

Dynamic recruitment and the physiological roles of the TPLATE complex in plant endocytosis

Jie Wang

Promotors:

Prof. Dr. Ir. Daniel Van Damme

Prof. Dr. Eugenia Russinova

Ghent University

Faculty of Sciences

Department of Plant Biotechnology and Bioinformatics

VIB Center for Plant Systems Biology

Thesis submitted in partial fulfillment of the requirement for the degree of Doctor of Philosophy in Science: Biochemistry and Biotechnology.

Academic year: 2020-2021



This manuscript and its content are presented in confidentiality, with the only purpose to evaluate the dissertation of Jie Wang, and cannot be revealed to third parties or used for other purposes without the permission of Prof. Dr. Daniel Van Damme.

This work was conducted in VIB department of Plant Systems Biology, Ghent University. Jie Wang was supported by the China Scholarship Council (CSC) for a predoctoral fellowship and by the Special Research Funds of Ghent University (BOF).

Examination Board

Promotor:

Prof. Dr.ir. Daniel Van Damme

Ghent University - Faculty of Sciences, Department of Plant Biotechnology and Bioinformatics

VIB - Center for Plant Systems Biology

Co-Promotor:

Prof. Dr. Eugenia Russinova

Ghent University - Faculty of Sciences, Department of Plant Biotechnology and Bioinformatics

VIB - Center for Plant Systems Biology

Examination committee:

Prof. Dr. Sofie Goormachtig (Chair)

Ghent University - Faculty of Sciences, Department of Plant Biotechnology and Bioinformatics

VIB - Center for Plant Systems Biology

Prof. Dr. Ir. Steffen Vanneste (Secretary)

Ghent University - Faculty of Sciences, Department of Plant Biotechnology and Bioinformatics

VIB - Center for Plant Systems Biology

Prof. Dr. Ruediger Simon

Heinrich-Heine University - Institute for Developmental Genetics

Prof. Dr. Charles Hachez

University of Louvain - Louvain Institute of Biomolecular Science and
Technology

Dr. Roman Pleskot

Ghent University - Faculty of Sciences, Department of Plant Biotechnology and
Bioinformatics

VIB - Center for Plant Systems Biology

Dr. Ana Fernandez

Ghent University - Faculty of Sciences, Department of Plant Biotechnology and
Bioinformatics

VIB - Center for Plant Systems Biology

Table of Contents

Scope and Objectives	- 1 -
Summary	- 3 -
Samenvatting	- 7 -
List of Abbreviations	- 11 -
Chapter One	- 15 -
Insight into the TPLATE complex: functions in clathrin-mediated endocytosis and beyond	- 15 -
Clathrin-Mediated Endocytosis	- 16 -
Clathrin-mediated endocytosis is a multi-step sequential process.....	
.....	- 18 -
Clathrin-mediated endocytosis requires adaptor protein complexes..	- 19 -
Two adaptor protein complexes coexist in plants.....	- 21 -
The canonical player: AP-2.....	- 21 -
A novel player: the TPLATE complex.....	- 23 -
A specific role for TPC in lignocellulosic cell wall formation?	- 24 -
Does TPC represent an ancient early nucleation module for CME?	
.....	- 25 -
Imaging tools to study CME in plants.....	- 27 -
Live-cell visualization of endocytosis in plants.....	- 27 -
Dynamic visualization and quantitative measurements are employed to study endocytosis in plants.....	- 28 -
Ultrastructural imaging of endocytosis in plants.....	- 32 -
Chemical and genetic tools to study CME in plants	- 34 -
Unravelling TPC function during CME and plant development requires additional tools.....	- 36 -
Does the AtEH/Pan1 proteins or whole TPC drive autophagy? ..	- 37 -
References	- 40 -

Chapter Two.....	- 49 -
High temporal resolution reveals simultaneous plasma membrane recruitment of the TPLATE complex subunits	- 49 -
Abstract	- 50 -
Introduction.....	- 51 -
Results.....	- 53 -
Lowering the experimental temperature reduces CME kinetics..	- 53 -
Lowering the temperature enhances the temporal resolution of plasma membrane recruitment.....	- 56 -
TPLATE is closely associated with the AtEH/Pan1 proteins at the plasma membrane.....	- 58 -
AtEHs/Pan1 and the core TPC subunits are simultaneously recruited to the PM	- 60 -
Discussion	- 63 -
Materials and Methods	- 68 -
References	- 82 -
Chapter Three.....	- 87 -
Characterization of TPLATE motif mutated isoforms	- 87 -
Abstract	- 88 -
Introduction.....	- 89 -
Results.....	- 90 -
Identification and evaluation of evolutionarily conserved TPLATE motifs	- 90 -
SANDWICH and PLATFORM subdomains are crucial for TPLATE function	- 94 -
Substitutions in the WDX domain partially affect TPLATE functionality	- 96 -
Discussion	- 101 -
The APPENDAGE domain but not the BODY and LINKER domains are essential for TPLATE function	- 101 -

Substituting SANDWICH and PLATFORM domains completely abolishes TPC assembly	- 102 -
WDX motif substitution mutant is a partially functional TPLATE mutant	- 103 -
Materials and methods	- 108 -
References	- 117 -
Chapter Four.....	- 121 -
Conditional destabilization of the TPLATE complex impairs endocytosis rather than autophagy	- 121 -
Abstract	- 122 -
Introduction.....	- 123 -
Results.....	- 126 -
Substitutions in the WDX domain destabilize the whole TPC ...	- 126 -
Destabilizing TPC does not lead to visible developmental defects in seedlings	- 127 -
Short-term heat stress induces aggregation of TPLATE proteins and results in cytoplasmic aggregation of TPLATE.....	- 128 -
Destabilizing TPC correlates with hypersensitivity to heat stress as well as accumulation of ubiquitinated proteins.....	- 130 -
The effect of destabilizing TPC is not phenocopied in atg mutants under stress.....	- 133 -
Destabilizing TPC by short-term heat stress does not inhibit autophagy	- 136 -
Inactivation of TPC by short-term heat stress efficiently impairs endocytosis.....	- 139 -
Discussion	- 142 -
mWDX-mediated destabilization of TPLATE is a novel conditional tool to study TPC's functions.	- 142 -
Autophagy relies on AtEH/Pan1 rather than on the whole TPC.....	- 144 -

Long-term heat stress resistance relies more on endocytic capacity than on autophagosomal degradation.	- 145 -
mWDX is a conditional tool to manipulate endocytosis specifically at the PM.	- 146 -
Materials and methods	- 154 -
References	- 161 -
Chapter Five	- 167 -
The TPLATE complex is essential for shoot apical meristem maintenance.....	- 167 -
Abstract	- 168 -
Introduction	- 169 -
Results.....	- 172 -
Destabilizing TPC affects SAM patterning and results in a multiple-shoot phenotype	- 172 -
Destabilizing TPC affects SAM patterning and results in ectopic PIN1 and DR5 expression	- 176 -
mWDX2 vegetative meristems exhibit re-specification of meristem identity	- 178 -
Destabilizing TPC results in hypersensitivity to CLV3 signaling	- 181 -
Destabilizing TPC results in impaired internalization of CLV1 in meristems	- 184 -
TPC targets more than the CLV1 receptor.....	- 185 -
Destabilizing TPC results in ectopic callose accumulation and altered cell wall morphology in vegetative meristems.....	- 188 -
Discussion	- 192 -
A threshold-dependent TPC function underpins SAM maintenance.	- 192 -
Re-specification of stem cell identity in mWDX2 vegetative SAM	- 194 -
WUS and CLV3 expression is dysregulated in mWDX2 vegetative	

SAM.....	- 194 -
TPC-dependent CME internalizes CLV receptors.....	- 196 -
Ectopic callose deposition causes the defects in mWDX2 vegetative SAM.....	- 198 -
Materials and methods	- 207 -
References	- 213 -
Chapter Six.....	- 221 -
Conclusions and Perspectives.....	- 221 -
TPC is recruited as octameric complex on the plasma membrane to fulfill its function in plant endocytosis.....	- 222 -
Slowing down endocytosis by lowering temperature contributes to improving temporal resolution of differential recruitment	- 223 -
The octameric TPC is required on the PM in plant endocytosis	- 224 -
TPC versus AP-2 recruitment	- 225 -
Development of tools to uncover TPC function.....	- 226 -
mWDX is a novel conditional tool to uncover the roles of TPC on the PM	- 229 -
mWDX links TPLATE-dependent endocytosis to the regulation of ROS homeostasis	- 231 -
mWDX reveals that TPC function is not required for autophagosome formation.....	- 232 -
mWDX associates TPLATE-dependent endocytosis with shoot apical meristem maintenance	- 233 -
Is TPLATE-dependent endocytosis required root apical meristem maintenance?.....	- 236 -
Is manipulation of TPC's function potentially applicable to agriculture?	- 237 -
References	- 239 -
Acknowledgments.....	- 243 -
Curriculum Vitae	- 247 -

Scope and Objectives

Clathrin-mediated endocytosis (CME) is the best-characterized and evolutionarily conserved pathway by which eukaryotic cells internalize extracellular materials and plasma membrane proteins, such as receptors and transporters, thereby controlling cellular homeostasis and many aspects of cellular signaling. Endocytosis in plants is essential not only for basic cellular functions but also for a plethora of physiological processes, including regulation of growth and development, nutrient uptake, and defense against pathogens. However, the precise mechanism of how endocytosis operates in plants remains quite elusive.

Clathrin does not bind membranes directly nor does it recognize the cargos that needs to be internalized. Thus, adaptor proteins act as essential links between the clathrin coat and the cargoes on the plasma membrane. Two types of multimeric adaptors function in plant endocytosis, the evolutionarily conserved AP-2 complex and the newly identified plant (and all amoeba species)-specific TPLATE (termed after the T-shaped cell plate localization at the end of cytokinesis when the cell plate fuses with the mother wall) complex (TPC/TSET). The jotnarlog (a homolog hidden from view as it is not present in the most studied model systems, named by the group of Joel Dacks after a hidden world in Norse mythology) TPC was identified as an octameric complex in *Arabidopsis* and as hexameric complex (TSET) in *Dictyostelium discoideum*. Over the past years, the lab has determined TPC as an essential adaptor complex during CME, which is essential for pollen and seedling development in plants. However, the exact mode-of-action of TPC remains largely unknown.

Two TPC subunits, AtEH1/Pan1 and AtEH2/Pan1, are likely auxiliary to the core TPC complex, as they do not co-purify with the other complex subunits in *Dictyostelium*, and they are not associated with the other TPC core components

when the complex was forced into the cytoplasm by truncating the TML (TPLATE Muniscin-Like) subunit. One aspect of my PhD study was to understand the recruitment mechanism of TPC on the PM using dynamic live-cell imaging. More specifically, my aim was to answer the question whether TPC was recruited as a whole or whether differential recruitment of AtEH/Pan1 vs the other TPC subunits occurred. In addition, recent work showed that AtEH1/Pan1 and AtEH2/Pan1 are also involved in actin cytoskeleton-regulated autophagy. However, whether this is an independent function of AtEH/Pan1 proteins or whether the whole TPC is required for autophagosome formation remains unclear. The male sterility or seedling lethality phenotype caused by mutations in single TPC subunits, blocks any genetic approach to study TPC functions in CME in relation to plant development. One of the concrete aims of my PhD projects was therefore to explore whether we could develop a partially complemented TPC background, which could overcome the genetic barrier caused by knockout or knockdown TPC subunits and which would allow us to study the functions of TPC in plant development. Moreover, such a tool would also allow evaluating the involvement of the TPC as a whole in the process of autophagy.

Summary

Clathrin-mediated endocytosis (CME) is the most prominent endocytic pathway in plants. It represents a major mechanism for regulating signaling, plant immunity and global responses, as many important plasma membrane (PM) proteins (including transporters and receptors) are established cargos for the CME pathway. As clathrin does not interact directly with membranes or cargos, the formation of the clathrin-coated vesicles (CCVs) requires the recruitment of adaptor proteins.

The TPLATE complex (TPC) represents an ancestral adaptor complex, which is however absent in present-day metazoans and yeasts, and has been so far only experimental characterized in plants and in *Dictyostelium*. In plants, TPC consists of eight components and functions as an early adaptor complex during CME. Knockdown or knockout of TPC single subunit leads to either pollen lethality or seedling lethality, revealing that TPC-dependent endocytosis is essential for plant life. While the hexameric TPC (TSET) still functions in plasma membrane turnover, the complex appears to be dispensable for *Dictyostelium*. TPC therefore remains only essential for life in the plant kingdom, suggesting fundamental differences in how the endocytic machinery operates in plants compared with animals and yeasts. In addition, two TPC subunits, AtEH1/Pan1 and AtEH2/Pan1, are involved in autophagy. These proteins or the whole TPC might therefore have multiple roles in both pathways. The research aims of my PhD study were to understand TPC's mode of recruitment to the PM as well as to dissect its physiological role in plant endocytosis, using a directed strategy to generate partial or conditional mutants.

The fact that AtEH1/Pan1 and AtEH2/Pan1 are auxiliary to the core TPC complex, suggests that they might be potentially recruited to the PM, independently of the other TPC subunits. To study the dynamic assembly of TPC at the PM, we employed dual-color live cell imaging at physiological and

at lowered temperature. My data in **Chapter 2** show that lowering the temperature slows down endocytosis and thereby enhances the temporal resolution of the recruitment of endocytic components. Lowering the temperature therefore has the potential to enhance the visualization of the differential recruitment of the endocytic players. The extremely strong spatial correlation between AtEH1/Pan1 and AtEH2/Pan1 and the TPC core subunits at endocytic foci as well as their simultaneous recruitment under both normal and lowered temperature conditions, led us to conclude that TPC is recruited to the PM as an octameric complex.

A targeted mutagenesis strategy was employed to identify partial loss of function alleles of TPLATE by mutating selected motifs, which we identified based on evolutionary conservation. In **Chapter 3**, I provide an overview and initial characterization of the different TPLATE mutated isoforms that were analyzed. This approach identified that SANDWICH and PLATFORM domains are essential for TPC assembly and functionality. Besides, our data also revealed that substituting the most conserved motif of TPLATE across plants as well as *Dictyostelium*, which we termed WDX, for stability in Chinese, dampens the efficiency of endocytosis while it conserves TPLATE functionality. The mWDX complemented line therefore represents a potential partially functional TPLATE allele.

In the following chapter, **Chapter 4**, I further characterized mWDX as a destabilized form of TPLATE, which leads to destabilization of the whole TPC in mWDX complemented *tplate(-/-)* KO lines. We further developed mWDX as a heat-inducible tool to inactivate TPC, as short-term heat-treatment delocalizes TPLATE from the PM and causes it to aggregate in the cytoplasm. This heat-inducible TPC inactivation tool provided us the opportunity to study the functions of TPC in autophagy and endocytosis. Our phenotypical analysis and confocal data confirm that TPC is essential for endocytosis and they support the hypothesis that it is not required for autophagosome formation.

Moreover, our data revealed that TPC-dependent endocytosis is required for heat stress tolerance.

In the last results chapter, **Chapter 5**, I discovered the importance of TPC in shoot apical meristem (SAM) maintenance. Our results revealed that mild destabilization of TPC results in a predominant double-shoot phenotype caused by the splitting of the meristem, randomized cell identity and disordered patterning in the vegetative SAM. We further revealed impaired internalization of CLV1 receptors from the PM and subsequent hypersensitivity to exogenous CLV3 peptide treatment in mWDX2 complemented lines. Moreover, the fact that CLV-type receptors are present, but that signaling is perturbed, together with observation of ectopic deposition of callose and thick cell walls in the vegetative meristems in mWDX2 plants, leads us to conclude that cell wall alterations are likely the causal to the observed mutant phenotype. These results together reveal that mildly perturbing TPC-dependent endocytosis predominantly leads to a manifestation of defects in SAM maintenance.

In the final chapter of this thesis, Chapter 6, I provide a general discussion of my research and provide some perspectives for future research.

Samenvatting

Clathrine-gemedieerde endocytose (CME) is de meest prominente internalizatieleroute bij planten. Het vertegenwoordigt een belangrijk mechanisme voor het reguleren van signalisatie, immuniteit van planten en globale reacties, aangezien veel prominente plasmamembraaneiwitten (inclusief transporters en receptoren) bevestigde cargos zijn voor de CME-route. Aangezien clathrine niet rechtstreeks interageert met membranen of cargo-eiwitten, vereist de vorming van clathrine gecoate vesikels (CCV's) de rekrutering van adaptereiwitten.

Het TPLATE-complex (TPC) vertegenwoordigt een voorouderlijk adaptercomplex, dat echter afwezig is in de huidige dieren en gisten, en tot dusver alleen experimenteel is gekarakteriseerd in planten en in *Dictyostelium*. In planten bestaat TPC uit acht componenten en fungeert het als een vroeg adaptercomplex tijdens CME. Knockdown of knockout van subeenheden van het TPC leidt ofwel tot pollenletaliteit of tot zaailingletaliteit, wat onthult dat TPC-afhankelijke endocytose essentieel is voor het leven van planten. Hoewel het hexamere TPC (TSET) nog steeds functioneert in plasmamembraantransport, lijkt het complex niet essentieel voor *Dictyostelium*. TPC blijft daarom alleen essentieel voor het leven in het plantenrijk, wat fundamentele verschillen blootlegt over hoe het endocytische proces in planten werkt in vergelijking met dieren en gisten. Daarnaast zijn twee TPC-subeenheden, AtEH1/Pan1 en AtEH2/Pan1, betrokken bij autofagie. Deze eiwitten of het hele TPC, kunnen daarom in beide routes meerdere functies vervullen. De onderzoeksdoelen van mijn doctoraatsonderzoek waren om de manier van rekrutering van het TPC aan het plasmamembraan te begrijpen en om de fysiologische rol ervan bij endocytose bij planten te ontleden, met behulp van een gerichte strategie om partiële of voorwaardelijke mutanten te genereren.

Het feit dat AtEH1/Pan1 en AtEH2/Pan1 geen deel uitmaken van het kern TPC, suggereert dat ze mogelijk onafhankelijk van de andere TPC-subeenheden zouden kunnen worden gerekruteerd naar het plasmamembraan. Om de dynamische assemblage van TPC aan het plasmamembraan te bestuderen, gebruikten we tweekleurige live-cel beeldvorming bij fysiologische en verlaagde temperatuur. Mijn gegevens in hoofdstuk 2 laten zien dat het verlagen van de temperatuur endocytose vertraagt en daardoor de temporele resolutie van de rekrutering van endocytische componenten verbetert. Het verlagen van de temperatuur heeft daarom potentieel om de visualisatie van de differentiële rekrutering van de endocytische spelers te verbeteren. De extreem sterke correlatie tussen de localisatie van AtEH1/Pan1 en AtEH2/Pan1 en de TPC-kernsubeenheden ter hoogte van endocytische foci, evenals hun gelijktijdige rekrutering onder zowel normale als verlaagde temperaturomstandigheden, hebben geleid tot de conclusie dat het TPC gerekruteerd wordt naar het plasmamembraan als een octameer complex.

Een gerichte mutagenesestrategie werd gebruikt om gedeeltelijk verlies van functionele allelen van TPLATE met partiële functie te identificeren. Dit gebeurde door motieven te muteren, die we identificeerden op basis van evolutionaire conservatie. In Hoofdstuk 3 geef ik een overzicht en een initiële karakterisatie van de verschillende mutanten die werden geanalyseerd. Deze aanpak identificeerde dat SANDWICH- en PLATFORM-domeinen essentieel zijn voor TPC-assemblage en functionaliteit. Bovendien toonden onze gegevens ook aan dat het vervangen van het meest geconserveerde motief van TPLATE tussen planten en *Dictyostelium*, dat we WDX noemden, voor stabiliteit in het Chinees, de efficiëntie van endocytose dempt terwijl de functionaliteit behouden blijft. WDX vertegenwoordigt daarom potentieel een gedeeltelijk functioneel TPLATE-allel.

In het volgende hoofdstuk, Hoofdstuk 4, heb ik mWDX verder gekarakteriseerd als een gedestabiliseerde vorm van TPLATE. Destabilisatie van TPLATE leidt tot destabilisatie van het hele complex in met mWDX

gecomplementeerde tplate(-/-) KO-lijnen. We hebben mWDX verder ontwikkeld als een door warmte induceerbare tool om het TPC conditioneel te inactiveren. Korte warmtebehandeling delocaliseert WDX weg van het plasmamembraan en zorgt voor een accumulatie van geaggregeerd complex in het cytoplasma. Deze hitte-induceerbare TPC-inactivatietool bood ons de mogelijkheid om de functies van TPC bij autofagie en endocytose te bestuderen. Onze fenotypische analyses en confocale beelden bevestigen dat TPC essentieel is voor endocytose en ze ondersteunen de hypothese dat het niet vereist is voor autofagosoomvorming. Bovendien toonden onze gegevens aan dat TPC-afhankelijke endocytose vereist is voor hittestress-tolerantie.

In het laatste hoofdstuk met resultaten, hoofdstuk 5, ontdekte ik het belang van het TPC bij de organisatie van het scheut apicaal meristeem (SAM). Onze resultaten toonden aan dat milde destabilisatie van TPC resulteert in een overheersend fenotype van planten met dubbele scheuten, veroorzaakt door de splitsing van het meristeem, gerandomiseerde celidentiteit en ongeordende cellulaire patronen in het vegetatieve SAM. We konden dit fenotype herleiden tot een verminderde internalisatie van CLV1-type receptoren aan het plasmamembraan en overgevoeligheid voor exogene CLV3-peptidebehandeling. Het feit dat receptoren van het CLV-type aanwezig zijn en functioneel zijn, maar dat de signalisatie verstoord is, samen met de observatie van de ectopische afzetting van callose en de aanwezigheid van dikke celwanden in de vegetatieve meristemen in WDX2-planten, leidde tot de conclusie dat celwandveranderingen oorzakelijk zijn voor de waargenomen mutante fenotypes. Deze resultaten samen tonen aan dat mild verstoorde TPC-afhankelijke endocytose voornamelijk leidt tot een manifestatie van defecten bij het in stand houden van het SAM.

In het laatste hoofdstuk van dit proefschrift, hoofdstuk 6, geef ik een algemene bespreking van mijn onderzoek en geef ik enkele perspectieven voor toekomstig onderzoek.

List of Abbreviations

Adaptor protein 2 complex	AP-2
AINTEGUMENTA	ANT
AlexaFluor 647-castesterone	AFCS
Arabidopsis thaliana EH domain containing protein 1/2	AtEH1/2
Autophagy related gene 8	ATG8
BARELY ANY MERISTEMS	BAM
Borate efflux transporter	BOR1
BRASSINOSTERIOD INSENSITIVE 1	BRI1
CALLOSE SYNTHASE 3	CALS3
Cellulose synthase complexes	CESA
Central zone	CZ
C-terminally encoded peptide	CEP
Clathrin heavy chains	CHCs
Clathrin light chains	CLCs
Clathrin-coated pits	CCPs
Clathrin-coated vesicles	CCVs
Clathrin-independent endocytosis	CIE
Clathrin-mediated endocytosis	CME
CLAVATA	CLV
CLAVATA 1	CLV1
CLAVATA 2	CLV2
CLAVATA3	CLV3
CLAVATA3/ESR-RELATED	CLE
Co-immunoprecipitation	Co-IP
Columella stem cells	CSCs
CORYNE	CRN
Day after germination	DAG

Dynamin-related proteins	DRPs
Early endosome	EE
EGFR-phosphorylated substrate protein 15	Eps15
Electron microscopy	EM
Endocytosis accessory proteins	EAPs
Endosidin 9	ES9
Epsin/AP180N-terminal homology	E/ANTH
FASCIATED EAR3	FEA3
Fer/CIP4 homology domain only	FCHo
FLAGELLIN SENSING 2	FLS2
Flotillin1	FLOT1
Fluorescence microscopes	FM
HAIRYMERISTEM	HAM
Immunoprecipitation	IP
Iron transporter	IRT1
Leucine-rich repeat receptor-like protein kinases	LRR-RLKs
Longin-like protein interacting with TPLATE adaptor	LOLITA
Mass spectrometry	MS
Modified pseudo-Schiff propidium iodide staining	mPS-PI
Neighbor of BRCA1	NBR1
Organizing center	OC
PEP RECEPTOR1	PEPR1
Peripheral zone	PZ
Phosphatidylinositol 4,5-bisphosphate	PtdIns(4,5)P2
PIN-FORMED	PIN
Plasma membrane	PM
Plasmodesmal-localized β -1,3 glucanase 1	PdBG1
Propidium iodide	PI
Quiescent center	QC

Reactive oxygen species	ROS
RECEPTOR-LIKE PROTEIN KINASE 2	RPK2
Respiratory burst oxidase homologs	RBOH s
Rib meristem	RM
Root apical meristem	RAM
Shoot apical meristem	SAM
Signal-to-noise ratio	SNR
Spinning disk microscopy	SD
Stem cell niche	SCN
Total internal reflection fluorescence microscopy	TIRF
TPLATE complex	TPC
TPLATE muniscin like	TML
TPLATE-associated SH3 domain containing protein	TASH3
TPLATE-associated WD40 domain containing protein 1/2	TWD40-1/2
Trans-Golgi network	TGN
Transmission electron microscopy	TEM
Tyrphostin A23	TyrA23
Variable angle epifluoresence microscopy	VAEM
Wendingxing	WDX
Wild type	WT
WUSCHEL	WUS
β -coatomer proteins motif	β -COP
μ -homology domain	μ HD

Chapter One

Insight into the TPLATE complex: functions in clathrin-mediated endocytosis and beyond

Jie Wang^{1,2}, Daniel Van Damme^{1,2,*}

¹Ghent University, Department of Plant Biotechnology and Bioinformatics, Technologiepark 71, 9052 Ghent, Belgium

²VIB Center for Plant Systems Biology, Technologiepark 71, 9052 Ghent, Belgium

This chapter serves as background information on the topic of clathrin-mediated endocytosis as well as overview of recent progress into TPC function in plants.

Author Contributions: JW wrote the initial draft of this chapter. DVD contributed to finalizing this paper

Chapter 1

Endocytosis is the process whereby eukaryotic cells generate small membrane vesicles to transport various cargo molecules from the plasma membrane (PM) into cells. This process is vital, not only for basic cellular functions but also to allow cells to respond quickly to extracellular stimuli, including stress, nutrient availability, hormone signalling and for cell plate formation and differentiation to occur (McMahon and Boucrot, 2011). Cargoes to be internalized by the endocytic pathway consist mainly of transmembrane proteins and their extracellular ligands, which are involved in a broad range of physiological processes (Kaksonen and Roux, 2018; Mettlen et al., 2018).

Different types of endocytic mechanisms exist in eukaryotes, the process can either depend on the scaffolding molecule clathrin or work independently of it (McMahon and Boucrot, 2011; Robinson, 2015; Paez Valencia et al., 2016). Clathrin-mediated endocytosis (CME) is however the most prominent and evolutionary conserved endocytic route for internalization of many cargoes in eukaryotes (Doherty and McMahon, 2009; McMahon and Boucrot, 2011; Bitsikas et al., 2014).

Clathrin-Mediated Endocytosis

CME is named after the key component of the endocytic machinery — the clathrin triskelia proteins, which comprise of heavy and light chain subunits (CHCs and CLCs). Clathrin was first identified as being the major protein making up the lattice-like coat around vesicles in pig brains (Pearse, 1976) and in soybean (Mersey et al., 1985). Clathrin self-assembles into a three-legged triskelium and assembles together with other cytosolic proteins at the endocytic site to form the clathrin-coated vesicles (CCVs) (Kaksonen and Roux, 2018). In plants, CCVs do not only form at the plasma membrane during endocytosis but also at the *trans*-Golgi network (TGN), which in plants represents an early endosome (EE) (Paez Valencia et al., 2016; Schwihla and Korbei, 2020).

Chapter 1

Clathrin-independent endocytosis (CIE) in *Arabidopsis* relies on flotillin1 (Flot1)-enriched membrane microdomains (Li et al., 2012), however the mechanics have yet to be clearly elucidated. The best-characterized endocytic pathway in plants depends on the coat protein clathrin. The *Arabidopsis* genome contains two *CHC* genes (*CHC1* and *CHC2*) which are highly identical (around 90%) and functionally partially redundant (Kitakura et al., 2011), and three *CLC* genes (*CLC1* to *CLC3*) which have at least 30% sequence homology with mammalian *CLCa* and *CLCb* (Wang et al., 2013). Mutants for *CLC1* show pollen lethality. On the other hand, *clc2* and *clc3* single mutants are viable but have shorter roots and longer hypocotyls than wild-type plants. The *clc2 clc3* double mutant is impaired in CME and displays stronger developmental defects than the corresponding single mutants, suggesting a partial functional redundancy between *CLC2* and *CLC3* (Wang et al., 2013). The respective *CHC* single mutants, however, show different phenotypes, where *chc2* plants display abnormal embryo and seedling development, but *chc1* mutants show no obvious phenotypes (Kitakura et al., 2011). Interfering with the function of *CHC* via overexpression of a dominant-negative C-terminal form of *CHC* (*CHC HUB*) that competes with the unimpaired *CHC* for *CLC* binding, the overexpression of *AUXILIN*, which inhibits endocytosis via blocking clathrin uncoating, and the application of a novel chemical inhibitor which binds *CHC* and disrupt its assembly into CCVs, highlight CME as the most prominent route for endocytosis in plant (Dhonukshe et al., 2007; Kitakura et al., 2011; Adamowski et al., 2018; Dejonghe et al., 2019).

Plants employ CME to maintain steady-state levels of many membrane proteins at the plasma membrane. In the absence of any stimulus, components on the PM are removed from the cell surface via constitutive internalization to specialized intracellular membranous compartments and recycled back to the plasma membrane. Plant cells can also modulate signalling events in response to external cues, for example during receptor-mediated endocytosis, where specific internalization of receptors bound to their ligands occurs (Traub, 2009;

Roy et al., 2014; Schwihla and Korbei, 2020). With the advent of *Arabidopsis* as a model system and the availability of a plethora of mutants, chemical tools and live imaging techniques, CME has been widely studied in plants over the past 15 years (Dhonukshe et al., 2007; Konopka and Bednarek, 2008b; Kitakura et al., 2011; Wang et al., 2013; Adamowski et al., 2018; Dejonghe et al., 2019). The hypothesized mechanism of CME in plants is still largely inferred from the more advanced studies in mammalian and yeast systems where CME components are highly conserved.

Clathrin-mediated endocytosis is a multi-step sequential process

Similar to mammalian systems, the dynamic and sequential CME process can be dissected into multi-sequential steps in plants (Fig 1), including initiation, cargo recruitment, coat assembly or maturation, scission and vesicle uncoating (McMahon and Boucrot, 2011; Zhang et al., 2015; Kaksonen and Roux, 2018; Mettlen et al., 2018). The formation of the CCPs require the recruitment of adaptor proteins and endocytic accessory proteins (EAPs) that interact with membrane lipids and sorting motifs in cargo proteins and then recruit clathrin from the cytoplasm to the initiation site at the PM (Paez Valencia et al., 2016). With the concentration of cargoes into growing CCPs and the further recruitment of numerous EAPs, the nascent CCPs undergo maturation until they are deeply invaginated while remain connected to the cell surface via a narrow neck. After the maturation of CCPs, the large GTPase dynamin is recruited to these narrow necks and catalyzes membrane scission (Paez Valencia et al., 2016; Schmid, 2017; Kaksonen and Roux, 2018; Mettlen et al., 2018). The released clathrin-coated vesicles are uncoated by the uncoating ATPase Hsc70 and auxilin-like proteins, and the uncoated vesicles deliver their contents via fusion to the TGN and EE for subsequent sorting back to the PM (recycling) and/or delivery to the vacuole (Schmid, 2017; Reynolds et al., 2018).

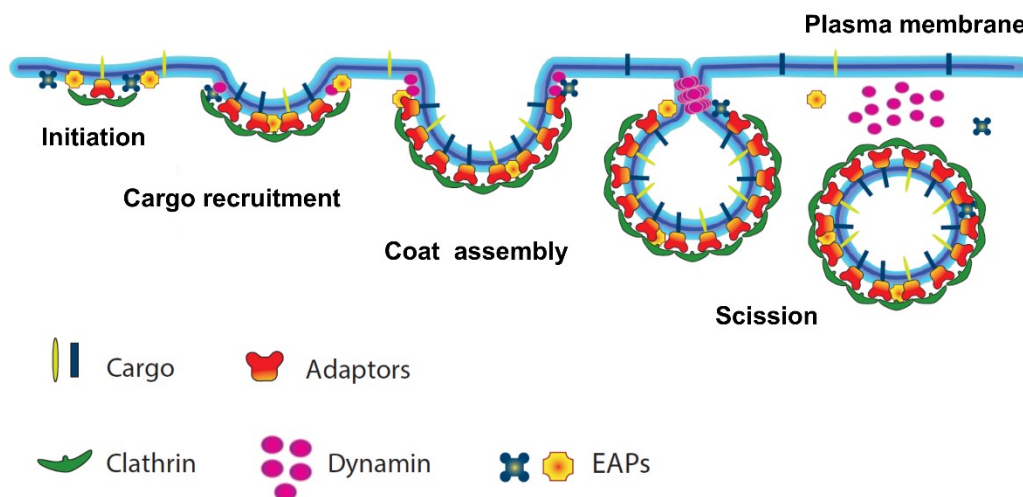


Figure 1. CME is a multi-stage process.

CME can be viewed as a multi-stage process on the PM that involves initiation, cargo recruitment, coat assembly or maturation and scission. CME is initiated by adaptor proteins that recognize sorting motifs of cargoes and recruit clathrin to form nascent CCPs. With the aid of numerous endocytic accessory proteins (EAPs), CCPs further concentrate cargoes as they grow and mature. After maturation of CCPs, dynamin is recruited to the necks of deeply invaginated coated pits and drives membrane fission and vesicle release. The released CCPs are uncoated and deliver their cargo to the TGN/EE for subsequent sorting back to the PM (recycling) and/or delivery to the vacuole for degradation. The figure is modified based on (Mettlen et al., 2018).

Clathrin-mediated endocytosis requires adaptor protein complexes

In mammalian systems, the initiation of CME depends on lipids, cargoes, and adaptor proteins. An endocytic event is initiated by clustering of the first endocytic proteins at the plasma membrane, forming the nucleus for the assembly of the vesicle coats. The initiation stage of CME defines the site where the endocytic vesicle will be formed and which cargo will be internalized (Kaksonen and Roux, 2018).

As clathrin does not bind membranes nor does it interact with the cargo proteins directly, the formation of the CCPs require the recruitment of adaptor proteins. They interact with membrane lipids and sorting motifs in cargo proteins and then bring clathrin from the cytoplasm to the initiation site at the

Chapter 1

PM (Fig 1). Adaptor proteins consist of multiple domains and motifs and interact with specific membrane phospholipids and cargo proteins, thus conferring specificity to the cargoes sequestered within the CCPs and, later, into the CCVs (McMahon and Boucrot, 2011; Paez Valencia et al., 2016; Reynolds et al., 2018).

In mammalian cells, many endocytic adaptor proteins are recruited to the plasma membrane by binding to phosphatidylinositol 4,5-bisphosphate [PtdIns(4,5)P₂], and this interaction is necessary for the assembly and function of the endocytic coat (Zoncu et al., 2007; Antonescu et al., 2011). In non-plant systems, the endocytic process is initiated by the heterotetrameric adaptor protein complex AP-2, which functions in CME that simultaneously binds clathrin, cargo proteins, and PtdIns(4,5)P₂ at the plasma membrane (Honing et al., 2005; Cocucci et al., 2012). In addition, AP-2 interacts with various EAPs, including the E/ANTH (epsin/AP180N-terminal homology) domain proteins epsin and AP180, the EGFR-phosphorylated substrate protein 15 (Eps15) proteins as well as muniscin proteins like the Fer/CIP4 homology domain only (FCHo) proteins and intersectins in mammals (Henne et al., 2010; Cocucci et al., 2012). In line with its nature as a major interaction hub in CME, the AP-2 complex is essential for embryonic development and morphogenesis in mammals (Mitsunari et al., 2005).

In addition to AP-2, the FCHo proteins were also proposed to be initiation factors in mammalian cells (Henne et al., 2010). It has been further shown that AP-2 is directly activated by the muniscin FCHo, by promoting a conformational change to the open/active form in the nematode *Caenorhabditis elegans*. AP-2 has been hypothesized to partite as two conformations which correlates with its function: the cytoplasmic locked form in which the binding sites for cargo-sorting motifs are blocked, and the open/active form in which cargo-binding sites are exposed and accessible (Jackson et al., 2010). In the absence of FCHo, AP-2 is inactive and endocytosis is reduced, reinforcing the idea that the assembly of a nucleation module precedes the activation of AP-2 at the clathrin-coated

Chapter 1

pit initiation sites (Hollopeter et al., 2014).

In mammalian cells, the open/closed conformation of AP-2 does not solely depend on FCHO as phosphorylation or PI(4,5)P₂ binding for example have also been shown to change AP-2 conformation. The initial recruitment of the closed/inactive AP-2 to the cytosolic face of the plasma membrane requires its interaction with PI(4,5)P₂ (Collins et al., 2002; Honing et al., 2005). The second binding site for PI(4,5)P₂ in the open conformation of AP-2 that stabilizes membrane engagement (Kadlecova et al., 2017). Phosphorylation of AP2 is suggested to play roles of enhancing the binding to PIP₂ and cargo (Honing et al., 2005) or promoting AP2 activity (Olusanya O, 2001) .

Two adaptor protein complexes coexist in plants

The muniscin protein family has likely evolved by combining the mu-HD of the TPC TML subunit with a BAR domain (Hirst et al., 2014). Muniscins such as the mammalian FCHO protein have a predominant and early role in CME (Henne et al., 2010; Cocucci et al., 2012). The nature of the CME initiation machinery in plants is still largely unknown and by default distinct from animal and yeast cells. Two candidates for initiation factors have been identified in plants, the conserved Adaptor protein 2 (AP-2) complex (Bashline et al., 2013; Di Rubbo et al., 2013; Fan et al., 2013; Kim et al., 2013; Yamaoka et al., 2013) and the TPLATE complex (Gadeyne et al., 2014).

The canonical player: AP-2

Arabidopsis contains five heterotetrameric adaptor protein complexes (AP-1 to AP-5), while only AP-2 has been shown to function specifically at the plasma membrane (Bashline et al., 2013; Di Rubbo et al., 2013; Fan et al., 2013; Kim et al., 2013; Yamaoka et al., 2013; Paez Valencia et al., 2016; Yoshinari et al., 2019). As the canonical CME adaptor complex, the evolutionarily conserved

Chapter 1

heterotetrameric AP-2 complex consists of two large (AP2A and AP2B respectively α and β), one medium (AP2M or μ) and one small subunit (AP2S or σ) has been well characterized in plants (Bleckmann et al., 2010; Di Rubbo et al., 2013; Fan et al., 2013; Kim et al., 2013). Unlike the fact that AP-2 is essential in animals, Arabidopsis plants which lack single AP-2 subunits (α -, μ -, and σ -subunits) are viable and exhibit pleiotropic defects in plant growth and development (such as reduced pollen production and viability, abnormal floral structures, and reduced vegetative growth), suggesting that plant cells can overcome the loss of single AP-2 subunits (Bashline et al., 2013; Fan et al., 2013; Kim et al., 2013; Yamaoka et al., 2013). Null mutations of AP-2 subunit (α - and μ - subunit) are viable in *Caenorhabditis elegans*, as the remaining subunits form hemicomplexes and retain some function (Gu et al., 2013). Recent work showed that, in Arabidopsis plants deficient in a given AP-2 subunit, the remaining subunits can still associate with the PM (Wang et al., 2016), suggest the relatively mild phenotype observed in *ap2* subunit mutants (Bashline et al., 2013; Di Rubbo et al., 2013; Fan et al., 2013; Kim et al., 2013; Yamaoka et al., 2013), is likely due to the formation of partially active AP-2 complexes.

An advantage of the viability of AP-2 subunit knockout alleles is the ability to examine the effect of mutations on CME dynamics and cargo selection *in vivo*. Plants impaired in AP-2 subunits showed generally altered endocytosis, in particular of the PIN-FORMED family of auxin efflux facilitators (PINs), the Brassinosteroid receptor BRASSINOSTEROID INSENSITIVE1 (BRI1), subunits of the primary cell wall forming complex CELLULOSE SYNTHASE6 (CESA6) and the borate efflux transporter (BOR1) (Bashline et al., 2013; Di Rubbo et al., 2013; Fan et al., 2013; Kim et al., 2013; Bashline et al., 2015; Yoshinari et al., 2019).

A novel player: the TPLATE complex

Next to AP-2, TPLATE complex (TPC) is another adaptor complex acting in endocytosis at the plasma membrane specifically (Van Damme et al., 2006; Van Damme et al., 2011; Gadeyne et al., 2014). This complex is named after TPLATE subunit, which is the founding member and recruited to the forming cell plate and to the plasma membrane region surrounding the cell plate insertion site (Fig 2A), appears as a “T” in Arabidopsis root cells (Van Damme et al., 2006). The cell plate-anchoring defects in silenced TPLATE BY-2 tobacco suspension cells, suggests the essential role of TPLATE for cell plate to anchor to the mother wall (Van Damme et al., 2006). Besides, the colocalization of TPLATE with clathrin (CLC2) at cell plate and PM, together with the interaction identified between TPLATE and clathrin (CLC2 and CHC1), as well as their similar behavior following caffeine treatment in BY-2 cells provided the initial clues to link TPLATE to clathrin-mediated endocytosis (Van Damme et al., 2011).

In addition to cell plate recruitment, TPLATE is dynamically recruited to the PM as endocytic foci, which mostly reside at the PM between 10-30s (Fig 2B) (Gadeyne et al., 2014; Wang et al., 2020a). TPC was identified as an octameric complex, that consists of TPLATE, TML, TASH3, LOLITA, TWD40-1, TWD40-2, AtEH1/Pan1 and AtEH2/Pan1, and interacts with clathrin (both CHCs and CLCs), AP-2, proteins containing the ANTH (AP180 N-terminal homology) domain, and dynamin-related proteins (DRPs) in plants (Fig 2D) (Gadeyne et al., 2014). In agreement with its essential role during CME and in contrast to AP-2, TPC is essential for plants as knockout or knockdown TPC single subunits results in pollen lethality or seedling lethality respectively (Van Damme et al., 2006; Gadeyne et al., 2014; Wang et al., 2019). Analysis of inducible knockdown mutants revealed defective internalization of the endocytic dye marker FM4-64 and various PM proteins, including CESA6, BRI1, PIN1 and PIN2 (Gadeyne et al., 2014; Sanchez-Rodriguez et al., 2018).

A specific role for TPC in lignocellulosic cell wall formation?

TPC is an evolutionary ancient adaptor complex which was simultaneously discovered in plants and in slime molds, where it is a hexameric complex (AtEH1/Pan and AtEH2/Pan1 were not co-purified with other subunits) and was termed TSET (Fig 2E), consisting of TPLATE, TSPOON, TCUP, TSAUCER and its two TTRAYS (Gadeyne et al., 2014; Hirst et al., 2014). In contrast to yeast and mammalian cells, plants and slime molds have retained this adaptor complex (Gadeyne et al., 2014; Hirst et al., 2014). Although TSET still functions in *Dictyostelium* plasma membrane turnover, the complex appears to be dispensable for the organism as a knockout in the small subunit is viable (Hirst et al., 2014). Plants therefore are the only kingdom where TPC is essential for life (Gadeyne et al., 2014; Hirst et al., 2014), suggesting that CME executes fundamentally differently in plants compared with animals and yeast systems.

One hypothesis why TPC was evolutionary retained in plants but not in animals and yeasts might very well be connected to a lignocellulosic cell wall. Loss-of-function of TPLATE subunit results in pollen lethality concomitant with ectopic callose deposition, which was also observed in TPLATE RNA interference (amiRNA) plants (Van Damme et al., 2006), suggesting TPC is implicated in cell wall modification. The somatic developmental defects (defective hypocotyl and root elongation, bulging cells) and male sterility caused by inducible down-regulation/loss-of-function of TPC (Van Damme et al., 2006; Gadeyne et al., 2014; Sanchez-Rodriguez et al., 2018; Wang et al., 2019), are similar to what was found in plants that exhibited impaired-function or loss-of-function of cellulose synthesis, respectively (Persson et al., 2007; McFarlane et al., 2014). TPC subunits show co-expression with primary cell wall genes (Sanchez-Rodriguez et al., 2018). Co-IP and BiFC experiments confirmed the interaction between TPC subunits and CESA6 (Sanchez-Rodriguez et al., 2018). Live-cell imaging further reflected the reduced internalization of CESA6 when TPC subunits function are impaired (Sanchez-

Chapter 1

Rodriguez et al., 2018), accounts for the cellulose deficiency in inducible TML down-regulation lines. Similar to the *ap2* mutant and inducible knockdown *tpc* mutants, the weak allele *twd40-2-3* of TWD40-2 (*twd40-2-1* and *twd40-2-2* are male sterile (Gadeyne et al., 2014)) that affects TPC subunit expression, also exhibited defective internalization of CESA6 (Bashline et al., 2015; Sanchez-Rodriguez et al., 2018). These results suggested that TPC functions are essential for the regulation of cellulose synthesis, which is essential and unique to plants.

Does TPC represent an ancient early nucleation module for CME?

Phylogenetic analysis suggests that TPC/TSET are evolutionarily ancient, arising between the advent of COPI and the functional specification of the AP adaptor complexes (Fig 2F), two of the primary coat/adapting complexes in eukaryotes (Hirst et al., 2014; Zhang et al., 2015). Several TPLATE subunits contain conserved domains like the SH3 domain in TASH3, the EPS15 homology (EH) domains in AtEH1 and AtEH2, and a μ -homology domain in TML, which is also present in the medium subunits of the AP- complexes. These domains are also found in the mammalian AP complexes, Eps15, intersectins, and the muniscins. These domains are generally involved in membrane interactions, cargo recognition, and binding and recruitment of accessory proteins (Zhang et al., 2015). The TML subunit could have evolved into the muniscin protein family (Hirst et al., 2014; Zhang et al., 2015), where the prominent member, FCHo in animal cells, acts as nucleation point for CME (Henne et al., 2010). In plants, TPC (visualized by its core subunits TPLATE and TML) is recruited to the PM preceding AP-2 (visualized by its large subunit AP2-A1), light clathrin2 (CLC2) and dynamin-related protein1c (DRP1c). This determines its essential role in the early endocytic stages (Gadeyne et al., 2014). Besides, TPC is required for AP-2 subunit recruitment to the PM (Gadeyne et al., 2014; Bashline et al., 2015; Wang et al., 2016). These results

together reveal that TPC shows functional similarities to the nucleation modules in mammalian system and could play a role as a CME nucleation complex in plants (Mayers et al., 2013).

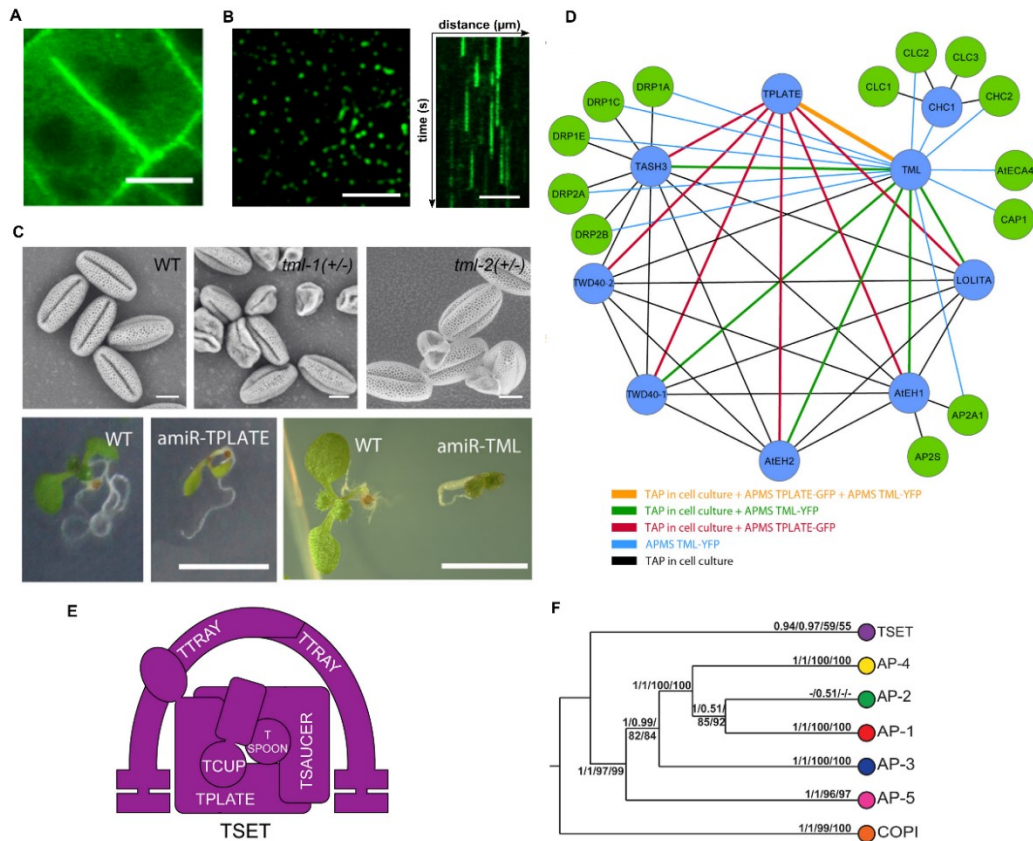


Figure 2. TPC functions as early adaptor proteins during CME.

(A) TPLATE-GFP is recruited to cell plate as well as the plasma membrane region surrounding the cell plate insertion site, shaping as a “ T ” in Arabidopsis root cells. **(B)** TPLATE-GFP is recruited to the PM as endocytic dots in Arabidopsis hypocotyl cells. Kymograph analysis indicates the residual life-time of TPLATE labelled endocytic foci on the PM. **(C)** Pollen lethality and seedling lethality phenotype caused by knockout or knockdown TPC single subunits. **(D)** Spoke-model interaction of TPC identified using various experiments as indicated in the legend. **(E)** Schematic diagram of the hexameric TPC (TSET) in *Dictyostelium*. **(F)** Simplified diagram of the concatenated tree showing the evolution of TSET, AP complexes and COPI. Pictures in this figure are modified from (Van Damme et al., 2011; Gadeyne et al., 2014; Hirst et al., 2014; Wang et al., 2020a).

Imaging tools to study CME in plants

Endocytosis is a dynamic cellular process that requires precise temporal and spatial orchestration of complex protein machinery to mediate membrane budding. To understand how this machinery works, many attempts have been made to visualize and quantify endocytosis.

Live-cell visualization of endocytosis in plants

Many efforts have been made to understand the roles of endocytosis in plants by the application of live cell imaging with fluorescent dyes or fluorescent-labelled cargoes. The lipophilic dye FM4-64, which only fluoresces when bound to membranes and is readily internalized into root cells through endocytosis, is widely employed to visualize and quantify endocytic flux (Di Rubbo et al., 2013; Gadeyne et al., 2014; Bashline et al., 2015; Dejonghe et al., 2016; Dejonghe et al., 2019; Wang et al., 2020a). FM4-64, when added, becomes an inherent part of the membrane and therefore will be likely internalized by multiple endocytic pathways. The extreme drop in FM4-64 internalization upon clathrin HUB overexpression indicates that CIE plays minor role for FM4-64 internalization in plants (Dhonukshe et al., 2007) as also in other systems, it was concluded that CIE does not majorly contribute to the bulk of material that is internalized (Bitsikas et al., 2014).

In addition to the endocytic tracer FM4-64, several bioactive fluorescent ligands have been developed to study receptor-mediated endocytosis (Irani et al., 2012; Di Rubbo et al., 2013). The bioactive fluorescent Brassinosteroid analog, AlexaFluor 647-castesterone (AFCS), was used to quantitatively study the endocytosis of ligand-bound BRI1 in living cells (Irani et al., 2012; Di Rubbo et al., 2013). More recently, the fluorescent tag TAMRA labelled endogenous peptide Pep1 and the bacterial peptide flg22 were used to examine trafficking of their cognate receptor PEP RECEPTOR1 (PEPR1) and FLAGELLIN SENSING 2 (FLS2) receptor kinase (Mbengue M, 2016; Ortiz-Morea et al.,

2016).

In addition to visualizing the fluorescently labelled ligand, visualization of fluorescent proteins tagged cargoes such as transporters and receptors localized on the PM contributes to understand the roles of endocytosis in these key physiological process in plants. Labelling with genetically encoded fusions to a fluorescent protein is the most widely used method for labelling proteins as the target protein and the fluorescent protein are produced as a translational fusion and thus are covalently linked. Besides, as the labelling occurs at the genetic level, nonspecific labelling can be avoided (Wang et al., 2018). Live cell imaging with labelled transporters and receptors such as those of the PINs, PEPR1, FLS22, BRI1, iron transporter (IRT1) and the boron exporter BOR1, revealed that endocytosis is essential for plants to response to hormone signalling (Dhonukshe et al., 2007; Kitakura et al., 2011; Di Rubbo et al., 2013; Du et al., 2013; Yu et al., 2016), environmental stimuli including plant pathogens (Mbengue M, 2016; Ortiz-Morea et al., 2016), and nutrient uptake (Barberon et al., 2011; Kasai et al., 2011; Yoshinari et al., 2016; Yoshinari et al., 2019). Compared to visualizing the fluorescent labelled ligand, which is reflecting the ligand-mediated endocytosis, visualizing the fluorescent tagged receptors detects not only the ligand-mediated internalization but also the constitutive internalization of the receptors itself (Mbengue M, 2016; Ortiz-Morea et al., 2016).

Dynamic visualization and quantitative measurements are employed to study endocytosis in plants

A striking feature of the endocytic machinery is that CCVs assemble at the plasma membrane through recruitment of endocytic proteins from the cytosol in a highly regular sequence and that different proteins arrive and leave in a specific order. In mammalian and yeast cells (with the exception of neuronal cells, which can do it much faster), it takes about 1-2 min for the whole endocytic

Chapter 1

event to happen, from initiation to vesicle formation (Lu et al., 2016; Picco and Kaksonen, 2018). The endocytic machinery of CME is well understood in mammalian and yeast systems, where more than 60 endocytosis accessory proteins (EAPs) have been well characterized in both model systems (Merrifield and Kaksonen, 2014; Lu et al., 2016; Kaksonen and Roux, 2018). However, CME in plants is more dynamic and the whole endocytic process spans less than 30 seconds. This high dynamicity partially explains the poor characterization of the sequential recruitment information we have on the endocytic machinery. Much of the current characterization of plant CME largely relied upon biochemical and pharmacological approaches using confocal microscopy, which are indirect and fail to capture the subtle roles of EAPs at CME sites with sufficient temporal resolution (Aguet et al., 2013; Johnson and Vert, 2017). CME is a highly dynamic process on the PM, thus direct monitoring the dynamics of single endocytic event contributes to understanding how the endocytic machinery in plants operates.

The development of live cell imaging techniques applicable to plant cells has greatly improved our ability to monitor dynamic events at the cell cortex. Among the live-cell imaging approaches to visualizing CME, spinning disc microscopy (SD) turned out to be an excellent choice as excitation is uniform throughout the illuminated area. Use of the pinholes allows one to select the cell surface plane and facilitates rapid acquisition (Johnson and Vert, 2017; Mettlen et al., 2018). Next to SD, other choices to image dynamic process on the cell surface is total internal reflection fluorescent microscopy (TIRF) or variable angle-TIRF, which has been referred as variable angle evanescent microscopy (VAEM). Taking advantage of the evanescent field results in the generation of a zone of fluorescence excitation with a typical probing depth of 100-160 nm along the z-direction from the glass-sample interface for visible light (Wang et al., 2018). These unique illumination techniques of TIRF/VAEM allow for the selective excitation of a limited portion of the sample adjacent to the glass slide, thus allows to capture dynamic events at the cell surface without background

Chapter 1

fluorescence from the sample interior and with extremely high spatiotemporal resolution (Johnson and Vert, 2017).

In plants, lifetimes of endocytic proteins are measured using time-lapse imaging of cells expressing fluorescent labelled proteins imaged via SD (Bashline et al., 2013; Gadeyne et al., 2014; Bashline et al., 2015; Dejonghe et al., 2016; Zhou et al., 2018; Dejonghe et al., 2019; Wang et al., 2020a) or TIRF/VAEM (Konopka et al., 2008; Konopka and Bednarek, 2008b, a; Ito et al., 2012; Johnson and Vert, 2017; Adamowski et al., 2018; Narasimhan et al., 2020). Imaging of fluorescently tagged clathrin and/or EAPs at the PM using SD or TIRFM/VAEM reveals dynamic foci of appearing and disappearing intensity reflecting the formation of CCPs and the internalization of budding CCVs away from the plane of focus, respectively. The time between the appearing foci and disappearing foci reflect the residual lifetime of fluorescent endocytic proteins labelled CCVs on the PM. Besides, live cell imaging of the dynamic behaviours between different endocytic players labelled by different fluorescent proteins (-GFP / -RFP) could reflect their different recruitment order during the formation of CCVs (Fujimoto et al., 2010; Fan et al., 2013; Gadeyne et al., 2014; Johnson and Vert, 2017; Narasimhan et al., 2020), contributing to unravelling the endocytic machinery in plant cells. By application of dual-colour live cell imaging, TPC has been determined as an early endocytic player during CME because of the observation that TPC subunits are recruited to the PM earlier than or concomitant with CLC2 (Gadeyne et al., 2014; Narasimhan et al., 2020), earlier than DRP1c or DRP1a (Gadeyne et al., 2014; Wang et al., 2020a), and prior to or concomitantly with the AP2 α subunit or AP2 μ (Gadeyne et al., 2014; Bashline et al., 2015).

Along with specific cell surface imaging techniques, automated image analysis algorithms which allow high throughput, unbiased and rapid analysis, have been widely employed to analyse CME events in the animal and the yeast fields (Jaqaman et al., 2008; Aguet et al., 2013; Compeer et al., 2018; Pascolutti et al., 2019; Wrobel et al., 2019). In plant CME research, however, image

Chapter 1

analysis still largely relies on manual analysis using kymographs generated from the time-lapse SD or TIRF or VAEM movies, which is labour intensive, time-consuming and susceptible to human subjectivity. To address these problems, the Trackmate tool which is a plug-in for the open source ImageJ/FIJI software platform that offers automated and manually segmentation and tracking (Tinevez et al., 2017), and the cmeAnalysis package (Aguet et al., 2013) for the MATLAB computing platform were employed for tracking and lifetime analysis of CME dynamics in plant cells (Johnson and Vert, 2017; Narasimhan et al., 2020). Automatic image analysis using the cmeAnalysis package was able to generate closely matched CLC2 lifetimes compared with reported manual measurement (Konopka et al., 2008; Narasimhan et al., 2020). The detection of the differential or concomitant recruitment between TPLATE and CLC2 was re-analyzed by automatic image analysis and it was concluded that TPC indeed arrives earlier than clathrin (Gadeyne et al., 2014; Narasimhan et al., 2020), suggesting it is a reliable tool to analyze CME images unbiasedly and rapidly, given that the signal to noise ratio of the images is sufficiently high. Often, when working with complemented mutant lines, with low expression levels, the signal to noise ratio is not sufficient to allow automated quantification (Wang et al., 2020a). Improving the analytical tools is therefore still required and this becomes increasingly necessary in order to quantitatively assess the spatiotemporal dynamics of endocytosis.

It has been revealed the significantly different lifetime between the two AP-2 subunits (AP2A1 and AP2M) at a single event resolution via the application of dynamic visualization and automatic images analysis (Johnson and Vert, 2017). However, whether it represents the differential recruitment between AP-2 subunits requires further study, as work such as live-cell imaging of dynamic behaviors of these subunits labelled with dual-color fluorescent proteins are lacking.

It appears that AtEHs/Pan1 proteins may be auxiliary to the core TPC complex, as these proteins were not associated with other TPC components

Chapter 1

when the complex was forced into the cytoplasm by truncation of the TML subunit in plants (Gadeyne et al., 2014), and also not copurified with the hexameric TPC complex in *Dictyostelium* (Hirst et al., 2014). These results suggest the possibility of differential recruitment between AtEHs/Pan1 and the six other TPC subunits on the PM in plants. This also leads to the question whether TPC is recruited to the PM as octameric complex to fulfill its function during CME or not. Monitoring the dynamic recruitment behavior between AtEHs/Pan1 and other TPC subunits contributes to answering this question.

Ultrastructural imaging of endocytosis in plants

Endocytosis is a spatial and temporal process that deforms a part of the plasma membrane into an invagination, which ultimately will give rise to a vesicle. The endocytic membrane invagination is a narrow tubule that extends up to 140 nm in length in yeast, and the size of the protein machinery that envelops the forming vesicle is approximately 200 nm in diameter in mammalian cells. The forming vesicle is thus an ellipsoid in yeast which is about 60 nm in length, and it is round and about 100 nm in diameter in mammalian cells (Picco and Kaksonen, 2018). Although fluorescence microscopes (FM) are excellent tools to observe dynamic processes in living cells, the limited spatial resolution (around 200 nm) determines they are unable to provide detailed information of the architecture of CCVs. This means that where the different endocytic proteins assemble and how they operate cannot be directly resolved by fluorescence microscopy. Super-resolution microscopy techniques can boost the resolution down to about 30 nm but this higher spatial resolution typically comes at the expense of temporal resolution (Picco and Kaksonen, 2018).

Electron microscopy (EM) and endocytosis is historically intimately linked. The first evidence of protein uptake via protein coated membrane vesicles forming from the plasma membrane was showed by application of EM (Roth and Porter, 1964). EM can reveal the cellular membranes and their shapes in

Chapter 1

detail, determines itself as an excellent tool for studying membrane trafficking processes. Besides, correlative electron and fluorescence microscopy has been developed to elucidate the ultrastructural details of dynamic and rare cellular events. By correlation the dynamics of key endocytic proteins (early and late markers) observed by fluorescence microscopy with the ultrastructural data obtained from electron tomograms, providing not only a quantitative four-dimensional description of an average endocytic event but also a resource for analysis of how proteins can dynamically shape membranes in vivo (Kukulski et al., 2011; Kukulski et al., 2012).

Although methods to isolate CCVs from *Arabidopsis* seedlings have been developed (Reynolds et al., 2014; Mosesso et al., 2018), only very recently high resolution images of clathrin coated pits from 'unroofed' *Arabidopsis* protoplasts were obtained (Narasimhan et al., 2020). The unroofing process which allows to look into the inside of the plasma membrane, and therefore provides a unique view of CCPs budding from the plasma membrane (Heuser, 1980). The EM analysis results revealed that clathrin-mediated endocytosis may follow a 'constant curvature' model. This means that clathrin assembly at the invagination directly bends the membrane, and the continuous polymerization of clathrin possibly sustains the curvature (Narasimhan et al., 2020). This is opposed to the constant area model, where clathrin is first deposited as a flat surface, which then later on bends. It was also shown that CME in plants does not require actin for functional endocytic pit progression, providing new insight into how endocytosis in plants differs from other model systems (Narasimhan et al., 2020). TPC is speculated as an initiation player during CME in plants, thus it will be interesting to perform similar experiments in conditions where TPC function is perturbed in order to provide new mechanistic insights about plant endocytosis.

Chemical and genetic tools to study CME in plants

Endocytosis has been so far manipulated in plants by the application of genetic tools and chemical tools that interfere with the functions of the endocytic players such as clathrin (Dhonukshe et al., 2007; Kitakura et al., 2011; Wang et al., 2013; Adamowski et al., 2018; Dejonghe et al., 2019), adaptor proteins (Bashline et al., 2013; Di Rubbo et al., 2013; Fan et al., 2013; Kim et al., 2013; Yamaoka et al., 2013; Gadeyne et al., 2014; Bashline et al., 2015; Wang et al., 2016; Sanchez-Rodriguez et al., 2018; Yoshinari et al., 2019) and dynamin-related proteins (Collings et al., 2008; Konopka and Bednarek, 2008a; Backues et al., 2010; Taylor, 2011; Yoshinari et al., 2016).

The viability of knockout mutants in clathrin (Kitakura et al., 2011; Wang et al., 2013), AP-2 (Bashline et al., 2013; Di Rubbo et al., 2013; Fan et al., 2013; Kim et al., 2013; Yamaoka et al., 2013; Wang et al., 2016; Yoshinari et al., 2019), and some dynamin-related proteins (Konopka and Bednarek, 2008a; Backues et al., 2010), allowed to characterize roles of CME in plants development such as floral organ development (Yamaoka et al., 2013), vegetative developmental defects (Fan et al., 2013; Wang et al., 2013). These mutants are also widely used to study the roles of CME in the regulation of various physiological processes including hormone signalling (Dhonukshe et al., 2007; Kitakura et al., 2011; Di Rubbo et al., 2013; Du et al., 2013; Yu et al., 2016), environmental stimuli including plant pathogens (Mbengue M, 2016; Ortiz-Morea et al., 2016), and nutrients uptake (Barberon et al., 2011; Kasai et al., 2011; Yoshinari et al., 2016; Yoshinari et al., 2019). Meanwhile, genetic studies and cellular imaging also indicated the functional redundancy among these proteins respectively (Backues et al., 2010; Wang et al., 2013; Wang et al., 2016). Manipulating the functions of clathrin has been achieved via overexpression of a dominant-negative C-terminal HUB of CHC that competes with the unimpaired CHC for CLC binding, and the overexpression of AUXILIN which likely blocks clathrin recruitment by continuous uncaging. These tools led to defective endocytosis

Chapter 1

of FM4-64 and PINs and somatic developmental defects in plants (Kitakura et al., 2011; Adamowski et al., 2018). Similarly, inducible overexpression of the dominant-negative of AP2M (*AP2MΔC*) resulted in reduced internalization of FM4-64, PIN2 and BRI1 as well as reduced root growth (Di Rubbo et al., 2013). Inducible overexpression of the dominant-negative of DRP1A (DRP1A K47A) inhibited BOR1 endocytosis, boron-induced BOR1 degradation and polar localization of BOR1 (Yoshinari et al., 2016), and the inducible expression of the dominant-negative DRP2A/B protein resulted in reduced endocytosis of FM4-64 (Taylor, 2011).

In addition to genetic approaches, chemical tools have been also developed to facilitate the studies of CME by providing small molecules that can interfere with CME in a conditional way. The phosphotyrosine analog tyrphostin A23 (TyrA23) is a drug that inhibits the interactions between the tyrosine motif of the cargo and medium subunit of the AP-2 (Banbury et al., 2003), and was until recently commonly used to interfere with endocytosis in plants (Van Damme et al., 2011; Irani et al., 2012; Di Rubbo et al., 2013; Wang et al., 2013; Dejonghe et al., 2016; Wang et al., 2016). In plants, TyrA23 has been shown to disrupt the PM association of AP2 α 1 (Di Rubbo et al., 2013; Kim et al., 2013), AP2 μ (Yamaoka et al., 2013), AP2 σ (Fan et al., 2013; Wang et al., 2016) and TPC subunit (TPLATE) (Van Damme et al., 2011), and it inhibited the internalization of a number of PM-resident proteins involved in hormone signaling (Dhonukshe et al., 2007; Irani et al., 2012), nutrient uptake (Barberon et al., 2011), and pathogen defense (Smith et al., 2014b; Smith et al., 2014a). However, recent work showed that the inhibition of TyrA23 on CME occurs through non-specific cytoplasmic acidification due to its protonophore activity, which thus undermines its use as a specific inhibitor of cargo recognition by the AP-2 adaptor complex (Dejonghe et al., 2016). Similar to TyrA23, Endosidin 9 (ES9) was recently characterized as a protonophore, its function as endocytic inhibitor, does however not entirely originate from cytoplasmic acidification as it also inhibited endocytosis at an increased apoplasmic pH (Dejonghe et al., 2016).

Chapter 1

Recent work showed that ES9 binds the N-terminal domain of CHC in *Arabidopsis*, and its improved analog ES9-17, which lacks the protonophore properties of ES9, overcomes the undesirable side effects of ES9 and retains the ability to bind CHC (Dejonghe et al., 2019). The development of ES9-17 therefore expanded the chemical tools for CME inhibition.

Besides TyrA23 and ES9, other CME inhibitors such as the dynamin inhibitor dynasore and the clathrin inhibitors pitstop which have been well established in mammalian systems (Macia et al., 2006; von Kleist et al., 2011), were recently employed to as CME inhibitors in plants (Sharfman et al., 2011; Dejonghe et al., 2016; Dejonghe et al., 2019). Recent work showed that dynasore as well as pitstop2 are not potent CME inhibitors in *Arabidopsis* (Dejonghe et al., 2016; Dejonghe et al., 2019).

Unravelling TPC function during CME and plant development requires additional tools.

Although TPC is determined as essential adaptor proteins in plants, little is known about its actual function. Knockout or knockdown TPC single subunit leads to pollen lethality and seedling lethality, and revealed the essential functions of TPC for pollen development and somatic development in plants (Van Damme et al., 2006; Gadeyne et al., 2014; Wang et al., 2019). At the same time, this also blocks genetic approaches to further study TPC function. Although inducible downregulation of TPC subunits can overcome the seedling lethality phenotype caused by constitutive silencing of TPC subunits, and resulted in impaired internalization of PM cargoes including BRI1, PINs and CESA6 (Gadeyne et al., 2014; Sanchez-Rodriguez et al., 2018), this approach still failed to provide more information regarding TPC functions, especially in adult plants. A weak allele of TWD40-2 (*twd40-2-3*) was identified which is viable and affected this TPC subunit expression. Analysis of this mutant revealed defective internalization of FM4-64 and CESA6, however only a mild

Chapter 1

macroscopic mutant phenotype (reduction in etiolated hypocotyl length and root growth) was detected (Bashline et al., 2015). Our recent work developed the mild downregulation lines of AtEH1/Pan1 via RNAi, which interfere with the formation of autophagosomes formation (Wang et al., 2019). However, the effect on CME in those lines has not been characterized yet. Besides, no chemical tools have been developed to target on TPC function as well as no dominant-negative mutants are available by far. Thus, new tools or partially functional mutants are required to dissect TPC function in CME.

Does the AtEH/Pan1 proteins or whole TPC drive autophagy?

Like endocytosis is essential for the turnover of extracellular and plasma membrane materials in plants, autophagy (self-eating in Greek) is another dynamic process which is essential for the turnover of intracellular materials such as cytoplasmic proteins and organelles to maintain cellular homeostasis (Roy et al., 2014; Marshall and Vierstra, 2018; Rodriguez et al., 2020). Autophagy is a conserved eukaryotic mechanism for cells to degrade dysfunctional or unnecessary cellular components including large protein complexes, protein and nucleic acid aggregates, lipid bodies, and even entirely damaged or superfluous organelles through double membrane compartments known as autophagosomes (Marshall and Vierstra, 2018; Wang et al., 2020b).

Autophagy was initially defined as a bulk degradation process, in which the cargoes of the autophagosomes are selected randomly. However, increasing evidences indicates the recruitment of cargoes are highly selectively and various selective autophagy pathway exist in plants (Avin-Wittenberg et al., 2018; Marshall and Vierstra, 2018; Avin-Wittenberg, 2019). The selectivity of cargoes recognitions is facilitated by autophagy receptor proteins, which possess affinities for specific cargoes and associate with the lipidated autophagy related gene 8 (ATG8)(Avin-Wittenberg et al., 2018; Avin-Wittenberg, 2019). ATG8 binds to a conserved sequence of the receptor proteins termed

Chapter 1

ATG8 interacting motif (AIM) in plants, which also known as the LC3-interacting region (LIR) in animals (Marshall and Vierstra, 2018).

The formation of the autophagosome is a complex, dynamic, and stepwise process that requires vesicle trafficking between donor and acceptor compartments, membrane expansion, and fusion, which is very likely to be regulated by the cytoskeleton (Wang et al., 2020b). AtEH/Pan1 proteins localize to the autophagosomes and interact with actin, like their yeast homologs Pan1p, localizing to ER-PM contact sites, where they play a key role in activating a novel degradation pathway (Wang et al., 2019). Overexpression of AtEH/Pan1 proteins boosts autophagosome formation, while knockdown expression of AtEH1/Pan1 results in susceptibility to nutrient depleted conditions (nitrogen and carbon) as well as a significant reduction of autophagosome formation, highlighting the essential roles of AtEHs/Pan1 proteins to drive autophagosome formation in plants under nutrient deprived conditions. Along with the involvement of AtEHs/Pan1 in this pathway, several other TPC and AP-2 subunits as well as clathrin are also implicated, as they are recruited to autophagosomes by AtEHs/Pan1 proteins upon induction of autophagy. Given that AtEHs/Pan1 proteins (AtEH1/Pan1 and AtEH2/Pan1) are likely auxiliary to the core TPC complex, suggests that they may function independently of the other TPC components (Gadeyne et al., 2014; Hirst et al., 2014). However, whether the implication of endocytic players in autophagy serves to degrade specific cargoes, whether this serves to degrade endocytic machinery (Liu et al., 2018) and whether, next to AtEH/Pan1, the whole TPC is required for this degradation pathway remains unclear. Consequently, new tools that manipulate TPC function are also required to dissect TPC function in autophagy.

In conclusion, TPC has been characterized as essential adaptor proteins during CME. The auxiliary feature of AtEHs/Pan1 to TPC determines that the recruitment machinery among TPC subunits requires being further characterized. Although AtEHs/Pan1 are involved in the novel degradation pathway at ER-PM contact site, whether this is causal to the evolutionary

Chapter 1

retention of TPC in plants is still unknown. The development of new tools interfering with TPC function, will contribute to dissect the functions of TPC involved in CME, autophagy as well as in plant development.

Chapter 1

References

Adamowski, M., Narasimhan, M., Kania, U., Glanc, M., De Jaeger, G., and Friml, J. (2018). A Functional Study of AUXILIN-LIKE1 and 2, Two Putative Clathrin Uncoating Factors in Arabidopsis. *Plant Cell* **30**: 700-716.

Aguet, F., Antonescu, C.N., Mettlen, M., Schmid, S.L., and Danuser, G. (2013). Advances in analysis of low signal-to-noise images link dynamin and AP2 to the functions of an endocytic checkpoint. *Dev Cell* **26**: 279-291.

Antonescu, C.N., Aguet, F., Danuser, G., and Schmid, S.L. (2011). Phosphatidylinositol-(4,5)-bisphosphate regulates clathrin-coated pit initiation, stabilization, and size. *Mol Biol Cell* **22**: 2588-2600.

Avin-Wittenberg, T. (2019). Autophagy and its role in plant abiotic stress management. *Plant Cell Environ* **42**: 1045-1053.

Avin-Wittenberg, T., et al. (2018). Autophagy-related approaches for improving nutrient use efficiency and crop yield protection. *J Exp Bot* **69**: 1335-1353.

Backues, S.K., Korasick, D.A., Heese, A., and Bednarek, S.Y. (2010). The Arabidopsis dynamin-related protein2 family is essential for gametophyte development. *Plant Cell* **22**: 3218-3231.

Banbury, A.N., Oakley, J.D., Sessions, R.B., and Banting, G. (2003). Tyrphostin A23 inhibits internalization of the transferrin receptor by perturbing the interaction between tyrosine motifs and the medium chain subunit of the AP-2 adaptor complex. *J. Biol. Chem.* **278**: 12022-12028.

Barberon, M., Zelazny, E., Robert, S., Conejero, G., Curie, C., Friml, J., and Vert, G. (2011). Monoubiquitin-dependent endocytosis of the iron-regulated transporter 1 (IRT1) transporter controls iron uptake in plants. *Proc Natl Acad Sci U S A* **108**: E450-458.

Bashline, L., Li, S., Zhu, X., and Gu, Y. (2015). The TWD40-2 protein and the AP2 complex cooperate in the clathrin-mediated endocytosis of cellulose synthase to regulate cellulose biosynthesis. *Proc Natl Acad Sci U S A* **112**: 12870-12875.

Bashline, L., Li, S., Anderson, C.T., Lei, L., and Gu, Y. (2013). The endocytosis of cellulose synthase in Arabidopsis is dependent on mu2, a clathrin-mediated endocytosis adaptin. *Plant Physiol* **163**: 150-160.

Bitsikas, V., Correa, I.R., Jr., and Nichols, B.J. (2014). Clathrin-independent pathways do not contribute significantly to endocytic flux. *eLife* **3**: e03970.

Bleckmann, A., Weidtkamp-Peters, S., Seidel, C.A., and Simon, R. (2010). Stem cell signaling in Arabidopsis requires CRN to localize CLV2 to the plasma membrane. *Plant Physiol* **152**: 166-176.

Cocucci, E., Aguet, F., Boulant, S., and Kirchhausen, T. (2012). The first five seconds in the life of a clathrin-coated pit. *Cell* **150**: 495-507.

Chapter 1

Collings, D.A., Gebbie, L.K., Howles, P.A., Hurley, U.A., Birch, R.J., Cork, A.H., Hocart, C.H., Arioli, T., and Williamson, R.E. (2008). Arabidopsis dynamin-like protein DRP1A: a null mutant with widespread defects in endocytosis, cellulose synthesis, cytokinesis, and cell expansion. *J Exp Bot* **59**: 361-376.

Collins, B.M., McCoy, A.J., Kent, H.M., Evans, P.R., and Owen, D.J. (2002). Molecular architecture and functional model of the endocytic AP2 complex. *Cell* **109**: 523-535.

Compeer, E.B., et al. (2018). A mobile endocytic network connects clathrin-independent receptor endocytosis to recycling and promotes T cell activation. *Nat Commun* **9**: 1597.

Dejonghe, W., et al. (2019). Disruption of endocytosis through chemical inhibition of clathrin heavy chain function. *Nat Chem Biol* **15**: 641-649.

Dejonghe, W., et al. (2016). Mitochondrial uncouplers inhibit clathrin-mediated endocytosis largely through cytoplasmic acidification. *Nat Commun* **7**: 11710.

Dhonukshe, P., Aniento, F., Hwang, I., Robinson, D.G., Mravec, J., Stierhof, Y.D., and Friml, J. (2007). Clathrin-mediated constitutive endocytosis of PIN auxin efflux carriers in Arabidopsis. *Curr Biol* **17**: 520-527.

Di Rubbo, S., et al. (2013). The clathrin adaptor complex AP-2 mediates endocytosis of brassinosteroid insensitive1 in Arabidopsis. *Plant Cell* **25**: 2986-2997.

Doherty, G.J., and McMahon, H.T. (2009). Mechanisms of endocytosis. *Annu Rev Biochem* **78**: 857-902.

Du, Y., Tejos, R., Beck, M., Himschoot, E., Li, H., Robatzek, S., Vanneste, S., and Friml, J. (2013). Salicylic acid interferes with clathrin-mediated endocytic protein trafficking. *Proc Natl Acad Sci U S A* **110**: 7946-7951.

Fan, L., Hao, H., Xue, Y., Zhang, L., Song, K., Ding, Z., Botella, M.A., Wang, H., and Lin, J. (2013). Dynamic analysis of Arabidopsis AP2 sigma subunit reveals a key role in clathrin-mediated endocytosis and plant development. *Development* **140**: 3826-3837.

Fujimoto, M., Arimura, S., Ueda, T., Takanashi, H., Hayashi, Y., Nakano, A., and Tsutsumi, N. (2010). Arabidopsis dynamin-related proteins DRP2B and DRP1A participate together in clathrin-coated vesicle formation during endocytosis. *Proc Natl Acad Sci U S A* **107**: 6094-6099.

Gadeyne, A., et al. (2014). The TPLATE adaptor complex drives clathrin-mediated endocytosis in plants. *Cell* **156**: 691-704.

Gu, M., Liu, Q., Watanabe, S., Sun, L., Hollopeter, G., Grant, B.D., and Jorgensen, E.M. (2013). AP2 hemicomplexes contribute independently to synaptic vesicle endocytosis. *eLife* **2**: e00190.

Henne, W.M., Boucrot, E., Meinecke, M., Evergren, E., Vallis, Y., Mittal, R., and McMahon, H.T. (2010). FCHO proteins are nucleators of clathrin-mediated endocytosis. *Science* **328**: 1281-1284.

Chapter 1

- Heuser, J.** (1980). Three-dimensional visualization of coated vesicle formation in fibroblasts. *J Cell Biol* **84**: 560-583.
- Hirst, J., Schlacht, A., Norcott, J.P., Traynor, D., Bloomfield, G., Antrobus, R., Kay, R.R., Dacks, J.B., and Robinson, M.S.** (2014). Characterization of TSET, an ancient and widespread membrane trafficking complex. *eLife* **3**: e02866.
- Hollopeter, G., Lange, J.J., Zhang, Y., Vu, T.N., Gu, M., Ailion, M., Lambie, E.J., Slaughter, B.D., Unruh, J.R., Florens, L., and Jorgensen, E.M.** (2014). The membrane-associated proteins FCHo and SGIP are allosteric activators of the AP2 clathrin adaptor complex. *eLife* **3**.
- Honing, S., Ricotta, D., Krauss, M., Spate, K., Spolaore, B., Motley, A., Robinson, M., Robinson, C., Haucke, V., and Owen, D.J.** (2005). Phosphatidylinositol-(4,5)-bisphosphate regulates sorting signal recognition by the clathrin-associated adaptor complex AP2. *Mol Cell* **18**: 519-531.
- Irani, N.G., et al.** (2012). Fluorescent castasterone reveals BRI1 signaling from the plasma membrane. *Nat Chem Biol* **8**: 583-589.
- Ito, E., Fujimoto, M., Ebine, K., Uemura, T., Ueda, T., and Nakano, A.** (2012). Dynamic behavior of clathrin in *Arabidopsis thaliana* unveiled by live imaging. *Plant J* **69**: 204-216.
- Jackson, L.P., Kelly, B.T., McCoy, A.J., Gaffry, T., James, L.C., Collins, B.M., Honing, S., Evans, P.R., and Owen, D.J.** (2010). A large-scale conformational change couples membrane recruitment to cargo binding in the AP2 clathrin adaptor complex. *Cell* **141**: 1220-1229.
- Jaqaman, K., Loerke, D., Mettlen, M., Kuwata, H., Grinstein, S., Schmid, S.L., and Danuser, G.** (2008). Robust single-particle tracking in live-cell time-lapse sequences. *Nat Methods* **5**: 695-702.
- Johnson, A., and Vert, G.** (2017). Single Event Resolution of Plant Plasma Membrane Protein Endocytosis by TIRF Microscopy. *Front Plant Sci* **8**: 612.
- Kadlecova, Z., Spielman, S.J., Loerke, D., Mohanakrishnan, A., Reed, D.K., and Schmid, S.L.** (2017). Regulation of clathrin-mediated endocytosis by hierarchical allosteric activation of AP2. *J Cell Biol* **216**: 167-179.
- Kaksonen, M., and Roux, A.** (2018). Mechanisms of clathrin-mediated endocytosis. *Nat Rev Mol Cell Biol* **19**: 313-326.
- Kasai, K., Takano, J., Miwa, K., Toyoda, A., and Fujiwara, T.** (2011). High boron-induced ubiquitination regulates vacuolar sorting of the BOR1 borate transporter in *Arabidopsis thaliana*. *J Biol Chem* **286**: 6175-6183.
- Kim, S.Y., Xu, Z.Y., Song, K., Kim, D.H., Kang, H., Reichardt, I., Sohn, E.J., Friml, J., Juergens, G., and Hwang, I.** (2013). Adaptor protein complex 2-mediated endocytosis is crucial for male reproductive organ development in *Arabidopsis*. *Plant Cell* **25**: 2970-2985.
- Kitakura, S., Vanneste, S., Robert, S., Lofke, C., Teichmann, T., Tanaka, H., and Friml, J.** (2011). Clathrin mediates endocytosis and polar distribution of PIN auxin transporters in *Arabidopsis*. *Plant Cell* **23**: 1920-1931.

Chapter 1

- Konopka, C.A., and Bednarek, S.Y.** (2008a). Comparison of the dynamics and functional redundancy of the Arabidopsis dynamin-related isoforms DRP1A and DRP1C during plant development. *Plant Physiol* **147**: 1590-1602.
- Konopka, C.A., and Bednarek, S.Y.** (2008b). Variable-angle epifluorescence microscopy: a new way to look at protein dynamics in the plant cell cortex. *Plant J* **53**: 186-196.
- Konopka, C.A., Backues, S.K., and Bednarek, S.Y.** (2008). Dynamics of Arabidopsis dynamin-related protein 1C and a clathrin light chain at the plasma membrane. *Plant Cell* **20**: 1363-1380.
- Kukulski, W., Schorb, M., Kaksonen, M., and Briggs, J.A.** (2012). Plasma membrane reshaping during endocytosis is revealed by time-resolved electron tomography. *Cell* **150**: 508-520.
- Kukulski, W., Schorb, M., Welsch, S., Picco, A., Kaksonen, M., and Briggs, J.A.** (2011). Correlated fluorescence and 3D electron microscopy with high sensitivity and spatial precision. *J Cell Biol* **192**: 111-119.
- Li, R., Liu, P., Wan, Y., Chen, T., Wang, Q., Mettbach, U., Baluska, F., Samaj, J., Fang, X., Lucas, W.J., and Lin, J.** (2012). A membrane microdomain-associated protein, Arabidopsis Flot1, is involved in a clathrin-independent endocytic pathway and is required for seedling development. *Plant Cell* **24**: 2105-2122.
- Liu, C., Shen, W., Yang, C., Zeng, L., and Gao, C.** (2018). Knowns and unknowns of plasma membrane protein degradation in plants. *Plant Sci* **272**: 55-61.
- Lu, R., Drubin, D.G., and Sun, Y.** (2016). Clathrin-mediated endocytosis in budding yeast at a glance. *J Cell Sci* **129**: 1531-1536.
- Macia, E., Ehrlich, M., Massol, R., Boucrot, E., Brunner, C., and Kirchhausen, T.** (2006). Dynasore, a cell-permeable inhibitor of dynamin. *Dev Cell* **10**: 839-850.
- Marshall, R.S., and Vierstra, R.D.** (2018). Autophagy: The Master of Bulk and Selective Recycling. *Annu Rev Plant Biol* **69**: 173-208.
- Mayers, J.R., Wang, L., Pramanik, J., Johnson, A., Sarkeshik, A., Wang, Y., Saengsawang, W., Yates, J.R., 3rd, and Audhya, A.** (2013). Regulation of ubiquitin-dependent cargo sorting by multiple endocytic adaptors at the plasma membrane. *Proc Natl Acad Sci U S A* **110**: 11857-11862.
- Mbengue M, B.G., Gervasi F, Beck M, Zhou J, Spallek T, Bartels S, Boller T, Ueda T, Kuhn H, Robatzek S.** (2016). Clathrin-dependent endocytosis is required for immunity mediated by pattern recognition receptor kinases. *Proc Natl Acad Sci USA* **113**: 11034-11039.
- McFarlane, H.E., Doring, A., and Persson, S.** (2014). The cell biology of cellulose synthesis. *Annu Rev Plant Biol* **65**: 69-94.
- McMahon, H.T., and Boucrot, E.** (2011). Molecular mechanism and physiological functions of clathrin-mediated endocytosis. *Nat Rev Mol Cell Biol* **12**: 517-533.

Chapter 1

Merrifield, C.J., and Kaksonen, M. (2014). Endocytic accessory factors and regulation of clathrin-mediated endocytosis. *Cold Spring Harb Perspect Biol* **6**: a016733.

Mersey, B.G., Griffing, L.R., Rennie, P.J., and Fowke, L.C. (1985). The isolation of coated vesicles from protoplasts of soybean. *Planta* **163**: 317-327.

Mettlen, M., Chen, P.H., Srinivasan, S., Danuser, G., and Schmid, S.L. (2018). Regulation of Clathrin-Mediated Endocytosis. *Annu Rev Biochem* **87**: 871-896.

Mitsunari, T., Nakatsu, F., Shioda, N., Love, P.E., Grinberg, A., Bonifacino, J.S., and Ohno, H. (2005). Clathrin adaptor AP-2 is essential for early embryonal development. *Mol Cell Biol* **25**: 9318-9323.

Mosesso, N., Blaske, T., Nagel, M.K., Laumann, M., and Isono, E. (2018). Preparation of Clathrin-Coated Vesicles From *Arabidopsis thaliana* Seedlings. *Front Plant Sci* **9**: 1972.

Narasimhan, M., Johnson, A., Prizak, R., Kaufmann, W.A., Tan, S., Casillas-Perez, B., and Friml, J. (2020). Evolutionarily unique mechanistic framework of clathrin-mediated endocytosis in plants. *eLife* **9**.

Olusanya O, A.P., Swedlow JR, Smythe E. . (2001). Phosphorylation of threonine 156 of the mu2 subunit of the AP2 complex is essential for endocytosis in vitro and in vivo. *Curr Biol* **11**.

Ortiz-Morea, F.A., et al. (2016). Danger-associated peptide signaling in *Arabidopsis* requires clathrin. *Proc Natl Acad Sci U S A* **113**: 11028-11033.

Paez Valencia, J., Goodman, K., and Otegui, M.S. (2016). Endocytosis and Endosomal Trafficking in Plants. *Annu Rev Plant Biol* **67**: 309-335.

Pascolutti, R., et al. (2019). Molecularly Distinct Clathrin-Coated Pits Differentially Impact EGFR Fate and Signaling. *Cell Rep* **27**: 3049-3061 e3046.

Pearse, B.M. (1976). Clathrin: a unique protein associated with intracellular transfer of membrane by coated vesicles. *Proc Natl Acad Sci U S A* **73**: 1255-1259.

Persson, S., Paredez, A., Carroll, A., Palsdottir, H., Doblin, M., Poindexter, P., Khitrov, N., Auer, M., and Somerville, C.R. (2007). Genetic evidence for three unique components in primary cell-wall cellulose synthase complexes in *Arabidopsis*. *Proc Natl Acad Sci U S A* **104**: 15566-15571.

Picco, A., and Kaksonen, M. (2018). Quantitative imaging of clathrin-mediated endocytosis. *Curr Opin Cell Biol* **53**: 105-110.

Reynolds, G.D., August, B., and Bednarek, S.Y. (2014). Preparation of enriched plant clathrin-coated vesicles by differential and density gradient centrifugation. *Methods Mol Biol* **1209**: 163-177.

Reynolds, G.D., Wang, C., Pan, J., and Bednarek, S.Y. (2018). Inroads into Internalization: Five Years of Endocytic Exploration. *Plant Physiol* **176**: 208-218.

Robinson, M.S. (2015). Forty Years of Clathrin-coated Vesicles. *Traffic* **16**: 1210-1238.

Chapter 1

Rodriguez, E., et al. (2020). Autophagy mediates temporary reprogramming and dedifferentiation in plant somatic cells. *EMBO J* **39**: e103315.

Roth, T.F., and Porter, K.R. (1964). Yolk Protein Uptake in the Oocyte of the Mosquito *Aedes Aegypti*. *L. J Cell Biol* **20**: 313-332.

Roy, R., Floyd, B.E., and Bassham, D.C. (2014). Autophagy and Endocytosis. *Cell Biology*: 1-26.

Sanchez-Rodriguez, C., et al. (2018). The Cellulose Synthases Are Cargo of the TPLATE Adaptor Complex. *Mol Plant* **11**: 346-349.

Schmid, S.L. (2017). Reciprocal regulation of signaling and endocytosis: Implications for the evolving cancer cell. *J Cell Biol* **216**: 2623-2632.

Schwihla, M., and Korbei, B. (2020). The Beginning of the End: Initial Steps in the Degradation of Plasma Membrane Proteins. *Front Plant Sci* **11**: 680.

Sharfman, M., Bar, M., Ehrlich, M., Schuster, S., Melech-Bonfil, S., Ezer, R., Sessa, G., and Avni, A. (2011). Endosomal signaling of the tomato leucine-rich repeat receptor-like protein LeEix2. *Plant J* **68**: 413-423.

Smith, J.M., Salamango, D.J., Leslie, M.E., Collins, C.A., and Heese, A. (2014a). Sensitivity to Flg22 is modulated by ligand-induced degradation and de novo synthesis of the endogenous flagellin-receptor FLAGELLIN-SENSING2. *Plant Physiol* **164**: 440-454.

Smith, J.M., Leslie, M.E., Robinson, S.J., Korasick, D.A., Zhang, T., Backues, S.K., Cornish, P.V., Koo, A.J., Bednarek, S.Y., and Heese, A. (2014b). Loss of *Arabidopsis thaliana* Dynamin-Related Protein 2B reveals separation of innate immune signaling pathways. *PLoS Pathog* **10**: e1004578.

Taylor, N.G. (2011). A role for *Arabidopsis* dynamin related proteins DRP2A/B in endocytosis; DRP2 function is essential for plant growth. *Plant Mol Biol* **76**: 117-129.

Tinevez, J.Y., Perry, N., Schindelin, J., Hoopes, G.M., Reynolds, G.D., Laplantine, E., Bednarek, S.Y., Shorte, S.L., and Eliceiri, K.W. (2017). TrackMate: An open and extensible platform for single-particle tracking. *Methods* **115**: 80-90.

Traub, L.M. (2009). Tickets to ride: selecting cargo for clathrin-regulated internalization. *Nat Rev Mol Cell Biol* **10**: 583-596.

Van Damme, D., Coutuer, S., De Rycke, R., Bouget, F.Y., Inze, D., and Geelen, D. (2006). Somatic cytokinesis and pollen maturation in *Arabidopsis* depend on TPLATE, which has domains similar to coat proteins. *Plant Cell* **18**: 3502-3518.

Van Damme, D., Gadeyne, A., Vanstraelen, M., Inze, D., Van Montagu, M.C., De Jaeger, G., Russinova, E., and Geelen, D. (2011). Adaptin-like protein TPLATE and clathrin recruitment during plant somatic cytokinesis occurs via two distinct pathways. *Proc Natl Acad Sci U S A* **108**: 615-620.

Chapter 1

von Kleist, L., et al. (2011). Role of the clathrin terminal domain in regulating coated pit dynamics revealed by small molecule inhibition. *Cell* **146**: 471-484.

Wang, C., Yan, X., Chen, Q., Jiang, N., Fu, W., Ma, B., Liu, J., Li, C., Bednarek, S.Y., and Pan, J. (2013). Clathrin light chains regulate clathrin-mediated trafficking, auxin signaling, and development in Arabidopsis. *Plant Cell* **25**: 499-516.

Wang, C., et al. (2016). Differential Regulation of Clathrin and Its Adaptor Proteins during Membrane Recruitment for Endocytosis. *Plant Physiol* **171**: 215-229.

Wang, J., Mylle, E., Johnson, A., Besbrugge, N., De Jaeger, G., Friml, J., Pleskot, R., and Van Damme, D. (2020a). High Temporal Resolution Reveals Simultaneous Plasma Membrane Recruitment of TPLATE Complex Subunits. *Plant Physiol* **183**: 986-997.

Wang, L., Xue, Y., Xing, J., Song, K., and Lin, J. (2018). Exploring the Spatiotemporal Organization of Membrane Proteins in Living Plant Cells. *Annu Rev Plant Biol* **69**: 525-551.

Wang, P., Gao, E., and Hussey, P.J. (2020b). Autophagosome Biogenesis in Plants: An Actin Cytoskeleton Perspective. *Trends Plant Sci* **25**: 850-858.

Wang, P., et al. (2019). Plant AtEH/Pan1 proteins drive autophagosome formation at ER-PM contact sites with actin and endocytic machinery. *Nat Commun* **10**: 5132.

Wrobel, A.G., et al. (2019). Temporal Ordering in Endocytic Clathrin-Coated Vesicle Formation via AP2 Phosphorylation. *Dev Cell* **50**: 494-508 e411.

Yamaoka, S., Shimono, Y., Shirakawa, M., Fukao, Y., Kawase, T., Hatsugai, N., Tamura, K., Shimada, T., and Hara-Nishimura, I. (2013). Identification and dynamics of Arabidopsis adaptor protein-2 complex and its involvement in floral organ development. *Plant Cell* **25**: 2958-2969.

Yoshinari, A., Fujimoto, M., Ueda, T., Inada, N., Naito, S., and Takano, J. (2016). DRP1-Dependent Endocytosis is Essential for Polar Localization and Boron-Induced Degradation of the Borate Transporter BOR1 in Arabidopsis thaliana. *Plant Cell Physiol* **57**: 1985-2000.

Yoshinari, A., Hosokawa, T., Amano, T., Beier, M.P., Kunieda, T., Shimada, T., Hara-Nishimura, I., Naito, S., and Takano, J. (2019). Polar Localization of the Borate Exporter BOR1 Requires AP2-Dependent Endocytosis. *Plant Physiol* **179**: 1569-1580.

Yu, Q., Zhang, Y., Wang, J., Yan, X., Wang, C., Xu, J., and Pan, J. (2016). Clathrin-Mediated Auxin Efflux and Maxima Regulate Hypocotyl Hook Formation and Light-Stimulated Hook Opening in Arabidopsis. *Mol Plant* **9**: 101-112.

Zhang, Y., Persson, S., Hirst, J., Robinson, M.S., van Damme, D., and Sanchez-Rodriguez, C. (2015). Change your TPLATE, change your fate: plant CME and beyond. *Trends Plant Sci* **20**: 41-48.

Zhou, J., et al. (2018). Regulation of Arabidopsis brassinosteroid receptor BRI1 endocytosis and degradation by plant U-box PUB12/PUB13-mediated ubiquitination. *Proc Natl Acad Sci U S A* **115**: E1906-E1915.

Chapter 1

Zoncu, R., Perera, R.M., Sebastian, R., Nakatsu, F., Chen, H., Balla, T., Ayala, G., Toomre, D., and De Camilli, P.V. (2007). Loss of endocytic clathrin-coated pits upon acute depletion of phosphatidylinositol 4,5-bisphosphate. *Proc Natl Acad Sci U S A* **104**: 3793-3798.

Chapter Two

High temporal resolution reveals simultaneous plasma membrane recruitment of the TPLATE complex subunits

Jie Wang^{1,2}, Evelien Mylle^{1,2}, Alexander Johnson³, Nienke Besbrugge^{1,2},
Geert De Jaeger^{1,2}, Jiří Friml³, Roman Pleskot^{1,2}, Daniel Van Damme^{1,2,*}

¹Ghent University, Department of Plant Biotechnology and Bioinformatics,
Technologiepark 71, 9052 Ghent, Belgium

²VIB Center for Plant Systems Biology, Technologiepark 71, 9052 Ghent,
Belgium

³Institute of Science and Technology Austria, 3400 Klosterneuburg, Austria

This chapter was published in *Plant Physiology* (DOI:10.1104/pp.20.00178)

* Corresponding author: Daniel.VanDamme@psb.vib-ugent.be

Author Contributions: JW, EM, AJ and NB designed and performed experiments and/or generated material. JW, EM, AJ, GDJ, JF, RP and DVD designed experiments, analyzed data and discussed results. JW, RP and DVD wrote the initial draft of the manuscript. AJ, GDJ, JF, RP and DVD contributed to finalizing the paper.

Abstract

The TPLATE complex (TPC) is a key endocytic adaptor protein complex in plants. TPC contains six evolutionary conserved subunits and two plant specific subunits, AtEH1/Pan1 and AtEH2/Pan1, although cytoplasmic proteins, are not associated with the hexameric subcomplex in the cytoplasm. To investigate the dynamic assembly of the octameric TPC at the plasma membrane (PM), we performed state-of-the-art dual-color live cell imaging at physiological and a lowered temperature. Our data show that lowering the temperature slows down endocytosis and thereby enhances the temporal resolution of the differential recruitment of endocytic components. Under both normal and lowered temperature conditions, the core TPC subunit TPLATE, and the AtEH/Pan1 proteins, exhibited simultaneous recruitment at the PM. These results, together with our co-localization analysis of different TPC subunits, allow us to conclude that in plant cells, TPC is not recruited to the PM sequentially but as an octameric complex.

Introduction

Clathrin-mediated endocytosis (CME) is the best-studied endocytic pathway in eukaryotes to internalize plasma membrane (PM) proteins and extracellular materials, commonly termed “cargo”, into cells (Dhonukshe et al., 2007; Robert et al., 2010; Kitakura et al., 2011; Bitsikas et al., 2014). The formation of clathrin-coated vesicles (CCVs) requires several highly coordinated stages: initiation, cargo selection, coat assembly, scission and vesicle uncoating (McMahon and Boucrot, 2011). Though the initiation of CME at the PM remains poorly understood in plants, similarly to other systems, adaptor proteins are presumed to recognize cargo proteins via cargo-recognition motifs and subsequently recruit clathrin triskelia through clathrin-binding motifs (Zhang et al., 2015). As clathrin does not bind directly to the PM nor to the cargo proteins, adaptor proteins thus play an essential role to link the PM and the clathrin cage (McMahon and Boucrot, 2011).

Two early-arriving adaptor protein complexes function at the PM in plants; the heterotetrameric Adaptor Protein-2 complex (AP-2) and the octameric TPLATE complex (TPC). AP-2 comprises of two large (AP2A and AP2B or α and β), one medium (AP2M or μ) and one small subunit (AP2S or σ) (Di Rubbo et al., 2013). TPC contains eight components; six that can be traced back to the Last Eukaryotic Common Ancestor: TPLATE, TML, TASH3, LOLITA, TWD40-1, TWD40-2, and two components, AtEH1/Pan1 and AtEH2/Pan1, which are plant-specific TPC subunits (Gadeyne et al., 2014; Hirst et al., 2014). AP-2 function is important for somatic plant development as single *Arabidopsis ap-2* mutants display developmental defects, yet still result in viable plants (Di Rubbo et al., 2013; Fan et al., 2013; Kim et al., 2013; Yamaoka et al., 2013). The TPC is essential for both pollen and somatic plant development as knockout, or knockdown, of single subunits of TPC in *Arabidopsis* leads to pollen or seedling lethality respectively (Van Damme et al., 2006; Gadeyne et al., 2014).

Chapter 2

TPC is an evolutionary ancient protein complex that has been so far experimentally characterized only in plants and in an amoeba, *Dictyostelium discoideum* (Gadeyne et al., 2014; Hirst et al., 2014). TPC in plants was identified as an octameric complex by tandem affinity purification (TAP) experiments (Gadeyne et al., 2014). Recently, we also identified an important role for the AtEH/Pan1 proteins in actin-regulated autophagy and in recruiting several components of the endocytic machinery to the AtEH/Pan1 positive autophagosomes (Gadeyne et al., 2014; Wang et al., 2019). TPC in *Dictyostelium* (described as TSET) was however identified as a hexameric complex lacking the AtEH/Pan1 homologs (Hirst et al., 2014). Although Amoebozoa contain homologous proteins to AtEH/Pan1, these resemble more closely Ede1 than Pan1 (Gadeyne et al., 2014; Wang et al., 2019).

Truncation of the TML subunit of TPC forces the complex into the cytoplasm and this correlates with the dissociation of AtEH/Pan1 proteins from the complex (Gadeyne et al., 2014). It therefore appears that TPC composition depends on its localization and that the two AtEH/Pan1 subunits might be peripherally associated with a hexameric subcomplex of TPC, which would resemble to TSET in *Dictyostelium*. To investigate whether there is a differential order of recruitment between both AtEH/Pan1 proteins and the remaining hexameric subcomplex, we performed dual color time-lapse microscopy of CME in etiolated *Arabidopsis* epidermal hypocotyl cells. We also took advantage of lowering the temperature of our samples to slow down CME and thereby increase the temporal resolution. Altogether, our data strongly suggest that TPC is recruited as the octameric complex to the PM, where it functions as the early adaptor complex for plant CME.

Results

Lowering the experimental temperature reduces CME kinetics

TPC is proposed to serve as an early adaptor complex (Gadeyne et al., 2014), however temporal resolution remains the biggest challenge to monitor the dynamic recruitment of different endocytic protein players (Fujimoto et al., 2010; Fan et al., 2013; Gadeyne et al., 2014; Bashline et al., 2015). As lowering the temperature generally slows down dynamics of cellular processes (Das et al., 1966), we hypothesized that by lowering the temperature, we could also slow down dynamics of endocytic events and therefore enhance the temporal visualization of the differential recruitment of the endocytic players at the PM.

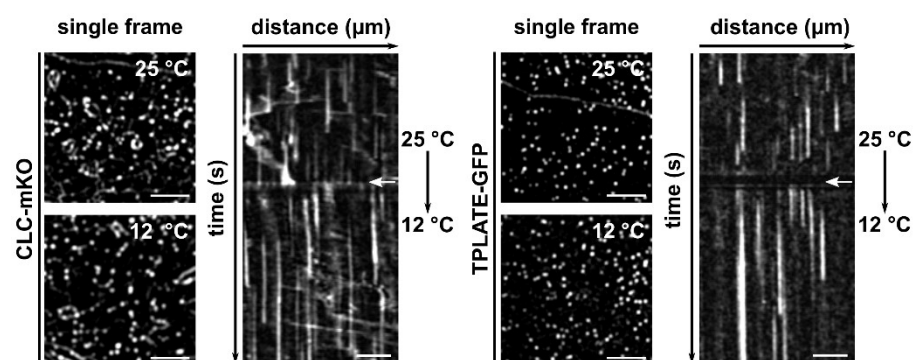


Figure 1. Endocytic dynamics alter immediately upon lowering the temperature.

Spinning disc images and representative kymographs showing endocytic foci and lifetimes of CLC2 (left) or TPLATE (right) in *Arabidopsis* etiolated hypocotyl epidermal cells at different temperatures. Cells were imaged at 25 °C for 2 minutes and then imaged at 12 °C for an additional 3 minutes. Images were acquired with a 1-second interval. White arrows on the kymographs indicate the position of the temperature shift. Scale bars of spinning disc images, 5 µm. Scale bars of kymographs, 30 µm. Time, 300s.

To time how intracellular dynamics respond to decreasing the temperature in plant cells, we firstly imaged *Arabidopsis* plants expressing the microtubule (MT) binding protein EB1a-GFP (Van Damme et al., 2004). Hypocotyl cells of *Arabidopsis* seedlings expressing EB1a-GFP were imaged at 20 °C for 5 min, then the temperature was lowered to 10 °C with the aid of the CherryTemp

Heater Cooler system and the effect on microtubule polymerization rate was assessed. Lowering the temperature had an immediate effect on the MT polymerization speed, measured as EB1a labeled tracks in time-projection images (Fig. S1 A). Visualization and quantification of the MT growth dynamics further confirmed that the temperature shift was transmitted to the seedling almost instantaneously (Fig. S1).

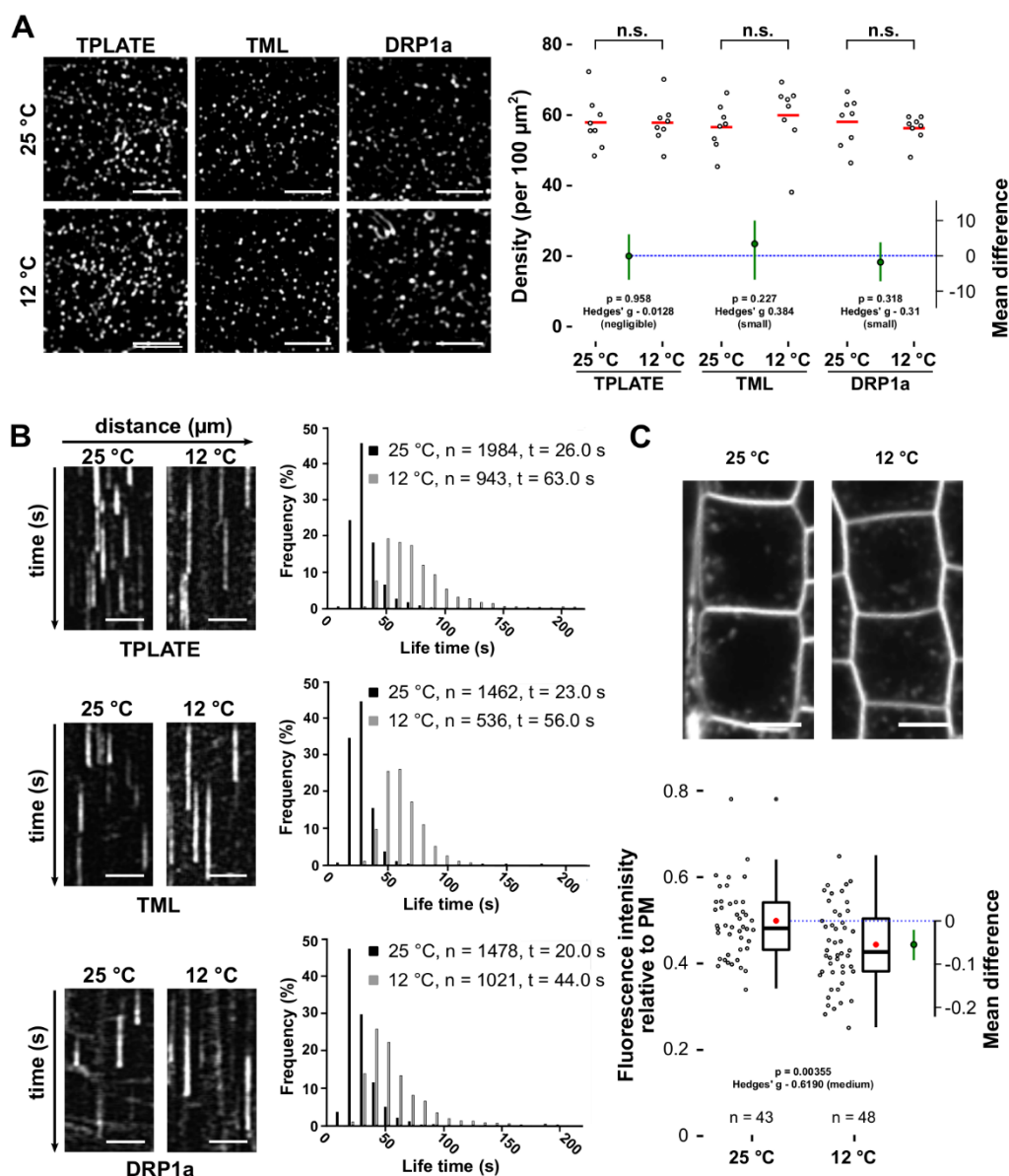


Figure 2. Lowering the temperature slows down CME.

(A) Spinning disk images and density quantification of TPLATE, TML and DRP1a-marked foci in epidermal hypocotyl cells at the permissive (25 degrees) and restrictive (12 degrees) temperature. The density of the foci is independent of the tested temperatures (n.s. not

Chapter 2

significant, Mann-Whitney U-test). The mean difference with the bootstrap 95% confidential interval (green circle and green line) is shown as a part of the plot. Hedges' g value is a standardized effect size indicating how much two groups differ from each other. For each transgenic line, 8 cells from 8 seedlings were imaged at both temperatures. Scale bars, 5 μm .

(B) Representative kymographs and histograms showing the life-time distribution of TPLATE, TML and DRP1a positive foci at both temperatures. Scale bars, 25 μm . Time, 120 s. Number of events (n) and mean lifetime \pm standard error (t) are indicated.

(C) Representative confocal images and Jitter and box plot quantification showing internalization of the FM4-64 dye (4 μM , 30mins) in Col-0 root epidermal cells at both temperatures. The red circle represents the mean. The p-value was calculated by the Welch two sample T-test. The mean difference with the bootstrap 95% confidential interval (green circle and green line) is shown on the right side of the plot. Hedges' g value is a standardized effect size. n represents the number of measurements (n = 43 cells for 25 $^{\circ}\text{C}$ and n = 48 cells for 12 $^{\circ}\text{C}$) from 11 individual roots respectively. Scale bar, 10 μm .

To examine the capacity of lowering the temperature to slow down endocytosis, etiolated hypocotyl cells expressing endocytic markers CLC2-mKO and TPLATE-GFP the temperature was shifted during image acquisition and no obvious defect in the recruitment was observed. Density analysis of early-arriving (TPLATE and TML) as well as late arriving DRP1A furthermore showed that lowering the temperature did not visually affect the PM recruitment of these endocytic markers while it prolonged their lifetime at the PM instantly (Fig. 1 and Fig. 2A).

To further evaluate how lowering the temperature affects the dynamic behavior of endocytic proteins, we carefully measured the dynamics of TPLATE, TML and DRP1a at different temperatures. Kymograph and histogram analysis of measured lifetimes confirmed that lowering the temperature from 25 to 10 $^{\circ}\text{C}$ correlated with a gradual increase in lifetime of endocytic proteins at the PM (Fig. S2). For TPLATE and TML, we observed a strong increase in average lifetime between 15 and 12 $^{\circ}\text{C}$. Therefore, we selected 25 $^{\circ}\text{C}$ and 12 $^{\circ}\text{C}$ as the two temperatures for our future experiments, the fold change in the mean lifetime for each studied protein between these two temperatures is around 2.2. Visualizing the individual lifetimes of the three markers at both temperatures in

a histogram showed a clear shift of the distribution to longer lifetimes (Fig. 2B) and this correlated with a significant reduction in the internalization of the styryl dye FM4-64, which is used as a proxy for endocytic flux (Van Damme et al., 2011; Bashline et al., 2013; Fan et al., 2013; Gadeyne et al., 2014; Dejonghe et al., 2016; Dejonghe et al., 2019) (Fig. 2C). Furthermore, photo-bleaching experiments showed a dramatic reduction in the recovery of endocytic foci at PM at the low temperature, in agreement with reduced dynamics of the process (Fig. S3). These results together, show that lowering the temperature using our experimental setup slows down CME efficiently and rapidly.

Lowering the temperature enhances the temporal resolution of plasma membrane recruitment.

Having established the effect of lowering the temperature on endocytic dynamics in *Arabidopsis* cells, we then examined whether we would be able to enhance the temporal difference between an early (TPLATE) player and a late one (DRP1A). We therefore generated a dual marker line of TPLATE-GFP (Van Damme et al., 2006) and DRP1a-mRFP (Mravec et al., 2011) and compared their temporal behavior at both temperatures. When imaged at 25 °C, the time-lapse images and kymographs showed multiple independent events where TPLATE-GFP foci clearly appeared earlier than DRP1a-mRFP at the PM, while they disappeared together (Fig. 3A, B and Fig. S4). Lowering the temperature prolonged the lifetime of both TPLATE-GFP and DRP1a-mRFP (the fold change in the mean lifetime is around 2.2, Fig. 3A-B), whereas their departure remained synchronized. Overall, the temporal difference between their PM recruitment was dramatically enhanced (Fig. 3A, B and Fig. S4), which resulted in a very significant mean difference of the paired lifetimes (Hedge's g value of -1.271, Fig. 3C).

Chapter 2

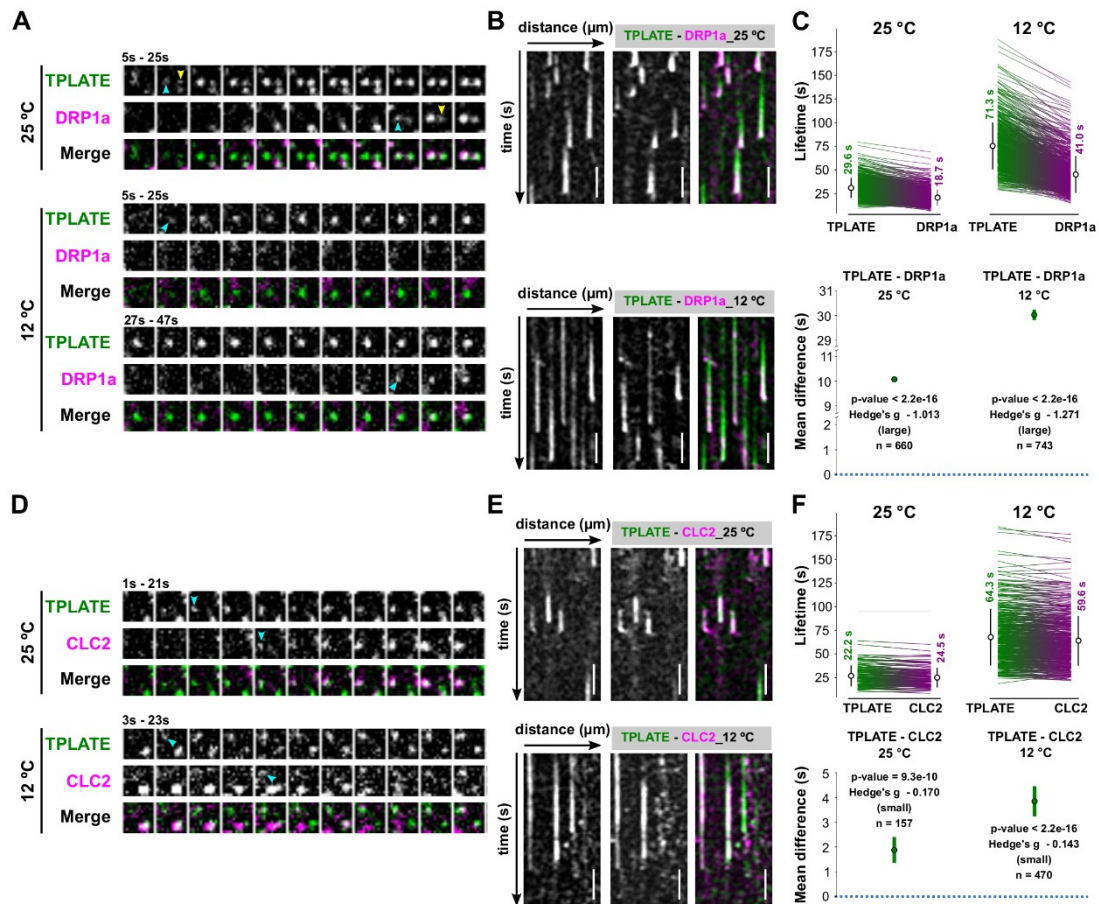


Figure 3. Lowering the temperature enhances the temporal resolution of plasma membrane recruitment.

(A and D) Representative time series of dual-color spinning disk movies (2s/f) showing the sequential recruitment between TPLATE and DRP1a or CLC2 at the different temperatures. Arrowheads mark the appearance of TPLATE or DRP1a and CLC2 at PM.

(B and E) Representative kymographs displaying the differential recruitment between TPLATE and DRP1a or CLC2 at different temperatures. Scale bar, 25 μm. Time, 120s.

(C and F) Paired comparison of the lifetimes of particular protein pairs at the different temperatures. On the sides of each plot for different combinations of constructs and temperatures, each line represents an individual pair with the mean (white circle) ± SD (black line) and the number represents the mean lifetime ± standard error. The p-value was calculated using the Wilcoxon Signed Rank test. The green circle in the bottom graph represents the paired mean difference with the bootstrap 95% confidential interval (green line). Hedges' g value is a standardized effect size indicating how much two groups differ from each other. n represents the number of events.

Chapter 2

We performed a similar experiment comparing TPLATE and CLC2, which were previously shown only to have minor differences in their PM recruitment (Gadeyne et al., 2014; Narasimhan et al., 2020). Here, we also observed a temperature-enhancing effect of their differential recruitment with TPLATE being recruited before CLC2, yet less pronounced than the difference between TPLATE and DRP1a (Fig. 3D to F and Fig. S4).

Taken together, these results show that lowering the temperature slows down dynamics of endocytosis as well as enhances the temporal resolution of recruitment of the endocytic proteins at the PM.

TPLATE is closely associated with the AtEH/Pan1 proteins at the plasma membrane

The absence of AtEH1/Pan1 and AtEH2/Pan1 as subunits of TSET (Hirst et al., 2014), together with the observation that inducing mislocalization of TPC to the cytoplasm leads to loss of those two subunits from the complex (Gadeyne et al., 2014) and the observation that AtEH/Pan1 proteins have a specific role in promoting autophagy (Wang et al., 2019), suggest that TPC could be in essence a hexameric complex, which temporarily gains two additional subunits. To reveal the temporal relationship among the TPC subunits, we visualized their dynamic behavior at the PM using multiple dual-color labeled lines. To evaluate the functional association of TPC subunits at PM, we crossed complemented mutant lines of core subunits (TPLATE, TML and TWD40-1) and generated double complemented homozygous mutant lines. We also combined complemented mutants of the core subunit TPLATE with AtEH1/Pan1 or AtEH2/Pan1 and generated the respective double complemented, double homozygous mutant lines. As a first indication for differential recruitment, we monitored the steady-state percentage of co-localization between the markers using an average projection of five consecutive frames. Comparing an early endocytosis marker such as TPLATE,

with a late marker such as DRP1A revealed that the differential arrival between those markers leads to a substantial non-colocalizing fraction (roughly 40%, Fig. 4A).

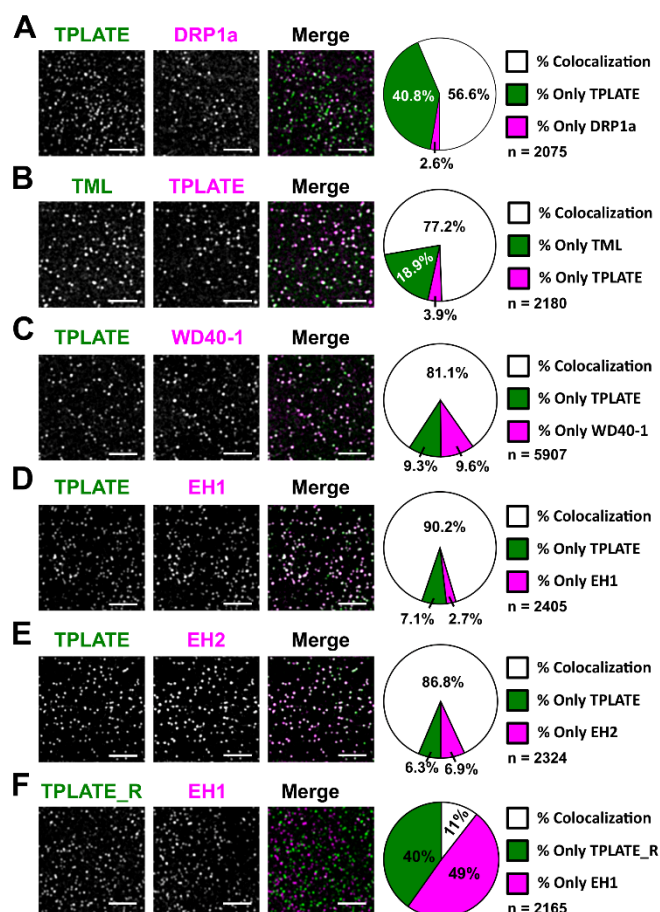


Figure 4. Colocalization analysis hints at a tight association between core and peripheral TPC subunits at the PM.

Representative spinning disk dual-color images and corresponding pie charts displaying the percentage of colocalization of dual-labeled endocytic foci. TPLATE was compared to a late endocytic marker, DRP1a (A), to both TML (B) and TWD40-1 (C), and to both AtEHs/Pan1 (D, E). A quality check for the used algorithm was performed by comparing rotated TPLATE (90° rotation; TPLATE_R) to AtEH1/Pan1 to control for random association of foci (F). Scale bars, 5 μ m. Z-projections of five consecutive frames with average intensity were used for quantification. Quantification (%) of colocalization as calculated using the DIANA algorithm. The high percentage of overlap between TPLATE and the AtEH/Pan1 proteins suggests a tight connection between those proteins at the plasma membrane.

Chapter 2

Combining TPLATE-TagRFP with TML-GFP resulted in around 77% of total foci where TML and TPLATE overlapped (Fig. 4B). We also tested functional association when combining TPLATE-GFP with a TWD40-1-mRuby3 complemented line (Fig. S5 and Table 1). Similarly, as for TML and TPLATE, combining TPLATE-GFP and TWD40-1-mRuby3 resulted in a very high percentage of colocalizing foci (Fig. 4C), confirming their intrinsic behavior as part of the same complex.

In *Arabidopsis* seedlings, AtEH1/Pan1 and AtEH2/Pan1 have so far been shown functionally associated with TPLATE at autophagosomes and to be delivered to the vacuole after carbon starvation and Conc A treatment (Wang et al., 2019). To address the recruitment of AtEH/Pan1 and TPLATE in endocytic foci at the PM, we combined AtEH/Pan1 with TPLATE in their respective complemented mutant backgrounds. Similar to the combination of the core subunits, both AtEH1/Pan1-mRuby3 and AtEH2/Pan1-mRuby3 showed a very high degree of colocalization with TPLATE-GFP at the PM (Fig. 4D and E). To exclude the possibility that TPLATE and AtEH/Pan1 foci overlapped due to the high density of endocytic foci, we performed a quality check of the algorithm used by comparing the colocalization percentage between TPLATE and AtEH1/Pan1 on images where the TPLATE channel was rotated 90 degrees. This rotation resulted in only around 10% of foci colocalizing (Fig. 5F), confirming that the observed high degree of colocalization is not random. These results also suggest a tight association between TPLATE and the AtEH/Pan1 proteins at the PM.

AtEHs/Pan1 and the core TPC subunits are simultaneously recruited to the PM

To further investigate TPC assembly at the PM at the level of the different subunits, we compared the recruitment and disassociation behavior among pairs of TPC subunits at 25 and 12 °C. As a benchmark, we compared the

Chapter 2

behavior of two closely related TPC subunits, TPLATE and TML, which by homology to other adaptor complexes are presumed to be part of the core of TPC.

Time-lapse imaging and kymograph analyses showed that dual-labeled TML-GFP and TPLATE-TagRFP foci appear and disappear simultaneously at the PM when imaged at 25 °C (Fig. 5A, 5B and S6). Lowering the temperature maintained this simultaneous appearing and disappearing behavior. However, there were very small changes in average lifetime, which were found to be negligible by their effect size (expressed as the Hedge's *g* value). These small changes could be explained by there being more signal noise and differential bleaching effects of the fluorophores during the image acquisition at the lower temperature conditions (Fig. 5A-5C and S6).

We next compared the PM appearance and disappearance behavior of AtEH/Pan1 and TPLATE. Similar to the recruitment behavior of TPLATE and TML foci, when imaged at 25 °C, both AtEH1/Pan1 and AtEH2/Pan1 foci simultaneously appeared and disappeared with TPLATE at the PM (Fig. 5D-5E, 5G-5H and S7). Lowering the temperature did not alter the simultaneous recruitment of TPLATE and AtEH/Pan1, and the respective Hedge's value remained very low (Fig. 5D-5I and S7). These results, together with our colocalization analysis, strongly suggest that AtEH/Pan1 subunits are simultaneously recruited to, and maintained, at PM with the other TPC subunits.

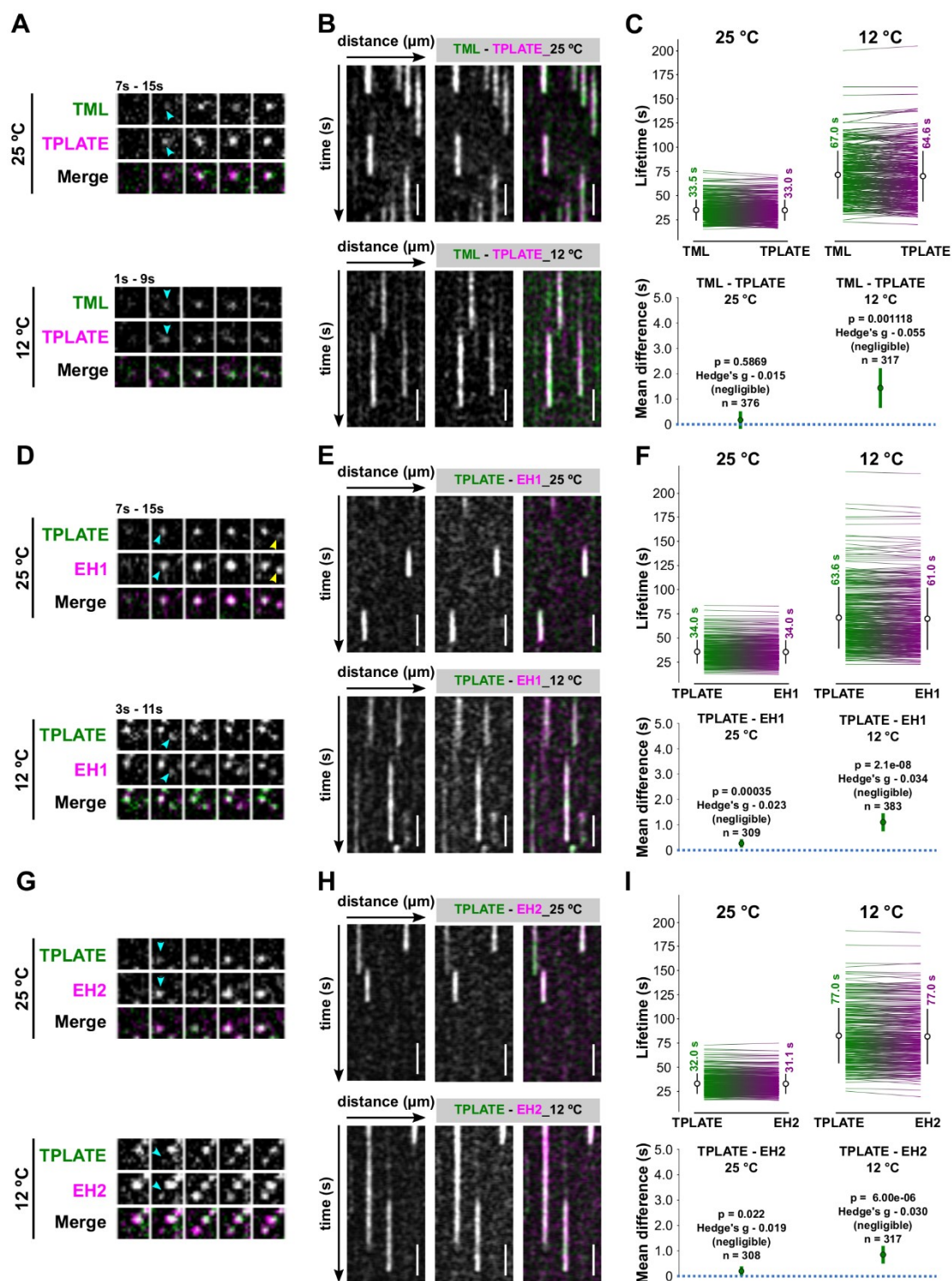


Figure 5. The AtEHs/Pan1 and the core TPC subunits are simultaneously recruited to the PM.

(A, D and G) Representative time series of dual-color spinning disk movies (2s/f) showing the recruitment between TPLATE and TML, EH1/Pan1 and EH2/Pan1 at different temperatures. Arrows mark the appearance of TPLATE or TML, EH1/Pan1 and EH2/Pan1 on the PM. (B, E and H) Representative kymographs displaying the recruitment of TPLATE versus TML, EH1/Pan1 and EH2/Pan1 at different temperatures. Scale bar, 25 μm . Time, 120s.

Chapter 2

(C, F and I) Paired comparison of the life-times of particular protein pairs at different temperatures. Each line on the sides of each plot represents an individual pair with the mean (white circle) \pm SD (black line) for different combinations of constructs and temperatures. Each number on the sides of each plot represent the mean lifetime \pm standard error. The p-value was calculated by the Wilcoxon Signed Rank test. The green circle in the bottom graph represents the paired mean difference with the bootstrap 95% confidential interval (green line). Hedges' g value is a standardized effect size indicating how much two groups differ from each other. n represents the number of events.

Discussion

Clathrin-mediated endocytosis is a highly dynamic process. It is best understood in mammalian and yeast model systems while little is known in plants. Although very fast endocytic events were observed in neurons (Balaji and Ryan, 2007), in yeast or cultured animal cells, the whole endocytic process takes up to minutes and the physiological role and precise temporal dynamics of endocytic proteins are well defined (Taylor et al., 2011; Lu et al., 2016; Ma et al., 2016; Picco and Kaksonen, 2018; Pascolutti et al., 2019; Wrobel et al., 2019). In plant cells, the endocytic process is much more dynamic, with larger clathrin cages being formed than those in yeast in shorter time periods (Narasimhan et al., 2020), which brings about more technical difficulties in monitoring the temporal recruitment of the diverse endocytic players (Zhang et al., 2015). To better understand the dynamics of endocytosis in plant cells, new approaches are required, which should provide us with enhanced temporal resolution.

Here, we report that lowering the temperature using a microfluidics-based on-slide approach can be used as a rapid and efficient tool to slow down intracellular dynamic processes in plant cells similar to earlier reports demonstrating temperature effects on endocytosis and synaptic vesicle recycling in animal cells (Pyott and Rosenmund, 2002; Bui and Glavinovic, 2014). The effect on microtubule growth rate was immediate and the

Chapter 2

dampening effect on the dynamic of endocytosis, as measured by the dwell time at the PM of several markers, FM-uptake as well as measuring recruitment by FRAP correlated with the reduction in temperature. Lowering the temperature however had no significant effect on the density of endocytic foci, suggesting that cargo proteins could still be adequately recognized.

Our data also show that the temporal resolution of the differential recruitment of endocytic players could be enhanced at lower temperatures, which was most apparent between early and late arriving endocytic proteins. Lowering the temperature also enabled us to slightly enhance the temporal difference between two early arriving proteins, TPLATE and CLC2, indicating that our approach worked. Given the temperature effect on the dynamics of plant processes, awareness should be increased to perform live-cell imaging in plants under accurate temperature control. No doubt this will substantially increase the robustness and reproducibility of future image data collection.

The TPC is an evolutionary ancient adaptor complex, which was not retained in yeast or animal cells (Hirst et al., 2014). It is proposed to function as an adaptor complex during CME and has been shown to be recruited to the PM earlier than Dynamin-related proteins while only slightly earlier than clathrin (Gadeyne et al., 2014; Narasimhan et al., 2020). *Dictyostelium discoideum* contains a similar complex, which however lacks the AtEH/Pan1 proteins and in contrast to TPC, TSET is not essential (Gadeyne et al., 2014; Hirst et al., 2014). These AtEH/Pan1 proteins both share their male sterility phenotype with the other TPC subunits (Van Damme et al., 2006; Gadeyne et al., 2014; Wang et al., 2019), they are dynamically recruited to the PM (Gadeyne et al., 2014; Wang et al., 2019), associated with the other TPC subunits as well as AP-2, but not when TPC is forced into the cytoplasm using proteomic manipulations (Gadeyne et al., 2014) and functionally associated with several endocytic players during autophagy (Wang et al., 2019). Here we investigated how these AtEH/Pan1 proteins are recruited to the PM in relation to the other TPC subunits. Our live-cell analysis could not identify any deviation in recruitment dynamics

Chapter 2

between AtEH/Pan1 and TPLATE, mirroring the results observed between the other core subunits TPLATE and TML. The small differences reported could be attributed to technical issues, including differential bleaching effects of fluorophores. The close association, as well as the simultaneous recruitment between TPLATE and AtEH/Pan1 labeled endocytic foci at the PM, therefore allow us to hypothesize that TPC is recruited to the PM as an octameric complex in plants. When combining TPLATE-TagRFP with TML-GFP, we observed unexpectedly high percentage of TML recruitment to PM without TPLATE (Fig. 4B). As this occurs in a double mutant double complemented background, we interpret this recruitment as independent of TPLATE and by extension, as independent of the complex. Under this hypothesis, and in agreement with the cytoplasmic localization of the complex containing a truncated TML(Gadeyne et al., 2014), this subunit likely plays a role in PM recruitment of TPC.

Altering the temperature will likely affect many plant processes, such as cytoskeleton dynamics, phosphoinositide production/conversion or membrane fluidity. However, our conclusions on the simultaneous recruitment of the various TPC subunits are independent of these temperature effects. Under normal conditions, there is a difference in recruitment between TPLATE and DRP1a or clathrin (Gadeyne et al., 2014; Narasimhan et al., 2020). Here, we describe that this difference increases upon lowering the temperature. We did not observe any significant differences between TPLATE and AtEH/Pan1 proteins, at either temperature, although this all happens in the same context of altered cytoskeleton, lipid conversion or membrane fluidity. The lack of statistical difference in the density of endocytic foci at 12°C or 25 °C indicates that effects on membrane fluidity, phosphoinositide levels and saturation degree of lipid acyl chains in our setup and are not majorly affected within the time-window that we use.

In plants, lifetimes of endocytic proteins are measured using time-lapse imaging of cells expressing fluorescent labeled proteins imaged via spinning

Chapter 2

disk microscopy (Bashline et al., 2013; Gadeyne et al., 2014; Bashline et al., 2015; Dejonghe et al., 2016; Zhou et al., 2018; Dejonghe et al., 2019) or total internal reflection fluorescence microscopy (TIRF) or variable angle epifluorescence microscopy (VAEM) (Konopka et al., 2008; Konopka and Bednarek, 2008b, a; Ito et al., 2012; Johnson and Vert, 2017; Narasimhan et al., 2020). Based on earlier work in the animal field (Jaqaman et al., 2008; Aguet et al., 2013; Compeer et al., 2018; Pascolutti et al., 2019; Wrobel et al., 2019), automated image analysis tools have recently been employed to analyze CME images unbiasedly and rapidly (Johnson and Vert, 2017; Narasimhan et al., 2020). Accurate detection of endocytic events requires high signal-to-noise ratio (SNR) images, a quality which is determined by multiple factors such as the susceptibility of the fluorophore to bleaching and the expression level of the fluorescent reporter and close-to-endogenous levels of fluorescent labeled endocytic proteins often failed to provide sufficient SNR for accurate lifetime measurements (Aguet et al., 2013). Here, we aimed at visualizing the recruitment dynamics of various TPC subunits at the PM. In order to avoid competition with endogenous subunits and to avoid over-expression effects such as induction of autophagy (Wang et al., 2019), we opted to work with double-labeled endocytic proteins in either single or double complemented *tpc* mutant background rather than use overexpression lines. Although our approach represents the optimal strategy from a biological perspective, our transgenic lines, especially those fused with red fluorescent proteins, and combined with extended imaging times under low temperature conditions failed to generate sufficient SNR images for automatic quantification. Actually, the only combination which yielded acceptable data when automatically quantified was our TPLATE-DRP1A combination, as the DRP1A is actually 35S-driven. We therefore generated kymographs of our dual-color endocytic spinning disc movies and measured the dwell-times of the proteins manually. We aimed at measuring several hundred events per experiment and combined measurements of independent persons to achieve an unbiased assessment of

Chapter 2

the data. We were unable to identify any recruitment of AtEH/Pan1 proteins at the PM which was independent of another TPC subunit. Our findings therefore show that the TPLATE adaptor protein complex is likely recruited to the PM as an octameric unit, both at normal and at lowered temperature conditions. We can however not exclude the possibility that the differential recruitment between the individual TPC subunits are too dynamic to monitor under our limiting, one-second temporal resolution, conditions. However, due to the fact that we were able to detect differences in the CLC2 and TPLATE dynamics, which are of the order of a few seconds, we hypothesize that TPC is recruited as an octameric unit at the PM during CME. The continuous development of novel microscopy as well as labeling techniques will help to overcome our current limitations of working with low-expressing functional fusions and will allow us to understand how endocytosis in plants is executed at high spatiotemporal resolution.

Materials and Methods

Molecular cloning

To yield the expression construct for TWD40-1, entry clones of TWD40-1 without a stop codon in pDONR221 (Gadeyne et al., 2014) were combined with pB7m34GW (Karimi et al., 2007), pDONRP4-P1R-Histone3p (Ingouff et al., 2017), and pDONRP2-P3R-mRuby3 (Wang et al., 2019) in a triple gateway LR reaction (Invitrogen) to generate pH3::TWD40-1-mRuby3. To yield a red fluorophore-tagged TPLATE, TPLATE without stop in pDONR207 (Van Damme et al., 2006) was combined with the Lat52 promoter in pDONRP4P1R (Van Damme et al., 2006), with TagRFP in pDONRP2P3R (Mylle et al., 2013) and with pH7m34GW (Karimi et al., 2007) in a triple gateway LR reaction (Invitrogen) to generate pLat52::TPLATE-TagRFP.

Plant Material

The *Arabidopsis* lines expressing EB1a-GFP (Van Damme et al., 2004), LAT52p::TPLATE-GFP (Van Damme et al., 2006; Gadeyne et al., 2014), TMLp::TML-GFP (Gadeyne et al., 2014), 35Sp::DRP1a-mRFP (Mravec et al., 2011) and 35Sp::CLC2(At2g40060)-mKO (Ito et al., 2012) were previously described. The dual-color line expressing TPLATE-GFP/CLC2-tagRFP in *tplate* homozygous background was reported previously (Gadeyne et al., 2014). The dual-marker lines expressing TPLATE-GFP/AtEH1/Pan1-mRuby3 or TPLATE-GFP/AtEH2/Pan1-mRuby3 in double homozygous mutant (*tplate ateh1/pan1* or *tplate ateh2/pan1*) background were reported before (Wang et al., 2019).

To generate TWD40-1-mRuby3 complemented lines, heterozygous mutants of *twd40-1-1* (Gadeyne et al., 2014) were transformed with pH3.3::TWD40-1-mRuby3 by floral dip. The T1 plants were selected for the complementation constructs on 1/2 MS plate supplemented with 10mg/L Basta. Resistant plants were genotyped to identify those with a *twd40-1-1* heterozygous mutant background. T2 plants expressing TWD40-1-mRuby3 were tested by

Chapter 2

genotyping PCR to identify homozygous lines for the *twd40-1-1* insertion mutations. Genotyping PCR was performed on genomic DNA isolated from rosette leaves. Genotyping primers for *twd40-1-1* are described before (Gadeyne et al., 2014).

For backcross experiments, the complemented lines of TWD40-1-mRuby3 as well as the heterozygous mutant plants of *twd40-1-1* were used as male to cross with Col-0 as female. The transfer of the T-DNA, causal to the functionality of the complementing fusion, was analyzed by genotyping PCR on F1 plants.

To generate dual-marker lines of TPLATE core subunits, a complemented *tplate* lines expressing pLat52::TPLATE-tagRFP was generated by dipping *tplate*(+/-) heterozygous plants with pLat52::TPLATE-TagRFP and selecting for the transformants. Homozygous *tplate*(-/-) plants were identified in the next generations by genotyping PCR.

Homozygous *tplate* mutant plants carrying pLat52::TPLATE-TagRFP were crossed with the complemented *tml-1* line expressing pTML::TML-GFP (Gadeyne et al., 2014). The complemented *twd40-1-1* lines expressing TWD40-1-mRuby3 were crossed with the complemented *tplate* line pLat52::TPLATE-GFP, respectively. F2 plants in double homozygous mutant background (*tml-1/tplate* or *tplate/twd40-1-1*) were identified by genotyping PCR. For the dual-color TPLATE-GFP/DRP1a-mRFP lines, the complemented *tplate* lines expressing Lat52p::TPLATE-GFP were crossed with 35Sp::DRP1a-mRFP expressing lines and F2 plants in *tplate* homozygous background were identified by genotyping PCR. Genotyping primers for *tplate*, *tml-1* and *twd40-1-1* are described before (Gadeyne et al., 2014).

Temperature modulation using the CherryTemp System

The CherryTemp system (Cherrybiotech), which enables ultra-fast temperature shifts between 5 °C and 45°C was used to modulate and maintain the temperature during the spinning disk imaging (<https://www.cherrybiotech.com/heater-cooler-for-microscopy>). Prior to

Chapter 2

imaging, a single etiolated seedling was laid between two coverslips with 1/2 strength MS liquid medium and incubated with the CherryTemp Heater Cooler device for five minutes to stabilize the temperature of the seedling (<https://www.cherrybiotech.com/heater-cooler-for-microscopy/temperature-control-for-plant-microscopy>).

FM4-64 Uptake

Prior to imaging, whole 6-day-old Col_0 seedlings were incubated with 4 μ M FM4-64 (Invitrogen) solution in 1/2 strength MS liquid medium between 2 coverslips at 25 °C or 12 °C for 30 minutes.

Live-cell Imaging

A Nikon Ti microscope with the Perfect Focus System (PFSIII) for Z-drift compensation, equipped with an Ultraview spinning-disk system (PerkinElmer) and two 512x512 Hamamatsu ImagEM C9100-13 EMccd cameras was used to image endocytic dynamics. Images of hypocotyl epidermal cells of 4-day old etiolated seedlings expressing single or dual-color fluorophore labeled proteins were acquired with a 100x oil immersion objective (Plan Apo, NA = 1.45). During imaging, the CherryTemp system was used to maintain the temperature of the samples constant.

Seedlings expressing GFP fused proteins were imaged with 488nm excitation light and an emission window between 500 nm and 530 nm in single camera mode, or 500 to 550 nm in dual camera mode. Seedlings expressing mKO, mRFP and tagRFP labeled proteins were imaged with 561 nm excitation light and an emission window between 570nm and 625nm in single camera mode or 580 to 630 nm in dual camera mode. Single-marker line movies were acquired with an exposure time of 500 ms/frame. Movies of 2 minutes in total were made. Dual-color lines were acquired either sequentially (one camera mode) or simultaneously (two camera mode) with an exposure time of 500 ms/frame. Single camera mode was used for density, colocalization (TML-

Chapter 2

TPLATE, TPLATE-DRP1A) and life-time (TML-DR1AP, TML-TPLATE 25°C) measurements. Dual camera mode was used for colocalization (TPLATE-AtEH1/Pan1, TPLATE-AtEH2/Pan1, TPLATE-TWD40-1, TPLATE-TWD40-2) and lifetime (TPLATE-AtEH1/Pan1, TPLATE-AtEH2/Pan1 and TML-TPLATE 12°C) measurements. For photo-bleaching experiments, seedlings were exposed to 100% power of laser for around 2s during the imaging, using the Photokinesis unit of the PE spinning disk system.

Root meristematic epidermal cells of 6-day-old seedlings were acquired with a Zeiss 710 inverted confocal microscope with the ZEN 2009 software package and equipped with a C-Apochromat 40x water Korr M27 objective (NA 1.2). FM4-64 was visualized using 561 nm laser excitation and a 650–750 nm detection window.

Quantification of measurements

Dynamics of EB1a-GFP were analyzed using ImageJ equipped with the Trackmate (v4.0.1) plugin (Tinevez et al., 2017). We used the LoG detector with an estimated blob diameter of 10 pixels, a threshold value of 1, using the median filter and sub-pixel localization. An auto initial thresholding, followed by a Linear motion LAP tracker with as parameters a 5 pixel initial search radius, a 5 pixel search radius and a 2 frames maximum frame gap correction, were applied. Tracks with a duration of less than 10 frames were excluded and the obtained median speed per track was converted to $\mu\text{m}/\text{min}$ using the pixel size values. Outliers for the median speed were defined by the iterative Median Absolute Deviation Method (MAD) (Leys et al., 2013) and their values were excluded. Three movies coming from two different seedlings were analyzed.

The density of labeled endocytic markers was measured in Matlab 2017b using the detection and tracking parts of the of the cmeAnalysis package and further processed as described in (Johnson and Vert, 2017; Narasimhan et al., 2020). Density calculations were obtained from all the tracks within the region of interest (ROI) over certain frames of the movies, which used to produce an

Chapter 2

average density. The ROI was selected on the middle of the image. The middle frame was used as a reference and the temporal range is based on the middle frame. We used the pixel size and the area to convert this to spots per μm^2 . For each of the analyzed sample set, eight cells from eight different seedlings were analyzed.

Objects based co-localization was performed using the ImageJ plugin Distance Analysis (DiAna) (Gilles et al., 2017). Prior to analyzing with DiAna, images were processed with ImageJ. Each channel was processed with a Walking Average of 4 and then merged (also rotated if required). Region of interest were selected based on that they excluded the border of the cells and still represented a good number of objects. Z-projection images were generated of five slices with average intensity. Each channel of Z-projected images was processed using Morphological filters from the MorphoLibJ plugin (Legland et al., 2016), using the parameters white top-hat, disk element and a 2 pixels radius. A first step in the DiAna plugin is to segment the objects for each channel, which is done by selecting the 3D Spot segmentation tool of the DiAna-Segment plugin. If requested, adapt the calibration by changing the pixel size to 1.00001 for all dimensions. Both the noise and seed threshold value were obtained by averaging the maximum intensity of three regions covering only background signal. The spot was defined with a minimum value of 4 and maximum value of 36 pixels. The option to exclude objects on XY edges was activated. Default values were used for the other parameters. Results for number of total objects (Tot) or touching objects (Tou) in image A/B obtained from Diana were recorded. The colocalization ratio of objects was calculated as follows:

$$\text{only (A) \%} = (\text{Tot A} - \text{Tou A}) / ((\text{TouA} + \text{TouB}) / 2 + (\text{Tot A} - \text{Tou A}) + (\text{Tot B} - \text{Tou B})) * 100$$

$$\text{only (B) \%} = (\text{Tot B} - \text{Tou B}) / ((\text{TouA} + \text{TouB}) / 2 + (\text{Tot A} - \text{Tou A}) + (\text{Tot B} - \text{Tou B})) * 100$$

$$\text{Colocalization \%} = 100\% - \text{only (A)\%} - \text{only (B)\%}$$

Chapter 2

As a control, one of the channels was rotated 90°C (no interpolation) and analyzed similarly as described above. For each of the analyzed sample set, a minimum of six cells coming from three different seedlings were analyzed.

Lifetimes of individual endocytic events were measured from kymographs generated by the Volocity software package (PerkinElmer). To measure paired lifetimes of dual-color kymographs, individual events showing good SNR (signal-noise ratio) in both channels were marked. Following the measurement of the lifetimes of the marker in the red channel, the lifetime of the marker in the green channel was analyzed. Data was further analyzed in Excel by checking the start position of X from each line of the kymograph to avoid mistakes in pairing the red and green channel values. Calculation to time (ns) of each line was done. Outliers for the life-time differences were defined by the iterative MAD (Leys et al., 2013) and their values were excluded. For each of the analyzed sample sets, minimum 9 movies spread among minimum 3 seedlings were analyzed. Except for TPLATE-GFP/CLC2-tagRFP for which 7 movies over 3 seedlings (12°C) and 5 movies over 2 seedlings (25°C) were analyzed. To generate unbiased data, paired lifetimes of endocytic events labeled by dual-color fluorophores were measured by independent persons.

Statistical analysis

The results were analyzed with the estimation method to calculate mean, mean differences, confidence intervals, and Hedges' g (Claridge-Chang and Assam, 2016; Ho et al., 2019). 95% confidence intervals for the mean differences were calculated using bootstrap methods (re-sampled 5000 times, bias-corrected, and accelerated). Effect size was measured using Hedges' g and accordingly to the standard practise is referred as 'negligible' ($g < 0.2$), 'small' ($0.2 < g < 0.5$), 'medium' ($0.5 < g < 0.8$) or 'large' ($g > 0.8$) (Cumming, 2012). Hedges' g is a quantitative measurement for the difference between means indicating how much two groups differ from each other, if Hedges' g equals 1, the two groups differ by 1 standard deviation. R version 3.6.2 and Rstudio 1.2.5001 were used

Chapter 2

to calculate the Wilcoxon Signed Rank test (paired samples), the Mann-Whitney U-test and the Welch two sample T-test (Team, 2019). All plots and figures were generated with Rstudio 1.2.5001 and Inkscape (version 0.92, <https://inkscape.org/>).

Acknowledgements

Research in the Van Damme lab is funded by the European Research Council T-Rex project number 682436 and by the Chinese Scholarship Council (CSC) (scholarship 201508440249 to J.W.). The acquisition of the CherryTemp Heater Cooler system (Cherrybiotech) was funded by VIB Tech Watch Initiative and by the Research Foundation Flanders (research grant 1511817N to D.V.D.). A.J. is supported by funding from the Austrian Science Fund (FWF): I3630B25 to J.F.

Chapter 2

Table 1. *twd40-1-1* plants expressing C-terminal fusions of TWD40-1 with mRuby3 allow transfer of the T-DNA via the male.

The table shows the result of the analysis of back-cross experiments between Col-0 as female (♀) and the *twd40-1-1* heterozygous plants with or without expression of TWD40-1-mRuby3 as male (♂). The analysis clearly shows that the mutation blocks transfer via the male and that this block is lifted by the presence of the fluorescent fusion construct, indicating that it is functional.

Back-cross to Col-0 (♀)	# plants	T-DNA transfer via ♂
<i>twd40-1-1</i> (+/-)	12	0
<i>twd40-1-1</i> (-/-) + TWD40-1-mRuby3 ♂	12	12

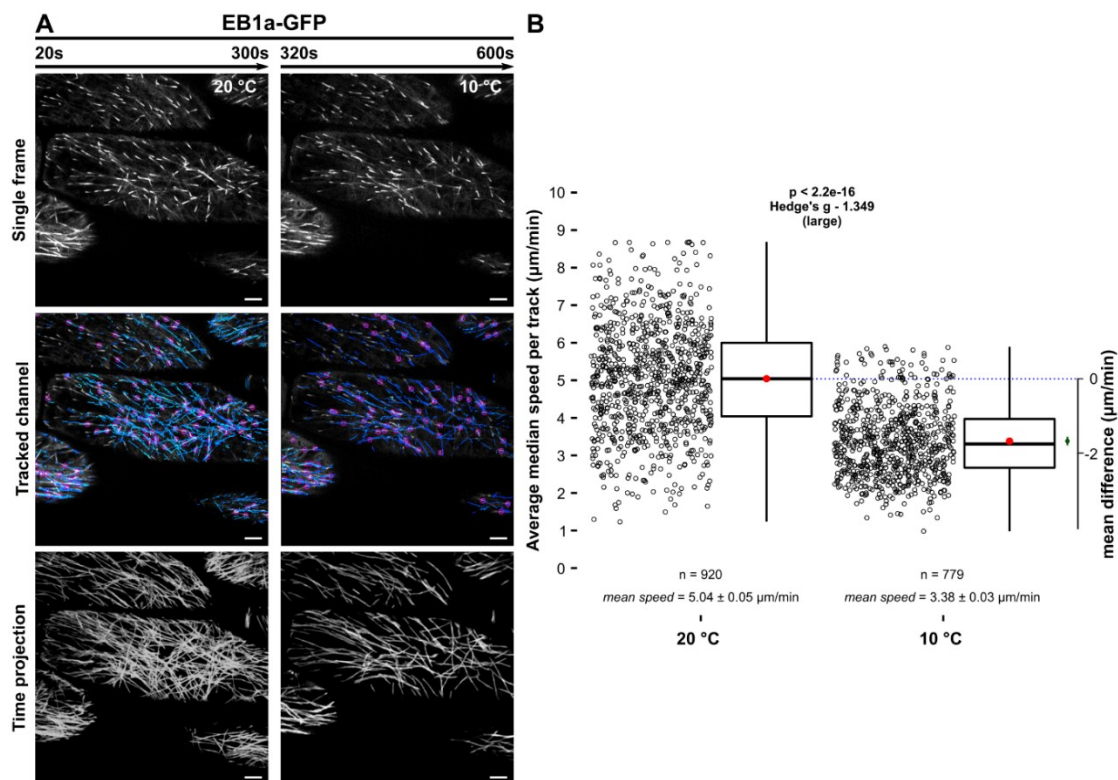


Figure S1. The CherryTemp system can be effectively used to quickly alter intracellular dynamics in plant cells.

(A) Representative spinning disk images of *Arabidopsis* hypocotyl cells expressing EB1a-GFP imaged consecutively at two temperatures using the CherryTemp system. The same cells were imaged at 10 °C for 5 minutes and then captured at 20 °C for another 5 minutes (1f/s). To quantify the microtubule dynamics, tracked channels were generated to calculate the speed of EB1a at both temperatures. Time projection max intensity images of 200 slices (200 seconds) at both temperatures show the difference in travelled distance at both temperatures. Scale bars, 5 μm .

(B) The jitter and box plot compare the average median track speed at both temperatures calculated from three independent movies. The red circle represents the mean. The p-value was calculated by the Mann-Whitney U-test. The mean difference with the bootstrap 95% confidential interval (green circle and green line) is shown on the right side of the plot. Hedges' g is a quantitative measurement for the difference between means indicating how much two groups differ from each other. n represents the number of tracks measured. The mean speed \pm standard error is presented.

Chapter 2

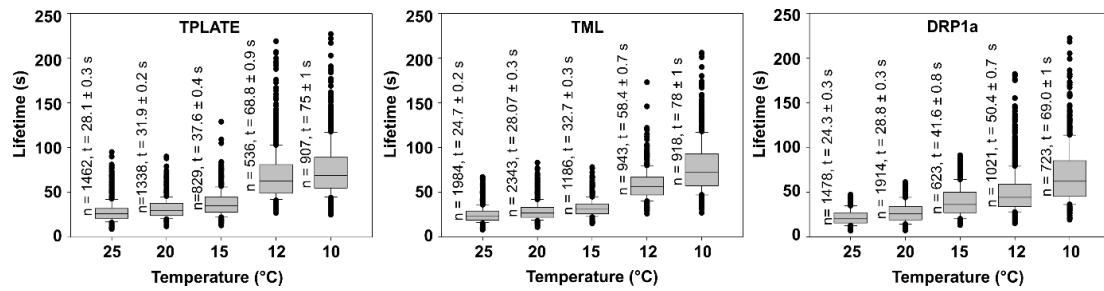


Figure S2. Lowering the temperature increases the lifetime of endocytic proteins at the plasma membrane.

Etiolated *Arabidopsis* hypocotyl epidermal cells expressing TPLATE-GFP, TML-GFP and DRP1a-mRFP were imaged at various temperatures and their individual lifetimes were quantified by kymograph analysis at each indicated temperature. The corresponding boxplot graphs show that both TPLATE, TML and DRP1a display increasing lifetimes with lowering the temperature. For each transgenic line, multiple cells from at least 3 independent seedlings at each temperature were imaged. n represents the number of tracks measured; t represents the mean lifetime \pm standard error for each construct at the given temperature.

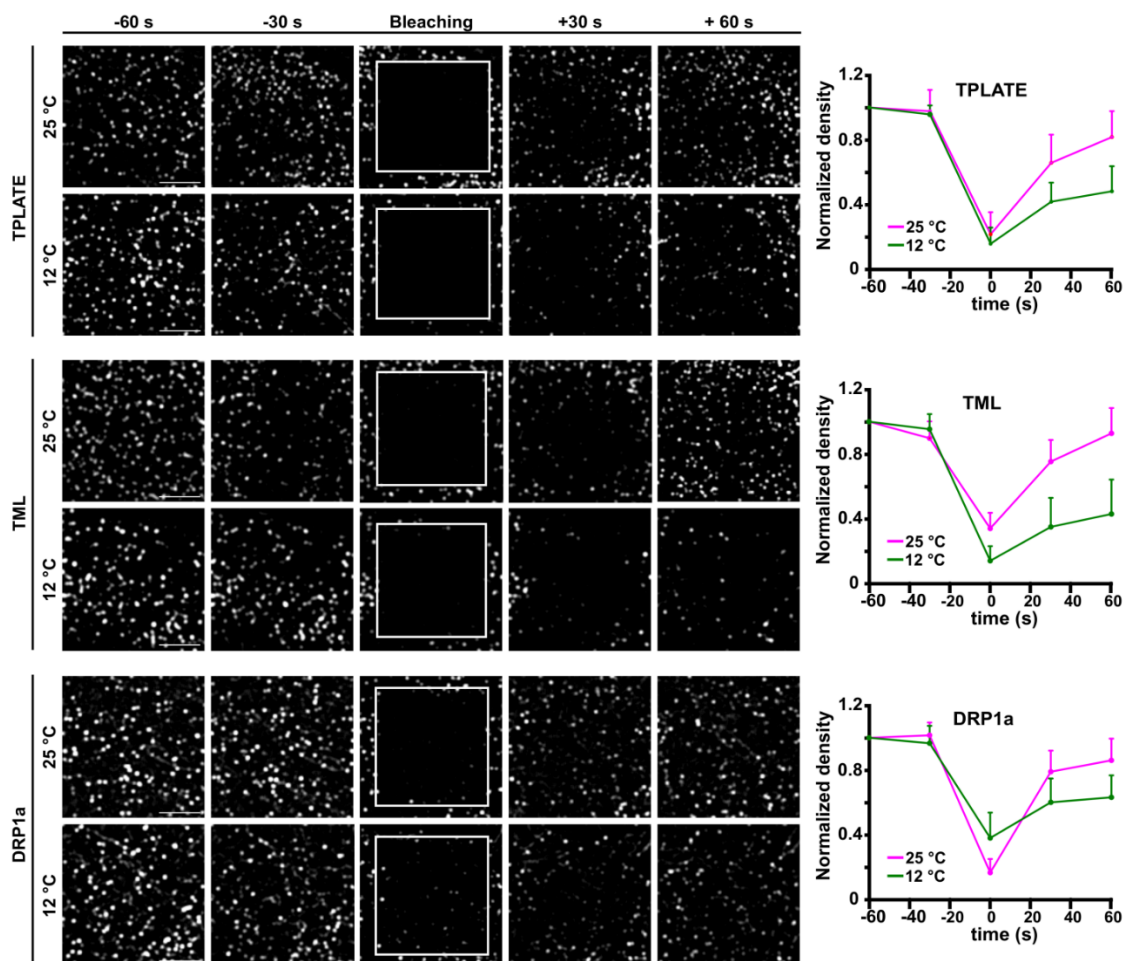


Figure S3. Lowering the temperature decreases the recruitment dynamics of the endocytic proteins.

Representative spinning disk images showing the density of labelled TPLATE, TML and DRP1a endocytic foci in etiolated *Arabidopsis* hypocotyl cells before (-) or after (+) photo bleaching at different temperatures. Scale bar, 5 μm . The density of the endocytic foci in the photo-bleached region (white box) at different time points before and after photo bleaching was quantified to yield the curves on the right. The density of each time point was normalized to the -60 s time point respectively. Number of cells, $15 \leq n \leq 22$ from at least 3 seedlings. For all three CME markers, the slope representing the increase in density after bleaching is lower at 12 °C (green) than it is at 25 °C (red), indicating that the dynamics by which the bleached proteins are exchanged at the plasma membrane are reduced at lower temperature.

Chapter 2

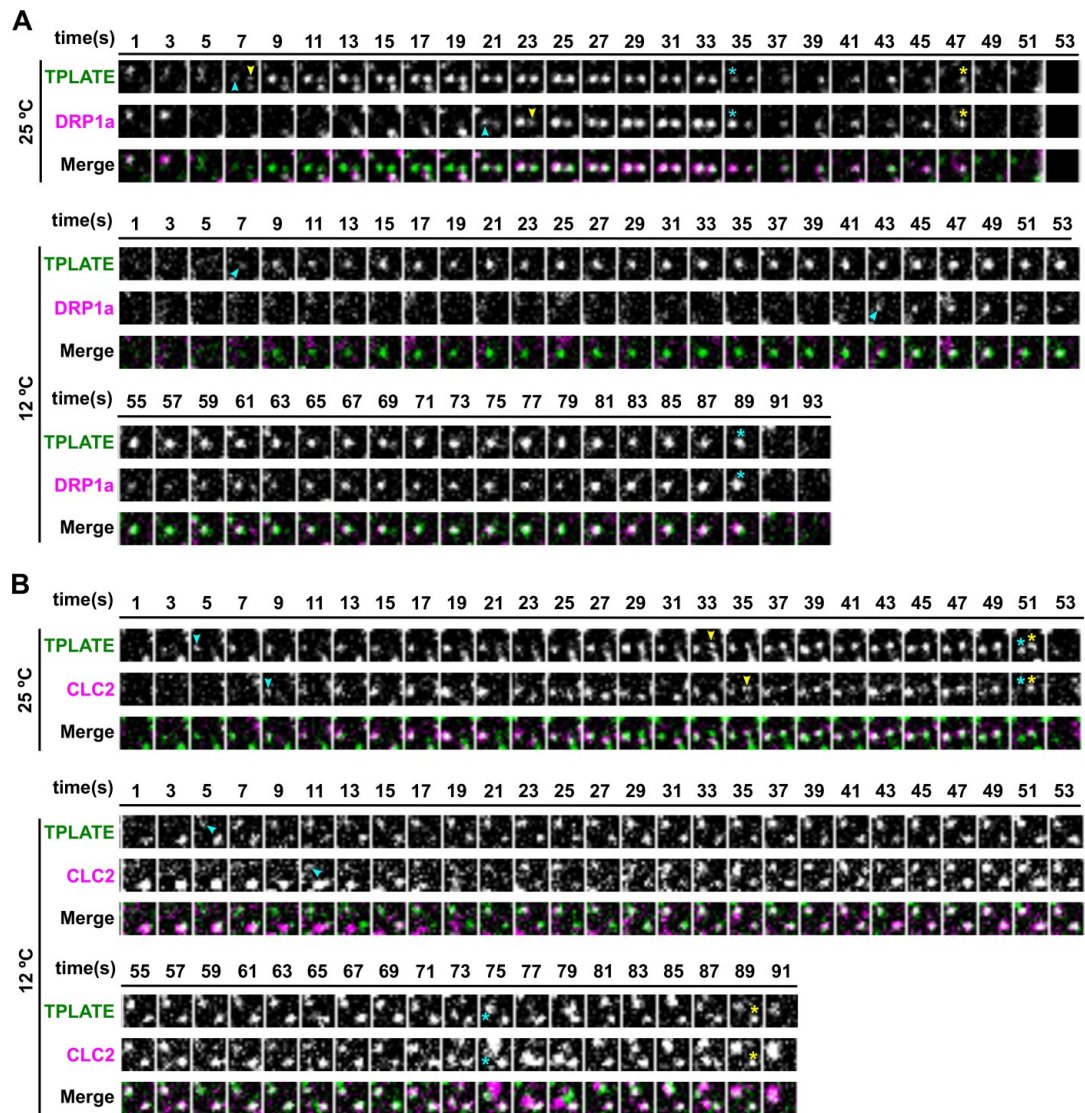


Figure S4. Lowering the temperature enhances the temporal resolution of recruitment. Time series of dual-color spinning disk movies showing the sequential recruitment between TPLATE and DRP1a (A) or CLC2 (B) at the different temperatures. Arrowheads mark the appearance and asterisks mark the disappearance of TPLATE or DRP1a and CLC2 at the PM. These image series are the extended versions of the series shown in Figure 3.

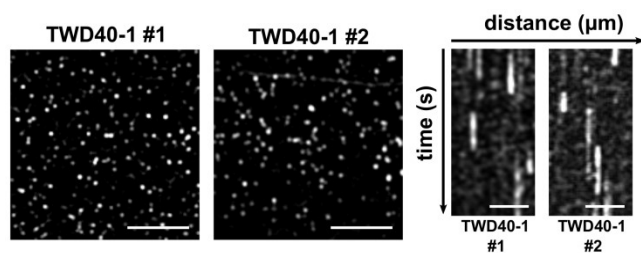


Figure S5. TWD40-1 localizes to the PM as endocytic foci.

Representative spinning disk images showing the TWD40-1 labeled endocytic foci and related kymograph in *Arabidopsis* etiolated hypocotyl cells. Scale bars of spinning discs images, 5 μm . Scale bars of kymograph, 25 μm .

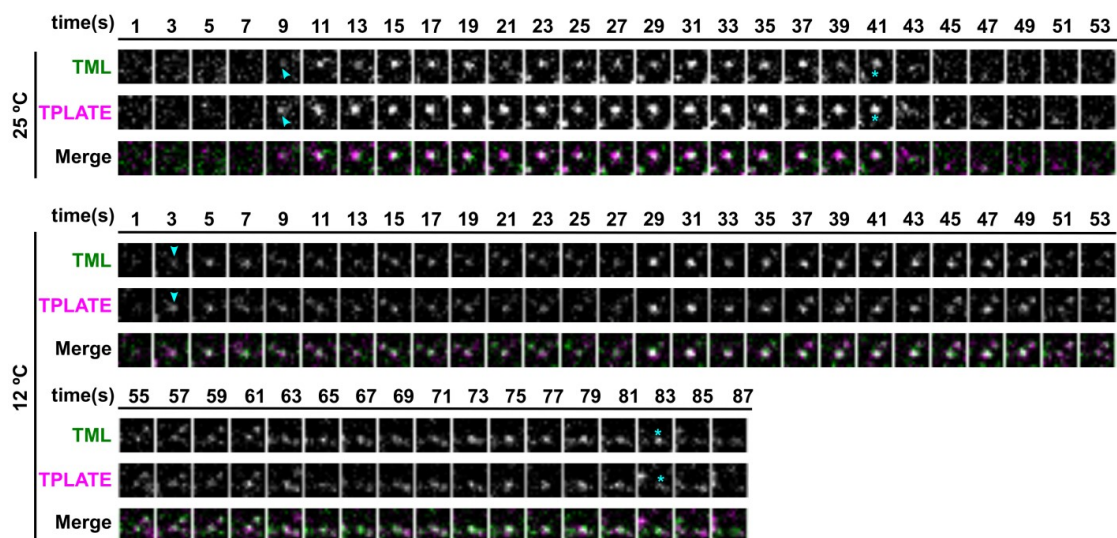


Figure S6. TPLATE and TML are recruited to the PM simultaneously.

Time series of dual-color spinning disk movies showing the simultaneous recruitment between TPLATE and TML at different temperatures. Arrowheads mark the appearance and asterisks mark the disappearance of TPLATE or TML on the PM. These image series are the extended versions of the series shown in Figure 5.

Chapter 2

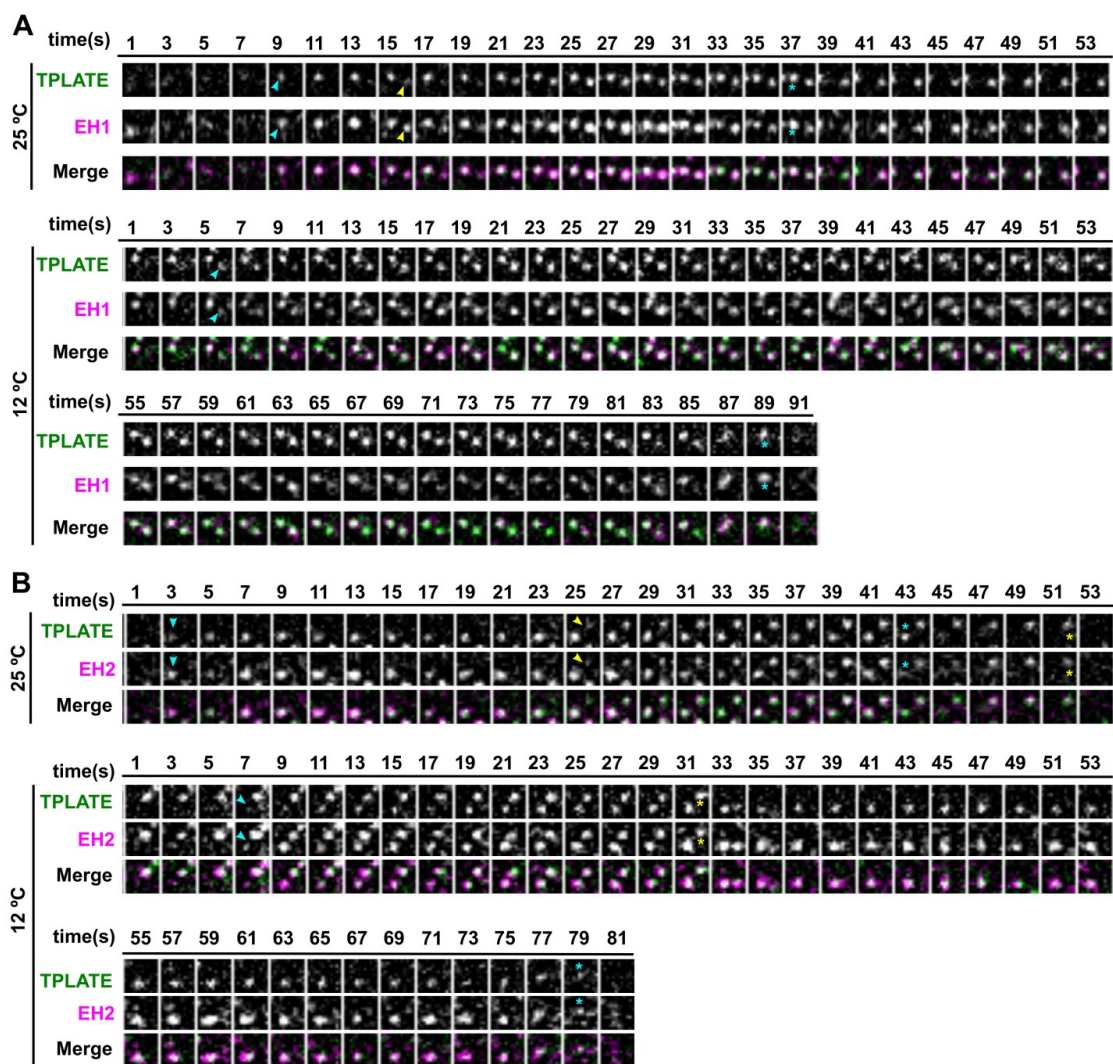


Figure S7. AtEH/Pan1 and TPLATE are recruited to the PM simultaneously.

Time series of dual-color spinning disk movies showing the simultaneous recruitment between TPLATE and AtEH1/Pan1 (A) or AtEH2/Pan1 (B) at different temperatures. Arrowheads mark the appearance and asterisks mark the disappearance of TPLATE or AtEH1/Pan1 and AtEH2/Pan1 on the PM. These image series are the extended versions of the series shown in Figure 5.

Chapter 2

References

Aguet, F., Antonescu, C.N., Mettlen, M., Schmid, S.L., and Danuser, G. (2013). Advances in analysis of low signal-to-noise images link dynamin and AP2 to the functions of an endocytic checkpoint. *Dev Cell* **26**: 279-291.

Balaji, J., and Ryan, T.A. (2007). Single-vesicle imaging reveals that synaptic vesicle exocytosis and endocytosis are coupled by a single stochastic mode. *Proc Natl Acad Sci U S A* **104**: 20576-20581.

Bashline, L., Li, S., Zhu, X., and Gu, Y. (2015). The TWD40-2 protein and the AP2 complex cooperate in the clathrin-mediated endocytosis of cellulose synthase to regulate cellulose biosynthesis. *Proc Natl Acad Sci U S A* **112**: 12870-12875.

Bashline, L., Li, S., Anderson, C.T., Lei, L., and Gu, Y. (2013). The endocytosis of cellulose synthase in Arabidopsis is dependent on mu2, a clathrin-mediated endocytosis adaptin. *Plant Physiol* **163**: 150-160.

Bitsikas, V., Correa, I.R., Jr., and Nichols, B.J. (2014). Clathrin-independent pathways do not contribute significantly to endocytic flux. *eLife* **3**: e03970.

Bui, L., and Glavinovic, M.I. (2014). Temperature dependence of vesicular dynamics at excitatory synapses of rat hippocampus. *Cogn Neurodyn* **8**: 277-286.

Claridge-Chang, A., and Assam, P.N. (2016). Estimation statistics should replace significance testing. *Nat Methods* **13**: 108-109.

Compeer, E.B., et al. (2018). A mobile endocytic network connects clathrin-independent receptor endocytosis to recycling and promotes T cell activation. *Nat Commun* **9**: 1597.

Cumming, G. (2012). *Understanding the new statistics: Effect sizes, confidence intervals, and meta-analysis.* (New York, NY, US: Routledge/Taylor & Francis Group).

Das, T.M., Hildebrandt, A.C., and Riker, A.J. (1966). Cine-photomicrography of low temperature effects on cytoplasmic streaming, nucleolar activity and mitosis in single tobacco cells in microculture. *Am J Bot* **53**: 253-259.

Dejonghe, W., et al. (2019). Disruption of endocytosis through chemical inhibition of clathrin heavy chain function. *Nat Chem Biol* **15**: 641-649.

Dejonghe, W., et al. (2016). Mitochondrial uncouplers inhibit clathrin-mediated endocytosis largely through cytoplasmic acidification. *Nat Commun* **7**: 11710.

Dhonukshe, P., Aniento, F., Hwang, I., Robinson, D.G., Mravec, J., Stierhof, Y.D., and Friml, J. (2007). Clathrin-mediated constitutive endocytosis of PIN auxin efflux carriers in Arabidopsis. *Curr Biol* **17**: 520-527.

Di Rubbo, S., et al. (2013). The clathrin adaptor complex AP-2 mediates endocytosis of brassinosteroid insensitive1 in Arabidopsis. *Plant Cell* **25**: 2986-2997.

Chapter 2

- Fan, L., Hao, H., Xue, Y., Zhang, L., Song, K., Ding, Z., Botella, M.A., Wang, H., and Lin, J.** (2013). Dynamic analysis of Arabidopsis AP2 sigma subunit reveals a key role in clathrin-mediated endocytosis and plant development. *Development* **140**: 3826-3837.
- Fujimoto, M., Arimura, S., Ueda, T., Takanashi, H., Hayashi, Y., Nakano, A., and Tsutsumi, N.** (2010). Arabidopsis dynamin-related proteins DRP2B and DRP1A participate together in clathrin-coated vesicle formation during endocytosis. *Proc Natl Acad Sci U S A* **107**: 6094-6099.
- Gadeyne, A., et al.** (2014). The TPLATE adaptor complex drives clathrin-mediated endocytosis in plants. *Cell* **156**: 691-704.
- Gilles, J.F., Dos Santos, M., Boudier, T., Bolte, S., and Heck, N.** (2017). DiAna, an ImageJ tool for object-based 3D co-localization and distance analysis. *Methods* **115**: 55-64.
- Hirst, J., Schlacht, A., Norcott, J.P., Traynor, D., Bloomfield, G., Antrobus, R., Kay, R.R., Dacks, J.B., and Robinson, M.S.** (2014). Characterization of TSET, an ancient and widespread membrane trafficking complex. *eLife* **3**: e02866.
- Ho, J., Tumkaya, T., Aryal, S., Choi, H., and Claridge-Chang, A.** (2019). Moving beyond P values: data analysis with estimation graphics. *Nat Methods* **16**: 565-566.
- Ingouff, M., Selles, B., Michaud, C., Vu, T.M., Berger, F., Schorn, A.J., Autran, D., Van Durme, M., Nowack, M.K., Martienssen, R.A., and Grimanelli, D.** (2017). Live-cell analysis of DNA methylation during sexual reproduction in Arabidopsis reveals context and sex-specific dynamics controlled by noncanonical RdDM. *Genes Dev* **31**: 72-83.
- Ito, E., Fujimoto, M., Ebine, K., Uemura, T., Ueda, T., and Nakano, A.** (2012). Dynamic behavior of clathrin in Arabidopsis thaliana unveiled by live imaging. *Plant J* **69**: 204-216.
- Jaqaman, K., Loerke, D., Mettlen, M., Kuwata, H., Grinstein, S., Schmid, S.L., and Danuser, G.** (2008). Robust single-particle tracking in live-cell time-lapse sequences. *Nat Methods* **5**: 695-702.
- Johnson, A., and Vert, G.** (2017). Single Event Resolution of Plant Plasma Membrane Protein Endocytosis by TIRF Microscopy. *Front Plant Sci* **8**: 612.
- Karimi, M., Depicker, A., and Hilson, P.** (2007). Recombinational cloning with plant gateway vectors. *Plant Physiol* **145**: 1144-1154.
- Kim, S.Y., Xu, Z.Y., Song, K., Kim, D.H., Kang, H., Reichardt, I., Sohn, E.J., Friml, J., Juergens, G., and Hwang, I.** (2013). Adaptor protein complex 2-mediated endocytosis is crucial for male reproductive organ development in Arabidopsis. *Plant Cell* **25**: 2970-2985.
- Kitakura, S., Vanneste, S., Robert, S., Lofke, C., Teichmann, T., Tanaka, H., and Friml, J.** (2011). Clathrin mediates endocytosis and polar distribution of PIN auxin transporters in Arabidopsis. *Plant Cell* **23**: 1920-1931.
- Konopka, C.A., and Bednarek, S.Y.** (2008a). Comparison of the dynamics and functional redundancy of the Arabidopsis dynamin-related isoforms DRP1A and DRP1C during plant development. *Plant Physiol* **147**: 1590-1602.

Chapter 2

Konopka, C.A., and Bednarek, S.Y. (2008b). Variable-angle epifluorescence microscopy: a new way to look at protein dynamics in the plant cell cortex. *Plant J* **53**: 186-196.

Konopka, C.A., Backues, S.K., and Bednarek, S.Y. (2008). Dynamics of Arabidopsis dynamin-related protein 1C and a clathrin light chain at the plasma membrane. *Plant Cell* **20**: 1363-1380.

Legland, D., Arganda-Carreras, I., and Andrey, P. (2016). MorphoLibJ: integrated library and plugins for mathematical morphology with ImageJ. *Bioinformatics* **32**: 3532-3534.

Leys, C., Ley, C., Klein, O., Bernard, P., and Licata, L. (2013). Detecting outliers: Do not use standard deviation around the mean, use absolute deviation around the median. *Journal of Experimental Social Psychology* **49**: 764-766.

Lu, R., Drubin, D.G., and Sun, Y. (2016). Clathrin-mediated endocytosis in budding yeast at a glance. *J Cell Sci* **129**: 1531-1536.

Ma, L., Umasankar, P.K., Wrobel, A.G., Lymar, A., McCoy, A.J., Holkar, S.S., Jha, A., Pradhan-Sundd, T., Watkins, S.C., Owen, D.J., and Traub, L.M. (2016). Transient Fcho1/2Eps15/RAP-2 Nanoclusters Prime the AP-2 Clathrin Adaptor for Cargo Binding. *Dev Cell* **37**: 428-443.

McMahon, H.T., and Boucrot, E. (2011). Molecular mechanism and physiological functions of clathrin-mediated endocytosis. *Nat Rev Mol Cell Biol* **12**: 517-533.

Mravec, J., et al. (2011). Cell plate restricted association of DRP1A and PIN proteins is required for cell polarity establishment in Arabidopsis. *Curr Biol* **21**: 1055-1060.

Mylle, E., Codreanu, M.C., Boruc, J., and Russinova, E. (2013). Emission spectra profiling of fluorescent proteins in living plant cells. *Plant Methods* **9**: 10.

Narasimhan, M., Johnson, A., Prizak, R., Kaufmann, W.A., Tan, S., Casillas-Perez, B., and Friml, J. (2020). Evolutionarily unique mechanistic framework of clathrin-mediated endocytosis in plants. *eLife* **9**.

Pascolutti, R., et al. (2019). Molecularly Distinct Clathrin-Coated Pits Differentially Impact EGFR Fate and Signaling. *Cell Rep* **27**: 3049-3061 e3046.

Picco, A., and Kaksonen, M. (2018). Quantitative imaging of clathrin-mediated endocytosis. *Curr Opin Cell Biol* **53**: 105-110.

Pyott, S.J., and Rosenmund, C. (2002). The effects of temperature on vesicular supply and release in autaptic cultures of rat and mouse hippocampal neurons. *J Physiol* **539**: 523-535.

Robert, S., et al. (2010). ABP1 mediates auxin inhibition of clathrin-dependent endocytosis in Arabidopsis. *Cell* **143**: 111-121.

Taylor, M.J., Perrais, D., and Merrifield, C.J. (2011). A high precision survey of the molecular dynamics of mammalian clathrin-mediated endocytosis. *PLoS Biol* **9**: e1000604.

Team, R.C. (2019). R: A language and environment for statistical computing.

Chapter 2

Tinevez, J.Y., Perry, N., Schindelin, J., Hoopes, G.M., Reynolds, G.D., Laplantine, E., Bednarek, S.Y., Shorte, S.L., and Eliceiri, K.W. (2017). TrackMate: An open and extensible platform for single-particle tracking. *Methods* **115**: 80-90.

Van Damme, D., Bouget, F.Y., Van Poucke, K., Inze, D., and Geelen, D. (2004). Molecular dissection of plant cytokinesis and phragmoplast structure: a survey of GFP-tagged proteins. *Plant J* **40**: 386-398.

Van Damme, D., Coutuer, S., De Rycke, R., Bouget, F.Y., Inze, D., and Geelen, D. (2006). Somatic cytokinesis and pollen maturation in Arabidopsis depend on TPLATE, which has domains similar to coat proteins. *Plant Cell* **18**: 3502-3518.

Van Damme, D., Gadeyne, A., Vanstraelen, M., Inze, D., Van Montagu, M.C., De Jaeger, G., Russinova, E., and Geelen, D. (2011). Adaptin-like protein TPLATE and clathrin recruitment during plant somatic cytokinesis occurs via two distinct pathways. *Proc Natl Acad Sci U S A* **108**: 615-620.

Wang, P., et al. (2019). Plant AtEH/Pan1 proteins drive autophagosome formation at ER-PM contact sites with actin and endocytic machinery. *Nat Commun* **10**: 5132.

Wrobel, A.G., et al. (2019). Temporal Ordering in Endocytic Clathrin-Coated Vesicle Formation via AP2 Phosphorylation. *Dev Cell* **50**: 494-508 e411.

Yamaoka, S., Shimono, Y., Shirakawa, M., Fukao, Y., Kawase, T., Hatsugai, N., Tamura, K., Shimada, T., and Hara-Nishimura, I. (2013). Identification and dynamics of Arabidopsis adaptor protein-2 complex and its involvement in floral organ development. *Plant Cell* **25**: 2958-2969.

Zhang, Y., Persson, S., Hirst, J., Robinson, M.S., van Damme, D., and Sanchez-Rodriguez, C. (2015). Change your TPLATE, change your fate: plant CME and beyond. *Trends Plant Sci* **20**: 41-48.

Zhou, J., et al. (2018). Regulation of Arabidopsis brassinosteroid receptor BRI1 endocytosis and degradation by plant U-box PUB12/PUB13-mediated ubiquitination. *Proc Natl Acad Sci U S A* **115**: E1906-E1915.

Chapter Three

Characterization of TPLATE motif mutated isoforms

Jie Wang^{1,2}, Klaas Yperman^{1,2}, Dominique Eeckhout^{1,2}, Jonah Nolf^{1,2}, Eliana Mor^{1,2}, Bert De Rybel^{1,2}, Roman Pleskot^{1,2}, & Daniel Van Damme^{1,2,*}

¹Ghent University, Department of Plant Biotechnology and Bioinformatics, Technologiepark 71, 9052 Ghent, Belgium

²VIB Center for Plant Systems Biology, Technologiepark 71, 9052 Ghent, Belgium

The Sandwich and Platform part of this chapter together with other data from the lab are part of a manuscript addressing the potential structure (Structural basis for the evolution of the endocytic TSET complex in plants). The manuscript is currently under review

.

The remaining data in this chapter together with the data in chapter four are combined into a manuscript characterizing a novel and conditional tool to manipulate endocytosis independently of its role in autophagy (Conditional destabilization of the TPLATE complex impairs endocytic internalization). The manuscript is currently being submitted for publication.

Author Contributions: JW and DVD designed the projects. JW generated all experimental materials and performed majority of experiments. KP helped with the western blots experiments. RP helped with AA alignment analysis. DE, JN, EM and BDR helped with IP-MS experiments and analysis. JW wrote the manuscript. DVD contributed to the revision of the manuscript.

Abstract

Clathrin-mediated endocytosis (CME) is the best-characterized endocytic pathway to regulate plasma membrane protein turnover in plants. The octameric TPLATE complex (TPC) serves as an essential adaptor complex during plant CME. Given the male sterility phenotype of single subunit *tpc* mutants, weak allele mutants or partially complemented *tplate* mutants are required to understand the function of the TPC. We employed a targeted mutagenesis strategy to identify partial loss of function alleles of *TPLATE* by mutating selected motifs. Substituting two evolutionary conserved motifs named SANDWICH and PLATFORM, locating at the APPENDAGE part of TPLATE, abolished PM recruitment and TPC assembly. Both SANDWICH and PLATFORM motif substitutions (named mSandwich and mPlatform) failed to complement the *tplate* T-DNA mutant. While substitutions in other domains including EF-LOOP, LINKER and WDX (named mEF-loops, mWDXs and mLinkers) maintained the PM recruitment as well as conserved the functionality of TPLATE. Among these functional TPLATE mutated isoforms, mWDX, in which the evolutionary most conserved motif of TPLATE was replaced, not only conserved the functionality of TPLATE but also impaired the efficiency of endocytosis. Thus, the mWDX complemented lines are potential partially functional alleles of TPLATE, contributing to further revealing the role of TPC.

Introduction

The TPC is an evolutionary ancient protein complex that so far has only been experimentally characterized in plants and *Dictyostelium* (Gadeyne et al., 2014; Hirst et al., 2014). In plants, TPC was identified as an octameric complex that acts as the key endocytic adaptor complex (Gadeyne et al., 2014). It is essential for both pollen development and plant development as knockdown or knockout TPC single subunit results in male sterility or seedling lethality (Van Damme et al., 2006; Gadeyne et al., 2014; Wang et al., 2019). In contrast to TPC in plant cells, *Dictyostelium* TPC was identified as a hexameric complex (named TSET), which still functions in plasma membrane turnover but appears to be dispensable for the organism (Hirst et al., 2014).

In *silico* studies on TPC have identified multiple putative protein domains and motifs in the various subunits. These domains putatively can function in clathrin binding, cargo sorting, AP-2 interactions, protein-protein interactions, Ca²⁺ binding, cargo recognition, or dynamin interaction (Gadeyne et al., 2014; Zhang et al., 2015). Our previous work showed that the μ -homology domain (μ HD) of TML is essential for plasma membrane recruitment and complete TPC assembly (Gadeyne et al., 2014). Our recent work showed that the N-terminal EH domains of AtEH1/Pan1 are required for its PM recruitment while the C-terminal is essential for autophagy (Wang et al., 2019). With the exception of these above reported domains, the function of the other motifs and domains in the TPC proteins remains to be determined.

The TPLATE subunit carries an armadillo repeat domain, an EF-hand motif as well as a highly conserved β -coatamer proteins motif (β -COP), which may be important to its function (Van Damme et al., 2006). The armadillo repeat domain in the N terminus of TPLATE is also largely found in AP complexes and COPI protein complex (Van Damme et al., 2006; Gadeyne et al., 2014; Hirst et al., 2014; Zhang et al., 2015). The β -COP motif is highly conserved in TPLATE isoforms across different genera (Van Damme et al., 2006). The amino acid

Chapter 3

residues at position 1, 5 and 12 of EF-hand motif are essential for Ca²⁺ binding (Janssens et al., 2003; Buevich et al., 2004). We however know little to nothing about the function of these TPLATE motifs or domains for TPC functioning.

The male sterility or seedling lethality of TPC single subunit causes a genetic barrier to study the somatic function of TPC in plants. Recently, a weak allele of the TPC subunit TWD40-2, *twd40-2-3*, did not cause the male sterility phenotype as observed for the strong *twd40-2-1* or *twd40-2-2* alleles (Gadeyne et al., 2014; Bashline et al., 2015). Similarly, to overcome the male sterility phenotype of *tplate* mutants, we employed a strategy to identify partial loss of function alleles of *TPLATE* by mutating selected motifs or conserved residues and we assessed the functionality of these TPLATE isoforms by their capacity to complement the *tplate* loss-of-function mutant.

Results

Identification and evaluation of evolutionarily conserved TPLATE motifs

TPC can be dated back to the last eukaryotic common ancestor and represents a missing link between COPI and AP complexes (Dacks and Field, 2018). Although, the most eukaryotic super groups contain a full or partial TPC, the complex was completely lost in animals and yeast (Hirst et al., 2014). The functional complex has been so far described only in two eukaryotic super groups, Archaeplastida (plants) and Amoebozoa (Gadeyne et al. 2014; Hirst et al., 2014). By application of an integrative structural approach, we revealed a first model of TPC architecture and showed the central location of the TPLATE subunit inside the complex (Figure 1A), indicating the essential role of TPLATE for TPC assembly (Yperman et al., 2020). Consequently, we targeted this subunit to manipulate TPC function.

To identify evolutionary conserved motifs, we compared the TPLATE subunit of functionally characterized TPCs and of closely related species and generated

Chapter 3

a multiple alignment of the TPLATE protein sequences based on selected plant and Amoebozoa species. We selected these motifs or domains either because of an earlier indication of their functionality from our previous work or because of amino acid conservation across plants species or across all species. These conserved amino acid residues were mutated to alanine, glycine or serine based on the original amino acid composition (Fig.1B). With our substitutions, we aimed to maintain similar flexibility and hydrophobicity, in order not to completely abolish TPLATE function.

The five mutated regions locate in three different parts of TPLATE; the body domain, the appendage domain and the linker region between these two parts (Fig. 1B). In the TPLATE body domain, we mutated the EF-loop in which the amino acid residues at position 1, 5 and 12 are essential for Ca²⁺ binding (Janssens et al., 2003; Buevich et al., 2004) and generated two different isoforms (Fig. 1B, mEF-loop1 and mEF-loop2). We also selected another motif which contained the hyper-conserved amino acids FREE across all the species (Fig. 1B and S1). We mutated either FREE alone or FREE along with a couple of flanking residues (Fig. 1B, named as mWDX1 and mWDX2, WDX stands for WenDingXing, which means stability in Chinese, will be explained further below). The Linker1 and Linker2 subdomain are quite conserved across plant species thus were also selected to be mutated (Fig. 1B and S1, named as mLinker1 and mLinker2). The APPENDAGE domain of TPLATE is analogous to the appendage domains of other coatomer complexes (i.e. COPI and AP complexes) and consists of two subdomains, a SANDWICH domain and a PLATFORM domain. The SANDWICH domain (earlier named β -COP motif) has been shown to be conserved in various plant species (Van Damme et al., 2006) and here we show that it is also conserved in amoebas (Fig. 1B and S1). We picked up the PLATFORM domain as it is very conserved across several selected species (Fig. 1B and S1). We mutated conserved residues in each of these domains (Fig. 1B, named mSandwich and mPlatform).

To gain insight into the roles of these conserved regions, GFP fusions

Chapter 3

of TPLATE substitution constructs were introduced into a *tplate* heterozygous mutant background followed by a complementation assay in T2 transgenics. The male sterility of the *tpc* mutant leads to a 1:1 segregation ratio of wild type plants (WT) versus heterozygous T-DNA insertion plants (Van Damme et al., 2006; Gadeyne et al., 2014; Wang et al., 2019). Functional complementation of these substituted TPLATE isoforms was evaluated via the segregation ratio of WT plants and T-DNA insertion plants among T2 transgenics whose parent line contained the T-DNA insertion in *tplate* (Fig. 1C). Plants carrying mSandwich and mPlatform isoforms showed a 1:1 ratio between WT and T-DNA insertion offspring, indicating that neither of these constructs could rescue the male sterility phenotype of the *tplate* mutant. Plants expressing mEF-Loop, mLinker and mWDX isoforms however yielded ratios of WT and T-DNA insertion offspring plants that deviated from 1:1, suggesting that they were at least partially functional (Table 1). Western blot analysis confirmed the presence of full-length of TPLATE, mEF-Loops, mLinkers and mWDXs proteins in these transgenic lines, along with the absence of endogenous TPLATE in two independently complemented lines (Fig. 3C). The results of our complementation analysis therefore showed that the substitutions of highly conserved motifs in the BODY did not abolish TPLATE functionality, in contrast to substitutions in the APPENDAGE domain, which produced TPLATE isoforms (mSandwich and mPlatform) that could not complement the male sterility phenotype of the *tplate* loss-of-function mutant.

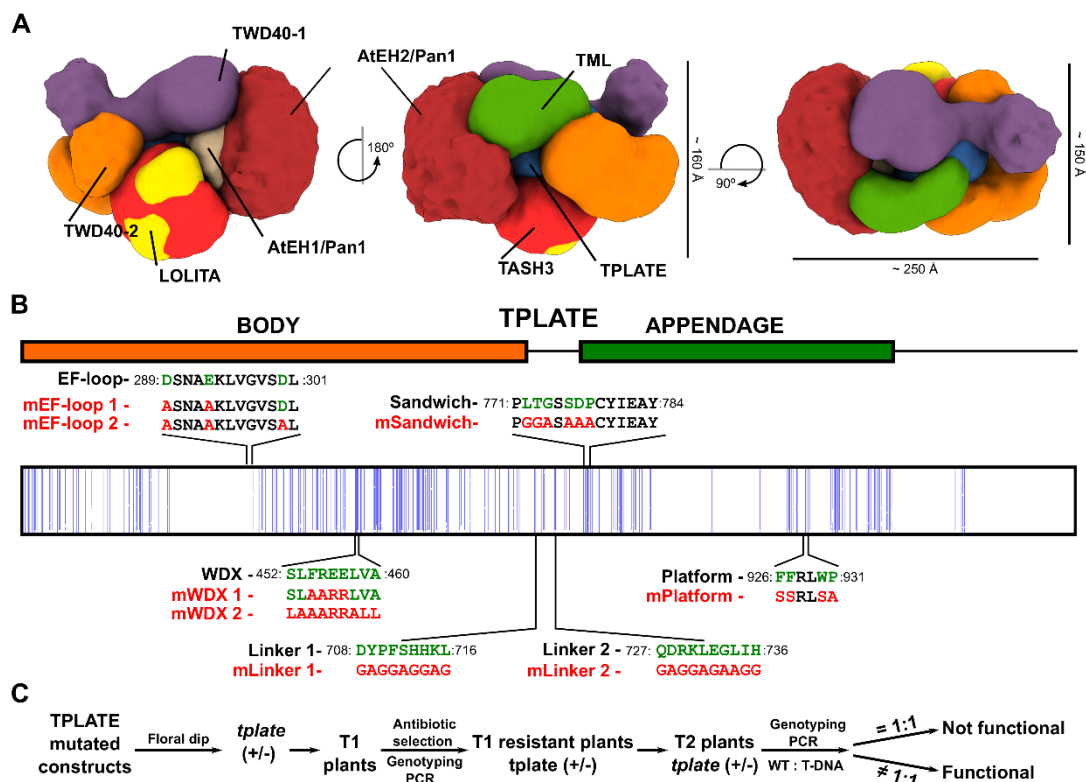


Figure 1. Identification and functionality assay of selected TPLATE motif mutants.

(A) The architecture of TPC as obtained by the integrative modelling platform. The localization of each subunit is defined by a density map, visualized here at a threshold equal to one-tenth of the maximum. The localization density map represents the probability of any volume element being occupied by a given subunit. The approximate dimensions of TPC are 150x160x250 Å. Image reproduced from (Yperman et al., 2020).

(B) Schematic representation of TPLATE domain organization. We aligned Arabidopsis TPLATE against various plant as well as Amoebozoa species. The schematic view of the amino acid alignment data shows highly conserved amino acids of TPLATE as vertical blue lines. The five motifs that we selected to mutate are plotted on the alignment. The conserved original amino acids of these motifs are highlighted in green and the corresponding substituted amino acids are indicated in red. Numbers represent the amino acid positions of these elements within Arabidopsis TPLATE.

(C) Schematic diagram employed to screen for functionality of the generated TPLATE isoforms. Given the male sterility phenotype of the *tplate* T-DNA line (AA: Aa =1:1), the ratio of WT:T-DNA among T2 transgenic *tplate* lines expressing the complementation construct of TPLATE, mutated in the selected motifs, was used to evaluate the functionality of these constructs.

SANDWICH and PLATFORM subdomains are crucial for TPLATE function

To gain insight into why the mSandwich and mPlatform isoforms were non-functional, we visualized their localization as well as recruitment behavior at the plasma membrane (PM). TPLATE localizes at the PM and is recruited to highly dynamic endocytic spots (Van Damme et al., 2011; Gadeyne et al., 2014). In contrast to TPLATE, which co-localized with FM4-64 at the PM in confocal sections of epidermal root cells, mSandwich and mPlatform isoforms failed to be recruited to the PM (Fig. 2A). To evaluate whether this represented reduced or abolished PM recruitment, we crossed TPLATE, mSandwich and mPlatform isoforms with the dynamin-related protein 1A (DRP1a)-mRFP reporter line (Mravec et al., 2011) and analyzed PM recruitment in etiolated hypocotyl cells. Similar as shown previously (Gadeyne et al., 2014), TPLATE and DRP1a co-localized at endocytic dots at the PM in epidermal cells of etiolated hypocotyls. The mSandwich and mPlatform isoforms however failed to be recruited to the endocytic dots at the PM in the focal plane of DRP1a (Fig. 2B). Kymograph analysis further confirmed that the dynamic recruitment behavior at the PM of TPLATE was completely abolished in mSandwich and mPlatform plants (Fig. 2C). Furthermore, this was not caused by reduced protein stability as full length-GFP fusions of mSandwich and mPlatform were present and stable (Fig. 2D). These results indicate that abolishing the function of the SANDWICH and PLATFORM domains impairs the stable PM recruitment of TPLATE, similar to what was observed previously for the truncated homology domain (μ HD) of TML, which relocated TPC to the cytoplasm (Gadeyne et al., 2014).

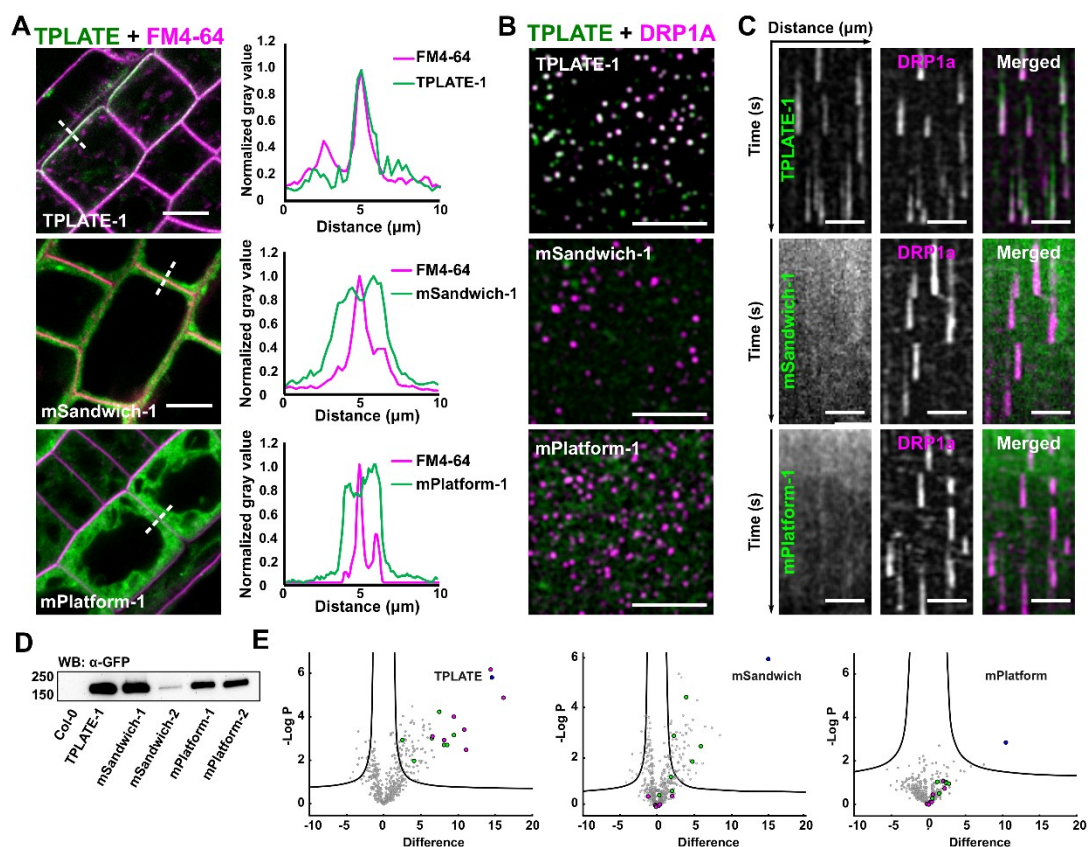


Figure 2. Substitutions in SANDWICH and PLATFORM domains disable TPLATE recruitment.

(A) Representative confocal images showing that TPLATE (WT) co-localizes with FM4-64 at the PM, while mSandwich and mPlatform display cytoplasmic localization. Scale bar = 10 μm . Intensity plots normalized to the highest fluorescence intensity along the white dashed line in (A) further clarify the presence or absence of PM localization of TPLATE compared with the mSandwich and mPlatform isoforms.

(B) Spinning disc images showing TPLATE and DRP1a co-recruitment at the PM as endocytic dots, whereas mSandwich and mPlatform are not present at the PM at the focal plane of DRP1a. Scale bar = 7 μm .

(C) Representative kymographs showing the dynamic co-localization of TPLATE and DRP1a during endocytic events and confirming the incapacity of mSandwich and mPlatform isoforms recruitment to the PM as endocytic dots. Time = 120s. Scale bar = 25 μm .

(D) Western blot using anti-GFP showing that full-length versions of the sandwich and platform motif mutations are stable. Two independent lines of each are shown. TPLATE-GFP is the positive and Col-0 is the negative control.

(E) Volcano plot showing the MS analysis following co-IP on complemented TPLATE as well as mSandwich and mPlatform lines compared with Col_0 plants. TPLATE is annotated and indicated in blue, other TPC subunits are not annotated and indicated as magenta, and other

Chapter 3

endocytic interactors (CHC 1 and 2, DRP1A, 1B and 1C, DRP2a and 2B) are indicated in green. Dots located above right curve presents the significantly detected proteins found when comparing TPLATE or TPLATE substitutions mutant with Col_0 using stringent parameters (FDR=0.01 and S0=1).

The μ HD of TML is essential for full TPC assembly, as truncating the μ HD of TML fails to recruit certain TPC components in the cytoplasm (Gadeyne et al., 2014). We further investigate whether TPC is well assembled in mSandwich and mPlatform transgenic lines. The -GFP fused TPLATE, mSandwich and mPlatform transgenic lines, together with Col_0, were performed with Immunoprecipitation (IP) experiments following with mass spectrometry (MS) analysis. Our MS results showing that, compared with Col_0, we significantly detected the TPC subunits as well as its interactors in TPLATE complemented lines (Fig. 2E). In contrast to TPLATE, we failed to significantly detect TPC subunits in both mSandwich and mPlatform plants compared with Col_0 (Fig. 2E). Although we were able to significantly detect certain endocytic interactors of TPC (CHC1 and CHC2; DRP1A and DRP1C) in mSandwich plants, we fail to detect any TPC interactors in mPlatform plants. These data together showing that, both SANDWICH and PLATFORM domains of TPLATE are essential for PM recruitment as well as for full TPC assembly. While unlike truncating the μ HD of TML, which still recruits the core TPC subunits in the cytoplasm (Gadeyne et al., 2014), substituting Sandwich and Platform domains of TPLATE, completely abolish the TPC complex assembly, suggested these two domains are essential for TPC stability.

Substitutions in the WDX domain partially affect TPLATE functionality

Both mEF-loops, mLinkers and mWDXs were sufficiently functional to be able to rescue the male sterility mutant phenotype of the *tplate* KO mutant (Table 1 and Fig. 3C). We subsequently examined whether these mutations, similar to the weak *twd40-2-3* allele, also had an effect on CME. Both mEF-Loops,

Chapter 3

mLinkers and mWDX co-localized with FM4-64 at the PM in root epidermal cells (Fig. 3A) and were recruited to the PM as endocytic dots in the epidermal cells of etiolated hypocotyls (Fig. 3B). The dynamic behavior of endocytic proteins is correlated with the efficiency of endocytosis as reduced or prolonged lifetimes correlate respectively with aborted or deficient CME (Fan et al., 2013; Bashline et al., 2015; Adamowski et al., 2018). Kymographs and lifetime analysis results showed that, compared to TPLATE, those motif substitutions isoforms exhibited various resident lifetimes at the PM. Both mLinker1 and mLinker2 showed a slightly but overall significantly decreased lifetime (Fig. 4A and B). Although mEF-loop1 hardly affected the average lifetime of TPLATE at the PM, both mEF-loop2 and mWDXs displayed severely prolonged resident lifetime of endocytic dots at the PM (Fig. 4A and B).

We were interested in those TPLATE mutated isoforms which showed prolonged lifetime at the PM which may correlate with a deficiency in CME. Given that both mWDX1 and mWDX2 complemented lines showed the most pronounced delayed lifetime at the PM, we further evaluated whether endocytosis was impaired in these lines. Compared to TPLATE, the internalization of the endocytic tracer FM4-64 was reduced in both mWDX1 and mWDX2 complemented lines, indicating that mWDX isoform, although functional enough to overcome the male sterility mutant phenotype, were slightly impaired in internalization (Fig. 5A).

The efficiency of endocytosis is determined by the dynamics as well as the amount of endocytic proteins, so we further evaluated the density of mWDX complemented lines at the PM. The mWDX complemented plants showed similar or slightly higher density at the PM compared with TPLATE, which could also be a result of their longer resident lifetimes (Fig. 5B).

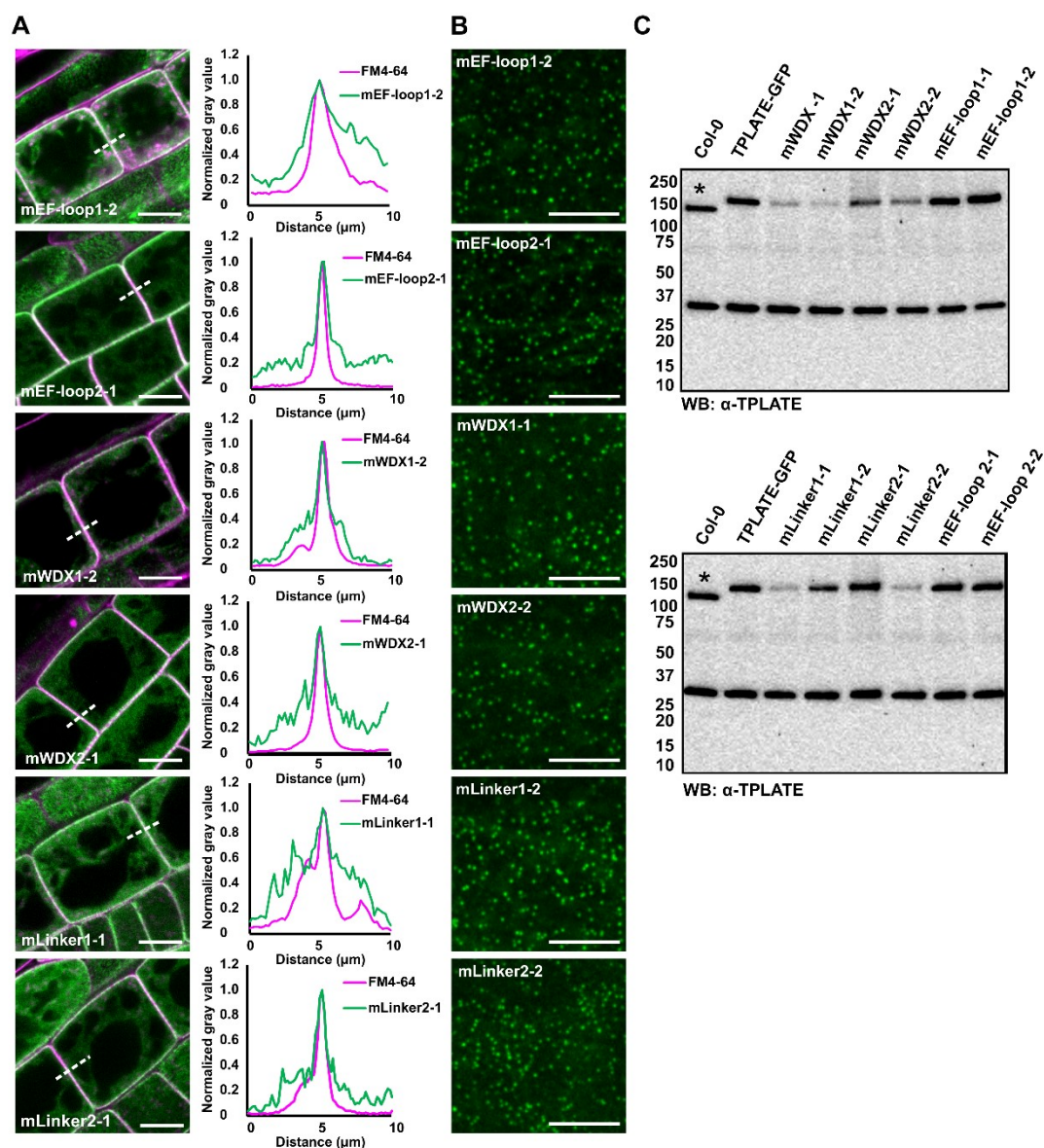


Figure 3. Substitutions in EF-loop, WDX and Linker domains conserve TPLATE PM recruitment.

(A) Representative confocal images showing that both of mEF-loops, mWDXs and mLinkers co-localize with FM4-64 at the PM. Plots of normalized fluorescence intensity along the white dashed line in confocal images further visualize the PM localization of these motif substitution mutants. Scale bar = 10 μ m.

(B) Spinning disc images displaying mEF-loops, mWDXs and mLinkers isoforms being recruited to endocytic spots on the PM. Scale bar = 7 μ m.

(C) Anti-TPLATE western blot detecting the presence of endogenous TPLATE in Col-0 (marked with an asterisk) and full length of GFP fusions of TPLATE as well as various mutated isoforms in the complemented *tplate* (-/-) background lines. The Western blot shown here confirms the complementation of the *tplate* T-DNA mutant background with these TPLATE mutated isoforms. Non-specific bands at the bottom of the blots serve as loading control.

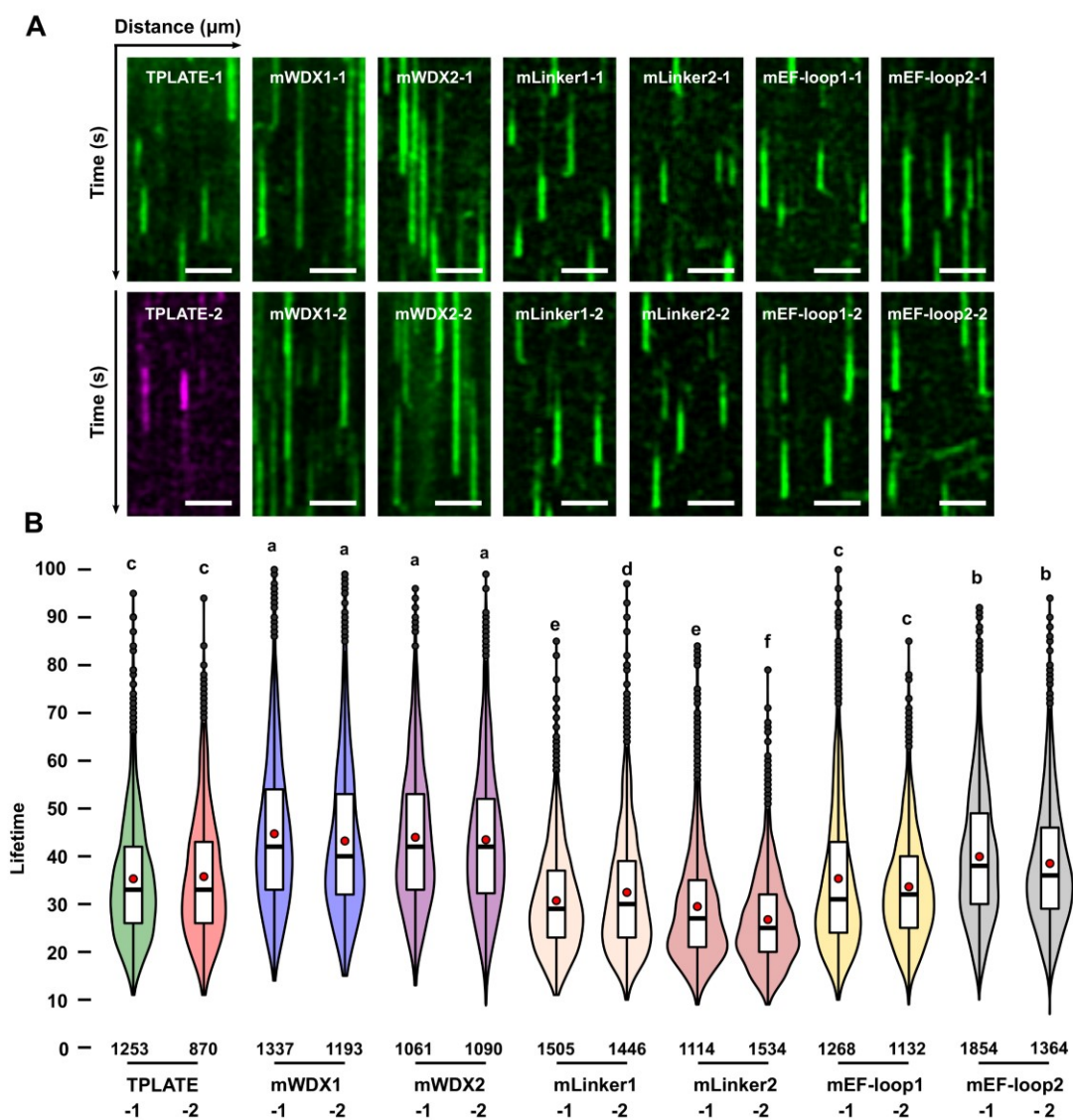


Figure 4. Substitutions in WDX domains of TPLATE delay endocytic events.

(A-B) Representative kymographs and violin plots showing that TPLATE mutated isoforms display variable dwell-times at the PM. Among these isoforms, both of mWDX1 and mWDX2 display the most pronounced delay in lifetime at the PM. Time = 120s. Scale bar = 25 μ m. The number of events analyzed for each independent line is indicated at the bottom of the graph. At least 12 movies from 4 seedlings were imaged for each independent transgenic line. Letters represent significantly different groups ($P < 0.001$) by one-way ANOVA analysis.

To further correlate the delay in dwell-time at the PM to the dynamics of the other CME machinery, we crossed the TPLATE and mWDX2 complemented lines with the DRP1a-mRFP marker, identified homozygous complemented *tplate(-/-)* lines and measured the dynamics of DRP1a-mRFP. The lifetime

distribution pattern of DRP1a-mRFP in mWDX and TPLATE complemented lines are quite similar. Unlike TPLATE, however, mWDX2 complemented plants exhibited a population of events with a more prolonged lifetime (> 30 s) of DRP1a-mRFP (Fig. 5C), indicating that the delay in CME is at least partially caused by a delay in fission.

Our data together clearly shows that the WDX domain in TPLATE contributes to the efficiency of endocytosis.

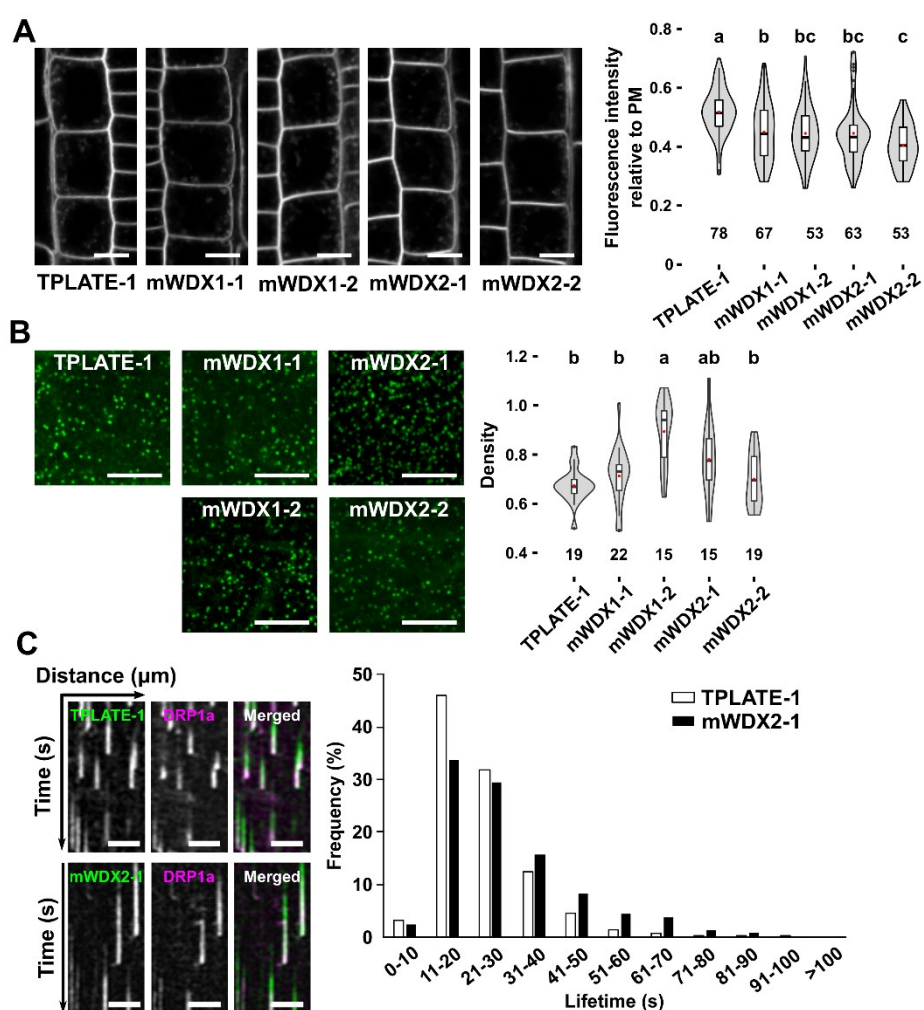


Figure 5. Substitutions in WDX domains of TPLATE impair endocytosis.

(A) Representative confocal images and quantification showing that both mWDX1 and mWDX2 complemented plants display reduced FM4-64 uptake in root apical epidermal cells. Scale bar = 10 μ m. Numbers represent the amount of cells analyzed. At least 8 independent roots of each transgenic line were analyzed. Red circles represent the mean. Letters represent significantly different groups (P < 0.001), evaluated by the Tukey multiple pairwise-comparisons test.

(B) Spinning disc images displaying mWDX1 and mWDX2 being recruited to endocytic spots

Chapter 3

on the PM. Scale bar = 7 μ m. Quantification the density of endocytic spots in TPLATE as well as independent line of mWDX1 and mWDX2 complemented plants. The “Find Maxima” tool of ImageJ was employed to quantify the density using the Z-projected images of 10 consecutive time lapse frames. Numbers of quantified cells from multiple seedlings (≥ 4 seedlings) are indicated. Red circles represent the mean. Letters represent significantly different groups ($P < 0.001$), evaluated by the Tukey multiple pairwise-comparisons test.

(C) Kymograph analysis and histogram representation of the quantification of the lifetime distribution of DRP1a in TPLATE and mWDX2 complemented lines. Scale bar = 25 μ m.

Discussion

The APPENDAGE domain but not the BODY and LINKER domains are essential for TPLATE function

Although the TPC has been hypothesized to possess many evolutionary conserved domains such as clathrin-binding boxes, AP-2 complex binding motifs, and sorting motifs by *in silico* predictions based on amino-acid motif conservation (Gadeyne et al., 2014), the function of these domains in TPC have not been experimentally studied. Truncation or site-directed mutagenesis strategies are widely used to explore the functions of domains of certain proteins (Daum et al., 2014; Gadeyne et al., 2014; Perales et al., 2016; Rodriguez et al., 2016; Wang et al., 2019; Moulinier-Anzola et al., 2020). Given the male sterility of knockout of TPC subunit (Van Damme et al., 2006; Gadeyne et al., 2014; Wang et al., 2019), to explore the function of TPLATE domains, it is an ingenious strategy to employ the domain substituted TPLATE constructs to heterozygous *tpalte* mutant. Our complementation screen clearly showed that the EF-loop motif, WDX domain located at the BODY domain and the Linker domains are not crucial for TPLATE function. While substituted the Sandwich and Platform subdomains located at the APPENDAGE domain of TPLATE, failed to rescue *tpalte* male sterile phenotype, suggested the importance role of APPENDAGE domain for TPLATE function.

Substituting SANDWICH and PLATFORM domains completely abolishes TPC assembly

Correct localization of proteins is crucial for their functions. Our recent work showed that the N-terminal part of AtEH/Pan1, containing the EH domains, are required for PM recruitment. While the C-terminal part of AtEH/Pan1 is essential for its co-localization with the ATG8 autophagy marker, as the N-terminal part alone did not cause excessive formation of autophagosomes. The N-terminal truncation of AtEH/Pan1, containing both EH domains, is supposed to be recruited to endocytic foci at the PM. However, whether it is built into the whole TPC remains unknown (Wang et al., 2019). It was also shown that the μ HD in the C-terminal of TML is required for its PM recruitment and for full TPC assembly (Gadeyne et al., 2014). A short C-terminal truncation of the μ HD (TML Δ C) relocated TML to the cytoplasm, whereas the TPC remained still partially assembled as the majority of TPC subunits could be identified via mass spec analysis using TML Δ C as bait. However, this cytoplasmic complex did not contain AtEH/Pan1 (Gadeyne et al., 2014). Given that TPC is recruited as octameric complex on the PM (Wang et al 2020), the disassembly of AtEH/Pan1 into TPC in the cytoplasm in plants together with the fact that AtEH/Pan1 proteins were not co-purified with the hexameric TPC in *Dictyostelium* (Gadeyne et al., 2014; Hirst et al., 2014)), further support that AtEH/Pan1 proteins are auxiliary to the other subunits constituting the hexameric TPC.

In contrast to the truncated TML, substitutions of SANDWICH and PLATFORM motifs in APPENDAGE domain completely abolished the PM recruitment of TPLATE and entirely abolished the assembly of TPC, contributing to the loss of TPLATE functionality. These two domains are therefore essential to stabilize TPC assembly. Our data does indicate that TPLATE can bind clathrin and this is in agreement with previous results where interaction between TPLATE and clathrin was shown via BiFC (Van Damme et al., 2011). We were however still able to detect CHCs and DRP1s in mSandwich

but not in mPlatform plants, which could indicate that the binding sites for those interactors could be related to the Platform domain. Further study such as ultrastructural analysis of TPC is required to further understand the details of the functions of APPENDAGE domain in TPLATE subunit.

WDX motif substitution mutant is a partially functional TPLATE mutant

Substituting the EF-loop, Linker and WDX domains conserved the PM recruitment of TPLATE, in agreement with the functionality assays. However, lifetime measurements indicated that these TPLATE mutated isoforms exhibited various subtle defects in the capacity to perform endocytosis.

The efficiency of endocytosis is determined by the residue lifetime of endocytic proteins on the PM as well as the amount of proteins. As the mEF-loop1, mLinker1 and mLinker2 complemented lines displayed slightly shorter or similar lifetime and comparable intensities on western (at least one line for mLinker1 and mLinker2 plants) compared with TPLATE, this suggests that their endocytic capacities would be less effected. The mEF-loop2 complemented plants showed delayed lifetime on the PM, and their proteins levels were similar or even stronger than TPLATE, suggested that it is likely a partially functional allele candidate. It has been reported that amino acid residues at position 1, 5 and 12 of EF-loop are essential for Ca²⁺ binding (Janssens et al., 2003; Buevich et al., 2004). We substituted EF-loop1 with two amino acid residues (at position 1 and 5) while substituted all three amino acid residues in EF-loop2, which may lead to different Ca²⁺ binding capacity of TPLATE EF-loop substitutions mutants. While mEF-loop2 showed longer lifetime than mEF-loop1 on the PM, may be attributed to their different Ca²⁺ binding capacity. However, further characterizations of mEF-loop2 such as endocytosis and Ca²⁺ binding capacity are required to determine it as a partially functional TPLATE allele.

The WDX motif in TPLATE is the evolutionary most conserved motif across plants as well as in Amoebozoa, suggesting that this motif may have a special

Chapter 3

role for TPC function. The extreme conservation of the FREE motif points to a specific interaction, which is however unknown. TPC is experimentally characterized in *Arabidopsis* as well as in *Dictyostelium*. TPC is essential for pollen development as well as somatic development in plants, however, it is not essential in *Dictyostelium* (Van Damme et al., 2006; Van Damme et al., 2011; Gadeyne et al., 2014; Hirst et al., 2014). Our data suggest that the severely prolonged PM resident lifetime, the reduction of FM4-64 internalization as well as the prolonged lifetime of DRP1a show us that the efficiency of endocytosis is partially affected in mWDX complemented lines. Besides, western blots results suggested that independent lines of mWDX1 and mWDX2 complemented lines are visibly less stable than TPLATE. Taken together, our results suggested that mWDX complemented lines are a partially functional TPLATE alleles.

It has been reported that the weak allele *twd40-2-3* of TWD40-2, showed mild developmental defects in hypocotyl and roots (Bashline et al., 2015). Our recent results also showed that downregulation of *AtEH/Pan1* results in susceptibility to nutrient deficiency (Wang et al., 2019). We also know that TPC serves as key adaptor protein for CME (Gadeyne et al., 2014). Whether mWDX complemented lines are phenotypically comparable to *twd40-2-3*, whether there is a link with autophagy, and how destabilization of TPC affects endocytosis will be further investigated in the following chapters.

Chapter 3

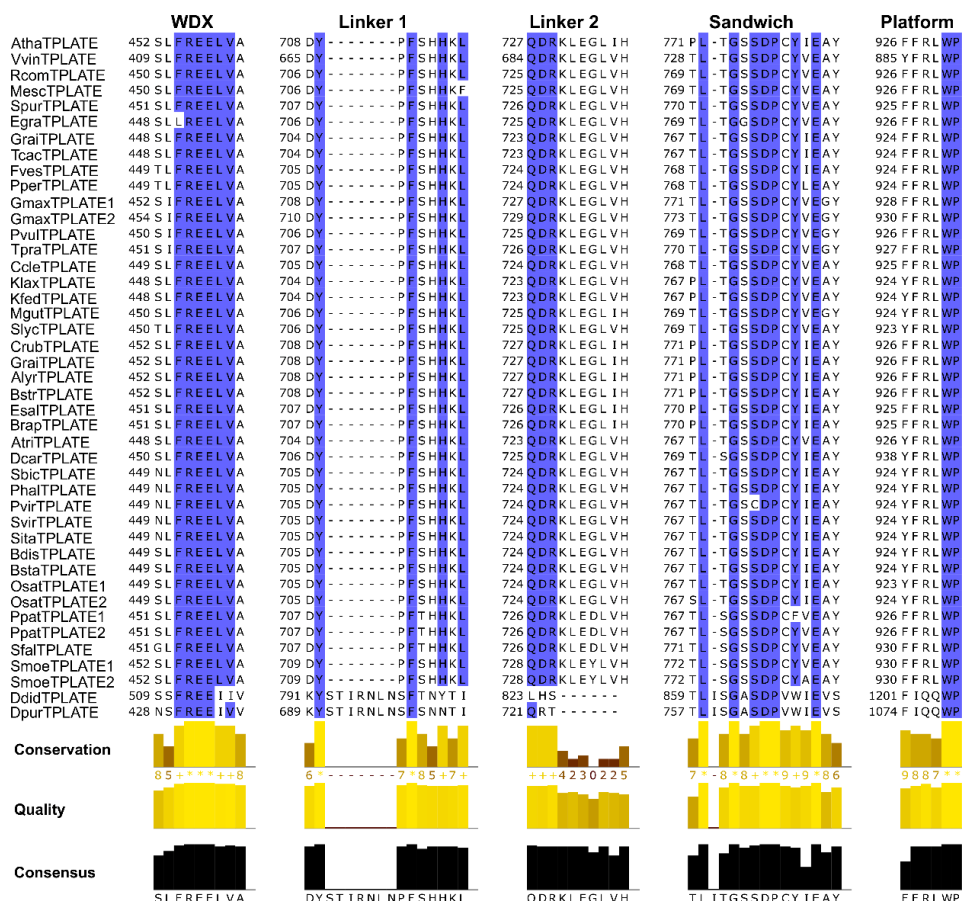


Figure S1. Identifying the highly conserved motifs in TPLATE across plant species as well as Dictyostelium.

Multiple sequence alignment of selected motifs from TPLATE proteins across selected plant species as well as selected amoebas. Only the sequences of selected motifs are shown. The alignment sequences only show the information about the selected motifs. Atha - *Arabidopsis thaliana*, Vvin - *Vitis vinifera*, Rcom - *Ricinus communis*, Mesc - *Manihot esculenta*, Spur - *Salix purpurea*, Egra - *Eucalyptus grandis*, Grai - *Gossypium raimondii*, Tcac - *Theobroma cacao*, Fves - *Fragaria vesca*, Pper - *Prunus persica*, Gmax - *Glycine max*, Pvul - *Phaseolus vulgaris*, Tpra - *Trifolium pretense*, Ccle - *Citrus clementina*, Klax - *Kalanchoe laxiflora*, Kfed - *Kalanchoe fedtschenkoi*, Mgut - *Mimulus guttatus*, Slyc - *Solanum lycopersicum*, Crub - *Capsella rubella*, Grai - *Gossypium raimondii*, Alyr - *Arabidopsis lyrata*, Bstr - *Boechera stricta*, Esal - *Eutrema salsugineum*, Brap - *Brassica rapa*, Atri - *Amborella trichopoda*, Dcar - *Daucus carota*, Sbic - *Sorghum bicolor*, Phal - *Panicum hallii*, Pvir - *Panicum virgatum*, Svir - *Setaria viridis*, Sita - *Setaria italica*, Bdis - *Brachypodium distachyon*, Bsta - *Brachypodium stacei*, Osat - *Oryza sativa*, Ppat - *Physcomitrella patens*, Sfal - *Sphagnum fallax*, Smoe - *Selaginella moellendorffii*, Ddid - *Dictyostelium discoideum*.

Chapter 3

Table 1. Segregation analysis of the TPLATE T-DNA in the offspring of *tplate* (+/-) plants expressing TPLATE motif substitution isoforms.

Segregation ratios of the progeny of *tplate* heterozygous mutants carrying various TPLATE motif substitution constructs. The male sterility phenotype of the *tplate* T-DNA insertion line causes the ratio between T-DNA: WT among the offspring progeny of *tplate* heterozygous mutants to equal 1:1. The ratio of T-DNA: WT among T2 transgenic plants of *tplate* mutants expressing TPLATE motif substitution constructs were identified by genotyping PCR to evaluate their functionality. At least 3 individual transgenic lines carrying TPLATE motif substitutions constructs were analyzed. The Chi square test was used to test whether the segregation ratio deviated from 1:1. $\chi^2_{0.05}(1) = 3.841$.

Mutant lines	Line Nr	T-DNA	WT	total	χ^2 (1:1)
mEF-loop1	-1	12	10	22	0.182
	-2	15	9	24	1.500
	-3	17	7	24	4.167
	Total	44	26	70	4.620
mEF-loop2	-1	16	8	24	2.667
	-2	22	2	24	16.667
	-3	17	7	24	4.167
	Total	55	17	72	20.056
mWDX1	-1	18	6	24	6.000
	-2	20	4	24	10.667
	-3	18	6	24	6.000
	Total	56	16	72	22.220
mWDX2	-1	21	3	24	13.500
	-2	22	2	24	16.667
	-3	18	6	24	6.000
	Total	61	11	72	34.720
mLinker1	-1	18	6	24	6.000
	-2	19	5	24	8.167
	-3	18	6	24	6.000
	Total	55	17	72	20.050
mLinker2	-1	16	8	24	2.667
	-2	20	4	24	10.667
	-3	21	3	24	13.500
	Total	57	15	72	24.500
mSandwich	-1	13	11	24	0.167
	-2	12	12	24	0.000
	-3	13	11	24	0.167
	Total	38	34	72	0.174

Chapter 3

(continued)					
	-1	11	13	24	0.167
	-2	8	14	22	1.637
mPlatform	-3	12	12	24	0.000
	Total	31	39	70	0.914

Materials and methods

Construction of multiple sequence alignment

To identify TPLATE homologues, the predicted proteins of each genome were searched using BLASTP (Altschul et al., 1997) with Arabidopsis TPLATE as an input sequence. Used databases were GenBank (<https://www.ncbi.nlm.nih.gov/genbank/>) and Joint Genome Institute (<https://genome.jgi.doe.gov/portal/>). Multiple sequence alignment was constructed with the MAFFT algorithm in eins mode (Kato et al., 2019) and visualized by the Jalview program (Waterhouse et al., 2009).

Molecular cloning

Primers used to generate TPLATE motif substitution fragments are listed in Table 2. Constructs carrying various mutations in conserved regions of TPLATE were generated by mutagenesis PCR. Two step PCR reactions were performed to introduce the mutations. The entry clone pDONR207-TPLATE without stop codon (Van Damme et al., 2004) was used as template with the combinations of sewing primers and mutation primers to obtain the mutated fragments respectively. Then sewing PCR reaction were performed with the mixture of mutation fragments as template and combinations of sewing primers. To generate the mEF-loop2 substitution isoform, two step PCR reactions was performed with mEF-loop1 as a template. To generate domain substituted TPLATE entry clones, all sewing PCR products were introduced into pDONR221 via Gateway BP reactions (Invitrogen) confirmed by sequencing.

To yield the expression constructs, the TPLATE and TPLATE motifs substituted entry clones were combined with pB7m34GW (Karimi et al., 2007), pDONRP4-P1r-Lat52 (Van Damme et al., 2006), and pDONRP2R-P3-EGFP (Van Damme et al., 2006) in triple gateway LR reactions (Invitrogen).

Arabidopsis transgenic lines and growth condition

Transgenic lines expressing isoforms of TPLATE are listed in Table 3. All the plants are in the Columbia-0 ecotype. The *tplate* heterozygous mutant plants, confirmed by genotyping PCR, were transformed by floral dip with various expression constructs of TPLATE substitution motifs fused to GFP under the control of the pLAT52 promoter, similar to the original complementation approach (Van Damme et al., 2006). Primary transformants (T1) were selected on ½ MS plate supplemented with 10mg/L Basta. All the resistant T1 plants put on soil were identified by genotyping PCR to identify transgenic plants possessing the *tplate* T-DNA insertion. Genotyping PCR reactions were performed again on T2 transgenic plants expressing different TPLATE motif substitution expression constructs to identify homozygous *tplate* mutants. Genotyping PCR was performed with genomic DNA extracted from rosette leaves. Genotyping LP and RP primers for *tplate* are described before (Van Damme et al., 2006), and the primer LBb 1.3 provided by SIGnAL website was used for T-DNA-specific primer.

To obtain dual-marker lines, mTPLATE/mSandwich/mPlatform and mWDX2-GFP expressing plants were crossed with 35Spro::DRP1a-mRFP expressing plants (Mravec et al., 2011), respectively. F1 plants (DRP1a cross with mSandwich and mPlatform plants) or F3 plants in the *tplate* homozygous background (DRP1a crossed with TPLATE and mWDX2 plants) were used to image.

Seeds were sterilized by chlorine gas sterilization and sown on ½ MS medium plates following a 3-day vernalization at 4°C. Then plates were exposed to continuous light at 21°C. To image the etiolated hypocotyls, plates were exposed to continuous light for 6 h and the kept in dark for 3 days.

Staining for live cell imaging

FM4-64 (Invitrogen) was stored at 4°C in 2 mM stock aliquots in water and protected from light at all times. Whole *Arabidopsis* seedlings were incubated

Chapter 3

with 1/2 strength MS liquid medium containing 2 μ M FM4-64 at room temperature for 15 minutes prior to confocal imaging.

Live cell imaging

The subcellular localization of TPLATE and TPLATE motif substitution isoforms was addressed by imaging root meristematic epidermal cells of 4 to 5-day-old seedlings on a Zeiss 710 inverted confocal microscope equipped with the ZEN 2009 software package and using a C-Apochromat 40x water Korr M27 objective (NA 1.2). EGFP was visualized with 488 nm laser excitation and 500-550 nm spectral detection and FM4-64 was visualized using 561 nm laser excitation and 650-750 nm spectral detection.

Dynamic imaging of TPLATE and TPLATE motif substitution isoforms at the PM was performed in etiolated hypocotyl epidermal cells using a Nikon Ti microscope equipped with an Ultraview spinning-disk system and the Volocity software package (PerkinElmer) as described previously (Gadeyne et al., 2014; Wang et al., 2019). Images were acquired with a 100 \times oil immersion objective (Plan Apo, NA = 1.45). The CherryTemp system (chapter 2) was used to maintain the temperature of samples constant at 20 $^{\circ}$ C during imaging.

Seedlings expressing GFP fused proteins were imaged with 488nm excitation light and an emission window between 500 nm and 530 nm in single camera mode, or 500 to 550 nm in dual camera mode. Seedlings expressing mRFP and tagRFP labeled proteins were imaged with 561 nm excitation light and an emission window between 570nm and 625nm in single camera mode or 580 to 630 nm in dual camera mode. Single-marker line movies were acquired with an exposure time of 500 ms/frame for 2 minutes. Dual-color lines were acquired either sequentially (one camera mode) or simultaneously (two camera mode) with an exposure time of 500 ms/frame. Single camera mode was used for density (TPLATE and mWDX2 plants), colocalization (TPLATE-DRP1a, mSandwich-DRP1A and mPlatform-DRP1a) and lifetime (TPLATE and TPLATE motif substitution isoforms) measurements. Dual camera mode was

Chapter 3

used for lifetime (TPLATE-DRP1a, WDX2-DRP1a) measurements.

Kymographs were generated using the Volocity software package and the lifetimes of individual endocytosis events were measured manually from the generated kymographs. Only endocytic events with a clear start or end present during the duration of the time lapse were retained for the measurements.

Density of endocytic dots were performed with movies exported from Volocity software package using ImageJ software. Movies were processed with “Walking Average” tool (Number of frames to average, 4) and following with Z-project of first 10 frames (with Max Intensity). Number of endocytic dots in certain region were counted using “Find Maxima” tool. To determine the threshold of “Prominence” when do the “Find maxima”, the Z-project images were processed with “MorphoLibJ” plugin (Plugins >>> MorphoLibJ>>> Morphological filters >>> Operation “White TOP Hat”; Element “disk”; Radius “2”) to get rid of background. Then the images were processed with “Gaussian Blur” filter (sigma =10) and run “Histogram” to get the “max value” for the “Prominence” threshold. Images after being processed with “MorphoLibJ” plugin were used to count endocytic dots.

Arabidopsis seedling protein extraction

Arabidopsis seedlings were grown for seven days on ½ MS medium under constant light. Seedlings were harvested, flash frozen and grinded in liquid nitrogen. Proteins were extracted in a 1:1 ratio, buffer (ml): seedlings(g), in HB+ buffer, as described before (Van Leene et al., 2007). Protein extracts were incubated for 30 min at 4°C on a rotating wheel before spinning down twice at 20000 g for 20 min. The supernatant was measured using Qubit (Thermofisher) and equal amount of proteins were loaded for analysis.

SDS-PAGE and western blot

Antibodies used in this study are listed in Table 4. Samples were analyzed by loading on 4-20% gradient gels (Biorad), after addition of 4x Laemmli sample

buffer (Biorad) and 10x NuPage sample reducing agent (Invitrogen). Gels were transferred to PVDF or Nitrocellulose membranes using the Trans-Blot® Turbo™ system (Biorad). Blots were imaged on a ChemiDoc™ Imaging System (Biorad) and the ImageJ program was used for a quantitative analysis.

Identification of interacting proteins using IP/MS-MS

Immunoprecipitation experiments were performed for three biological replicates as described previously (De Rybel et al., 2013), using 3g of 4-day old seedlings from TPLATE-GFP, Sandwich-GFP or Platform-GFP transgenic lines. Interacting proteins were isolated by applying total protein extracts to α GFP-coupled magnetic beads (Milteny Biotech). Three replicates of T-Plate-GFP (see Supplemental Dataset 1_tab 2A), Sandwich-GFP (see Supplemental Dataset 1_tab 2B) or Platform-GFP (see Supplemental Dataset 1_tab 2C) were compared to three replicates of 3g seedlings of Col-0 WT controls. Tandem mass spectrometry (MS) and statistical analysis using MaxQuant and Perseus software was performed as described previously (Wendrich et al., 2017).

Peptides were analyzed by LC-MSMS on Q Exactive (ThermoFisher Scientific) as previously reported (Nelissen et al., 2015). The raw data was searched with MaxQuant (Tyanova et al., 2016) using standard parameters (Supplemental Table 1). To determine the significantly enriched proteins in bait samples versus control samples, the MaxQuant protein groups file (Supplemental Dataset 1) was uploaded in Perseus software (Tyanova et al., 2016). Reverse, contaminant and only identified by site identifications were removed, samples were grouped by the respective triplicates and filtered for minimal 2 valid values per triplicate. LFQ values were transformed to log₂, and missing values were imputed from normal distribution using standard settings in Perseus, width of 0.3 and down shift of 1.8. Next, ttests were performed using the logged LFQ values, and the result was visualized in volcano plots, using permutation-based FDR to determine the significantly different proteins between bait and control. As cut-off, FDR=0.05, S0=1 was applied. Lists of the significantly enriched

Chapter 3

proteins with each of the baits can be found in Supplemental Dataset (2A, 2B, 2C). Mass spec data can be visited via the following link:
<https://floppy.psb.ugent.be/index.php/apps/files/?dir=/Mass%20spec%20data&fileid=4200182>

Chapter 3

Table 2. Primers used for mutagenesis PCR.

Primer name	Sequence
Sewing primer	Fwd ggggacaagttgtacaaaaagcaggctATGGACATTCTTTTGCTCAGATCC
	Rev ggggaccacttgtacaagaagctgggtGTAACTTTGGTATATTTCTATCTTTGCA
mEF-loop1	Fwd ATGCCACCGTTGTGGCCTCCAACGCCGCGAAGCTGGTTGG
	Rev CCAACCAGCTTCGCGGCCTGGAGGCCACAACGGTGGCAT
mEF-loop2	Fwd TCTCAGCGTTGGTTACCCATTTGGCGCCATTCTTGG
	Rev ACCAACGCTGAGACGCCAACCCAGCTTCGCG
mWDX1	Fwd TTAGCAGCTAGACGACTGGTGGCAATGCTTGTGGAAAGC
	Rev CAGTCGTCTAGCTGCTAAGCTCTTACTGGTAACACTATTGAGATCATCTTT AATCCTTG
mWDX2	Fwd TTAGCGGCAGCTAGACGAGCATTATTGATGCTTGTGGAAAGCTGCTTCC AGTTG
	Rev CAATAATGCTCGTCTAGCTGCCGCTAACTTACTGGTAACACTATTGAGAT CATCTTTAATCCTTGC
mLinker1	Fwd GGTGCAGGCGGTGCTGGAGGTGCAGGAAGTTCAGTTTACGAACCA TCAGCTGC
	Rev TCCTGCACCTCCAGCACCGCCTGCACCTCCTTGTCTCACTAACTCCA GCCCAC
mLinker2	Fwd GGTGCAGGCGGTGCTGGAGCTGCAGGTGGAAAGGCCATTCTCGAGCT TTGGAGG
	Rev TCCACCTGCAGCTCCAGCACCGCCTGCACCAGCAGCTGATGGTTCGTA AAACTGAACAG
mSandwich	Fwd GGTGGAGCAAGCGCAGCTGCCTGCTATGGAGCAGCTTACCATTAGCA GATAAAATGATGGAAGG
	Rev TGCTCCATAGCAGGCAGCTGCGCTTGCTCCACCAGGATATGCTGTGGG AGGAACCTTGATAGAAG
mPlatform	Fwd TCTAGTCGTTTGTGAGCAAGCTTGCCAGCTGTTGCAGAGTACAC
	Rev TGCTGACAAACGACTAGACTCGACTGGTGAGATTTTGTGCGGTAG

Chapter 3

Table 3. Plants materials used in this study

	Background	Antibiotic selection	Source
<i>tplate</i>	<i>tplate (+/-), tplate (+/+)</i>	Kanamycin	(Van Damme et al., 2006)
LAT52p::TPLATE-GFP	<i>tplate (-/-)</i>	Hygromycin	(Van Damme et al., 2006)
LAT52p::TPLATE-tagRFP	<i>tplate (-/-)</i>	Hygromycin	Chapter 2
LAT52p::mEF-loop1-GFP	<i>tplate (-/-)</i>	Basta	This study
LAT52p::mEF-loop2-GFP	<i>tplate (-/-)</i>	Basta	This study
LAT52p::mWDX1-GFP	<i>tplate (-/-)</i>	Basta	This study
LAT52p::mWDX2-GFP	<i>tplate (-/-)</i>	Basta	This study
LAT52p::mLinker1-GFP	<i>tplate (-/-)</i>	Basta	This study
LAT52p::mLinker2-GFP	<i>tplate (-/-)</i>	Basta	This study
LAT52p::mSandwich-GFP	<i>tplate (+/-), tplate (+/+)</i>	Basta	This study
LAT52p::mPlatform-GFP	<i>tplate (+/-), tplate (+/+)</i>	Basta	This study
LAT52p::TPLATE-GFP x 35Sp::DRP1a-mRFP	<i>tplate(-/-) drp(+/-),</i>		This study
LAT52p::mWDX2-GFP x 35Sp::DRP1a-mRFP	<i>tplate(-/-) drp(+/-),</i>		This study
LAT52p::mSandwich-GFP x 35Sp::DRP1a-mRFP	<i>tplate(+/-) drp(+/-), F1</i>		This study
LAT52p::mPlatform-GFP x 35Sp::DRP1a-mRFP	<i>tplate(+/-) drp(+/-), F1</i>		This study

Chapter 3

Table 4. Antibodies used in this study

Antibody	dilution	Incubation time	Source
a-TPLATE2	<i>1/1000</i>	1h	(Dejonghe et al., 2019)
a-GFP-HRP	1/1000	1h-o/n	Miltenyi Biotec GFP/HRP antibody (130-091-833)
a-rabbit	1/10000	1h	Amersham ECL Mouse IgG, HRP- linked whole Ab (NA931)

References

Adamowski, M., Narasimhan, M., Kania, U., Glanc, M., De Jaeger, G., and Friml, J. (2018). A Functional Study of AUXILIN-LIKE1 and 2, Two Putative Clathrin Uncoating Factors in Arabidopsis. *Plant Cell* **30**: 700-716.

Altschul, S.F., Madden, T.L., Schaffer, A.A., Zhang, J., Zhang, Z., Miller, W., and Lipman, D.J. (1997). Gapped BLAST and PSI-BLAST: a new generation of protein database search programs. *Nucleic Acids Res* **25**: 3389-3402.

Bashline, L., Li, S., Zhu, X., and Gu, Y. (2015). The TWD40-2 protein and the AP2 complex cooperate in the clathrin-mediated endocytosis of cellulose synthase to regulate cellulose biosynthesis. *Proc Natl Acad Sci U S A* **112**: 12870-12875.

Buevich, A.V., Lundberg, S., Sethson, I., Edlund, U., and Backman, L. (2004). NMR studies of calcium-binding to mutant alpha-spectrin EF-hands. *Cell Mol Biol Lett* **9**: 167-186.

Dacks, J.B., and Field, M.C. (2018). Evolutionary origins and specialisation of membrane transport. *Curr Opin Cell Biol* **53**: 70-76.

Daum, G., Medzihradzky, A., Suzaki, T., and Lohmann, J.U. (2014). A mechanistic framework for noncell autonomous stem cell induction in Arabidopsis. *Proc Natl Acad Sci U S A* **111**: 14619-14624.

De Rybel, B., Moller, B., Yoshida, S., Grabowicz, I., Barbier de Reuille, P., Boeren, S., Smith, R.S., Borst, J.W., and Weijers, D. (2013). A bHLH complex controls embryonic vascular tissue establishment and indeterminate growth in Arabidopsis. *Dev Cell* **24**: 426-437.

Dejonghe, W., et al. (2019). Disruption of endocytosis through chemical inhibition of clathrin heavy chain function. *Nat Chem Biol* **15**: 641-649.

Fan, L., Hao, H., Xue, Y., Zhang, L., Song, K., Ding, Z., Botella, M.A., Wang, H., and Lin, J. (2013). Dynamic analysis of Arabidopsis AP2 sigma subunit reveals a key role in clathrin-mediated endocytosis and plant development. *Development* **140**: 3826-3837.

Gadeyne, A., et al. (2014). The TPLATE adaptor complex drives clathrin-mediated endocytosis in plants. *Cell* **156**: 691-704.

Hirst, J., Schlacht, A., Norcott, J.P., Traynor, D., Bloomfield, G., Antrobus, R., Kay, R.R., Dacks, J.B., and Robinson, M.S. (2014). Characterization of TSET, an ancient and widespread membrane trafficking complex. *eLife* **3**: e02866.

Janssens, V., Jordens, J., Stevens, I., Van Hoof, C., Martens, E., De Smedt, H., Engelborghs, Y., Waelkens, E., and Goris, J. (2003). Identification and functional analysis of two Ca²⁺-binding EF-hand motifs in the B"/PR72 subunit of protein phosphatase 2A. *J Biol Chem* **278**: 10697-10706.

Karimi, M., Depicker, A., and Hilson, P. (2007). Recombinational cloning with plant gateway vectors. *Plant Physiol* **145**: 1144-1154.

Chapter 3

Katoh, K., Rozewicki, J., and Yamada, K.D. (2019). MAFFT online service: multiple sequence alignment, interactive sequence choice and visualization. *Brief Bioinform* **20**: 1160-1166.

Moulinier-Anzola, J., Schwihla, M., De-Araujo, L., Artner, C., Jorg, L., Konstantinova, N., Luschnig, C., and Korbei, B. (2020). TOLs Function as Ubiquitin Receptors in the Early Steps of the ESCRT Pathway in Higher Plants. *Mol Plant* **13**: 717-731.

Mravec, J., et al. (2011). Cell plate restricted association of DRP1A and PIN proteins is required for cell polarity establishment in Arabidopsis. *Curr Biol* **21**: 1055-1060.

Nelissen, H., et al. (2015). Dynamic Changes in ANGUSTIFOLIA3 Complex Composition Reveal a Growth Regulatory Mechanism in the Maize Leaf. *Plant Cell* **27**: 1605-1619.

Perales, M., Rodriguez, K., Snipes, S., Yadav, R.K., Diaz-Mendoza, M., and Reddy, G.V. (2016). Threshold-dependent transcriptional discrimination underlies stem cell homeostasis. *Proc Natl Acad Sci U S A* **113**: E6298-E6306.

Rodriguez, K., Perales, M., Snipes, S., Yadav, R.K., Diaz-Mendoza, M., and Reddy, G.V. (2016). DNA-dependent homodimerization, sub-cellular partitioning, and protein destabilization control WUSCHEL levels and spatial patterning. *Proc Natl Acad Sci U S A* **113**: E6307-E6315.

Tyanova, S., Temu, T., Sinitcyn, P., Carlson, A., Hein, M.Y., Geiger, T., Mann, M., and Cox, J. (2016). The Perseus computational platform for comprehensive analysis of (prote)omics data. *Nat Methods* **13**: 731-740.

Van Damme, D., Bouget, F.Y., Van Poucke, K., Inze, D., and Geelen, D. (2004). Molecular dissection of plant cytokinesis and phragmoplast structure: a survey of GFP-tagged proteins. *Plant J* **40**: 386-398.

Van Damme, D., Coutuer, S., De Rycke, R., Bouget, F.Y., Inze, D., and Geelen, D. (2006). Somatic cytokinesis and pollen maturation in Arabidopsis depend on TPLATE, which has domains similar to coat proteins. *Plant Cell* **18**: 3502-3518.

Van Damme, D., Gadeyne, A., Vanstraelen, M., Inze, D., Van Montagu, M.C., De Jaeger, G., Russinova, E., and Geelen, D. (2011). Adaptin-like protein TPLATE and clathrin recruitment during plant somatic cytokinesis occurs via two distinct pathways. *Proc Natl Acad Sci U S A* **108**: 615-620.

Van Leene, J., et al. (2007). A tandem affinity purification-based technology platform to study the cell cycle interactome in Arabidopsis thaliana. *Mol Cell Proteomics* **6**: 1226-1238.

Wang, P., et al. (2019). Plant AtEH/Pan1 proteins drive autophagosome formation at ER-PM contact sites with actin and endocytic machinery. *Nat Commun* **10**: 5132.

Waterhouse, A.M., Procter, J.B., Martin, D.M., Clamp, M., and Barton, G.J. (2009). Jalview Version 2--a multiple sequence alignment editor and analysis workbench. *Bioinformatics* **25**: 1189-1191.

Wendrich, J.R., Boeren, S., Moller, B.K., Weijers, D., and De Rybel, B. (2017). In Vivo Identification of Plant Protein Complexes Using IP-MS/MS. *Methods Mol Biol* **1497**: 147-158.

Chapter 3

Yperman, K., et al. (2020). The TPLATE subunit is essential for structural assembly of the endocytic TSET complex.

Zhang, Y., Persson, S., Hirst, J., Robinson, M.S., van Damme, D., and Sanchez-Rodriguez, C. (2015). Change your TPLATE, change your fate: plant CME and beyond. *Trends Plant Sci* **20**: 41-48.

Chapter Four

Conditional destabilization of the TPLATE complex impairs endocytosis rather than autophagy

Jie Wang^{1,2}, Klaas Yperman^{1,2}, Peter Grones^{1,2}, Qihang Jiang^{1,2}, Dominique Eeckhout^{1,2}, Jonah Nolf^{1,2}, Bert De Rybel^{1,2}, Roman Pleskot^{1,2*} & Daniël Van Damme^{1,2*}

¹Ghent University, Department of Plant Biotechnology and Bioinformatics, Technologiepark 71, 9052 Ghent, Belgium

²VIB Center for Plant Systems Biology, Technologiepark 71, 9052 Ghent, Belgium

Data in this chapter together with part of chapter three was prepared as story which addresses a heat-inducible tool that delocalizes TPLATE from PM to manipulate endocytosis (Conditional destabilization of the TPLATE complex impairs endocytic internalization). The manuscript is currently being submitted for publication.

Author Contributions: JW, RP and DVD designed the experiments. JW generated all experimental materials and performed the overall majority of the experiments. PG performed the immunolocalization experiments. DE, EM, JN and BDR performed the IP-MS experiments and analysis. KY and QJ helped with phenotyping experiments and biochemistry. JW wrote the manuscript. RP and DVD guided this project and contributed to the revision of this chapter.

Abstract

Clathrin-mediated endocytosis (CME) is the best-characterized endocytic pathway to regulate plasma membrane protein turnover and the octameric TPLATE complex (TPC) serves as an essential adaptor complex in this process. Two subunits of TPC, AtEH1/Pan1 and AtEH2/Pan1 drive autophagosome formation and recruit several other endocytic players, which are also degraded in the vacuole under nutrient stress conditions. However, whether TPC as a whole is required to drive autophagy in plants or whether this represents an independent function of the AtEH/Pan1 proteins remains unknown. Here, we showed previously that mutating a specific motif of TPLATE results in destabilizing TPC and we termed this unstable form of TPLATE, WDX (安定性). We further develop mWDX2 as a heat-inducible tool to inactivate TPC. This tool allows us to study the immediate effect of disrupting TPC function on endocytosis and autophagy. TPC harboring mWDX2 is hypersensitive to short-term heat stress, which causes the delocalization of TPLATE away from the PM and causes it to aggregate in the cytoplasm within few hours. Mild heat stress also causes seedling lethality upon prolonged exposure. mWDX plants and autophagy mutants exhibit differential phenotypes under heat stress and carbon starvation conditions. Heat stress-induced aggregated as well as ubiquitinated proteins accumulated heavily in the absence of a functional TPC and this was independent of the autophagosomal degradation pathway. TPC inactivation by short-term heat stress did not impair autophagosome formation, while it highly efficiently inhibited endocytosis. These data together reveal that the whole TPC is essential for endocytosis while not for autophagy. Our data therefore support the hypothesis that AtEH/Pan1 proteins function in autophagy independent of the other TPC subunits.

Introduction

To regulate a plethora of physiological processes to allow efficient growth and to respond to ever changing environmental conditions, plants require to regulate the turnover of extracellular and plasma membrane materials as well as the intracellular materials efficiently. Plant cells employ endocytosis to regulate the turnover of extracellular and plasma membrane materials. Endocytosis is a conserved pathway in which cargo is internalized from the extracellular space and the plasma membrane via transport vesicles. These vesicles are either recycled back to the plasma membrane or, they are targeted to the vacuole for degradation (Roy et al., 2014). Endocytic internalization is essential for plants to regulate a plethora of physiological processes such as hormone responses (Paciorek et al., 2005; Sutter et al., 2007; Irani et al., 2012; Di Rubbo et al., 2013; Du et al., 2013; Yu et al., 2016), pathogenic defense responses (Smith et al., 2014b; Smith et al., 2014a; Mbengue M, 2016; Xiaoyang, 2017) and nutrient availability (Takano et al., 2010; Barberon et al., 2011; Yoshinari et al., 2019).

Clathrin-mediated endocytosis (CME) is the best-characterized endocytosis mechanism in plants. As clathrin does not bind directly to the membrane or to cargo receptors, adaptor proteins act as essential link between the clathrin coat and the plasma membrane (McMahon and Boucrot, 2011; Zhang et al., 2015; Paez Valencia et al., 2016). Two early adaptor protein complexes coexist on the PM: the canonical AP-2 complex and the newly identified TPLATE complex (TPC) in plants (Di Rubbo et al., 2013; Gadeyne et al., 2014). AP-2 comprises of two large (AP2A and AP2B or α and β), one medium (AP2M or μ) and one small subunit (AP2S or σ)(Di Rubbo et al., 2013). The AP-2 complex is essential in animals (Mitsunari et al., 2005), while plants that lack AP-2 subunits (*Arabidopsis* mutants for AP-2 α -, μ -, and σ -subunits) are still viable. TPC was identified as an octameric complex that functions as essential CME adaptor proteins in plants (Gadeyne et al., 2014). Although yeast and metazoans lack

Chapter 4

clearly definable TPC subunit homologs, TPC was identified as a hexameric complex in *Dictyostelium*, which is however not essential anymore (Hirst et al., 2014). Indicative its critical function in plants, knockout of single TPC subunit leads to pollen lethality and knockdown TPC single subunits results in seedling lethality (Van Damme et al., 2006; Gadeyne et al., 2014; Wang et al., 2019), which strongly prevents any functional genetic approach to reveal TPC function. The analysis of inducible knockdown mutants (estradiol-induced expression of *amiR-TML* and *amiR-TPLATE*) reveals defective internalization of various PM proteins including BRI1, PIN1, PIN2 and cellulose synthase complexes (CESA) (Gadeyne et al., 2014; Sanchez-Rodriguez et al., 2018). Reduced internalization of CESA was also observed in the non-lethal allele *twd40-2-3*, which is a weak allele of TWD40-2 that affects this particular TPC subunit's expression as *twd40-2-1* and *twd40-2-2* are male sterile (Gadeyne et al., 2014; Bashline et al., 2015). However, functionality of TPC during CME still remains largely unknown during plant development.

In addition to endocytosis, plants utilize autophagy to regulate the turnover of intracellular materials such as cytoplasmic proteins and organelles to maintain cellular homeostasis. Autophagy is a conserved intracellular degradation process to degrade cytoplasmic components, including dysfunctional or unnecessary proteins and organelles, by sequestering them into autophagosomes, which are double-membraned vesicles. The cargo engulfed by autophagosomes is then trafficked to the vacuole to be degraded (Avin-Wittenberg et al., 2018; Marshall and Vierstra, 2018; Avin-Wittenberg, 2019). Autophagy functions essentially to regulate fitness, longevity, and fecundity, underpinning plant tolerance to various biotic and abiotic stresses (Avin-Wittenberg et al., 2018; Marshall and Vierstra, 2018; Avin-Wittenberg, 2019). Plants with an impaired autophagy mechanism (*atg* mutants) display early senescence, hypersensitivity to abiotic stresses, and susceptibility to carbon and nitrogen starvation (Hanaoka et al., 2002; Thompson et al., 2005; Chung et al., 2010; Suttangkakul et al., 2011; Zhou et al., 2013; Baxter et al., 2014; Li et al.,

Chapter 4

2014; Qi et al., 2017; Huang et al., 2019; Wang et al., 2019).

The two TPC subunits, AtEH1 and AtEH2, were not associated with the other TPC core components when the complex was forced into the cytoplasm by truncating the TML subunit. Similarly, these proteins did not co-purify with the other complex proteins in *Dictyostelium*, suggesting that they may be auxiliary components to the core TPC complex (Gadeyne et al., 2014; Hirst et al., 2014). Both AtEH proteins show homology with the yeast ARP2/3 complex activator Pan1p, and therefore were named as AtEH1/Pan1 and AtEH2/Pan1 (Wang et al., 2019). Our recent work showed that AtEH/Pan1 proteins are also involved in actin cytoskeleton regulated autophagy (Wang et al., 2019). AtEH/Pan1 proteins co-localized with both early and mature autophagosome markers. Enhanced expression of AtEH/Pan1 proteins boosts actin-dependent autophagy while lowering AtEH/Pan1 expression reduces autophagosome formation under stress conditions. Besides, AtEH/Pan1 and ATG8-positive autophagosomes also recruit several other endocytic players and some of those have been shown to be also degraded in the vacuole under nutrient stress conditions (Wang et al., 2019). However, whether TPC as a whole is required to drive autophagy in plants or whether this represents an independent function of the AtEH/Pan1 proteins, with the remaining endocytic proteins being rather cargo remains unknown.

In my previous chapter (chapter 3), I identified WDX domain substitutions in TPLATE as partially functional TPLATE alleles with a delay in endocytosis. Here, I show that substituting the WDX domains leads to a destabilization of the whole TPC. Moreover, short-term heat treatment enhances this destabilization and boosts the PM delocalization and aggregation of TPLATE in the cytoplasm, which results in a quick disruption of TPC function. We employed this heat-inducible inactivated TPC to further study TPC-dependent endocytosis as well as understand its role in autophagy.

Results

Substitutions in the WDX domain destabilize the whole TPC

In my previous chapter, our western blots results suggested the stability issues in the mWDX alleles as the protein levels of TPLATE-GFP in *tplate* (-/-) were relatively similar to the levels of endogenous TPLATE in Col-0, while full length bands of mWDX-GFP were significantly weaker for several independent lines (Chapter 3, Figure 3). To examine the stability of TPLATE, mWDX1 and mWDX2, transgenic lines were analyzed via co-immunoprecipitation (Co-IP) experiments. Our Co-IP analysis revealed increased degradation of the bait proteins mWDX1-GFP and mWDX2-GFP compared to TPLATE-GFP (Fig. 1A) and a reduced amount of the other subunits WD40-2 and AtEH1/2 co-purifying together with both mWDX isoforms (Fig. 1B). These results suggested that substituting the WDX motif therefore seems to not only destabilize TPLATE, but also likely impairs the interactions between TPLATE and the other complex subunits. To confirm the destabilization of whole TPC, we performed IP-MS experiments with TPLATE and mWDX transgenic lines. To do this, we only took into account peptides that were identified in all three experiments. We calculated the average intensity of all common peptides and normalized this to the intensities of the common peptides of the bait. Relative to the bait protein, the average intensity of commonly detected peptides for all other TPC subunits as well as DRP1a was strongly reduced in mWDX alleles compared to the non-mutated TPLATE (Fig. 1C). Our MS results further confirmed the destabilization of the whole TPC in mWDX alleles. These results together revealed that WDX domain is essential to maintain the stability of the TPC.

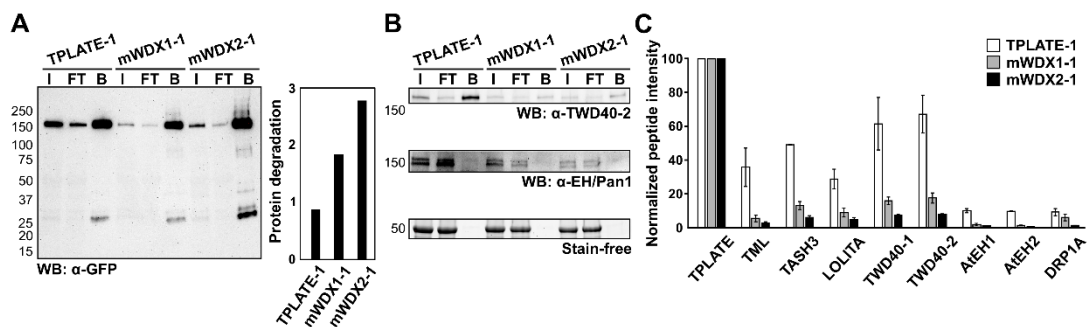


Fig 1. WDX domain substitutions destabilize the whole TPC

(A) Co-IP of complemented TPLATE and mWDX complemented lines. Input (I), flow through (FT) and bound fractions were analyzed using an anti-GFP antibody. Protein degradation was quantified as the ratio between the grey value of the full-length band and all smaller degradation bands from panel A.

(B) TPC subunit interaction analysis using anti-TWD40-2 and anti-EH/Pan1 antibodies on Input (I), flow through (FT) and bound (B) fractions. Stain-free detection was used as loading control.

(C) MS analysis following co-IP on complemented TPLATE and mWDX lines. For each TPC subunit, the intensity of peptides present in all experiments was averaged and normalized to the value of the bait protein. Standard deviations are based on three technical repeats.

Destabilizing TPC does not lead to visible developmental defects in seedlings

Compared with the loss-of-function mutants *twd40-2-1* and *twd40-2-2*, which are male sterile (Gadeyne et al., 2014), the weak allele *twd40-2-3* is viable due to the mild reduction of TWD40-2 and exhibit mild reduction of root and hypocotyl growth compared to WT plants (Bashline et al., 2015). In addition to severe seedling growth retardation, inducible downregulation of TPLATE and TML also results in defects in graviperception (Gadeyne et al., 2014). Given that mWDX is a destabilizing form of TPLATE, which destabilizes the whole TPC and impairs the efficiency of endocytosis, it may also cause plant developmental defects. We firstly examined whether destabilizing TPC by WDX substitutions would cause similar mutant phenotypes as reported for *twd40-2-3* or downregulation of TPC subunits. Our phenotypical analysis however

showed similar root growth and gravitropic responses between TPLATE and mWDX2 complemented lines (Fig S1).

To further examine whether combining mWDX alleles and *twd40-2-3* would exhibit an enhanced phenotype such as male sterility or more severe developmental defects, we crossed *twd40-2-3* into TPLATE and mWDX2 complemented lines respectively. We identified homozygous double mutants from the offspring (Fig S2 A). This revealed that mWDX2 complements the *tplate* KO mutation sufficiently and that the increased destabilization of TPC, even when combined with reduced levels of TWD40-2, fails to cause male sterility. Furthermore, mWDX2 and TPLATE in *tplate/twd40-2-3* exhibited similar root growth and hypocotyl length (Fig S2B), which is in contrast to the *ap2m-1 twd40-2-3* double mutants which exhibited enhanced defects in root growth (Bashline et al., 2015). These results together suggested that destabilizing TPC fails to cause visible developmental defects in roots as well as in hypocotyls.

Short-term heat stress induces aggregation of TPLATE proteins and results in cytoplasmic aggregation of TPLATE.

In vivo, the yields of functional protein, solubility, and proper cellular or extracellular localization are often correlated with protein stability (Goldenzweig and Fleishman, 2018). Misfolding and aggregation of proteins can be accelerated under stress, like high temperature, denaturing conditions, or altered pH (Goldenzweig and Fleishman, 2018). This is in accordance with the fact that proteins have a higher propensity to aggregate at higher temperatures (Zhou et al., 2013; Zhou et al., 2014). Given that we could not enhance the mutant phenotype of mWDX by combining it genetically with a weak allele of TWD40-2, we investigated whether we could enhance the destabilization of mWDX-containing TPC by augmenting the temperature *in vivo*. We therefore subjected TPLATE and mWDX2 complemented lines to short-term heat stress.

Time-course experiments were performed to monitor the effect of heat treatment on the TPLATE localization in TPLATE and mWDX2 complemented lines. When treated with 35 °C up to 6h, TPLATE conserved its PM localization and exhibited no aggregation in TPLATE complemented lines (Fig. 2A and Fig. S3). Conversely, mWDX2 displayed increasing sizes of cytoplasmic aggregates and gradually lost its PM localization after heat treatment, thus visualizing the heat-inducible aggregation and PM de-localization of mWDX2 mutants (Fig. 2A and Fig S3). Besides, the reduced size of aggregated TPLATE proteins as well as the increasing cytoplasmic GFP signal after 2h recovery (Fig. 2A), suggested the refolding or degradation of aggregated TPLATE proteins under normal condition.

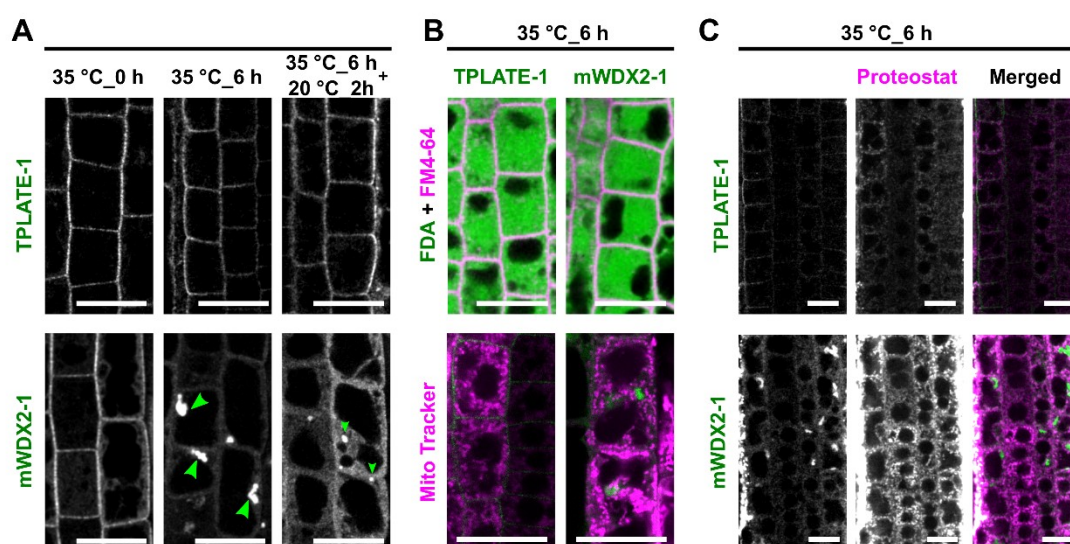


Figure 2. Short-term heat treatment induces aggregation of mWDX2.

(A) Confocal images of root cells from TPLATE and mWDX2 complemented lines subjected to short-term heat treatment followed by a recovery period. 5-day old seedlings, grown vertically on ½ MS media at 20 degrees were subjected to 35 °C for 0 h, 6 h and allowed to recover at 20°C for 2h. After treatment, seedlings were imaged immediately. Green arrowheads indicate the aggregated TPLATE proteins in the cytoplasm. Scale bars equal 20 μm.

(B) Confocal images of FDA staining (top) and Mito Tracker red (CM-H₂XRos, bottom) in TPLATE and mWDX2 complemented lines. 5-day old seedlings grown at 20 °C were treated with 35 °C for 6 hours and then stained with FDA (co-stained with FM4-64) or Mito Tracker red for 15min. Scale bar = 25 μm.

(C) Confocal images of Proteostat staining in TPLATE and mWDX2 complemented lines. 5-day old seedlings grown at 20 °C were exposed to 35 °C for 6 hours followed by Proteostat staining

Chapter 4

at 20 °C for 30 minutes. Scale bar = 25 µm.

To evaluate the cell viability, we performed FM4-64 and FDA co-staining as well as Mitotracker Red staining (Greco et al., 2012; Jones et al., 2016) on roots of TPLATE and mWDX2 complemented plants after short-term heat stress. After 35 °C treatment for 6h, both TPLATE and mWDX2 plants are able to convert FDA to its fluorescent form and show similar mitochondria staining (Fig. 2B), confirming that cell viability and mitochondrial function was not affected.

Heat shock readily causes protein misfolding and aggregation in a variety of cellular systems (Mogk et al., 2018). The ProteoStat dye binds selectively to aggregates of misfolded proteins and is widely employed to assess protein aggregates in cells and tissues (Shen et al., 2011; Nakajima and Suzuki, 2013). To compare the aggregation of proteins under our stress conditions, we performed ProteoStat staining in TPLATE and mWDX2 complemented plants after short-term heat treatment. Compared with TPLATE complemented lines, the ProteoStat application specifically revealed increased amounts of aggregated proteins in mWDX2 plants upon short-term heat stress (Fig. 2C).

Our data together revealed that short-term heat treatment induces the aggregation of TPLATE in the cytoplasm, although along with massive accumulation of aggregated proteins, but that cell viability is not differentially affected by the treatment.

Destabilizing TPC correlates with hypersensitivity to heat stress as well as accumulation of ubiquitinated proteins.

TPC is essential for plant survival as inducible knockdown of TPC single subunits results in seedling lethality (Gadeyne et al., 2014). Considering the dramatic reduction of TPLATE levels on the PM after only 6h heat treatment, we explored the effect of the reduced stability of TPLATE on seedling development. Seedlings of TPLATE and mWDX2 complemented lines were

Chapter 4

subjected to long-term heat stress. When seedlings were exposed to 35 °C for 3 days, primary root growth was dramatically reduced in mWDX2 complemented plants compared to TPLATE-GFP expressing plants (Fig. 3A). One-day prolongation of this stress caused extensive whitening of the cotyledons in mWDX2 complemented plants, unlike to TPLATE-GFP complemented lines which retained green cotyledons (Fig. 3B). To further analyze how quickly heat stress affects cellular viability, we compared root apical meristems of TPLATE and mWDX2 complemented lines following 6, 30 or 55h at 35°C. Whereas only few TPLATE seedlings showed dead root cells at these time points, all WDX2 root meristems were severely affected after 30h (Fig. S4). Our phenotypical analysis revealed that destabilizing the whole TPC by substituting the WDX domain leads to hypersensitivity to heat stress.

To further correlate TPC stability with the hypersensitivity to heat stress, we examined TPLATE protein levels in TPLATE and mWDX2 complemented plants after 3- day heat stress treatment. Heat stress hardly affected Full-length TPLATE-GFP levels, whereas only faint band remained in mWDX2 plants following heat treatment (Fig. 3C), confirming that the reduction of TPLATE protein level contributes to the inhibition of root growth under heat treatment as well as the observed seedling lethality.

Aggregation of ubiquitinated proteins by heat stress is highly proteotoxic to plants and correlates to whitening leaves (Zhou et al., 2013; Zhou et al., 2014). Given mWDX2 plants exhibited massive whitening of the leaves, we examined the accumulation of ubiquitinated proteins in TPLATE and mWDX2 complemented plants under long-term heat treatment. Along with the reduction of TPLATE proteins in mWDX2 complemented plants, western blot using anti-ubiquitin clearly showed increasing amounts of ubiquitinated proteins in mWDX2 complemented plants following heat stress, whereas levels of ubiquitinated proteins were similar at normal or elevated temperatures for TPLATE complemented plants (Fig. 3C).

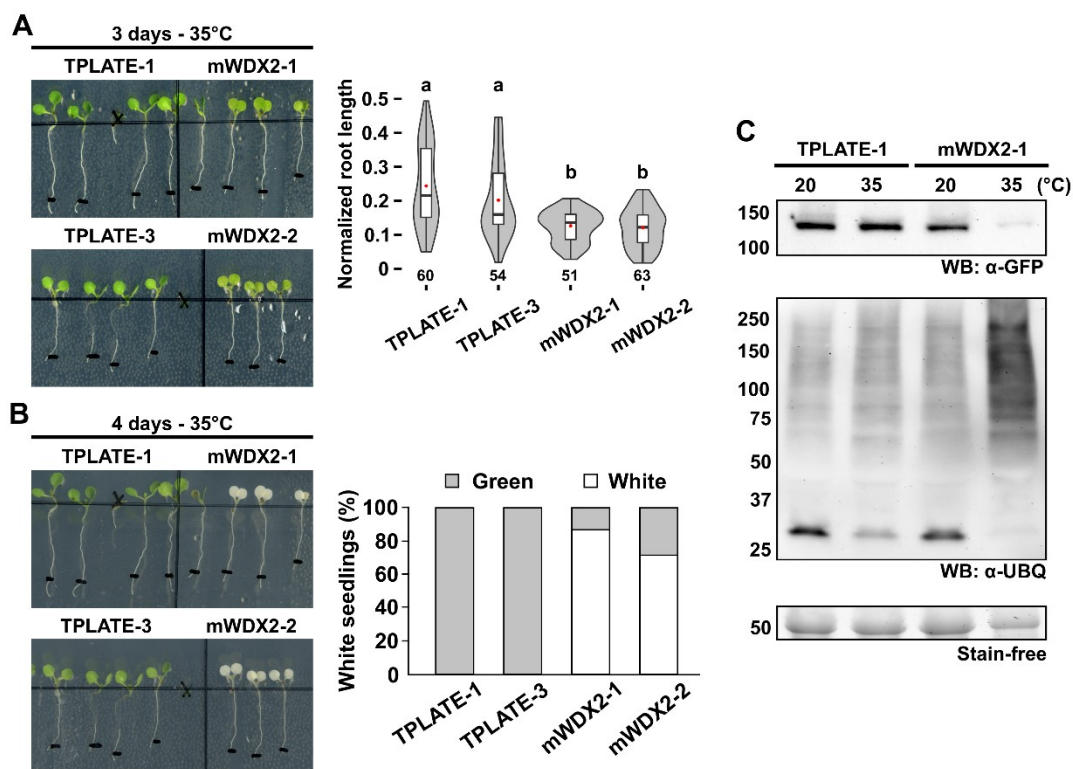


Figure 3 Heat stress hypersensitivity by destabilizing TPC in mWDX2-complemented lines correlates with the accumulation of ubiquitinated proteins.

(A) Phenotypic comparison between mWDX2 and TPLATE complemented lines in response to heat stress. Seedlings were grown vertically at 20 °C for 5 days and then moved to 35 °C for 3 days. Normalized primary root length of TPLATE versus mWDX2 lines following a 3-day heat treatment were quantified. For each seedling, root length grown at 35 °C was normalized to the root length at 20 °C. mWDX2 root length following heat treatment significantly differs from that of independent TPLATE lines (one-way anova, $p < 0.001$). The number of seedlings analyzed is indicated at the bottom of the graph.

(B) Phenotypic comparison between mWDX2 and TPLATE complemented lines in response to heat stress. The seedlings shown here are same ones as shown in panel A. Seedlings were grown vertically at 20 °C for 5 days and then moved to 35 °C for 4 days. Survival rate of TPLATE and mWDX2 complemented plants after a 4-day heat treatment were quantified. Numbers of seedlings analyzed are indicated in panel A.

(C) Western blot detection of TPLATE-GFP and mWDX2-GFP using anti-GFP and ubiquitinated proteins using anti-ubiquitin in TPLATE and mWDX2 complemented lines without or with heat treatment (35 °C for 3 days). The stain free gel detection serves as loading control.

Taken together, these results suggested that inactivating TPC by heat results in massive aggregation of misfolded and ubiquitinated proteins thus contributes to the hypersensitivity to heat stress.

The effect of destabilizing TPC is not phenocopied in atg mutants under stress.

Autophagy promotes plant viability during abiotic stress conditions, as *atg* mutants are hypersensitive to abiotic stresses (Avin-Wittenberg, 2019). The extensive whitening of cotyledons in mWDX2 complemented plants under heat stress reminded us of the senescence phenotype of autophagy-defective mutants under heat stress (Zhou et al., 2013; Zhou et al., 2014; Sedaghatmehr et al., 2019). Heat shock is proposed to induce autophagy, which then targets heat-denatured protein aggregates for degradation (Zhou et al., 2013; Yang et al., 2016; Avin-Wittenberg, 2019; Jung et al., 2020). The massive accumulation of aggregated proteins and ubiquitinated proteins under short-term and long-term heat stress, suggested the possibility that autophagy is impaired in mWDX2 plants under heat stress.

Our recent work revealed that the AtEH/Pan1 TPC subunits are involved in an actin cytoskeleton-regulated autophagy pathway between the ER-PM contact sites and the vacuole (Wang et al., 2019). To clarify whether the hypersensitivity of mWDX2 plants to heat stress is a consequence of impaired autophagy, we compared TPLATE, mWDX2 complemented lines and known *atg* mutants defective in autophagy, *atg5* and *atg7*, under heat stress. 3-day treatment of 35 °C reduced root growth in *atg5-1* and *atg7-3* mutants, compared with the TPLATE complemented line. However, root growth in mWDX2 complemented lines was more severely reduced (Fig. 4A and 4B). 4-day treatment of 35 °C caused whitening of the cotyledons in mWDX2 complemented lines, while both *atg5* and *atg7* mutants were significantly less affected and resembled the TPLATE complemented line (Fig. 4C and 4D).

Chapter 4

Besides, western blots using anti-ubiquitin further revealed the differences of accumulation of ubiquitinated proteins by heat stress between mWDX2 and *atg* mutants. After 3-day heat stress treatment, massive accumulation of ubiquitinated proteins was detected in mWDX2 plants while little increase was observed in TPLATE complemented lines as well as *atg* mutants (Fig. 4E). The different performance between mWDX2 and *atg* mutants under heat stress suggests that the hypersensitivity to heat stress in mWDX complemented plants is likely not a consequence of impaired autophagy.

Autophagy-defective mutants are typically characterized by their hypersensitivity to nutrient deprivation (Doelling et al., 2002; Hanaoka et al., 2002; Thompson et al., 2005; Xiong et al., 2005; Phillips et al., 2008; Yoshimoto et al., 2009; Chung et al., 2010; Suttangkakul et al., 2011; Li et al., 2014; Qi et al., 2017). Downregulation of AtEH/pan1 leads to susceptibility to nutrient deficiency, especially carbon depletion stress (Wang et al., 2019). To further evaluate whether destabilizing TPC results in susceptibility to nutrient deficiency, we further compared TPLATE, mWDX2 plants and *atg5* and *atg7* mutants under carbon starvation. Long-term constant dark exposure leads to significant reduction of root growth as well as yellowing of cotyledons in *atg* mutants, in contrast to TPLATE and mWDX2 complemented lines (Fig. 4F- 4H), indicating that the AtEH/Pan1-dependent actin cytoskeleton regulated autophagy pathway is not impaired in mWDX complemented plants under carbon starvation.

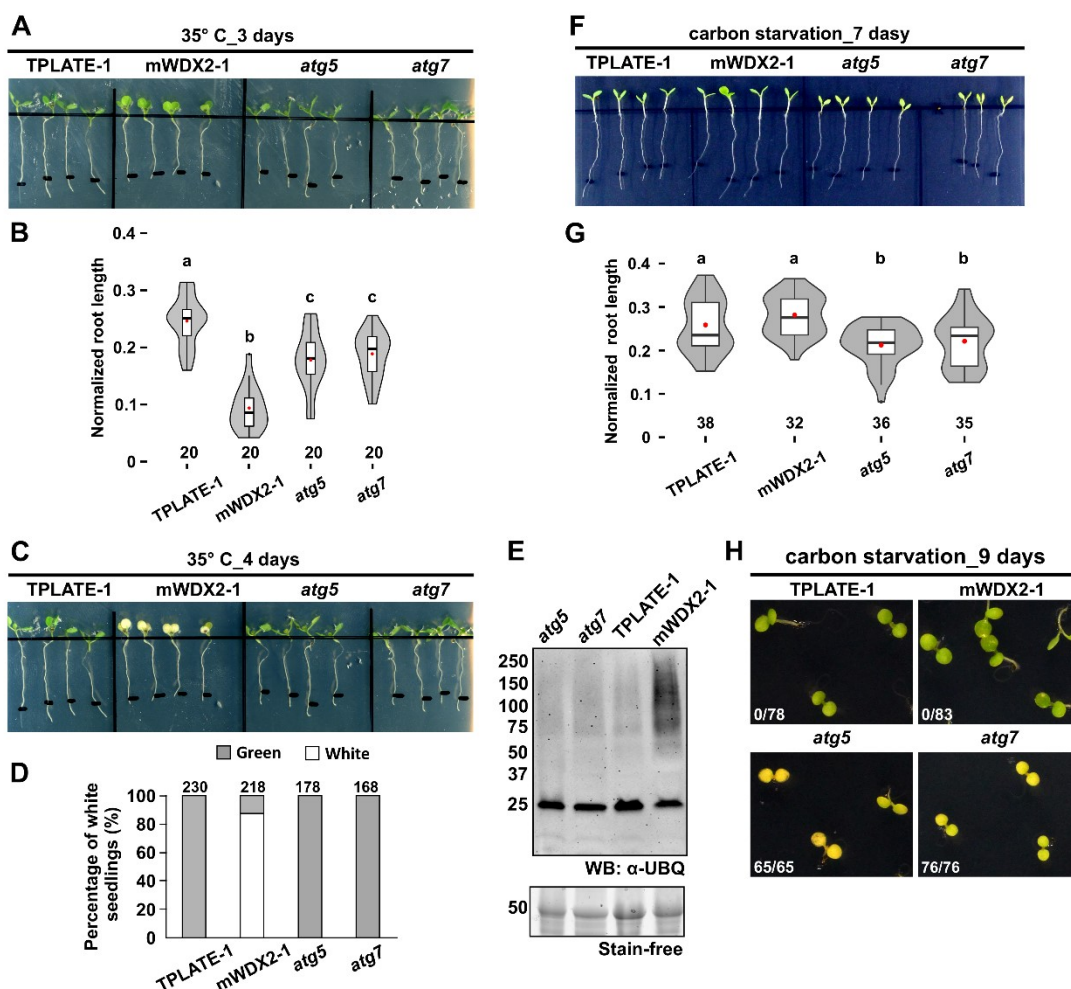


Figure 4. Destabilized TPC by mWDX2 complementation fails to phenocopy autophagy mutants under heat stress and carbon starvation.

(A-D) Phenotypical comparison between mWDX2, TPLATE complemented lines and *atg5-1* and *atg7-3* mutants in response to heat stress. Seedlings were grown vertically at 20 °C for 5 days and then moved to 35 °C for 3 days (A) or 4 days (C). Normalized primary root length of TPLATE versus mWDX2 lines following a 3-day heat treatment were quantified (B). After 4-day heat treatment, the ratio of whitening versus green seedlings was visually quantified (D). mWDX2 root length following heat treatment significantly differs from that of TPLATE, *atg5* and *atg7* (one-way anova, $p < 0.001$). The number of seedlings analyzed is indicated.

(E) Western blot detection using anti-ubiquitin with detergent for TPLATE and mWDX2 complemented lines as well as for *atg* mutants after heat treatment (35 °C for 3 days). The stain-free gel serves as loading controls.

(F-H) Seedling phenotype in response to carbon starvation of TPLATE and mWDX2 plants compared with *atg5-1* and *atg7-3* mutants. Seedlings were grown vertically or horizontally on ½ MS solid medium without sucrose at 20 °C for 5 days followed by 7-day (F) or 9-day (H) constant dark (-C). For root growth measurement, root growth grown in dark for 7 days was

Chapter 4

normalized to the 5-day root growth under light conditions (G). The numbers in the violin plot represent the number of seedlings measured. TPLATE and mWDX2 root length following carbon starvation significantly differs from that of *atg5* and *atg7* (one-way anova, $p < 0.001$). To quantify the yellowing of cotyledons, seedlings were grown horizontally and visually scored after a 9-day carbon starvation treatment.

Destabilizing TPC by short-term heat stress does not inhibit autophagy

Short-term heat shock was already employed as a strategy to study autophagy in plants (Zhou et al., 2013; Yang et al., 2016; Jung et al., 2020). To test how fast and extensive autophagy responses to our heat stress conditions, we subjected seedlings expressing the autophagic vesicle marker YFP-ATG8a to our short-term heat stress. Confocal imaging showed increasing detection of ATG8e-labelled autophagic bodies in root apical meristems within the first 6h following the start of the stress (Fig 5A). To measure the effect of short-term heat treatment on autophagic flux, we exposed YFP-ATG8e seedlings to short-term heat shock together with concanamycin A (ConcA), which suppresses autophagic body breakdown and stabilizes their contents in vacuoles (Marshall and Vierstra, 2018; Wang et al., 2019; Jung et al., 2020). Without ConcA treatment, cytoplasmic puncta decorated with YFP-ATG8e were less frequently observed in the vacuoles of root meristematic cells as well as elongated cells than upon ConcA treatment (Fig 5B). These data together suggested that short-term heat stress induces autophagy rapidly and efficiently and maintains autophagic flux, in agreement with recent published work (Jung et al., 2020).

Given the different responses to long-term heat treatment between mWDX2 and *atg* mutants, we further monitored autophagosome formation under short heat shock. Seedlings of *atg* mutants, TPLATE and mWDX2 complemented lines expressing mCherry-ATG8e were subjected to our short-term heat stress. Although TPLATE was removed from the PM and aggregated in the cytoplasm, mWDX2 roots exhibited comparable amounts of mCherry-ATG8e labeled autophagosomes. Conversely, mCherry-ATG8e labeled autophagosomes were

Chapter 4

hardly observed in both *atg* mutants (Fig 5C). The massive detection of autophagosomes in mWDX2 roots suggested that destabilizing TPC does not affect autophagy under heat stress. Besides, in mWDX2 roots, the co-localization between mcherry-ATG8e labeled autophagosomes and the aggregated TPLATE spots (Fig 5C), indicated that autophagy likely plays a role in the clearance of the aggregated TPLATE proteins destabilized by heat stress.

Our recent work showed that AtEH/Pan1 is important for autophagosome formation as overexpression of AtEH/Pan1 boosts autophagosome formation while down-regulation blocks this. Besides, AtEH/Pan1 proteins recruited other endocytic proteins including several TPC subunits, AP-2 subunits and clathrin to AtEH/Pan1 labeled autophagosomes (Wang et al., 2019). To determine whether aggregated TPLATE structures are able to recruit other endocytic players, we examined DRP1a and AtEH2/Pan1 localization under heat stress. The mWDX2-GFP complemented lines carrying DRP1a-mRFP and F2 seedlings expressing functional mWDX2-GFP and AtEH2/Pan1 were exposed to short-term heat stress and imaged. Our confocal images revealed that DRP1a was recruited to the aggregated structures, suggesting a direct interaction between TPLATE and DRPs, which is in agreement with the MS data of the Sandwich isoform where DRP1a was co-identified with TPLATE, independent of TPC assembly (Chapter 3). Conversely, aggregated mWDX2 failed to recruit AtEH2/Pan1 (Fig 5D). The observation that AtEH/Pan1 proteins were not aggregated together with mWDX2, their role in autophagy and the fact that autophagy was not inhibited upon functional inactivation of TPLATE suggests the possibility that AtEH/Pan1 proteins might drives autophagosome formation independent of the other TPLATE complex subunits.

Taken together, our data revealed that destabilizing TPC by short-term heat shock does not inhibit autophagosomes formation.

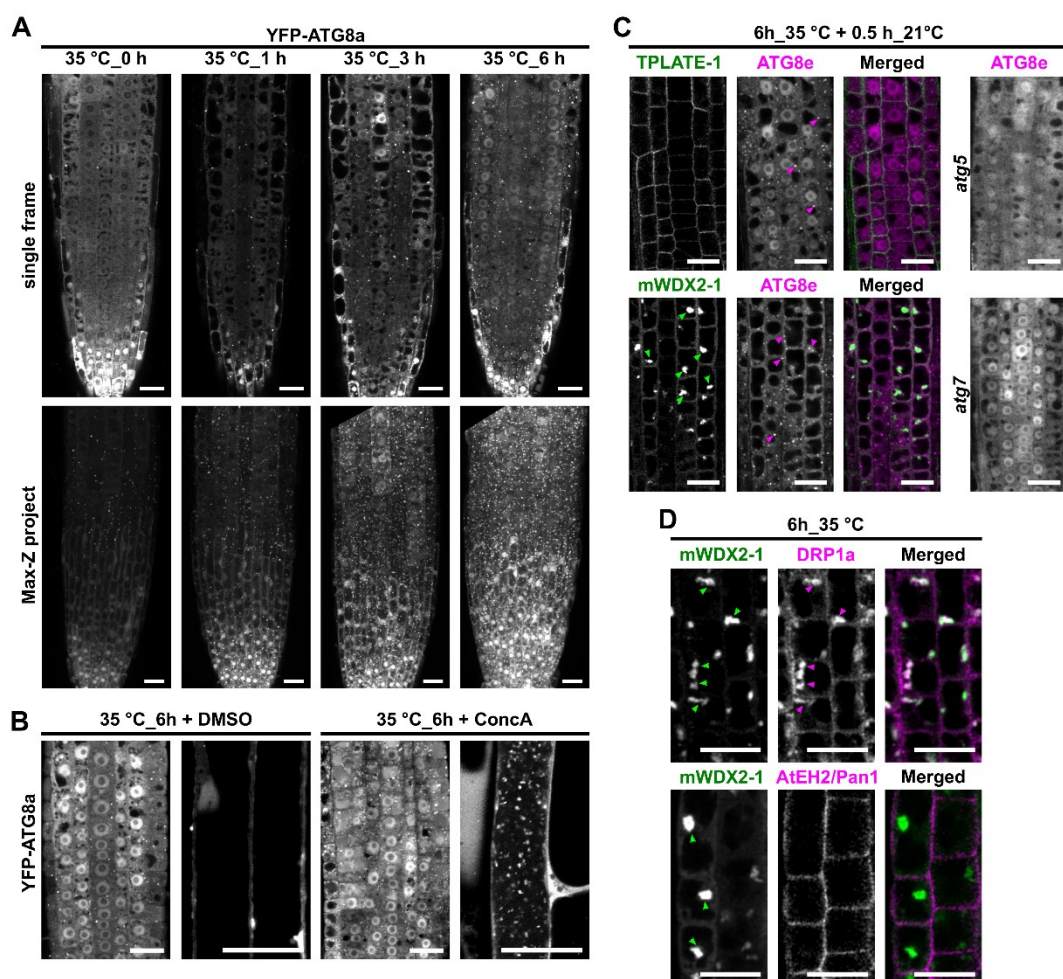


Figure 5. Destabilizing TPC fails to inhibit autophagosome formation under heat stress.

(A) Confocal images of root cells from YFP-ATG8a expressing lines upon time series of heat treatment. 5-day old seedlings, grown vertically on $\frac{1}{2}$ MS media at 20 degrees were subjected to 35 °C for certain hours and imaged immediately. Scale bars = 20 μ m.

(B) Confocal images of root cells from YFP-ATG8a expressing lines upon 6h heat treatment. 5-day old seedlings, grown vertically on $\frac{1}{2}$ MS media at 20 degrees were subjected to 35 °C with or without 1 μ M ConCA treatment. Seedlings were imaged immediately. Scale bars = 25 μ m.

(C) Confocal images of mCherry-ATG8e in TPLATE and mWDX2 complemented lines as well as in *atg* mutants. 5-day old seedlings grown at 20 °C were treated with 35 °C for 6 hours and then recovered at 20 °C for 30mins. Scale bar = 25 μ m. Green arrowheads indicate the aggregated TPLATE and red arrowheads indicate the overlap of autophagosomes with aggregated TPLATE labelled spots.

(D) Confocal images of DRP1a-mRFP and AtEH2/Pan1-mRuby3 in TPLATE and mWDX2 complemented lines. 5-day old seedlings grown at 20 °C were treated with 35 °C for 6 hours and then imaged. Scale bar = 25 μ m.

Inactivation of TPC by short-term heat stress efficiently impairs endocytosis.

TPC serves as an early adaptor protein complex that internalizes PM cargoes during CME in plants (Gadeyne et al., 2014; Sanchez-Rodriguez et al., 2018). Our previous work already showed that destabilizing TPC partially affected the efficiency of endocytosis (Chapter 3). Given that destabilized TPLATE proteins were removed from the PM and aggregated in the cytoplasm, we further generally evaluated the endocytic capacity of WDX2-complemented lines under short-term heat stress. In line with the aggregation of TPLATE in cytoplasm, mWDX2 plants exhibited a strong reduction (more than 40%) of FM4-64 uptake after short-term heat stress (Fig 6A), similar to what was observed upon strong downregulation of TPC single subunits (Gadeyne et al., 2014). Considering that mWDX2 plants only exhibited around 20% reduction of FM4-64 uptake under normal conditions (Chapter 3, Fig 5A), our data suggested that heat stress induces aggregation of TPLATE in the cytoplasm further impaired TPLATE-dependent endocytosis.

Our previous work showed that loss-of-function of TPLATE leads to ectopic callose deposition in mature pollen as well as in Arabidopsis roots (Van Damme et al., 2006). Given the loss of PM localization and the impairment of endocytosis caused by heat inactivated TPLATE, we further examined the callose deposition in mWDX2 plants after short-term heat treatment. When grown at 20 °C, both TPLATE and mWDX2 complemented lines exhibited predominant callose deposition on the cell plate (Fig. S5). After short-term heat treatment, only a bit of callose deposition was detected on the cell plate or cell walls in TPLATE roots. Conversely, massive callose deposition was observed in the cell walls (Fig 5B), further supports the inactivation of TPC function by heat treatment.

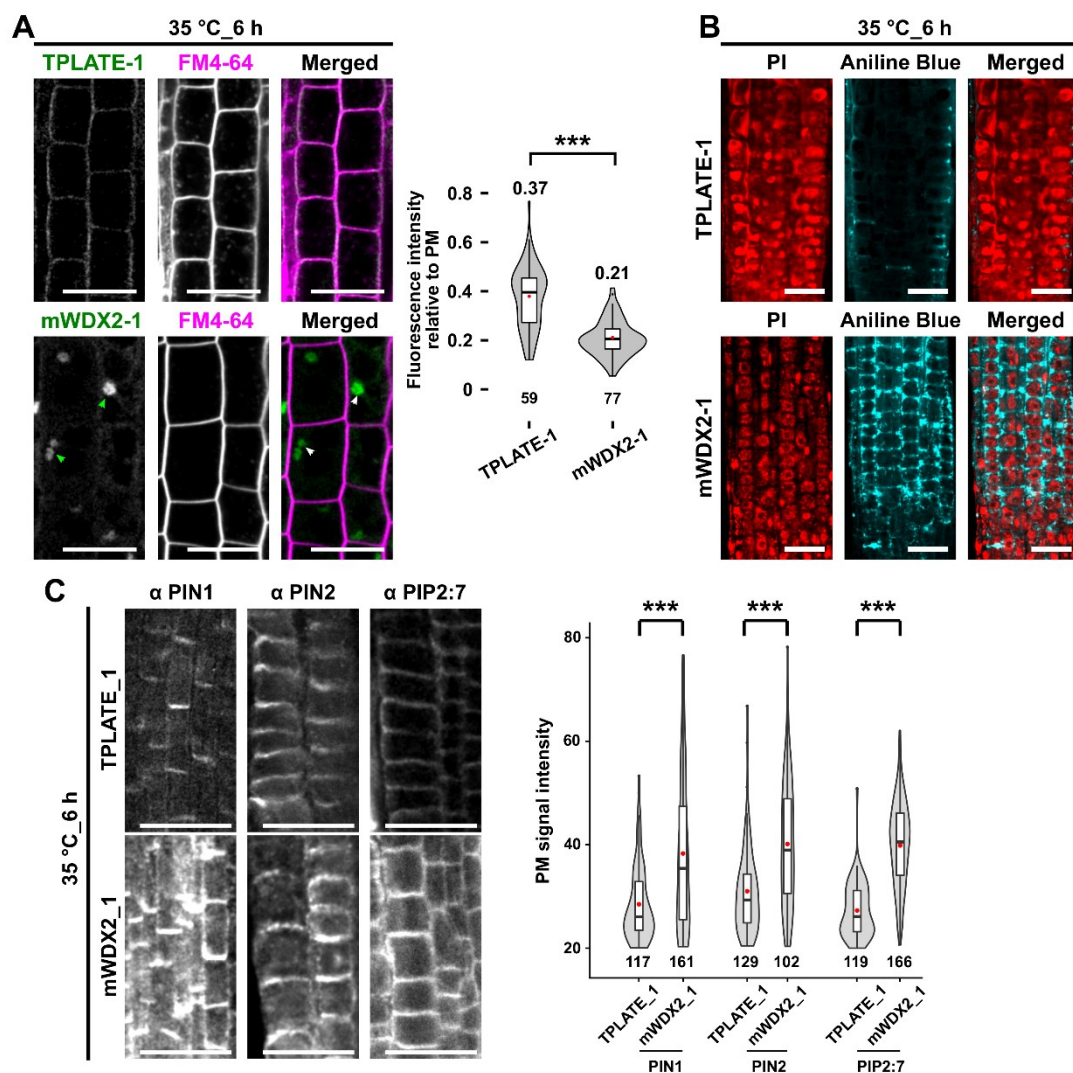


Figure 6. Destabilizing TPC by short-term heat stress impairs endocytosis.

(A) Confocal images and quantification of FM4-64 uptake in TPLATE and mWDX2 complemented lines. 5-day old seedlings grown at 20 °C were treated with 35 °C for 6 hours and then incubated in ½ MS liquid media supplemented with 2 μM FM4-64 at 20 °C for 15 minutes. Scale bar = 25 μm. Image quantification was done on 10 roots for each transgenic line respectively. Numbers at the bottom represent the amount of cells analyzed while numbers at the top indicate the mean values. ***, $p < 0.001$ for T-test.

(B) Confocal images of Aniline Blue and PI co-staining in TPLATE and mWDX2 complemented roots. 5-day old seedlings grown at 20 °C were treated with 35 °C for 6 hours and then stained with Aniline Blue for 2 hours following with PI staining for 5 mins. Scale bar = 25 μm.

(C) Representative immunolocalizations and quantification of fluorescence intensity on the PM of endogenous PIN1, PIN2 and PIP2:7 proteins after 6h heat treatment in TPLATE and mWDX2 complemented seedlings. Numbers of measured cells were indicated at the bottom. At least 6 transgenic plants for each protein were imaged and measured. ***, $p < 0.001$ for T-test.

Chapter 4

TPC has been associated with the internalization of cargoes on the PM (Gadeyne et al., 2014; Sanchez-Rodriguez et al., 2018). To further evaluate the specific internalization of PM cargoes, we examined the PM accumulation of several reported cargoes that undergoes CME (Dhonukshe et al., 2007; Li et al., 2011; Gadeyne et al., 2014). After short-term heat stress, immunolocalization of PIN1, PIN2 and PIP2;7 proteins on the PM were examined in TPLATE and mWDX2 complemented lines. Consistent with the reduction of FM4-64 internalization, we observed strong PM accumulation of PIN1, PIN2 and PIP2;7 proteins in mWDX2 plants (Fig 6C). Our mWDX2 complemented line therefore represent a novel conditional tool to impair endocytosis of various PM cargo proteins

Taken together, our data suggested that the heat-inducible aggregation of TPLATE in the cytoplasm results in heat-inactivation of TPC and blocked TPLATE-dependent endocytosis. Our mWDX complemented lines therefore represent a novel conditional tool to impair endocytosis specifically without affecting TGN function or autophagy (Fig 7). The whitening of cotyledons observed in mWDX complemented lines under prolonged heat stress is likely caused by constantly blocked endocytosis rather than impaired autophagy.

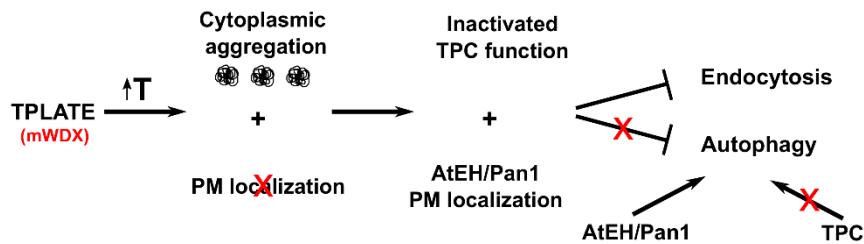


Figure 7. Mechanistic model shows the roles of TPC in endocytosis and autophagy.

The mWDX presents a destabilizing TPLATE allele in which TPLATE, and by extension, the whole TPC can be destabilized by heat. Short-term heat-treatment increases TPC destabilization and delocalizes TPLATE from the plasma membrane to aggregates in the cytoplasm, thus inactivating TPC function. The delocalization of TPLATE fails to affect AtEH/Pan1 proteins localization on the PM. AtEH/pan1 and several other TPC subunits are implicated in actin-regulated autophagosomal degradation (Wang et al., 2019). Inactivating TPC impairs endocytosis however does not impair autophagy, suggesting that it is AtEH/Pan1 proteins rather than the whole TPC that drive the actin-regulated autophagy pathway between the ER-PM CS and the vacuole in plants.

Discussion

mWDX-mediated destabilization of TPLATE is a novel conditional tool to study TPC's functions.

Our previous data in chapter 3 suggested that substituting the WDX domain of TPLATE results in partially functional TPLATE alleles as those mutations conserve TPLATE functionality and PM recruitment, while they impair the efficiency of TPLATE-dependent endocytosis. Indeed, our Co-IP and IP-MS results revealed that mutating the WDX domain of TPLATE destabilizes the whole TPC, which would be in agreement with the observation that mWDX-complemented *tplate* (-/-) mutants are only partially functional. The deficiency of endocytosis under normal conditions, including prolonged residual PM retention of TPLATE, reduction of FM4-64 uptake and prolonged lifetime of DRP1a observed in mWDX2 plants, can also be attributed to the destabilization of the whole TPC which makes that a longer time is needed for CCV formation.

Chapter 4

Destabilizing TPC fails to provide adequate amounts of functional TPC to efficiently perform endocytosis, which resembles to what happens in the viable weak allele of TWD40-2 (Bashline et al., 2015).

While deficient endocytosis does not always result in reduction of root and hypocotyl growth in Arabidopsis, as the loss-of-function *ap2m-1* fails to inhibit root growth while exhibits prolonged hypocotyl length (Bashline et al., 2015; Sanchez-Rodriguez et al., 2018). The reason why destabilizing TPC fails to cause root growth and graviperception defects could be blamed to that there are still enough endocytosis to execute these developmental processes. Despite the reduction of TWD40-2 caused by the weak allele and the destabilizing TPC caused by mWDX2, it appears plants can utilize the rest of TWD40-2 proteins to build-in adequate TPC to fulfill its function in plant endocytosis. As a consequence, we failed to observe enhanced phenotype in the combination of mWDX2 and *twd40-2-3* plants.

To overcome the male sterility and seedling lethality caused by knockout or knockdown single TPC subunits, strategies such as inducible knockdown/overexpression or mild downregulation of certain TPC subunits was employed previously to study the role of TPC in endocytosis and autophagy (Gadeyne et al., 2014; Bashline et al., 2015; Sanchez-Rodriguez et al., 2018; Wang et al., 2019). In this study, we employed the strategy that the destabilized form of TPLATE can be boosted by short-term heat stress to obtain the heat-inducible inactivated TPC mutants. Our live cell imaging data revealed that short-term heat treatment of mWDX2 is a rapid and efficient way to delocalize TPLATE from the PM and aggregate it into the cytoplasm, hereby disrupting TPC function.

All TPC subunits are recruited simultaneously to highly dynamic endocytic spots at the PM to act as essential adaptor protein complex to execute CME (Gadeyne et al., 2014; Wang et al., 2020). Next to their role in endocytosis, several TPC subunits are also implicated in actin-regulated autophagosomal degradation (Wang et al., 2019). This heat-inducible-inactivated TPLATE

isoform that we describe and characterize here provides us with an opportunity to further study TPC function in endocytosis as well as in autophagy.

Autophagy relies on AtEH/Pan1 rather than on the whole TPC.

AtEH/Pan1 are essential for autophagy, as mild downregulation of *AtEH1/Pan1* expression (about 30% reduction) renders plants susceptible to nutrient deficiency, especially to fixed-carbon starvation (Wang et al., 2019). If the whole TPC is involved in autophagy, given the severe destabilization of TPC in both mWDX1 and mWDX2 complemented plants, susceptibility to fixed-carbon starvation was expected to be observed in mWDX plants as well. However, mWDX2 plants performed similarly to TPLATE complemented lines, which is unlike *atg* mutants under fixed-carbon starvation. The resistance of mWDX2 plants to carbon starvation could be explained by the fact that the destabilization of TPC caused by substituting the WDX motif in TPLATE likely does not affect the functions of AtEH/Pan1 in autophagy. Thus, there are still enough AtEH/Pan1 proteins to function in autophagy under carbon limiting conditions. These results suggested that AtEH/Pan1 but not whole TPC is required for autophagy under fixed-carbon starvation.

In addition to inducing the aggregation of destabilized proteins, short-term heat treatment also induces autophagy (Sedaghatmehr et al., 2019; Jung et al., 2020). Our live cell imaging of the autophagy marker confirmed that 6 h heat treatment induces sufficient autophagosome formation without blocking autophagic flux, in agreement with previous work (Jung et al., 2020). We observed comparable numbers of autophagosomes in both TPLATE and mWDX2 complemented lines, while we rarely detected these in *atg* mutants. Besides, we also detected massive autophagosome formation in the cells presenting the aggregated TPLATE structures in mWDX2 plants. TPLATE has been shown to co-localize with AtEH/Pan1 in autophagosomes in the vacuole after fixed-carbon starvation (Wang et al., 2019). Here, we failed to detect any

Chapter 4

TPLATE localized to the ATG8e labelled autophagosomes. These results further support that TPC is not required for autophagosomes formation under heat stress. The overlap between aggregated TPLATE structures and ATG8e labelled autophagosomes in mWDX2 plants, is indicative for the possibility that autophagy might be involved in the clearance of aggregated TPLATE proteins.

Our recent work showed that TPC is required to the PM as octameric complex, while AtEH1 and AtEH2, were not associated with the other TPC core components when the complex was forced into the cytoplasm by truncating the TML subunit (Gadeyne et al., 2014; Wang et al., 2020). The aggregated TPLATE structure in the cytoplasm recruited DRP1a while it failed to recruit AtEH2/Pan1, indicating that AtEH/Pan1 can function independent of other TPC subunits, likely in autophagy. However, we do not have evidence to show that AtEH/Pan1 are required for autophagosomes formation under heat stress. Recent work showed that the receptor of aggrephagy NEIGHBOR OF BRCA1 (NBR1) is crucial for the heat-induced formation of autophagosomes (Jung et al., 2020). Although our previous work showed the partial colocalization between AtEH1/Pan1 and NBR1 in autophagosomes (Wang et al., 2019), it is not under heat stress. Monitoring autophagosome formation in lines with reduced *AtEH1/Pan1* expression will contribute to answering whether AtEH/Pan1 play a role in autophagosome formation under short-term heat stress.

Long-term heat stress resistance relies more on endocytic capacity than on autophagosomal degradation.

Autophagy helps plants to tackle different types abiotic stress, including heat stress (Avin-Wittenberg et al., 2018; Avin-Wittenberg, 2019), as short-term heat shock following with recovery at normal condition for several days causes the seedling lethality in *atg* mutants (Zhou et al., 2013; Zhou et al., 2014; Sedaghatmehr et al., 2019). While it appears that autophagy is not essential for seedlings to tolerate long-term heat stress. The *atg* mutants failed to exhibit

Chapter 4

seedlings lethality under prolonged heat stress, which is coherent with the previous work (Dundar et al., 2019). Besides, recent work showed that prolonged heat treatment (37 °C, 12h) inhibited autophagosome formation (Jung et al., 2020). These results together support that the accumulation of ubiquitinated proteins and seedlings lethality observed in mWDX2 plants under long-term heat stress is not caused by a defect in autophagy.

TPC serves as essential adaptor proteins during CME and knockdown single TPC subunits leads to seedling lethality (Gadeyne et al., 2014). Thus, the seedling lethality observed in mWDX2 plants under long-term heat stress is likely caused by constant inactivation of TPC by aggregated destabilized mWDX2 in the cytoplasm, which blocks TPLATE-dependent endocytosis.

mWDX is a conditional tool to manipulate endocytosis specifically at the PM.

Genetic and chemical tools to manipulate endocytosis have been extensively investigated via interfering with the functions of endocytic players such as clathrin (Dhonukshe et al., 2007; Kitakura et al., 2011; Wang et al., 2013; Adamowski et al., 2018; Dejonghe et al., 2019), adaptor proteins (Bashline et al., 2013; Di Rubbo et al., 2013; Fan et al., 2013; Kim et al., 2013; Yamaoka et al., 2013; Bashline et al., 2015; Wang et al., 2016; Yoshinari et al., 2019) and dynamin-related proteins (Collings et al., 2008; Konopka and Bednarek, 2008; Backues et al., 2010; Taylor, 2011; Yoshinari et al., 2016). The chemical inhibitors used to affect CME in plants have been described to possess undesirable side effects (Dejonghe et al., 2016) or to affect proteins which are not only specific for endocytosis, e.g. clathrin itself as it is also involved in TGN trafficking (Wang et al., 2013; Dejonghe et al., 2019). The same is true for several genetic tools currently available to affect CME in plants (Kitakura et al., 2011; Wang et al., 2013; Yoshinari et al., 2016; Adamowski et al., 2018). Manipulation of TPC, functioning exclusively at PM, represents a very good

Chapter 4

candidate to affect CME more specifically. So far however, there are no chemical tools to target TPC functions or dominant-negative mutants available. The only tools to manipulate TPC function in viable plants consist of knock-down mutants with very mild reduction of expression and consequently similar mild effects on CME (Gadeyne et al., 2014; Bashline et al., 2015; Sanchez-Rodriguez et al., 2018; Wang et al., 2019).

By application the conditional tool that delocalizes TPLATE from PM by short-term heat treatment, we are able to show that autophagy is not affected under this condition. Thus, this conditional tool can be used to specifically manipulate the endocytic machinery via inactivating TPC function. For example, our tool provides us an opportunity to evaluate AP-2 dependent endocytosis. It has been hypothesized that TPC and AP-2 function cooperatively as well as distinctly during CME (Gadeyne et al., 2014; Bashline et al., 2015). TPC seems to recruit or stabilize AP-2 at the plasma membrane, as downregulation of TPC subunits results in reduced PM intensity (TML silencing) as well as altered dynamics (e.g. in the *twd40-2-3* mutant) of AP-2 subunits (Gadeyne et al., 2014; Bashline et al., 2015). The recruitment of AP-2 subunits (PM intensity and dynamics) in *mWDX2* seedlings under short-term heat treatment are deserved to be further investigated. Additionally, we were also able to show that disrupting TPC blocks uptake of the endocytic tracer FM4-64 and causes accumulation of various known endocytic cargoes at the plasma membrane. Our conditional tool also provides us with an opportunity to identify novel or specific cargoes for TPC during CME. To achieve this aim, comparative membrane proteomics will be performed between TPLATE and *mWDX2* complemented lines under short-term heat treatment.

In conclusion, we used the destabilization defect of the *mWDX*-complemented *tplate(-/-)* mutant to our advantage and developed one of the first tools to inducibly interfere with TPC function within hours whereas previously reported inducible silencing reported before had visible phenotypes following several days of induction (Gadeyne et al., 2014). We show that our

Chapter 4

tool is highly efficient in disrupting endocytosis while not impairing autophagy.

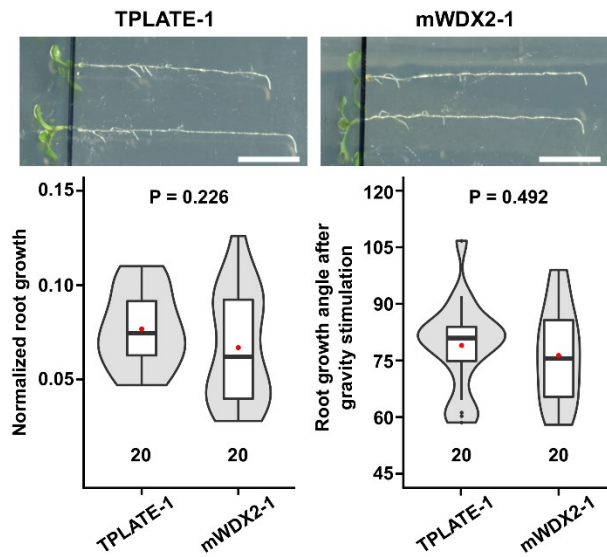


Figure S1. Destabilized TPC by mWDX2 complementation does not significantly affect root growth and gravitropic responses.

Root growth and gravitropic response of 8-day-old seedlings from TPLATE and mWDX2 complemented lines. The 8-day-old seedlings, grown vertically on 1/2 MS medium were rotated 90 degrees followed by 16h of gravistimulation. Normalized root growth was calculated as the ratio between the root growth after rotation and it before rotation respectively. Gravitropic bending was measured as the root growth angle after gravistimulation. The number of seedlings analyzed is indicated. Scale bar = 1cm.

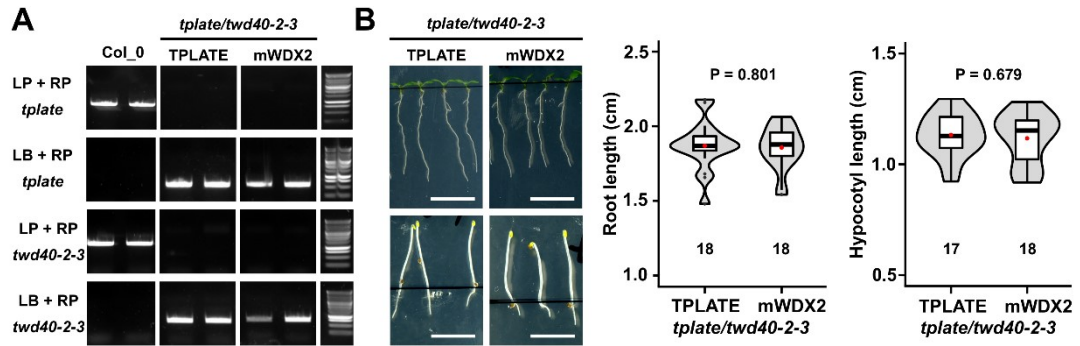


Figure S2. Combining mWDX2 and *twd40-2-3* exhibits no additive effect.

(A) Genotyping PCR analysis confirming the viability of double homozygous mutants after crossing plants from TPLATE and mWDX2 complemented lines with *twd40-2-3*. LP and RP are gene specific primers flanking the T-DNA and LB is the T-DNA specific primer.

(B) Phenotypic comparison and quantification between TPLATE and mWDX2 in *tplate/twd40-2-3* plants. Roots of 1-week-old seedlings and hypocotyls of 4-day-old dark-grown seedlings were measured. Scale bar = 1cm.

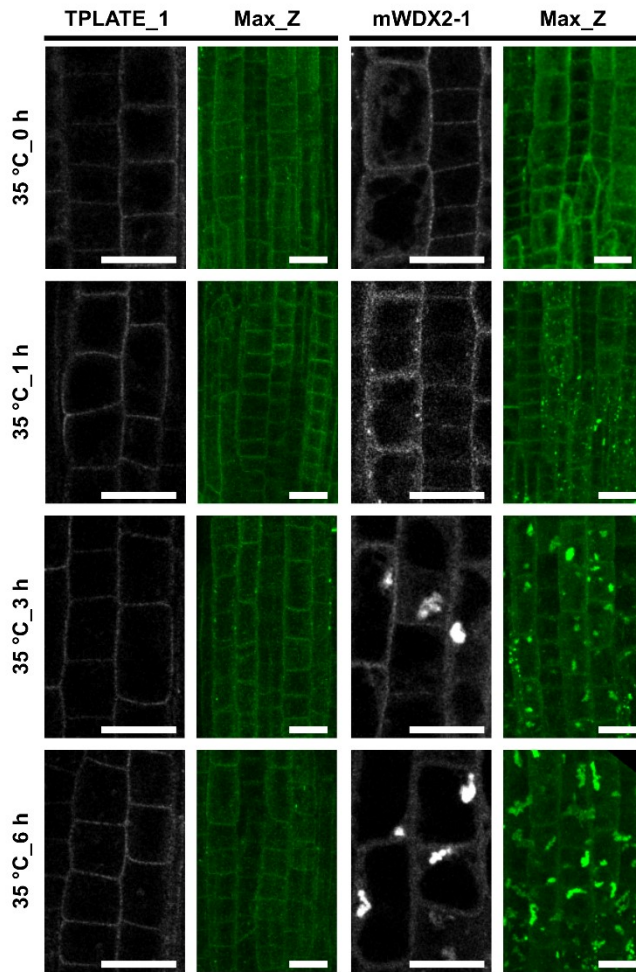


Figure S3. Short-term heat treatment induces time-dependent aggregation of mWDX2. Confocal images of root cells from TPLATE and mWDX2 complemented *tplate(-/-)* mutant lines subjected to short-term heat treatment. 5-day old seedlings, grown vertically on $\frac{1}{2}$ MS media at 20 degrees were subjected to 35 °C for 0 h, 1 h, 3 h and 6 h and imaged immediately following the treatment. The images present single optical sections (greyscale) as well as maximum Z-projections (green) at lower magnification. Scale bars equal 20 μ m.

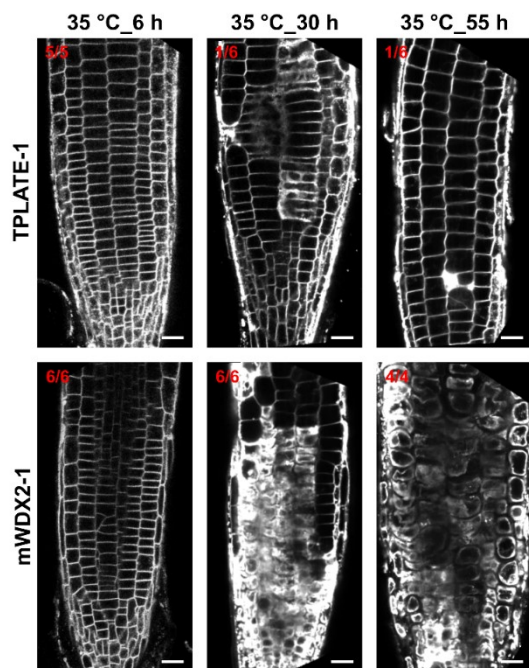


Figure S4. Long-term heat treatment induces severe cell death in mWDX2 roots.

Confocal images of roots from TPLATE and mWDX2 complemented *tplate(-/-)* mutant lines upon heat treatment. 5-day old seedlings, grown vertically on $\frac{1}{2}$ MS media at 20 degrees were subjected to 35 °C for 6 h, 30 h, and 55 h. Seedlings were stained with FM4-64 and imaged immediately. The numbers indicate the amount of seedlings showing the dead cells phenotype after heat treatment out of the total number of seedlings imaged. Scale bars equal 20 μ m.

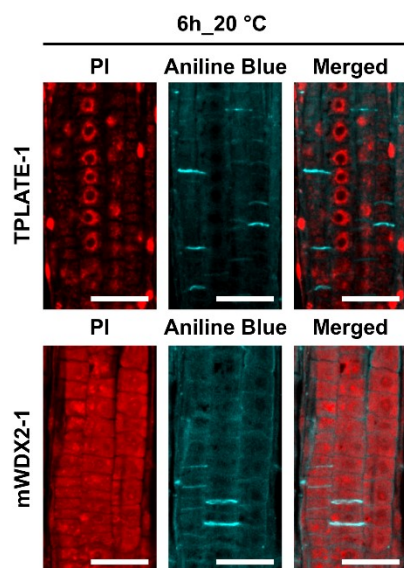


Figure S5. Callose accumulates predominately at cell plates in TPLATE and mWDX2 complemented lines at room temperature.

Representative confocal images of Aniline Blue and PI co-staining in TPLATE and mWDX2 complemented *tplate(-/-)* lines. 5-day old seedlings grown at 20 °C were treated with 20 °C for 6 hours and then stained with Aniline Blue for 2 hours following with PI staining for 15 mins. Scale bar = 25 μ m. The apparent difference of PI staining could be caused by inefficient wash-out of the fixative solution.

Materials and methods

Plant materials and growth conditions

Seeds were sterilized by chlorine gas sterilization and sown on ½ MS medium plates. After a 3-day vernalization period, seedlings were grown ½ MS media in a growth chamber under continuous light conditions at 20°C.

All the plants used in this study are from the Col-0 ecotype. TPLATE and mWDX2 transgenic lines were described in Chapter 3. The weak allele *twd40-2-3* of TWD40-2-3 was crossed with TPLATE and mWDX2 complemented line, respectively. F2 plants were identified by genotyping PCR to obtain homozygous mutant background (*tplate/twd40-2-3*). The pUBQ10::YFP-ATG8a and pUBQ10::mCherry-ATG8e reporter lines, *atg5-1* and *atg7-3* mutants are described before (Wang et al., 2019). The same male plant of the mCherry-ATG8e reporter line was used to cross with *atg5*, *atg7*, TPLATE and mWDX2 complemented lines. F2 plants were identified by genotyping PCR to obtain homozygous mutant background (*atg5-1*, *atg7-3*, *tplate* for TPLATE and mWDX2). The progeny expressing mCherry-ATG8 were selected based on fluorescence. The dual-color line expressing mWDX2-GFP and DRP1a-mRFP was described in Chapter 3. To obtain the dual color line expressing mWDX2-GFP and AtEH2/Pan1-mRuby3, the pLAT52-mWDX2-GFP complemented line was crossed with the pH3.3-AtEH2/Pan1-mRuby3 complemented line (Wang et al., 2019). Heterozygous F2 plants were used for imaging.

Staining for live cell imaging

The 5-day-old seedlings grown at 20 °C were treated at 35 °C for 6h and then processed with specific stainings and imaged with a Leica SP8X confocal microscope. During the staining, the staining solution was protected from light.

For FM4-64 uptake, seedlings were incubated with 1/2 strength MS liquid medium containing 2 µM FM4-64 at 20 °C for 15 minutes prior to confocal imaging. For FM4-64 and FDA co-staining, whole *Arabidopsis* seedlings were

Chapter 4

incubated with 1/2 strength MS liquid medium supplemented with 5µg/mL FDA and 2 µM FM4-64 at room temperature for 15 minutes prior to confocal imaging. The MitoTracker Red CMXRos (ThermoFisher) was used to stain the mitochondria. Whole *Arabidopsis* seedlings were incubated with 1/2 strength MS liquid medium supplemented with 100nM MitoTracker Red at room temperature for 15 minutes. To stain aggregated proteins, whole *Arabidopsis* seedlings were incubated with 1/2 strength MS liquid medium supplemented with 1µl/ml PROTEOSTAT dye (ENZ-51035-0025, Enzo) or 0.25 µl/ml (ENZ-51035-K100, Enzo) at 20 °C for 30 minutes prior to confocal imaging. Callose staining was performed as described before (Kulich et al., 2015). Seedlings were incubated in KH₂PO₄ (pH = 9.5) solution supplemented with 0.01% (w/v) aniline blue for 2 h with vacuum. After aniline blue staining, samples were stained with PI (0.01mg/mL) for 5 minutes.

Immunofluorescence

Arabidopsis roots were analyzed by immunofluorescence as described before (Sauer et al., 2006). The anti-PIN1 antibody (1:600) (donated by Dr. Ranjan Swarup), the anti-PIN2 antibody (Abas et al., 2006) (1:600) and the PIP2 antibody (Agrisera) were used as well as the fluorochrome-conjugated secondary anti-sheep-antibodies Alexa488 for PIN1 and the anti-rabbit-Alexa555 (1:600) (Dianova) for PIN2, and PIP2. Imaging was performed with a Leica SP8X confocal microscope, using a 20x objective (HC PL APO CS2 20x/0.75 DRY). Fluorophores were excited using a White Light laser with 488 nm (Alexa488) or 555 nm (Alexa555) excitation wavelength detected with a Hybrid detector with a gain of 100, (HyD 495nm - 549nm or HyD 561nm - 621nm) and time gating between 1-8 ns. Pictures were analyzed by ImageJ.

Live cell imaging

Arabidopsis seedlings were imaged between slide and cover glass. The stained seedlings after heat treatment were imaged using a Leica SP8X microscope

Chapter 4

equipped with a WhiteLight laser. Images were taken using a 40x water-corrected objective (40x HC APO CS2, NA= 1.10). Fluorescence for FM4-64 (excitation 561 nm, emission 650-750 nm), FDA (excitation 488 nm, emission 500-550 nm), MitoTracker Red (excitation 579 nm, emission 600-650 nm), PROTEOSTAT (excitation 488 nm, emission 500-540 nm), aniline blue (excitation 405 nm, emission 490-510 nm) were collected with Hybrid detectors (HyDTM).

Fluorescence for GFP (excitation 488 nm, emission 500-540 nm), YFP (excitation 514 nm, emission 520-550 nm), mRFP/mCherry/mRuby3 (excitation 561 nm, emission 590nm-650nm) were imaged with the WhiteLight laser and collected with hybrid detector (HyDTM) using a time-gating window between 0.3-6.0 ns. Images of the dual-color lines were acquired in line sequential mode.

Phenotypical analysis

For the root growth and gravitropic response analysis of TPLATE and mWDX2 complemented lines, the 8-day-old seedlings grown vertically on 1/2 MS medium were rotate 90 degrees following with 16h gravistimulation. Root growth before/after rotation was measured with Image J with NeuronJ plugin respectively. Normalized root growth was calculated as the ratio between the root growth after rotation and it before rotation respectively. The gravitropic bending was measured with Image J as described before (Du et al., 2013).

To compare the root growth and etiolated hypocotyl length, 1-week-old seedlings grown under continuous light (root growth) and 4-day-old seedlings under dark (hypocotyl elongation) were scanned and measured with Image J with NeuronJ plugin respectively.

For heat treatment phenotypical analysis, 5-day-old seedlings were grown vertically on 1/2 MS medium (without sucrose) under continuous light conditions ($68 \mu\text{E m}^{-2} \text{s}^{-1}$ photosynthetically active radiation) at 20°C in the growth chamber. For the treatment, they were moved to Lovibond incubators with continuous light ($75 \mu\text{E m}^{-2} \text{s}^{-1}$ photosynthetically active radiation) at 35 °C for 3 or 4

Chapter 4

additional days. Prior to moving plants to the incubator, root growth was marked. Root growth of seedlings was measured with ImageJ equipped with the NeuronJ plugin. After 4-day heat treatment, seedlings exhibited whitening cotyledons were visually counted.

For fixed-carbon starvation phenotypical analysis, seedlings were grown on $\frac{1}{2}$ MS medium without sucrose vertically or horizontally in the growth chamber under continuous light conditions at 20°C for 5 days. After that, root growth was marked, and the plates were covered by aluminum foil and kept in constant dark for extra one week (root growth) or 9 days (cotyledons observations). Root growth of seedlings was measured with Image J equipped with the NeuronJ plugin. The percentage of yellowing seedlings was visually determined.

SDS-PAGE and western blot

Samples were analyzed by loading on 4-20% gradient gels (Biorad), after addition of 4x Laemmli sample buffer (Biorad) and 10x NuPage sample reducing agent (Invitrogen). Gels were transferred to PVDF or Nitrocellulose membranes using the Trans-Blot® Turbo™ system (Biorad). Blots were imaged on a ChemiDoc™ Imaging System (Biorad) and the ImageJ program was used for a quantitative analysis.

Arabidopsis seedling protein extraction

Arabidopsis seedlings were grown for seven days on $\frac{1}{2}$ MS medium under constant light. Seedlings were harvested, flash frozen and grinded in liquid nitrogen. Proteins were extracted in a 1:1 ratio, buffer (ml): seedlings (g), in HB+ buffer, as described in (Van Leene et al., 2007). Protein extracts were incubated for 30 min at 4°C on a rotating wheel before spinning down twice at 20000 g for 20 min. The protein content of the supernatant was measured using Qubit (Thermofisher) and equal amounts of proteins were loaded for analysis.

Co-immunoprecipitation

Arabidopsis seedlings were grown for seven days on ½ MS medium at 20°C under constant light. Seedlings were harvested, flash frozen and grinded in liquid nitrogen. Proteins were extracted in a 1:1 ratio, buffer (ml): seedlings (g), in 50 mM Tris-HCl, 150mM NaCl, 5mM DTT supplemented with 1x cOmplete™ ULTRA Tablets, Mini, EDTA-free, EASYpack Protease Inhibitor Cocktail (Roche). Proteins extracts were incubated for 30 min at 4°C on a rotating wheel and cleared by subsequent centrifugation at 20000 g for 20 min. The protein content of the supernatant was measured using Qubit (Thermofisher) and an equal amount of total proteins were incubated with 20µl GFP-Trap, magnetic agarose beads (Chromotek, gtma-20, lot 90122001MA). Beads were washed three times with lysis buffer and eluted by boiling at 70°C for 10 min. Protein degradation was analyzed by ImageJ by comparing band intensities (grey values) of full-length protein versus all smaller molecular weight breakdown products.

Isolation of ubiquitinated proteins

Seedlings were grown vertically in the growth chamber under continuous light conditions at 20°C for 5 days, followed by either growth at 20 °C or 35 °C for extra 3 days. Seedlings were harvested and subsequently retched after flash freezing in liquid nitrogen. Proteins were extracted in a 1:1 ratio, buffer (ml): seedlings (g), in 100mM Tris, 10mM NaCl, 5mM DTT, 1mM EDTA and 1x cOmplete™ ULTRA Tablets, Mini, EDTA-free, EASYpack Protease Inhibitor Cocktail (Roche). Proteins extracts were incubated for 30 min at 4°C on a rotating wheel and cleared by two subsequent centrifugations at 4000 g for 5 min. The supernatant was measured using Qubit (Thermofisher) and an equal amount of total protein was used for SDS-PAGE.

Identification of interacting proteins using IP/MS-MS

Immunoprecipitation experiments were performed for three biological replicates as described previously (De Rybel et al., 2013), using 3g of 4-day old seedlings. Interacting proteins were isolated by applying total protein extracts to α GFP-coupled magnetic beads (Milteny Biotech). Three replicates of TPLATE motif substitution mutants (mWDX1 and mWDX2) were compared to three replicates of Col-0 and TPLATE-GFP (in *tplate(-/-)*) as controls. Tandem mass spectrometry (MS) and statistical analysis using MaxQuant and the Perseus software was performed as described previously (Wendrich et al., 2017).

Relative amounts of TPC subunits as well as DRP1a detected compared to the bait protein (TPLATE-GFP, mWDX1-GFP or mWDX2-GFP) were calculated based on peptide intensity levels. Peptides of the three bait proteins as well as of each specific TPC subunit and DRP1a that were identified in all experiments as well as in all three biological repeats by MS/MS or by matching and for which an intensity value was assigned were selected for the quantification. The total number of common peptides that were taken into account for the measurement are as follows: TPLATE (29), TASH3 (11), LOLITA (1), TWD40-1 (13), TWD40-2 (20), AtEH1 (2), AtEH2 (2) and DRP1a (6). Peptides used for the calculations of the respective proteins are color coded in supplemental data source 2. The intensities of the common peptides for each subunit were normalized to the averaged intensity of the bait proteins. The normalized intensity values of each prey peptide were then averaged for each prey protein, the standard deviation was calculated, and the values were plotted in Figure 1C. The MS data regarding TPLATE and WDX in this chapter can be visited via the following link: <https://floppy.psb.ugent.be/index.php/apps/files/?dir=/Mass%20spec%20data&fileid=4200182>

Chapter 4

Table 1. Antibodies used in this study

	<i>Dilution</i>	<i>Incubation time</i>	<i>Source</i>
a-TPLATE2	1/1000	1h	(Dejonghe et al., 2019)
a-GFP-HRP	1/1000	1h-o/n	Miltenyi Biotec GFP/HRP antibody (130-091-833)
a-TWD40-2 serum	1/100	1h	(Bashline et al., 2015)
a-EH1/2/Pan1	1/200	3h	(Wang et al., 2019)
a-rabbit	1/10000	1h	Amersham ECL Mouse IgG, HRP-linked whole Ab (NA931)
a-mouse	1/10000	1h	Amersham ECL Rabbit IgG, HRP-linked whole Ab (NA934)
anti-PIN1	1/600		donated by Dr. Ranjan Swarup
anti-PIN2	1/600		(Abas et al., 2006)
anti-PIP2	1/600		Agrisera
anti-rabbit-Alexa555	1/600		Dianova
anti-sheep Alexa488	1/600		Dianova

References

- Abas, L., Benjamins, R., Malenica, N., Paciorek, T., Wisniewska, J., Moulinier-Anzola, J.C., Sieberer, T., Friml, J., and Luschign, C.** (2006). Intracellular trafficking and proteolysis of the Arabidopsis auxin-efflux facilitator PIN2 are involved in root gravitropism. *Nat Cell Biol* **8**: 249-256.
- Adamowski, M., Narasimhan, M., Kania, U., Glanc, M., De Jaeger, G., and Friml, J.** (2018). A Functional Study of AUXILIN-LIKE1 and 2, Two Putative Clathrin Uncoating Factors in Arabidopsis. *Plant Cell* **30**: 700-716.
- Avin-Wittenberg, T.** (2019). Autophagy and its role in plant abiotic stress management. *Plant Cell Environ* **42**: 1045-1053.
- Avin-Wittenberg, T., et al.** (2018). Autophagy-related approaches for improving nutrient use efficiency and crop yield protection. *J Exp Bot* **69**: 1335-1353.
- Backues, S.K., Korasick, D.A., Heese, A., and Bednarek, S.Y.** (2010). The Arabidopsis dynamin-related protein2 family is essential for gametophyte development. *Plant Cell* **22**: 3218-3231.
- Barberon, M., Zelazny, E., Robert, S., Conejero, G., Curie, C., Friml, J., and Vert, G.** (2011). Monoubiquitin-dependent endocytosis of the iron-regulated transporter 1 (IRT1) transporter controls iron uptake in plants. *Proc Natl Acad Sci U S A* **108**: E450-458.
- Bashline, L., Li, S., Zhu, X., and Gu, Y.** (2015). The TWD40-2 protein and the AP2 complex cooperate in the clathrin-mediated endocytosis of cellulose synthase to regulate cellulose biosynthesis. *Proc Natl Acad Sci U S A* **112**: 12870-12875.
- Bashline, L., Li, S., Anderson, C.T., Lei, L., and Gu, Y.** (2013). The endocytosis of cellulose synthase in Arabidopsis is dependent on mu2, a clathrin-mediated endocytosis adaptin. *Plant Physiol* **163**: 150-160.
- Baxter, A., Mittler, R., and Suzuki, N.** (2014). ROS as key players in plant stress signalling. *J Exp Bot* **65**: 1229-1240.
- Chung, T., Phillips, A.R., and Vierstra, R.D.** (2010). ATG8 lipidation and ATG8-mediated autophagy in Arabidopsis require ATG12 expressed from the differentially controlled ATG12A AND ATG12B loci. *Plant J* **62**: 483-493.
- Collings, D.A., Gebbie, L.K., Howles, P.A., Hurley, U.A., Birch, R.J., Cork, A.H., Hocart, C.H., Arioli, T., and Williamson, R.E.** (2008). Arabidopsis dynamin-like protein DRP1A: a null mutant with widespread defects in endocytosis, cellulose synthesis, cytokinesis, and cell expansion. *J Exp Bot* **59**: 361-376.
- Dejonghe, W., et al.** (2019). Disruption of endocytosis through chemical inhibition of clathrin heavy chain function. *Nat Chem Biol* **15**: 641-649.
- Dejonghe, W., et al.** (2016). Mitochondrial uncouplers inhibit clathrin-mediated endocytosis largely through cytoplasmic acidification. *Nat Commun* **7**: 11710.

Chapter 4

Dhonukshe, P., Aniento, F., Hwang, I., Robinson, D.G., Mravec, J., Stierhof, Y.D., and Friml, J. (2007). Clathrin-mediated constitutive endocytosis of PIN auxin efflux carriers in Arabidopsis. *Curr Biol* **17**: 520-527.

Di Rubbo, S., et al. (2013). The clathrin adaptor complex AP-2 mediates endocytosis of brassinosteroid insensitive1 in Arabidopsis. *Plant Cell* **25**: 2986-2997.

Doelling, J.H., Walker, J.M., Friedman, E.M., Thompson, A.R., and Vierstra, R.D. (2002). The APG8/12-activating enzyme APG7 is required for proper nutrient recycling and senescence in Arabidopsis thaliana. *J Biol Chem* **277**: 33105-33114.

Du, Y., Tejos, R., Beck, M., Himschoot, E., Li, H., Robatzek, S., Vanneste, S., and Friml, J. (2013). Salicylic acid interferes with clathrin-mediated endocytic protein trafficking. *Proc Natl Acad Sci U S A* **110**: 7946-7951.

Dundar, G., Shao, Z., Higashitani, N., Kikuta, M., Izumi, M., and Higashitani, A. (2019). Autophagy mitigates high-temperature injury in pollen development of Arabidopsis thaliana. *Dev Biol* **456**: 190-200.

Fan, L., Hao, H., Xue, Y., Zhang, L., Song, K., Ding, Z., Botella, M.A., Wang, H., and Lin, J. (2013). Dynamic analysis of Arabidopsis AP2 sigma subunit reveals a key role in clathrin-mediated endocytosis and plant development. *Development* **140**: 3826-3837.

Gadeyne, A., et al. (2014). The TPLATE adaptor complex drives clathrin-mediated endocytosis in plants. *Cell* **156**: 691-704.

Goldenzweig, A., and Fleishman, S.J. (2018). Principles of Protein Stability and Their Application in Computational Design. *Annu Rev Biochem* **87**: 105-129.

Greco, M., Chiappetta, A., Bruno, L., and Bitonti, M.B. (2012). In *Posidonia oceanica* cadmium induces changes in DNA methylation and chromatin patterning. *J Exp Bot* **63**: 695-709.

Hanaoka, H., Noda, T., Shirano, Y., Kato, T., Hayashi, H., Shibata, D., Tabata, S., and Ohsumi, Y. (2002). Leaf senescence and starvation-induced chlorosis are accelerated by the disruption of an Arabidopsis autophagy gene. *Plant Physiol* **129**: 1181-1193.

Hirst, J., Schlacht, A., Norcott, J.P., Traynor, D., Bloomfield, G., Antrobus, R., Kay, R.R., Dacks, J.B., and Robinson, M.S. (2014). Characterization of TSET, an ancient and widespread membrane trafficking complex. *eLife* **3**: e02866.

Huang, L., Yu, L.J., Zhang, X., Fan, B., Wang, F.Z., Dai, Y.S., Qi, H., Zhou, Y., Xie, L.J., and Xiao, S. (2019). Autophagy regulates glucose-mediated root meristem activity by modulating ROS production in Arabidopsis. *Autophagy* **15**: 407-422.

Irani, N.G., et al. (2012). Fluorescent castasterone reveals BRI1 signaling from the plasma membrane. *Nat Chem Biol* **8**: 583-589.

Jones, K., Kim, D.W., Park, J.S., and Khang, C.H. (2016). Live-cell fluorescence imaging to investigate the dynamics of plant cell death during infection by the rice blast fungus *Magnaporthe oryzae*. *BMC Plant Biol* **16**: 69.

Chapter 4

Jung, H., Lee, H.N., Marshall, R.S., Lomax, A.W., Yoon, M.J., Kim, J., Kim, J.H., Vierstra, R.D., and Chung, T. (2020). Arabidopsis cargo receptor NBR1 mediates selective autophagy of defective proteins. *J Exp Bot* **71**: 73-89.

Kim, S.Y., Xu, Z.Y., Song, K., Kim, D.H., Kang, H., Reichardt, I., Sohn, E.J., Friml, J., Juergens, G., and Hwang, I. (2013). Adaptor protein complex 2-mediated endocytosis is crucial for male reproductive organ development in Arabidopsis. *Plant Cell* **25**: 2970-2985.

Kitakura, S., Vanneste, S., Robert, S., Lofke, C., Teichmann, T., Tanaka, H., and Friml, J. (2011). Clathrin mediates endocytosis and polar distribution of PIN auxin transporters in Arabidopsis. *Plant Cell* **23**: 1920-1931.

Konopka, C.A., and Bednarek, S.Y. (2008). Comparison of the dynamics and functional redundancy of the Arabidopsis dynamin-related isoforms DRP1A and DRP1C during plant development. *Plant Physiol* **147**: 1590-1602.

Kulich, I., Vojtikova, Z., Glanc, M., Ortmannova, J., Rasmann, S., and Zarsky, V. (2015). Cell wall maturation of Arabidopsis trichomes is dependent on exocyst subunit EXO70H4 and involves callose deposition. *Plant Physiol* **168**: 120-131.

Li, F., Chung, T., and Vierstra, R.D. (2014). AUTOPHAGY-RELATED11 plays a critical role in general autophagy- and senescence-induced mitophagy in Arabidopsis. *Plant Cell* **26**: 788-807.

Li, X., Wang, X., Yang, Y., Li, R., He, Q., Fang, X., Luu, D.T., Maurel, C., and Lin, J. (2011). Single-molecule analysis of PIP2;1 dynamics and partitioning reveals multiple modes of Arabidopsis plasma membrane aquaporin regulation. *Plant Cell* **23**: 3780-3797.

Marshall, R.S., and Vierstra, R.D. (2018). Autophagy: The Master of Bulk and Selective Recycling. *Annu Rev Plant Biol* **69**: 173-208.

Mbengue M, B.G., Gervasi F, Beck M, Zhou J, Spallek T, Bartels S, Boller T, Ueda T, Kuhn H, Robatzek S. (2016). Clathrin-dependent endocytosis is required for immunity mediated by pattern recognition receptor kinases. *Proc Natl Acad Sci USA* **113**: 11034-11039.

McMahon, H.T., and Boucrot, E. (2011). Molecular mechanism and physiological functions of clathrin-mediated endocytosis. *Nat Rev Mol Cell Biol* **12**: 517-533.

Mitsunari, T., Nakatsu, F., Shioda, N., Love, P.E., Grinberg, A., Bonifacino, J.S., and Ohno, H. (2005). Clathrin adaptor AP-2 is essential for early embryonal development. *Mol Cell Biol* **25**: 9318-9323.

Mogk, A., Bukau, B., and Kampinga, H.H. (2018). Cellular Handling of Protein Aggregates by Disaggregation Machines. *Mol Cell* **69**: 214-226.

Nakajima, Y., and Suzuki, S. (2013). Environmental stresses induce misfolded protein aggregation in plant cells in a microtubule-dependent manner. *Int J Mol Sci* **14**: 7771-7783.

Paciorek, T., Zazimalova, E., Ruthardt, N., Petrasek, J., Stierhof, Y.D., Kleine-Vehn, J., Morris, D.A., Emans, N., Jurgens, G., Geldner, N., and Friml, J. (2005). Auxin inhibits endocytosis and promotes its own efflux from cells. *Nature* **435**: 1251-1256.

Chapter 4

Paez Valencia, J., Goodman, K., and Otegui, M.S. (2016). Endocytosis and Endosomal Trafficking in Plants. *Annu Rev Plant Biol* **67**: 309-335.

Phillips, A.R., Suttangkakul, A., and Vierstra, R.D. (2008). The ATG12-conjugating enzyme ATG10 Is essential for autophagic vesicle formation in *Arabidopsis thaliana*. *Genetics* **178**: 1339-1353.

Qi, H., Xia, F.N., Xie, L.J., Yu, L.J., Chen, Q.F., Zhuang, X.H., Wang, Q., Li, F., Jiang, L., Xie, Q., and Xiao, S. (2017). TRAF Family Proteins Regulate Autophagy Dynamics by Modulating AUTOPHAGY PROTEIN6 Stability in *Arabidopsis*. *Plant Cell* **29**: 890-911.

Roy, R., Floyd, B.E., and Bassham, D.C. (2014). Autophagy and Endocytosis. *Cell Biology*: 1-26.

Sanchez-Rodriguez, C., et al. (2018). The Cellulose Synthases Are Cargo of the TPLATE Adaptor Complex. *Mol Plant* **11**: 346-349.

Sauer, M., Balla, J., Luschnig, C., Wisniewska, J., Reinohl, V., Friml, J., and Benkova, E. (2006). Canalization of auxin flow by Aux/IAA-ARF-dependent feedback regulation of PIN polarity. *Genes Dev* **20**: 2902-2911.

Sedaghatmehr, M., Thirumalaikumar, V.P., Kamranfar, I., Marmagne, A., Masclaux-Daubresse, C., and Balazadeh, S. (2019). A regulatory role of autophagy for resetting the memory of heat stress in plants. *Plant Cell Environ* **42**: 1054-1064.

Shen, D., Coleman, J., Chan, E., Nicholson, T.P., Dai, L., Sheppard, P.W., and Patton, W.F. (2011). Novel cell- and tissue-based assays for detecting misfolded and aggregated protein accumulation within aggresomes and inclusion bodies. *Cell Biochem Biophys* **60**: 173-185.

Smith, J.M., Salamango, D.J., Leslie, M.E., Collins, C.A., and Heese, A. (2014a). Sensitivity to Flg22 is modulated by ligand-induced degradation and de novo synthesis of the endogenous flagellin-receptor FLAGELLIN-SENSING2. *Plant Physiol* **164**: 440-454.

Smith, J.M., Leslie, M.E., Robinson, S.J., Korasick, D.A., Zhang, T., Backues, S.K., Cornish, P.V., Koo, A.J., Bednarek, S.Y., and Heese, A. (2014b). Loss of *Arabidopsis thaliana* Dynamin-Related Protein 2B reveals separation of innate immune signaling pathways. *PLoS Pathog* **10**: e1004578.

Suttangkakul, A., Li, F., Chung, T., and Vierstra, R.D. (2011). The ATG1/ATG13 protein kinase complex is both a regulator and a target of autophagic recycling in *Arabidopsis*. *Plant Cell* **23**: 3761-3779.

Sutter, J.U., Sieben, C., Hartel, A., Eisenach, C., Thiel, G., and Blatt, M.R. (2007). Abscisic acid triggers the endocytosis of the *Arabidopsis* KAT1 K⁺ channel and its recycling to the plasma membrane. *Curr Biol* **17**: 1396-1402.

Takano, J., Tanaka, M., Toyoda, A., Miwa, K., Kasai, K., Fuji, K., Onouchi, H., Naito, S., and Fujiwara, T. (2010). Polar localization and degradation of *Arabidopsis* boron transporters through distinct trafficking pathways. *Proc Natl Acad Sci U S A* **107**: 5220-5225.

Chapter 4

Taylor, N.G. (2011). A role for Arabidopsis dynamin related proteins DRP2A/B in endocytosis; DRP2 function is essential for plant growth. *Plant Mol Biol* **76**: 117-129.

Thompson, A.R., Doelling, J.H., Suttangkakul, A., and Vierstra, R.D. (2005). Autophagic nutrient recycling in Arabidopsis directed by the ATG8 and ATG12 conjugation pathways. *Plant Physiol* **138**: 2097-2110.

Van Damme, D., Coutuer, S., De Rycke, R., Bouget, F.Y., Inze, D., and Geelen, D. (2006). Somatic cytokinesis and pollen maturation in Arabidopsis depend on TPLATE, which has domains similar to coat proteins. *Plant Cell* **18**: 3502-3518.

Van Leene, J., et al. (2007). A tandem affinity purification-based technology platform to study the cell cycle interactome in Arabidopsis thaliana. *Mol Cell Proteomics* **6**: 1226-1238.

Wang, C., Yan, X., Chen, Q., Jiang, N., Fu, W., Ma, B., Liu, J., Li, C., Bednarek, S.Y., and Pan, J. (2013). Clathrin light chains regulate clathrin-mediated trafficking, auxin signaling, and development in Arabidopsis. *Plant Cell* **25**: 499-516.

Wang, C., et al. (2016). Differential Regulation of Clathrin and Its Adaptor Proteins during Membrane Recruitment for Endocytosis. *Plant Physiol* **171**: 215-229.

Wang, J., Mylle, E., Johnson, A., Besbrugge, N., De Jaeger, G., Friml, J., Pleskot, R., and Van Damme, D. (2020). High Temporal Resolution Reveals Simultaneous Plasma Membrane Recruitment of TPLATE Complex Subunits. *Plant Physiol* **183**: 986-997.

Wang, P., et al. (2019). Plant AtEH/Pan1 proteins drive autophagosome formation at ER-PM contact sites with actin and endocytic machinery. *Nat Commun* **10**: 5132.

Xiaoyang, L.S.Q.P. (2017). Agrobacterium delivers VirE2 protein into host cells via clathrin-mediated endocytosis. *Sci Adv* **3**: e1601528.

Xiong, Y., Contento, A.L., and Bassham, D.C. (2005). AtATG18a is required for the formation of autophagosomes during nutrient stress and senescence in Arabidopsis thaliana. *Plant J* **42**: 535-546.

Yamaoka, S., Shimono, Y., Shirakawa, M., Fukao, Y., Kawase, T., Hatsugai, N., Tamura, K., Shimada, T., and Hara-Nishimura, I. (2013). Identification and dynamics of Arabidopsis adaptor protein-2 complex and its involvement in floral organ development. *Plant Cell* **25**: 2958-2969.

Yang, X., Srivastava, R., Howell, S.H., and Bassham, D.C. (2016). Activation of autophagy by unfolded proteins during endoplasmic reticulum stress. *Plant J* **85**: 83-95.

Yoshimoto, K., Jikumaru, Y., Kamiya, Y., Kusano, M., Consonni, C., Panstruga, R., Ohsumi, Y., and Shirasu, K. (2009). Autophagy negatively regulates cell death by controlling NPR1-dependent salicylic acid signaling during senescence and the innate immune response in Arabidopsis. *Plant Cell* **21**: 2914-2927.

Yoshinari, A., Fujimoto, M., Ueda, T., Inada, N., Naito, S., and Takano, J. (2016). DRP1-Dependent Endocytosis is Essential for Polar Localization and Boron-Induced Degradation of the Borate Transporter BOR1 in Arabidopsis thaliana. *Plant Cell Physiol* **57**: 1985-2000.

Chapter 4

Yoshinari, A., Hosokawa, T., Amano, T., Beier, M.P., Kunieda, T., Shimada, T., Hara-Nishimura, I., Naito, S., and Takano, J. (2019). Polar Localization of the Borate Exporter BOR1 Requires AP2-Dependent Endocytosis. *Plant Physiol* **179**: 1569-1580.

Yu, Q., Zhang, Y., Wang, J., Yan, X., Wang, C., Xu, J., and Pan, J. (2016). Clathrin-Mediated Auxin Efflux and Maxima Regulate Hypocotyl Hook Formation and Light-Stimulated Hook Opening in Arabidopsis. *Mol Plant* **9**: 101-112.

Zhang, Y., Persson, S., Hirst, J., Robinson, M.S., van Damme, D., and Sanchez-Rodriguez, C. (2015). Change your TPLATE, change your fate: plant CME and beyond. *Trends Plant Sci* **20**: 41-48.

Zhou, J., Wang, J., Cheng, Y., Chi, Y.J., Fan, B., Yu, J.Q., and Chen, Z. (2013). NBR1-mediated selective autophagy targets insoluble ubiquitinated protein aggregates in plant stress responses. *PLoS Genet* **9**: e1003196.

Zhou, J., Zhang, Y., Qi, J., Chi, Y., Fan, B., Yu, J.Q., and Chen, Z. (2014). E3 ubiquitin ligase CHIP and NBR1-mediated selective autophagy protect additively against proteotoxicity in plant stress responses. *PLoS Genet* **10**: e1004116.

Chapter Five

The TPLATE complex is essential for shoot apical meristem maintenance

Jie Wang^{1,2}, Roman Pleskot^{1,2}, Riet De Rycke^{1,2}, Carlos Galván-Ampudia³, NJO Maria Fransiska^{1,2}, Grégoire Denay⁴, Qihang Jiang^{1,2}, Rüdiger Simon⁴, Tom Beeckman^{1,2}, Teva Vernoux³, Daniel Van Damme^{1,2,*}

¹Ghent University, Department of Plant Biotechnology and Bioinformatics, Technologiepark 71, 9052 Ghent, Belgium

²VIB Center for Plant Systems Biology, Technologiepark 71, 9052 Ghent, Belgium

³Laboratoire de Reproduction et de Développement des Plantes, INRA, CNRS, ENS de Lyon, UCB Lyon 1, Université de Lyon, France

⁴Institute for Developmental Genetics, Heinrich Heine University Düsseldorf, Universitätsstraße 1, 40225 Düsseldorf, Germany

This chapter is in preparation

* Corresponding author: Daniel.VanDamme@psb.vib-ugent.be

Author Contributions: JW and DVD designed the experiments. JW generated all experimental materials and performed the majority of the experiments. RP helped with the Co-IP experiment and CGA helped with the imaging of flower meristems. NMF helped with microtomy experiments. RDR helped with the TEM experiments. QJ helped with identifying crosses plants. RS provided unpublished materials. TB and TV contributed to constructive suggestions. JW wrote the initial manuscript. DVD contributed to the revision of the manuscript.

Abstract

TPLATE complex (TPC) serves as a key endocytic adaptor complex at the plasma membrane (PM) and it is essential for pollen and somatic plant development. The male sterility and seedling lethality caused by knockout or knockdown of single TPC subunits prevent to uncover the roles of TPC during plant development. Here, by employing the partially functional TPLATE mutant, mWDX, we discovered the importance of TPC in shoot apical meristem (SAM) maintenance. Our results revealed that mild destabilization of TPC results in a predominant double-shoot phenotype caused by the splitting of the meristem which is consistent with the split *WUSCHEL* gene expression at the periphery. The vegetative meristem in mWDX2-complemented plants exhibited randomized cell identity and disordered patterning. The deficiency of endocytosis in mWDX2 complemented lines results in impaired internalization of CLV1 receptor from the PM and subsequent hypersensitivity to exogenous CLV3 peptide treatment. Due to the deficient endocytosis, mWDX2 seedlings also exhibited ectopic deposition of callose and thick cell walls in the vegetative meristems. Altogether, our results reveal that mildly perturbing TPC-dependent endocytosis predominantly leads to a manifestation of defects in SAM maintenance.

Introduction

Plant stem cells are defined by their ability to both renew themselves and to generate daughter cells to produce new tissues, residing in microenvironments called meristems (Heidstra and Sabatini, 2014; Kitagawa and Jackson, 2019; Uchida and Torii, 2019). Plants possess two primary meristems, the shoot apical meristem (SAM) and the root apical meristem (RAM), located at the tip of stem and the tip of the root respectively, that continuously produce cells for organ formation and growth throughout the life (Gaillochet et al., 2015; Greb and Lohmann, 2016).

The SAM is a dome-shaped tissue located at the shoot apex that maintains a group of pluripotent stem cells that enable plants to continuously generate all aerial tissues. In *Arabidopsis*, the SAM can be subdivided into three distinct cell layers (L1-L3): L1 and L2 cells constitute the two outermost layers and generate epidermal and subepidermal tissues, respectively. While L3 cells divide in all orientations and give rise to the internal tissues (Heidstra and Sabatini, 2014; Gaillochet and Lohmann, 2015; Somssich et al., 2016; Soyars et al., 2016; Truskina and Vernoux, 2018; Uchida and Torii, 2019). Superimposed on the layers organization, the SAM can also be organized into a central zone (CZ) that contains slowly dividing stem cells, the organizing center (OC) located beneath the CZ acts to instruct and maintain pluripotency of stem cells in the CZ, a surrounding peripheral zone (PZ) consists of more rapidly dividing cells that generates the lateral organs, and an underlying rib meristem zone (RM) where cells have a flattened shape as the first indication of differentiation toward central stem tissue (Vernoux et al., 2010; Aichinger et al., 2012; Heidstra and Sabatini, 2014; Gaillochet and Lohmann, 2015; Greb and Lohmann, 2016; Somssich et al., 2016; Soyars et al., 2016; Uchida and Torii, 2019). The zonation into functional domains in the SAM is dynamic as shown by several molecular markers (Reddy and Meyerowitz, 2005; Muller et al., 2006; Yadav et al., 2010)

Chapter 5

The maintenance of SAM homeostasis largely depends on a feedback loop between the homeodomain transcription factor *WUSCHEL* (*WUS*) and the *CLAVATA* (*CLV*) signaling pathway (Brand et al., 2000; Schoof et al., 2000). While *WUS* is expressed in the OC, *WUS* moves from the OC to the entire CZ via plasmodesmata [59, 60] and activates *CLAVATA3* (*CLV3*) expression by directly binding to the *CLV3* promoter (Mayer et al., 1998; Yadav et al., 2011; Daum et al., 2014; Perales et al., 2016). *CLV3* encodes a secreted peptide, which is a negative regulator of *WUS* expression via a signaling cascade which starts by the perception of *CLV3* by overlapping leucine-rich receptors located at the plasma membrane (Clark et al., 1997; Jeong et al., 1999; Deyoung and Clark, 2008; Muller et al., 2008; Atsuko Kinoshita, 2010; Hu et al., 2018). Thus, the *WUS-CLV* feedback loop forms a self-correcting mechanism to maintain a stem cell pool of constant size.

In *Arabidopsis*, Leucine-rich repeat receptor-like protein kinases (LRR-RLKs), including *CLAVATA 1* (*CLV1*), *BARELY ANY MERISTEMS* (*BAM*) and *RECEPTOR-LIKE PROTEIN KINASE 2* (*RPK2*), a receptor-like protein *CLAVATA 2* (*CLV2*) and a pseudo kinase *CORYNE* (*CRN*) are involved in the perception of the *CLV3* signal to repress *WUS* expression (Clark et al., 1997; Jeong et al., 1999; Deyoung and Clark, 2008; Muller et al., 2008; Atsuko Kinoshita, 2010; Hu et al., 2018). Of these, *CLV1* is the primary receptor for *CLV3* in the control of SAM homeostasis. *CLV1* is highly expressed and functions in the *WUS*-expressing RM cells in the SAM and can bind *CLV3* peptide directly via the extracellular LRR domain (ectodomain) with high affinity (Ogawa et al., 2008; Nimchuk et al., 2015). Genetic analysis and cell biology studies suggest *CLV1* functions in parallel with *CLV2/CRN* receptor complex (Muller et al., 2008; Bleckmann et al., 2010; Guo et al., 2010), while other work supports the idea that they could also work cooperatively as *CLV2/CRN* do not bind *CLV3* directly and thus serve as co-receptor of *CLV1* (Shinohara and Matsubayashi, 2015; Somssich et al., 2015). Although *CLV1* represses the expression of its closely related paralogs *BAM* in the RM, *BAM1* can bind *CLV3*

Chapter 5

peptide *in vitro* and thus partially compensates the loss of CLV1 (Deyoung and Clark, 2008; Nimchuk et al., 2015; Shinohara and Matsubayashi, 2015). Cell biology studies revealed that CLV1 undergoes CLV3-dependent trafficking from the plasma membrane (Nimchuk et al., 2011). Whether this serves to maintain or attenuate signaling in order to maintain SAM homeostasis remains to be uncovered.

Cell-to-cell signaling is a key organizing principle in plant development. SAM maintenance requires the precise coordination of cell division and differentiation, which depends on the directional intercellular transport of mobile signals. It has been shown that symplastic movement of WUS from the OC to the CZ through plasmodesmata is necessary to maintain stem cell fate; blocking its movement or degrading WUS in stem cells results in stem cell depletion (Yadav et al., 2011; Daum et al., 2014; Ma et al., 2019). Although cell biology and genetic data showed that CLV3 can move several cell layers to the WUS domain in the organizing center (Lenhard and Laux, 2003), little is known about CLV3 peptide movement (Kitagawa and Jackson, 2019).

Clathrin-mediated endocytosis (CME) is the major endocytic pathway that internalizes the receptors from PM. This can be either ligand-binding dependent or independent, it can serve recycling or degradation and it can lead to signaling attenuation, or to maintain signaling via endosomal signaling continuation (Paez Valencia et al., 2016; Claus et al., 2018). The octameric TPLATE complex (TPC), serves as an adaptor complex at the PM, and is essential for CME in plants (Gadeyne et al., 2014; Wang et al., 2020). Knockout or knockdown of single subunits of TPC in *Arabidopsis* leads to pollen or seedling lethality respectively, revealing that TPC is essential for both pollen and somatic plant development (Van Damme et al., 2006; Gadeyne et al., 2014; Wang et al., 2019). Although the weak allele *twd40-2-3* of TWD40-2 is viable while exhibited mild phenotype (Bashline et al., 2015). We know little about the roles of TPC during plant development, because of the male sterility and the seedling lethality. In our previous work (chapter 3 and chapter 4), we identified a partially

functional TPC mutant named mWDX via substituting the mWDX domain of TPLATE, which resulted in destabilizing the whole TPC, thus partially affecting TPLATE functionality. Here we show, using mWDX complemented lines, a substantial contribution of TPC-dependent CME to the SAM maintenance.

Results

Destabilizing TPC affects SAM patterning and results in a multiple-shoot phenotype

My data in chapter 4 showed that our partially functional allele of TPLATE (mWDX2) failed to show obvious developmental defects at the seedling developmental stage. To further determine whether our mWDX complemented lines showed any aberrant phenotypes, growth of mWDX plants was monitored and compared with TPLATE at different developmental stages. Compared with TPLATE complemented lines, mWDX plants displayed pleiotropic developmental phenotypes.

At the vegetative stage, seedlings of mWDX1 and mWDX2 plants lacked the typical spiral phyllotaxis displayed by TPLATE complemented lines, Col-0 and *tplate*(+/-) seedlings. Instead, they showed an altered phyllotactic patterning that we termed “butterfly-shape” phyllotactic patterning (Fig 1A and Fig S1A). In two-week-old TPLATE complemented lines, Col-0 and *tplate* (+/-) seedlings, the first pair of true rosette leaves emerged simultaneously, and all the subsequent leaves arose following a spiral phyllotaxy, characterized by the ‘golden angle’ of about 137.5°. mWDX1 and mWDX2 plants, in contrast, generated two-pair of leaves simultaneously after the emergence of the first pair of true leaves resembling a “butterfly” (Figure 1A and Fig S1A). This two-pair of leaves belonged to two developmental centres, which developed simultaneously as two individual shoots (Fig 1A and Fig S1B). Although single shoot, fasciated-shoot, triple-shoot, and even a higher order shoot phenotype

could also be observed in mWDX1 and mWDX2 plants, statistics confirmed the double-shoot phenotype as the predominant phenotype of mWDX1 and mWDX2 plants (Fig 1A-B and Fig S1 B-C). Given the fact that independent lines of mWDX1 and mWDX2 plants showed the similar ratio of mutant phenotype, we performed further studies using the somewhat stronger mWDX2 plants.

The control of meristematic activity is crucial for plants to maintain tissue homeostasis. The altered vegetative phyllotactic patterning was accompanied with an enlarged vegetative meristem (Williams et al., 2005; Mandel et al., 2014; Mandel et al., 2016). To understand what happens with the mWDX2 meristems, we firstly compared the vegetative SAMs of TPLATE and mWDX2 seedlings using the modified pseudo-Schiff propidium iodide staining technique (mPS-PI) (Truernit et al., 2008). Compared with TPLATE seedlings, mWDX2 seedlings showed visible smaller sizes of the first-pair true leaves, indicating a developmental delay of leaf primordia initiation in mWDX2 seedlings (Fig 1C). The meristem of TPLATE seedling was dome-shaped and well organized. In contrast, mWDX meristems were more dome-shaped with enlarged size (with increasing width and height) and disorganized (Fig 1C-D). The huge cells and the aberrant-oriented cells indicated that the SAM patterning in mWDX2 seedlings were randomized (Fig 1C).

mPS-PI staining stained starch deposits in the columella stem cells (CSCs) of the root apical meristem (RAM) are regarded as a symptom of loss of stemness (Stahl et al., 2013). The meristematic cells in TPLATE meristem lacked the mPS-PI stainable starch deposits, while meristematic cells in mWDX2 meristems showed massive deposition of mPS-PI stainable starches (Fig 1C). However, no evidences so far link the starch deposition to meristematic cell fate in SAM.

To further understand what causes the observed double-shoot phenotype in mWDX2 plants, we also examined the TPLATE and mWDX2 vegetative SAMs at the histological level in seedlings of different age. Histological sections from 2DAG (day after germination) seedlings showed that TPLATE seedlings

Chapter 5

displayed relative flat but already dome-shaped and organized SAMs, while mWDX2 seedlings exhibited enlarged and disorganized SAMs. Meristematic cells were small and dark-stained in TPLATE meristems, while the huge and transparent cells located at the summit of mWDX2 meristems indicates the alteration of cell identity (Fig 1E and S2). Sections from older seedlings showed that TPLATE plants possessed a well-organized and dome-shaped meristem. Whereas mWDX2 seedlings mostly exhibited different extent of split meristems. Unlike the uniformly stained TPLATE meristems, mWDX2 meristems typically visibly displayed two toluidine blue stained meristematic cell regions in the PZ, which were separated by a group of large and transparent cells located at the CZ and OC. (Fig 1E and S2). The typical split meristem likely accounts for the predominant double-shoot phenotype in mWDX2 plants (Fig1A and 1B).

Therefore, our data showed that TPLATE is required to maintain the SAM homeostasis as destabilizing TPLATE results in double-shoot phenotype, likely caused by the splitting of the vegetative meristem.

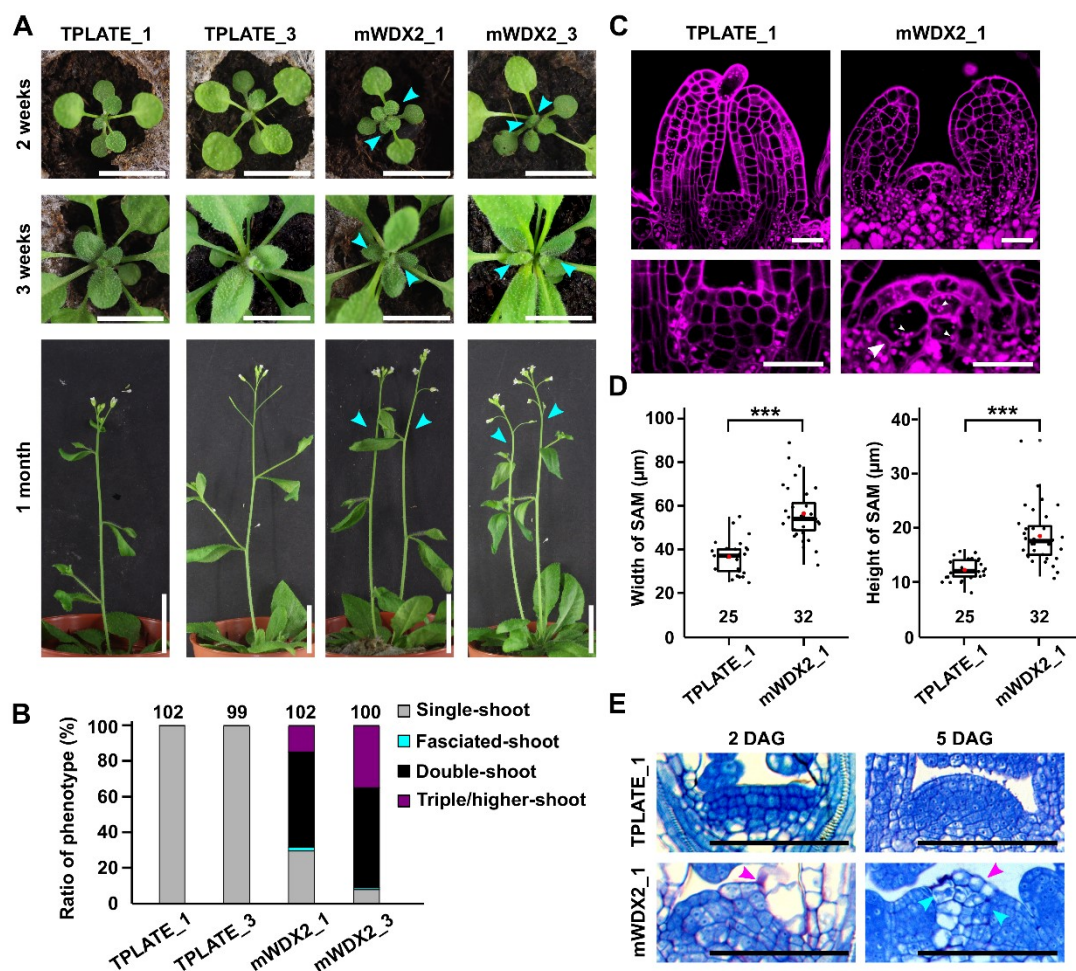


Figure 1. Destabilizing TPC affects SAM patterning and results in a multiple-shoot phenotype.

(A-B) Phenotype comparison (A) and quantification (B) of TPLATE and mWDX2 complemented plants at differential developmental stages. Two independent complemented lines of TPLATE and mWDX2 s mutants, fused to GFP (TPLATE_1 and mWDX2_1) and to mScarlet (TPLATE_3 and mWDX2_3), were grown at 21 °C in a growth chamber and imaged. Cyan arrowheads mark the altered phyllotaxis (2 weeks), emerging double-shoot (3 weeks) as well as two primary shoots in adult mWDX plants (one month). Shoot numbers in one-month-old plants of TPLATE and mWDX2 plants were quantified. Numbers at the top of bar chart indicate the amount of plants monitored. For 2 weeks and 3 weeks plants, scale bar = 1 cm. For one-month old plants, scale bar = 2 cm.

(C-D) Representative confocal images and quantification of the vegetative SAMs from TPLATE and mWDX2 seedlings after mPS-PI staining. 3-day old etiolated seedlings grown on $\frac{1}{2}$ MS medium were exposed to extra one-day light conditions priors to fixation. Large white arrowheads mark the huge cells and small white arrowheads mark the starch deposits in the SAMs of mWDX2 plants. Scale bar = 25 μm . The width and height of SAMs were quantified. Numbers for quantification are indicated at the bottom. ***, P < 0.001 for T-test.

(E) Histological sections of vegetative meristems from different aged seedlings of TPLATE as well as mWDX2 complemented lines. The 5 DAG (day after germination) and 2 DAG old seedlings were processed for microtomy and stained with 0,05% Toluidine blue. Magenta arrowheads indicate the defects while cyan arrowheads indicate individual meristematic regions marked by dense by Toluidine blue staining. Scale bar = 100 μ m.

Destabilizing TPC affects SAM patterning and results in ectopic PIN1 and DR5 expression

Changes in the spatial and temporal distribution of auxin act as key developmental signals during plant development. Polar auxin transport mediated by PIN1, the founding member of the PIN-FORMED (PIN) family of auxin efflux transporters, generates auxin maxima and minima, which are essential for organ initiation as well as SAM maintenance (Benková E, 2003; Reinhardt et al., 2003b; Heisler et al., 2005; Kierzkowski et al., 2013)

The trafficking and localization of plasma membrane-localized auxin carriers is under tight regulation. It has been shown that interfering with the functions of endocytic players results in disruption of the internalization or subcellular localization of PIN proteins at the PM (Kitakura et al., 2011; Fan et al., 2013; Wang et al., 2013; Gadeyne et al., 2014). To determine whether PIN1 internalization and localization is affected in mWDX2 vegetative meristems, we crossed the functional pPIN1:PIN1-GFP reporter (Benková E, 2003) into our TPLATE as well as mWDX2 complemented lines. In the vegetative SAMs of TPLATE seedlings, *PIN1* was mainly expressed in the L1 layer of the meristem and PIN1-GFP was polarly localized on the PM (Fig 2A), in agreement with previous reports (Reinhardt et al., 2003b; Guenot et al., 2012; Pfeiffer et al., 2016). In mWDX2 vegetative meristems, however, *PIN1* expression was massively observed in the PZ (not only in the L1 cells but also in the inner layer cells) but completely abolished by the huge cells located at the summit of meristem (Fig 2A), echoing our split meristem phenotype (Figure 1E). Besides,

increased amounts of PIN1 visibly localized on the PM in mWDX2 vegetative SAM (Fig 2A), suggested the impairment of PIN1 internalization in the mWDX2 meristem.

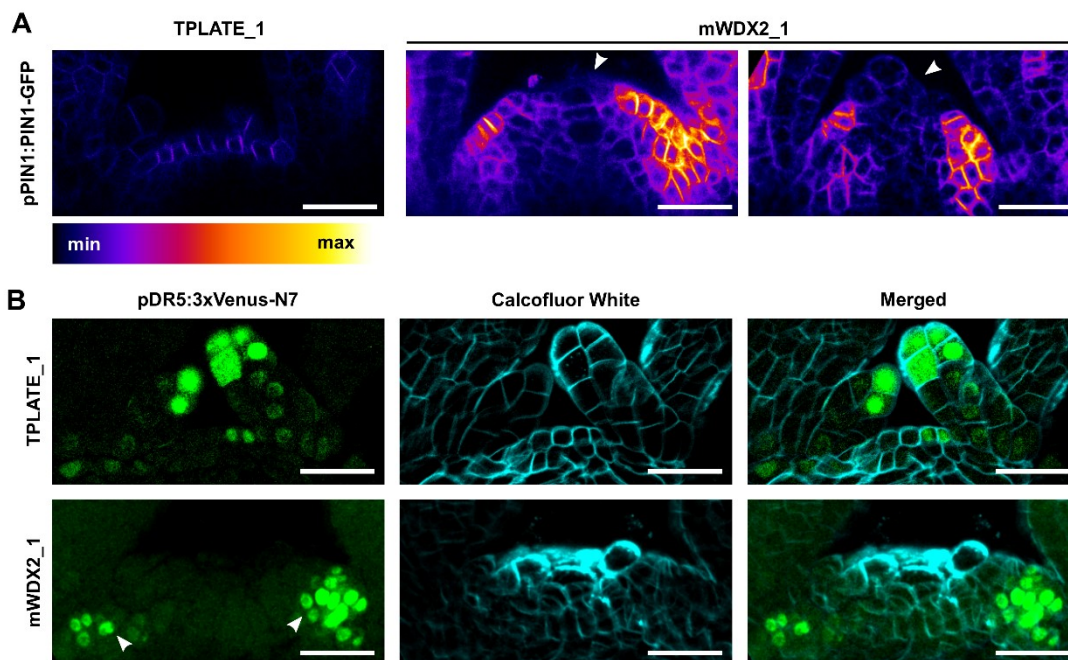


Figure 2. Destabilizing TPC affects SAM patterning and results in ectopic *PIN1* and *DR5* expression.

(A) Representative confocal images of PIN1 localization in the vegetative SAM of TPLATE and mWDX2 seedlings. The SAMs of 3-day-old seedlings expressing pPIN1-PIN1-GFP in TPLATE and mWDX2 complemented lines were imaged without fixation. White arrowheads indicate the absence of PIN1-GFP on the PM in the L1 cells of the CZ in WDX2 meristems. Scale bar = 25 μ m.

(B) Representative confocal images showing DR5 expression patterns in the vegetative SAMs of TPLATE and mWDX2 complemented lines. The SAMs of 3-day-old seedlings expressing pDR5:3xVenus-N7 in TPLATE and mWDX2 complemented lines were treated with ClearSee and stained with Calcofluor White prior to imaging. Scale bar = 25 μ m.

The *PIN1* expression pattern is dependent on the distribution of auxin in the meristem, which in turn depends on its transport (Heisler et al., 2005). The formation of auxin maxima in the L1 layer of the PZ is the first sign of incipient primordia position and associated lateral organs (Benková E, 2003; Reinhardt et al., 2003b; Heisler et al., 2005). The ectopic expression of *PIN1* promoted us

to examine the auxin maxima in our mWDX2 vegetative meristems. We made use of the auxin reporter line pDR5::3xVENUS-N7 (Heisler et al., 2005) in our TPLATE and mWDX2 complemented lines using the ClearSee technique (Kurihara et al., 2015). In the vegetative meristems of TPLATE seedlings, *DR5* was mainly expressed in the newly forming leaf primordia and the L1 layer of the PZ (Fig 2B), which is in line with the reported findings (Benková E, 2003). However, in the mWDX2 vegetative SAMs, expanded *DR5* expression was observed in the PZ, consistent with the ectopic *PIN1* expression in the PZ of mWDX2 meristems (Fig 2A and 2B). It is therefore possible that the extended auxin maxima contribute to the altered phyllotaxis in mWDX2 plants.

Although the auxin output minima has been functionally connected to stem cell identity, as induced stem cell loss in the CZ boosted the expression of *DR5v2* reporter (Ma et al., 2019). We failed to detect *DR5* expression in the CZ cells of mWDX2 vegetative SAM, although the expanded cell suggested they were differentiated or dead (Fig 2B).

Taken together, our data suggested the polar transport and distribution of auxin is affected in our mWDX2 vegetative meristems.

mWDX2 vegetative meristems exhibit re-specification of meristem identity

The split vegetative meristems in mWDX2 seedlings recalled us the classical SAM microsurgical ablation experiments in tomato where removal of the entire CZ and OC resulted in the re-establishment of a new meristem center or even a splitting of the meristem, along with ectopic tomato *WUS* gene expression or a doubling of the center of *WUS* expression (Reinhardt et al., 2003a).

To gain insight into the defects in mWDX2 meristem, we examined the expression of *WUS* and *CLV3* in the vegetative SAM. The transcriptional reporters pCLV3:mCherry-NLS and pWUS:3xVENUS-NLS were crossed into

our TPLATE and mWDX2 complemented lines (Pfeiffer et al., 2016). In TPLATE vegetative SAM, *WUS* and *CLV3* were normally expressed in the OC and CZ respectively (Fig 3A and 3B), which is in agreement with previous reports (Mayer et al., 1998; Fletcher et al., 1999; Pfeiffer et al., 2016). In mWDX2 vegetative meristems, the split *WUS* expression domain located in the PZ of mWDX2 vegetative meristem confirmed the re-establishment of two functional meristems (Fig 3A), in line with reported findings (Reinhardt et al., 2003a).

Live-cell imaging following induced down-regulation of *CLV3* or induced enhancement of *WUS* activity revealed that ectopic *WUS* expression induced expansion of *CLV3* expression into the PZ in SAM and re-specification of cells in the PZ back to stem cell identity (Reddy and Meyerowitz, 2005; Yadav et al., 2010). Unlike the vegetative SAM in TPLATE-GFP complemented lines, *CLV3* expression largely extended into the PZ, OC and even the RZ in mWDX-complemented lines, suggested a transition of the cells in these regions into the pluripotent stem cells of the CZ (Figure 3B).

The massively ectopic expression of *WUS* and *CLV3* in mWDX2 vegetative SAMs suggested a mixture of cell identities in the meristem. To test this hypothesis, we combined TPLATE and mWDX2 complemented lines expressing *WUS* and *CLV3* reporter lines respectively. The *CLV3* and *WUS* expression only overlapped in several L3 cells in TPLATE vegetative SAM, however, largely overlapped in the PZ, OC and the RZ even in some L1 and L2 cells in mWDX2 meristems (Figure 3C). The large overlap of the *WUS* and *CLV3* expression domains confirmed that cells in mWDX2 vegetative meristems underwent mixed identities since they expressed markers for both stem cell and organizing center fate.

Taken together, our data suggests that mWDX2 vegetative SAM undergoes a re-establishment of SAM with mixed cell identity.

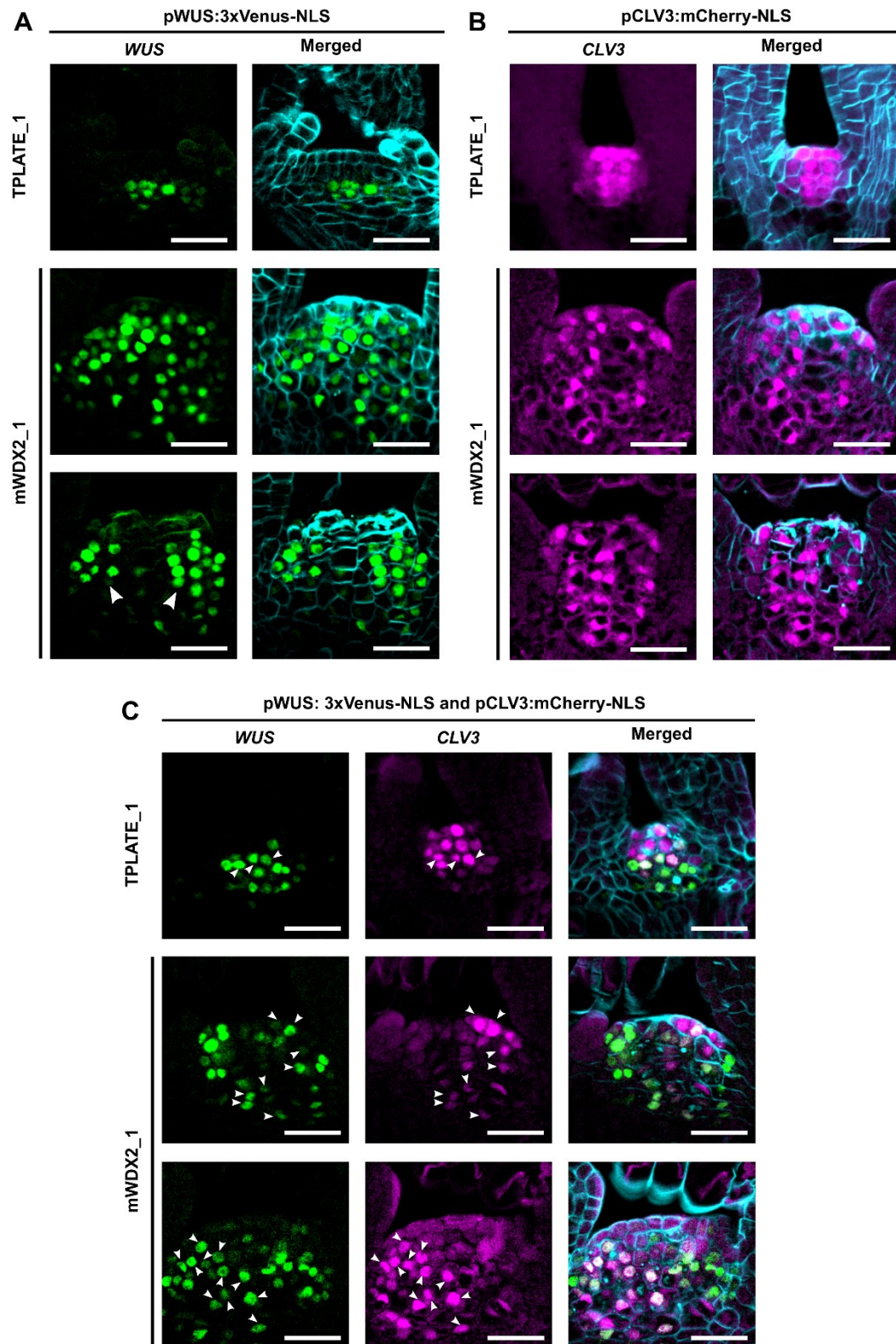


Figure 3. Destabilizing TPC affects SAM patterning and results in ectopic *WUS* and *CLV3* expression.

(A-B) Confocal images showing the *WUS* (A) or *CLV3* (B) expression patterns in the vegetative SAMs of TPLATE and mWDX2 complemented lines. The 3-day-old seedlings expressing the

Chapter 5

WUS or *CLV3* reporter in TPLATE and mWDX2 complemented lines were treated with ClearSee, stained with calcofluor white and imaged. White arrowheads in panel A indicate two *WUS* expression domains. Scale bar = 25 μ m.

(C) Confocal images showing the overlap of *WUS* and *CLV3* expression in vegetative SAMs of TPLATE and mWDX2 complemented lines. The TPLATE and mWDX2 complemented lines expressing *WUS* and *CLV3* were crossed. The 3-day-old seedlings were treated with ClearSee, stained with calcofluor white and imaged. The white arrowheads indicate the overlap between *WUS* and *CLV3* expression. Scale bar = 25 μ m.

Destabilizing TPC results in hypersensitivity to CLV3 signaling

Induced down-regulation of *CLV3* results in expanded *CLV3* and *WUS* expression in SAM (Reddy and Meyerowitz, 2005). The expanded *CLV3* and *WUS* expression therefore suggests a dysfunctional *CLV3*-mediated signaling pathway in mWDX2 vegetative meristems (Figure 3), which could be due to the dysfunction of *CLV* receptors or *CLV3* peptide. To differentiate between these processes, we evaluated the functions of receptors in mWDX2 vegetative SAM.

To generally evaluate *CLV* receptors function in mWDX2 vegetative meristems, mWDX2 and TPLATE complemented seedlings were exposed to synthesized *CLV3* peptide. TPLATE and mWDX2 seedlings grew normally when treated without or with low dose of *CLV3* peptides, even during long-term treatment (Fig 4A). However, mWDX2 seedlings exhibited hypersensitivity to higher concentrations of *CLV3* peptide as an increasing number of terminated SAM were found in mWDX2 seedlings compared to TPLATE seedlings at both 100nM and 1 μ M concentration of *CLV3* peptide (Fig 4A-B). To confirm the hypersensitive response of mWDX2 seedlings to *CLV3* peptide treatment, we further examined *WUS* promoter activity under *CLV3* peptide treatment. We crossed the *WUS* reporter line *pWUS-GUS* (Su et al., 2009) into TPLATE and the mWDX2 complemented lines and screened for homozygous lines of *pWUS-GUS* expression. After short-term treatment with *CLV3* peptide, *WUS* promoter activity in TPLATE and mWDX2 vegetative SAM was scored by GUS staining.

Compared with the control condition, both 10 nM and 100 nM CLV3 peptide treatment maintained a strong GUS staining of *WUS* promoter activity in TPLATE vegetative SAM (Fig 4C-D). In mWDX2 vegetative SAMs, however, *WUS* expression was dampened in a dose-dependent manner (Fig 4C-D), coherent with the terminated SAM phenotype (Fig 4A-B). Our data suggests that the CLV receptors in vegetative SAM of mWDX2 are able to perceive exogenously applied CLV3 peptide and that signal transduction is enhanced or sustained longer under these conditions.

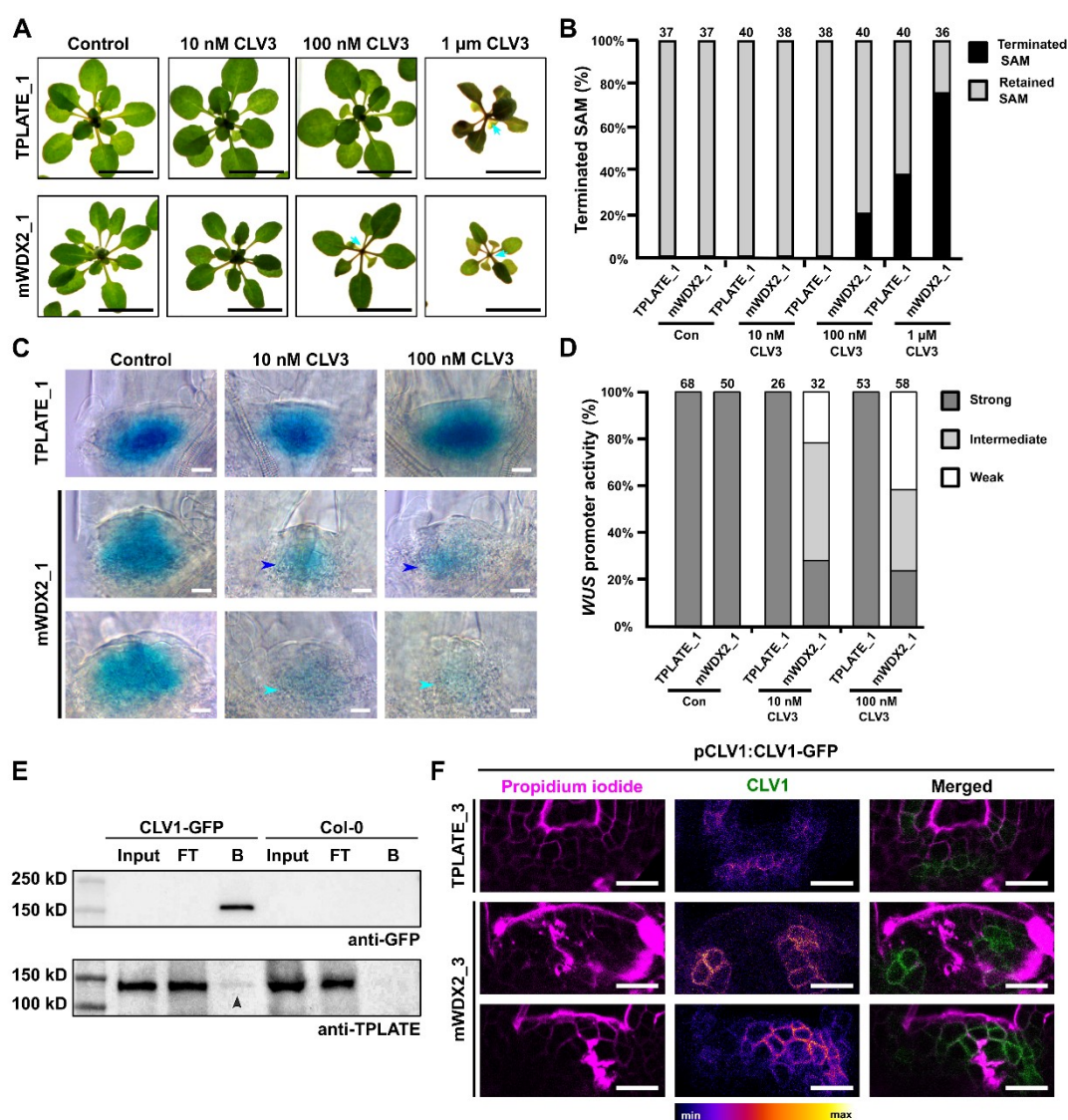


Figure 4. Destabilizing TPC results in hypersensitivity to CLV3 treatment as well as CLV1 accumulation at the PM.

(A) Phenotypical comparison of TPLATE and mWDX2 rosettes treated with or without different

Chapter 5

doses of CLV3 peptide. Plants were grown on ½ MS medium (without sucrose) supplemented with or without different doses of CLV3 peptide for 3 weeks. Cyan arrows indicate terminated SAM. Scale bar = 1cm.

(B) Quantification of the amount of meristems that terminated in function of the dose of CLV3. Numbers for quantification are indicated at the top of bar chart.

(C-D) Representative images (C) and quantification (D) of WUS expression in the vegetative SAMs of TPLATE and mWDX2 seedlings treated with or without CLV3 peptide. 3-day-old seedlings grown on ½ MS medium supplemented with different doses of CLV3 were fixed and GUS staining was performed for 3 hours. The intermediate (blue arrows) and weak (cyan arrows) WUS expression is indicated in the SAMs of mWDX seedlings after CLV3 peptide treatment. Scale bar = 50 µm. WUS expression after CLV3 treatment was scored and quantified. Numbers are indicated at the top of bar chart.

(E) Co-immunoprecipitation of TPLATE with CLV1-GFP. Total extracts of flowers expressing CLV1-GFP or the wild type (Col-0) were incubated with agarose-conjugated anti-GFP antibodies and probed with anti-GFP or anti-TPLATE antibodies.

(F) Confocal images showing enhanced PM localization of CLV1-GFP in mWDX2 vegetative meristems than in vegetative meristems of TPLATE-complemented lines. Scale bar = 20 µm.

Several CLAVATA3/ESR-RELATED (CLE) peptides were reported to inhibit root growth in *Arabidopsis* (Ito et al., 2006; Stahl et al., 2013; Hu et al., 2018). To test whether mWDX2 seedlings could response hypersensitively to other CLE peptides, we surveyed TPLATE and mWDX2 seedlings to 14 CLE peptides. Given the fact that *WUS-GUS* expression in mWDX2 SAM were hypersensitive to the super low dose of CLV3 peptide treatment. To perform CLE assay on primary root growth, seedlings were grown on 1/2 MS medium supplemented with 10 nM concentration of different CLE peptides. Mostly, the response of mWDX2 seedlings was largely similar to the TPLATE complimented line. However, mWDX2 seedlings showed hypersensitivity to CLV3, CLE 10 and CLE 40 peptides (Fig S3 A-B). A normalized root growth assay further confirmed the hypersensitivity of mWDX2 seedlings to low dose of CLV3 and CLE 40 peptides treatment (Fig S4 A-B).

CLE40 peptide is the closest homolog of CLV3 in *Arabidopsis*, which has been proven to play essential roles in the control of columella stem cells (CSCs)

in *Arabidopsis* root meristem while it could also function similar as CLV3 peptide in the SAM (Hobe et al., 2003; Ito et al., 2006; Stahl et al., 2009; Stahl et al., 2013). To further specify the hypersensitivity of mWDX2 seedlings to low doses of CLV3 and CLE 40 peptides, we also examined the response of mWDX2 seedlings to other peptides such as flg22, AtPEP1 and CEP (C-terminally encoded peptide), which have been shown to affect root growth (Roberts et al., 2016; Poncini et al., 2017). Generally, mWDX2 seedlings responded to these peptides similarly to TPLATE seedlings, although slight but statistically significant difference was found between TPLATE and mWDX2 seedlings responded to low dose of AtPEP1 treatment (Fig S4 A-B). Our data clearly showed that destabilizing TPC results in hypersensitivity to CLV3 and CLE40 treatment, suggested enhanced signaling of the receptors that recognize these peptides when treated with exogenous levels of peptide.

Destabilizing TPC results in impaired internalization of CLV1 in meristems

CLV1 mediates the CLV3 and CLE40 signaling pathway in both the SAM and RAM and CLV1 might undergo CLV3-dependent internalization to shut down CLV3 signaling in the SAM (Fletcher et al., 1999; Ogawa et al., 2008; Stahl et al., 2009; Nimchuk et al., 2011; Stahl et al., 2013; Shinohara and Matsubayashi, 2015). TPC functions at the PM to regulate the turnover of endocytic cargoes (Gadeyne et al., 2014), destabilizing TPC thus likely contributes to reducing the internalization of CLV1-GFP and consequently sustaining the signaling in meristems. The hypersensitive response of mWDX2 seedlings to exogenous CLV3 and CLE40 peptides treatment promote us to examine whether TPC-dependent endocytosis was involved in the internalization of CLV1.

To examine the interaction between TPC and CLV1, co-immunoprecipitation (Co-IP) experiments were performed with flower meristems expressing functional pCLV1:CLV1-GFP constructs. Our Co-IP analysis revealed a weak but reliable interaction between TPLATE and CLV1-GFP, when CLV1 was

precipitated via GFP-Trap (Fig 4E). To further test the involvement of TPC in the CLV1 internalization activated by CLV3, we monitored the PM localization of CLV1-GFP in TPLATE and mWDX2 vegetative meristems expressing the functional CLV1-GFP. A single locus CLV1-GFP transgenic line was screened and crossed into mScarlet fused TPLATE and mWDX2 complemented lines. Homozygous lines expressing CLV1-GFP in TPLATE and mWDX2 complemented lines were screened for imaging. Our preliminary live-cell imaging data showed that CLV1-GFP localized on the PM in both TPLATE and mWDX2 vegetative meristems (Fig 4F). While ectopic and more CLV1-GFP was observed to localize on the PM in vegetative meristems of mWDX2 compared to TPLATE seedlings (Fig 4F). Additionally, our data showed that TPLATE-GFP localized on the PM while mWDX2-GFP was more cytoplasmatic in flower meristems (Fig S5A). Similar to the vegetative SAMs, more CLV1-GFP was also observed to localize on the PM in mWDX2 flower meristems than in TPLATE flower meristem (Fig S5B). These results together suggest that CLV1-GFP internalization is likely impaired in mWDX2 meristems. Given the impaired internalization of reported cargoes in mWDX2 seedlings (Chapter 3 and 4), and the observed interaction between TPLATE and CLV1 in co-IP (Figure 4E), impaired endocytosis caused by destabilizing TPC likely contributes to the observed meristem accumulation of CLV1 in mWDX2 plants.

Taken together, our data suggested that destabilizing TPC results in hypersensitivity to CLV3 signaling under conditions of exogenously applied CLV3 peptide, which could be a consequence of impaired internalization of CLV receptors.

TPC targets more than the CLV1 receptor.

Given the complexity and redundancy of CLV1-mediated signaling, we further examined whether TPC is involved in regulation of other CLV1-related receptors. The *clv1* null mutant (*clv1-101*) shows a weak effect on shoot

Chapter 5

appearance whereas *clv1* missense mutations are dominant-negative and result in strong developmental phenotypes, similar to the *clv3* null mutant (Dievart et al., 2003; Atsuko Kinoshita, 2010). Besides, the weak phenotype of the *clv1* mutant could be enhanced by additional mutations in other receptors (Deyoung and Clark, 2008; Muller et al., 2008; Atsuko Kinoshita, 2010). To further illustrate the function of TPC in the CLV signaling pathway, we crossed the *clv1* null mutant (*clv1-101*) into TPLATE and mWDX2 complemented lines. Phenotypic analysis showed that the combination of TPLATE complemented line with *clv1-101* generally resembles *clv-101* single mutants, except a small group of the crossed plants which showed a fasciated-shoot phenotype (Fig 5A and 5C). In contrast, combining mWDX2 complemented lines with *clv1-101* maintained the double-shoot or even triple shoot of mWDX2 single mutants, and a large population of crossed plants exhibited a severely fasciated-shoot phenotype which was not observed before in mWDX2 plants (Fig 5B-C and Fig S1). These plants resembled higher order *clv* mutants or the *clv3* mutant (Fletcher et al., 1999; Deyoung and Clark, 2008; Muller et al., 2008; Nimchuk, 2017; Hu et al., 2018). Our genetic data further supports that TPC is likely involved in controlling the activity of several CLV-type receptors, presumably through internalization.

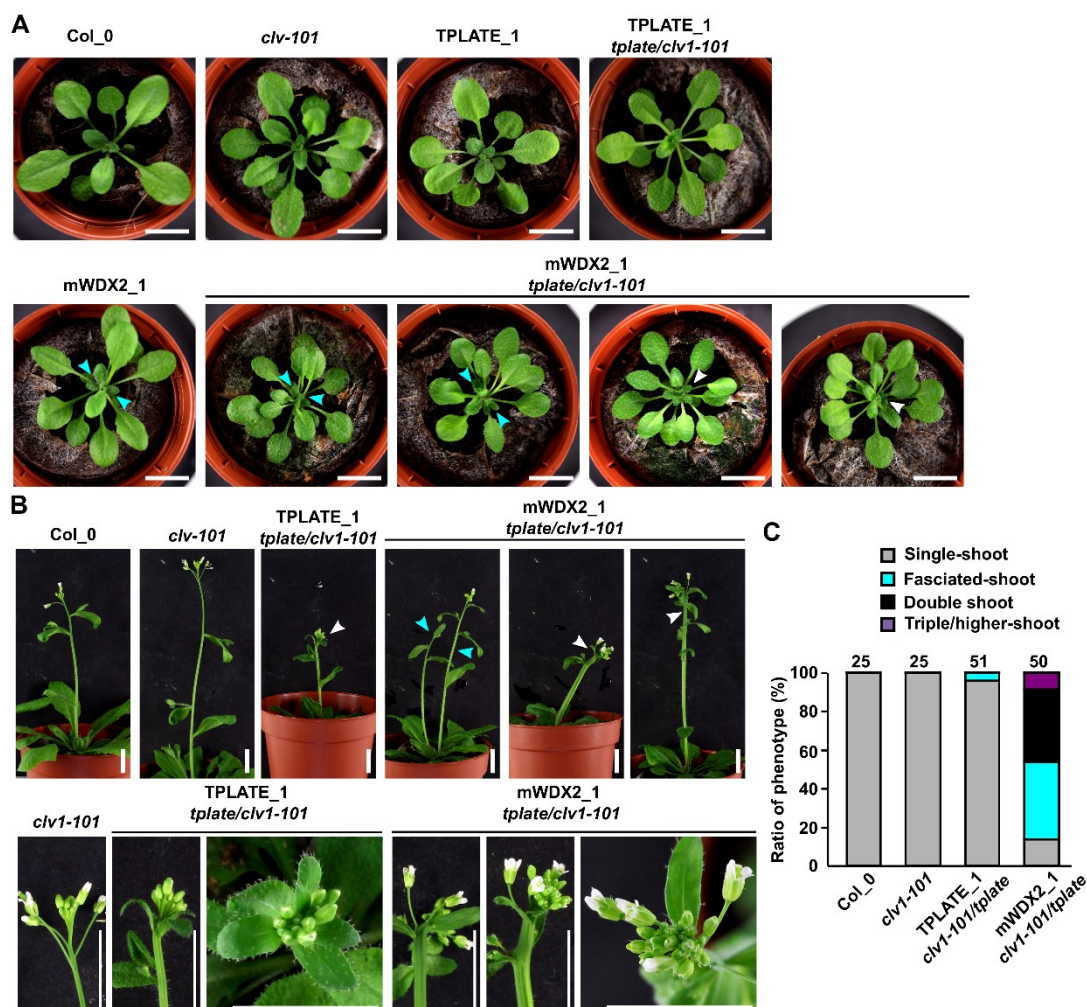


Figure 5. Destabilizing TPC enhances the *clv1* null mutant phenotype.

(A) Phyllotaxis phenotype comparison between Col-0, *clv1-101*, TPLATE, mWDX2, as well as TPLATE and mWDX-2 crossed with *clv1-101* plants. 3-week old plants grown in a growth chamber were imaged. Cyan arrowheads indicate emerging double-shoots and white arrowheads indicate severely fasciated shoots. Scale bar = 1cm.

(B-C) Shoot phenotype comparison (B) and quantification (C) between Col-0, *clv1-101*, TPLATE and mWDX-2 in a *tplate clv1-101* double homozygous mutant background. One-month-old plants grown in a growth chamber were imaged. Cyan arrowheads mark the double-shoot and triple- shoot while white arrowheads mark severely fasciated-shoots. Numbers for the quantification of the shoot phenotypes are indicated at the top of bar chart. Scale bar = 1cm.

Destabilizing TPC results in ectopic callose accumulation and altered cell wall morphology in vegetative meristems.

Impaired internalization of CLV1 in WDX2 vegetative SAM can explain the hypersensitivity of mWDX2 seedlings (SAM and RAM) to exogenous CLV3 peptide treatment. At the same time, this also suggests dysfunctional CLV3 signalling under normal conditions, which would otherwise lead to SAM termination. The presence of CLV1 at the PM, together with the absence of enhanced CLV1 signaling might be caused by the inability of CLV1 to perceive endogenous CLV3. The disordered SAM patterning as well as the randomized cell identity could be a barrier for perception of CLV1 to the CLV3 peptide.

TPC's functions has been linked to modulating cell wall components such as callose deposition and cellulose synthesis (Van Damme et al., 2006; Sanchez-Rodriguez et al., 2018). Disruption of TPC function leads to somatic and pollen developmental defects which could be traced back to the altered cell wall composition such as reduced cellulose contents and ectopic callose deposition respectively (Van Damme et al., 2006; Sanchez-Rodriguez et al., 2018).

To further reveal what could be the causal to the observed SAM defects in mWDX2 seedlings, we further examined callose accumulation in TPLATE and mWDX2 vegetative SAMs. Aniline blue staining revealed that callose deposition is detected at low levels in TPLATE vegetative SAM where it was mainly deposited into newly formed cell plates. However, in mWDX2 vegetative meristems, Z-projection images revealed numerous depositions of callose located at the top of meristems, typically in the L1 and L2 cells (Fig 5A). The intensive staining of cell walls in L1 and L2 cells, suggested the occurrence of an irregular cell wall pattern in mWDX2 vegetative SAM. Besides, the calcofluor white staining also revealed substantial cell wall thickenings at the top of mWDX2 vegetative SAMs (Fig 3A-B). Propidium iodide (PI) staining revealed frequent events of cell death only in the L1 cells of mWDX2 meristems, which is either a cause or a consequence of massive callose and cell wall depositions.

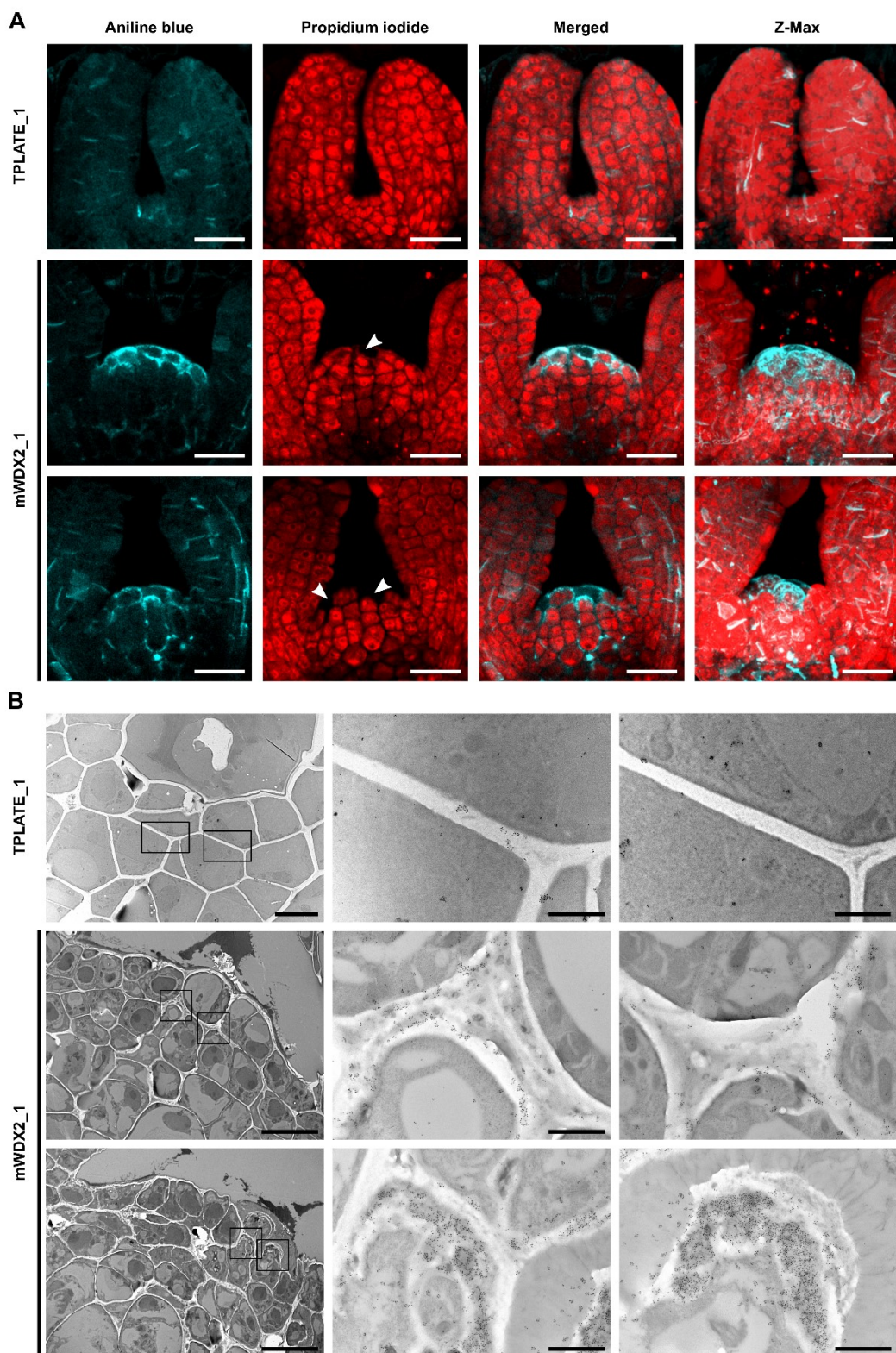


Figure 6. Destabilizing TPC results in ectopic callose deposition and aberrant cell wall depositions in vegetative SAM

(A) Representative confocal images showing callose depositions in the vegetative SAM of TPLATE seedlings and mWDX2 complemented lines. 3-day old seedlings were fixed with acetic

Chapter 5

acid: ethanol (1:3) solution and stained with aniline blue and PI. White arrowheads indicate dead cells.

(B) Immunoelectron microscopy sections of the vegetative SAMs from TPLATE and mWDX2 seedlings using a callose-specific antibody. The blow-up images are indicated by the black squares in the overview panels on the right. Left panel, scale bar = 10 μm . Right panel, scale bar = 1 μm .

To further specifically clarify callose depositions and altered cell wall morphology, vegetative SAM morphology was determined by means of transmission electron microscopy (TEM). As the irregular pattern of extra cell wall material is indicative of callose deposition, callose formation was examined by immunogold labeling. Using a specific antibody against callose, massive callose deposits were detected, predominantly in the thick cell walls between L1 and L2 cells in mWDX2 vegetative SAMs, while little labeling was found in the walls of TPLATE-complemented lines (Fig 6B). The thickened cell wall with massive callose depositions may explain the differentiated huge cells group that split the vegetative meristem. Furthermore, huge amounts of antibody-labeled callose spots were observed in the border between the dead L1 cells and the adjacent L2 cells in mWDX2 vegetative meristems, in agreement with our aniline blue staining (Fig 6A and 6B). These, therefore likely correlate with the cell death of the L1 cells. This observation recalled us the ectopic accumulation of callose in *tplate* shriveled pollen, which also correlated with pollen cell death (Van Damme et al., 2006).

Cell to cell communication is essential for stem cell maintenance (Daum et al., 2014; Liu et al., 2017). Callose deposition controls the permeability of the plasmodesmata, which is essential for symplastic cell to cell communication. Ectopic overexpression of CALLOSE SYNTHASE 3 (CALS3), which promotes callose deposition in the SAM, results in blocking the symplastic WUS movement from the OC to the CZ and thus causes stem cell depletion (Vaten et al., 2011; Daum et al., 2014; Ma et al., 2019). Given the massively ectopic callose deposition observed in mWDX2, the cell to cell communications

between different cells, layers or zonation are likely also affected in mWDX2 vegetative meristems.

Taken together, our data suggests that dampened endocytosis by destabilizing TPC results in accumulation of callose and aberrant cell wall depositions in the vegetative meristems of Arabidopsis.

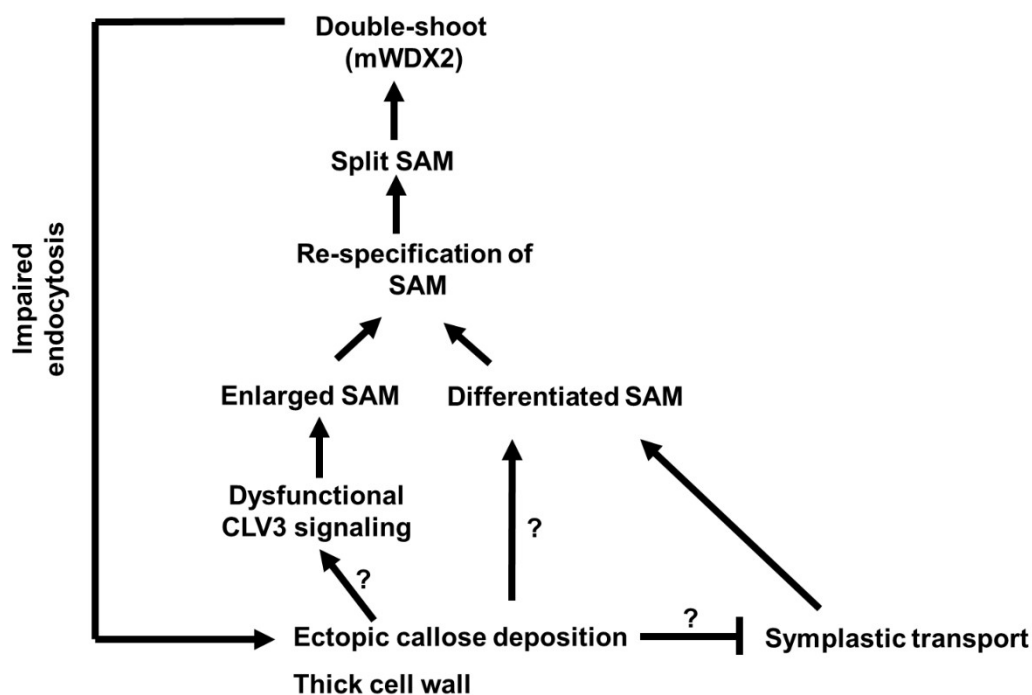


Figure 7. Model how TPC-dependent endocytosis is required for shoot apical meristem maintenance.

Destabilizing TPC via WDX complementation results in a predominant double-shoot phenotype, which can be traced back to split vegetative SAMs that are a consequence of the re-specification of SAM meristematic identity. The re-specification of vegetative SAMs in mWDX2 plants can be preceded by the formation of enlarged and differentiated meristems. Dysfunctional CLV3 signalling contributes to the enlarged SAM in mWDX2 plants. The dysfunction of CLV3 signalling as well as the differentiated SAM could be the consequence of the ectopic callose deposition and thick cell walls, which may contribute to blocking the trafficking and perception of CLV3 by CLV1 and its related receptors, as well as blocking the cell to cell communication.

Discussion

A threshold-dependent TPC function underpins SAM maintenance.

CME is critical for plant development as interfering with the function of endocytic players leads to pollen lethality or various plant developmental defects (Kitakura et al., 2011; Di Rubbo et al., 2013; Yoshinari et al., 2016; Adamowski et al., 2018). Mutations in single subunits of the Adaptor Protein-2 complex (AP-2) results in viable plants that however display various developmental defects, including abnormal embryo, seedling, and floral organ development (Fan et al., 2013; Kim et al., 2013; Yamaoka et al., 2013; Bashline et al., 2015). By contrast, knockout of single subunits of the TPLATE adaptor protein complex TPC (6/8 of TPC subunits), similar to the single subunit knockout mutant of clathrin light chain 1 (CLC1) and the dynamin related protein1c (DRP1c), causes male sterility (Van Damme et al., 2006; Backues et al., 2010; Wang et al., 2013; Gadeyne et al., 2014; Wang et al., 2019). Moreover, knockdown of single TPC subunits results in seedling lethality, respectively (Gadeyne et al., 2014). Although the importance of CME in the regulation of plant development has been addressed, the roles of CME in SAM maintenance are not well understood. Our partially functional TPLATE complemented line (mWDX), obtained by complementing the *tplate* T-DNA KO line with a mWDX-motif substituted form of TPLATE, exhibited a predominant double shoot phenotype caused by split vegetative meristem, and thereby linked TPLATE-dependent endocytosis to meristem maintenance (Fig 1, S1,S2 and 7).

Our independent mutations (mWDX1 and mWDX2) as well as independent lines (as well as independent fusions with GFP and mScarlet) suggested that the double-shoot phenotype is caused by TPC deficiency. Besides, our fasciated-shoot, double-shoot or multiple-shoot phenotype observed in mWDX2 plants correlates with our TPLATE RNAi lines, further supported this idea. Although the recent identified weak allele of TWD40-2, *twd40-2-3*, only

Chapter 5

exhibited a mildly aberrant phenotype (slight reduction in root growth and hypocotyl length) and showed normal shoot development under our growth conditions. Given the mild reduction of TWD40-2 in *twd40-2-3*, still adequate amounts of TPC are likely functional in *twd40-2-3* (Bashline et al., 2015). While the low amount TPLATE as well as the destabilization of the whole TPC, resulted in inadequate functional TPC in mWDX2 plants, which seems to be below the critical threshold in mWDX2 vegetative SAMs.

We mostly observed relative normal flowers (fasciated-siliques or double-siliques were also observed in some old flowers) suggesting that the flower meristems in mWDX2 plants are less affected. This is similar to the recently identified mutant of FASCIATED EAR3 (FEA3) receptor, which showed fasciated inflorescence stems with enlarged SAMs while flower and silique development were normal (Je et al., 2016). The phenotypical differences between the vegetative SAM and the inflorescence or floral meristem, or between the observed defects in the SAM and milder defects in RAM might be caused by the different activity of the pollen specific tomato promoter pLAT52 (Bate et al., 1996).

The pLAT52 promoter was originally employed to drive TPLATE to overcome its male sterility phenotype in the *tplate* KO mutant (Van Damme et al., 2006). However, the functional pLAT52::TPLATE-GFP fusion also showed expression in vegetative Arabidopsis cells, indicating that this tomato promoter is not pollen specific in Arabidopsis (Bate et al., 1996; Van Damme et al., 2006; Van Damme et al., 2011; Gadeyne et al., 2014). However, it remains unknown whether this promoter exhibits spatio-temporal or tissue specific expression levels in Arabidopsis. Further experiments to examine the expression pattern and dynamics of the pLAT52 promoter, by for example performing pLAT52::NLSYFP-GUS expression analysis, are required to answer this question.

Re-specification of stem cell identity in mWDX2 vegetative SAM

The re-specification of cells in the PZ back to stem cell identity has been proposed by microsurgical ablation experiments (Reinhardt et al., 2003a; Adibi et al., 2016). After ablation the CZ together with the OC in tomato SAM, two new *WUS* expressing centers reinitiated in plants which failed to replace the lesions in the meristem (Reinhardt et al., 2003a). While in mWDX2 vegetative meristems, it appears that the cells in the CZ and OC are differentiated and plants failed to replace them. This thus results in re-establishment of two or more new functional meristems (Fig 3 and 7). The split *WUS* expression domains in the PZ as well as the two independent normal shoots generated simultaneously from the split vegetative meristem supports this hypothesis. The ectopic expression of *CLV3* in the PZ also confirmed the re-specification of PZ cells back to stem cells. While the large overlap between *CLV3* expression and *WUS* expression cells suggested the mixture of cell identity.

It is still not completely clear what causes the developmental dynamics of the meristem identity in mWDX2 plants. We already observed disordered meristem patterning and randomized cell identity in 3-day old mWDX2 seedlings, which is a quite young developmental stage as it normally takes 2 days for seeds to germinate under our growth conditions. Further experiments to check the SAM patterning at the early embryo developmental stages will contribute to answering this question. Besides, the timepoint when mWDX2 meristems will start to exhibit defects may correlate with the dynamic behavior of the pLAT52 promoter activity and maybe even the re-specification of the meristematic cells in the SAM might also be linked to a re-activation of this promoter.

WUS and CLV3 expression is dysregulated in mWDX2 vegetative SAM

The expanded *WUS* expression domain reminds us of dysfunctional *CLV3* signaling in the mWDX2 vegetative meristem (Fig 3 and 7). The expanded *WUS* expression however fails to shift to the L1 layer of the meristem in the *clv3*

Chapter 5

mutant (Brand et al., 2000; Reddy and Meyerowitz, 2005). The ectopic *WUS* expression observed in L1 cells in mWDX2 vegetative meristems, suggests therefore that pathways, other than the CLV3-signaling pathway are affected. Knockout all CLV3 receptors, as in *clv1 bam1/2/3* quadruple mutants, exhibit extreme meristem over-proliferation beyond what is observed in *clv3* mutants, suggesting that additional CLE genes could buffer stem cell homeostasis in *Arabidopsis* (Nimchuk et al., 2015; Nimchuk, 2017). Recent work showed that the loss of function of the tomato *CLV3* ortholog (*SICLV3*) can be actively compensated by tomato *CLE9* (*SICLE9*). In *Arabidopsis*, loss of *CLV3* can be passively compensated by many *CLE* genes (Rodriguez-Leal et al., 2019). Thus, it is likely that signaling via other CLE peptides is dysfunctional as well in mWDX2 vegetative meristems.

The *WUS* distribution and HAM family activity together define *CLV3* expression pattern (Uchida and Torii, 2019). Recent work showed that the *CLV3* activation in the lower OC is prevented by the activity of HAIRYMERISTEM (HAM) family proteins, which are GRAS-domain transcription factors. Expression patterns of HAM family members and *CLV3* are nearly complementary along the apical–basal axis, and *CLV3* expression expands into the lower part of the SAM in absence of HAM family activity (Zhou et al., 2018). Thus, the deep ectopic expression of *CLV3* in the RM suggested that *CLV3* expression might be dysregulated as well.

A reversed expression pattern of *CLV3* and *WUS* was observed in the floral meristem in the double mutant of PLT-clade genes *AINTEGUMENTA* (*ANT*) and its closely related gene *AINTEGUMENTA-LIKE6/PLT3* (*AIL6/PLT3*). *CLV3* expression is shifted downward and overlaps with the region where *WUS* is normally expressed, however *WUS* expression is shifted upward and expands into the L1 and L2 layers (Krizek, 2009). The mechanism behind this unusual expression pattern is however largely unknown.

TPC-dependent CME internalizes CLV receptors

To prevent complete repression of *WUS* transcription, which would lead to catastrophic meristem termination, the CLV pathway must be downregulated after CLV3 peptide perception and subsequent signaling (Somssich et al., 2016). Thus, it is proposed that CLV1 undergoes CLV3-dependent trafficking from the plasma membrane to the vacuolar compartment to dampen CLV1 signaling (Nimchuk et al., 2011; Somssich et al., 2015). Cell biology research suggested that, in order to rapidly detect CLV3, CLV3 receptors form receptor complexes (CLV1-CLV1 homomeric, CLV2-CRN heteromeric, and CLV1-CLV2-CRN multimeric receptor complexes) that are regarded as in a “ready” state on the PM (Somssich et al., 2015; Yamaguchi et al., 2016). After perception of CLV3 peptide, increased numbers of CLV1-CLV2-CRN multimeric receptor complexes forming within subdomains of the plasma membrane might be internalized, thus this could serve as a means to shutting down the CLV3 signaling pathway (Somssich et al., 2015; Somssich et al., 2016).

TPC-dependent endocytosis functions to regulate the turnover of cargoes at the PM (Gadeyne et al., 2014; Bashline et al., 2015; Sanchez-Rodriguez et al., 2018). Our Co-IP data showed the interaction between TPLATE and CLV1. We observed CLV1 accumulation on the PM in mWDX2 meristems suggesting the impairment of CLV1 internalization although we do not know whether there are receptor complexes. The impaired internalization of CLV1, however, could be the consequences of either the impaired endocytosis or the failure of ligand perception of CLV1-GFP in mWDX2 meristems. Given the delayed endocytosis as well as the PM accumulated cargoes in mWDX2 seedlings (Chapter 3 and 4), the reduction of CLV1-GFP internalization in mWDX2 meristems could be partially attributed to the impaired endocytic capacity caused by destabilizing TPC in mWDX2 meristems.

Considering the disordered SAM patterning accompanied with the randomized cell identity, the ectopic callose deposition and thick cell walls

Chapter 5

observed in mWDX2 vegetative meristems might also contribute to affecting the efficiency for CLV1 to perceive CLV3 peptide under normal conditions. Our exogenous CLV3 peptide treatment experiments proved that CLV1 can transduce more CLV3-dependent signaling under exogenously applied CLV3 peptides conditions. Thus, examining the CLV1 PM accumulation in mWDX2 vegetative meristems combined with exogenous CLV3 treatment will contribute to addressing whether impaired CLV1 internalization, or impaired ligand perception is the main consequence of reduced endocytosis.

Endocytosis is proposed to dampen CLV3 signaling in plants (Nimchuk et al., 2011; Somssich et al., 2015). It appears that the hypersensitive response of mWDX2 vegetative SAMs and roots to exogenous CLV3 peptide is the consequence of deficient endocytosis to internalize receptor/receptor complexes to shut down CLV3 signaling. Our data showed that destabilizing TPC results in more specific hypersensitivity to several CLE peptides than other types of peptides under our tested conditions. This might be explained by the CLE signaling pathway acting as a more sensitive pathway than other peptide signaling pathways or that the other pathways have additional layers of control next to internalization. The SAM and RAM maintenance largely relies on the accurate regulation of CLE signaling which TPC-dependent endocytosis is likely involved in.

Additionally, our genetic data further suggested that TPC-dependent CME likely internalizes other receptors next to CLV1 as combining the mWDX2 mutant with *clv1-101* resulted in an enhanced phenotype beyond that of *clv1-101*. The mild phenotype of *clv1* can be partially attributed to the redundancy between *CLV1* and *BAMs*. *BAMs* display around 80% identity with *CLV1* in their kinase domains and they bind CLV3 with similar kinetics (DeYoung et al., 2006; Guo et al., 2010; Shinohara and Matsubayashi, 2015). Besides, *BAMs* can form multimeric complexes with *CLV1* in *N. benthamiana* and in *Arabidopsis* SAMs (Guo et al., 2010). It seems *BAM* receptors not normally function in the *CLV1* pathway in wild-type plants as *CLV1*-mediated signaling represses the

expression of *BAMs* (Nimchuk et al., 2015; Nimchuk, 2017). While *BAMs* can partially compensate for the loss of *CLV1* (Nimchuk, 2017). Based on these reported results, it is likely that TPC-dependent CME is also involved in the internalization of *BAMs* from the PM.

Ectopic callose deposition causes the defects in mWDX2 vegetative SAM

TPC was revealed to play specific roles in lignocellulosic cell wall formation, including cellulose synthesis, next to regulation the callose deposition in pollen and seedlings (Van Damme et al., 2006; Sanchez-Rodriguez et al., 2018). We could correlate the defective SAM patterning (differentiated and randomized cell identity) with massively ectopic callose deposition and thick cell walls in *mWDX2* seedlings. Besides, the dead cells observed in the L1 cells in *WDX2* meristems were also accompanied by massive amounts of ectopic callose deposition, which is similar to the observation in *tplate* KO pollen (Van Damme et al., 2006). Consequently, we speculated that the ectopic callose deposition and thick wall observed in the *mWDX2* meristems, on the one hand might contribute to the dead/differentiated cells at the summit and central zone of the meristem, on the other hand, it may also block the cell-to-cell communication between different functional zones (Fig 7).

The spatiotemporal zonation in the SAM is maintained by cell-to-cell signaling systems that specify cell specific transcriptional activity in the different zones to balance cellular division and regulate differentiation. To function as the central mobile signal in stem cell maintenance, *WUS* protein moves from the OC to the CZ via PD and activates *CLV3* expression in the CZ (Yoshida et al., 2011; Daum et al., 2014; Perales et al., 2016). Recent work showed that ectopic expression of an inactive version of *WUS* (*WUS*-delta Box) driven by the *ML1* promoter was able to move to the L2 and L3 layer cells. Thus, this seems a good candidate to evaluate the cell-to-cell communication in *mWDX2* vegetative meristems. Comparing the movement of labelled *ML1*-driven inactive *WUS* in

Chapter 5

TPLATE and mWDX2 vegetative meristems will contribute to addressing the effect of mWDX on cell-to-cell communications.

On the other hand, the regulation of the apoplastic space, or the extracellular matrix, is also important for receptor-ligand interactions (Janocha and Lohmann, 2018). The cell wall likely acts as a selective barrier to many biomolecules, which might also include CLE peptides. CLE peptides are supposed to move several cell layers before they are perceived by receptors and repress *WUS* expression (Brand et al., 2000; Schoof et al., 2000; Je et al., 2016). The randomized SAM pattern as well as the defective (thick) cell walls might also dampen CLE peptide movement, in particular CLV3, leading to a deficiency of CLV3 perception by its receptors. As the CLV3 peptide has never been localized *in vivo* (Kitagawa and Jackson, 2019), we cannot show how it could migrate in WDX2 vegetative meristem.

To further stress whether the ectopic callose is the casual of the defects we observed in mWDX2 meristems, it is essential to show whether the defective SAM patterning could be rescued by removing the ectopic callose deposition. Overexpression of the plasmodesma-localized β -1,3 glucanase 1 (PdBG1) is able to regulate callose accumulation in Arabidopsis roots (Benitez-Alfonso et al., 2013). We could apply a similar strategy and overexpress PdBG1 in mWDX2 to examine whether degrading the ectopic callose depositions will inhibit the cell death/differentiation in the mWDX2 meristem and thus convert the split meristem and double-shoot phenotype.

Our findings show that TPC-dependent CME is required for SAM maintenance. Deficient endocytosis caused by destabilizing TPC results in dysregulation of cells identity and a randomized cellular-pattern of the vegetative SAM which is correlated with dysfunctional CLV3 signaling and ectopic callose depositions in mWDX2 plants.

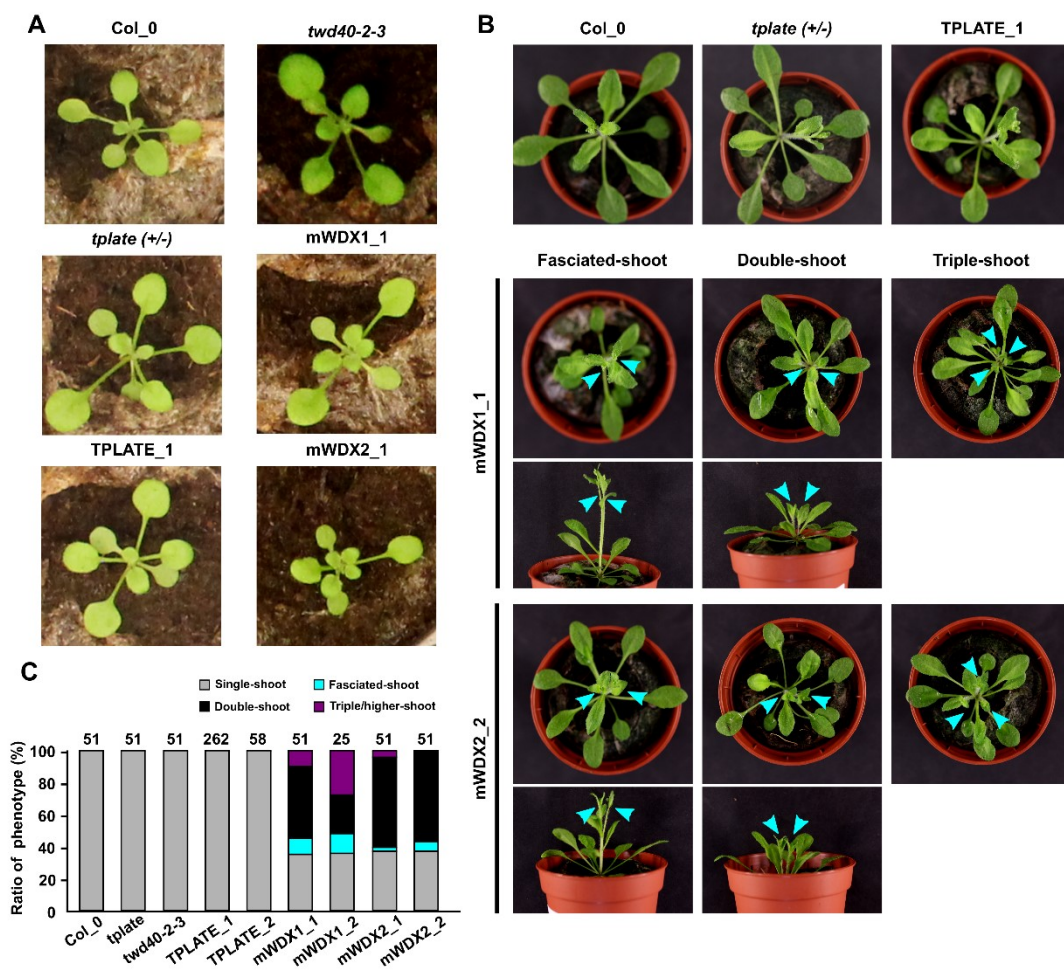


Figure S1. Destabilizing TPC result in multiple-shoot phenotypes.

(A) Phenotypical phyllotaxis comparison between Col-0, *tplate(+/-)*, TPLATE and mWDX1 and mWDX2 complemented plants. 2-week old plants grown in the greenhouse were imaged. mWDX1 and mWDX2 plants show a “butterfly” shape phyllotaxis as two pair of leaves, which belong to two centers, are generated simultaneously.

(B-C) Shoot phenotypical comparison and quantification between Col-0, *tplate(+/-)*, TPLATE and mWDX1 and mWDX2 s complemented plants. 3-week-old plants grown in the greenhouse were imaged. Cyan arrowheads mark fasciated-shoots, double-shoots and triple- shoots in mWDX1 and mWDX2 complemented plants. Shoot numbers used for the quantification are indicated at the top of bar chart.

Chapter 5

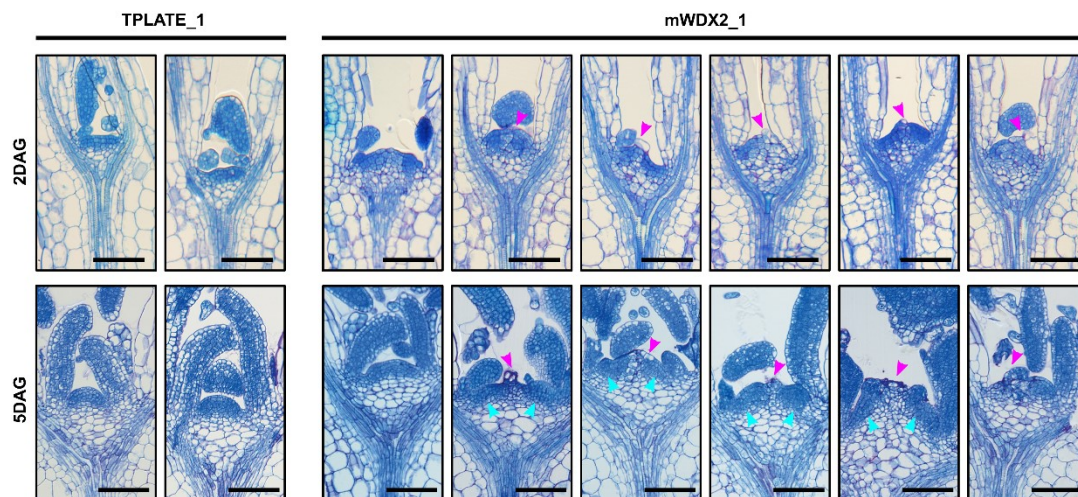


Figure S2. Destabilizing TPC causes different extent of defects in vegetative meristems. Histological sections of vegetative meristems from seedlings (2DAG and 5DAG) stained with Toluidine blue. Magenta arrowheads indicate the defects while cyan arrowheads indicate separate meristematic regions. Scale bar = 100 μ m.

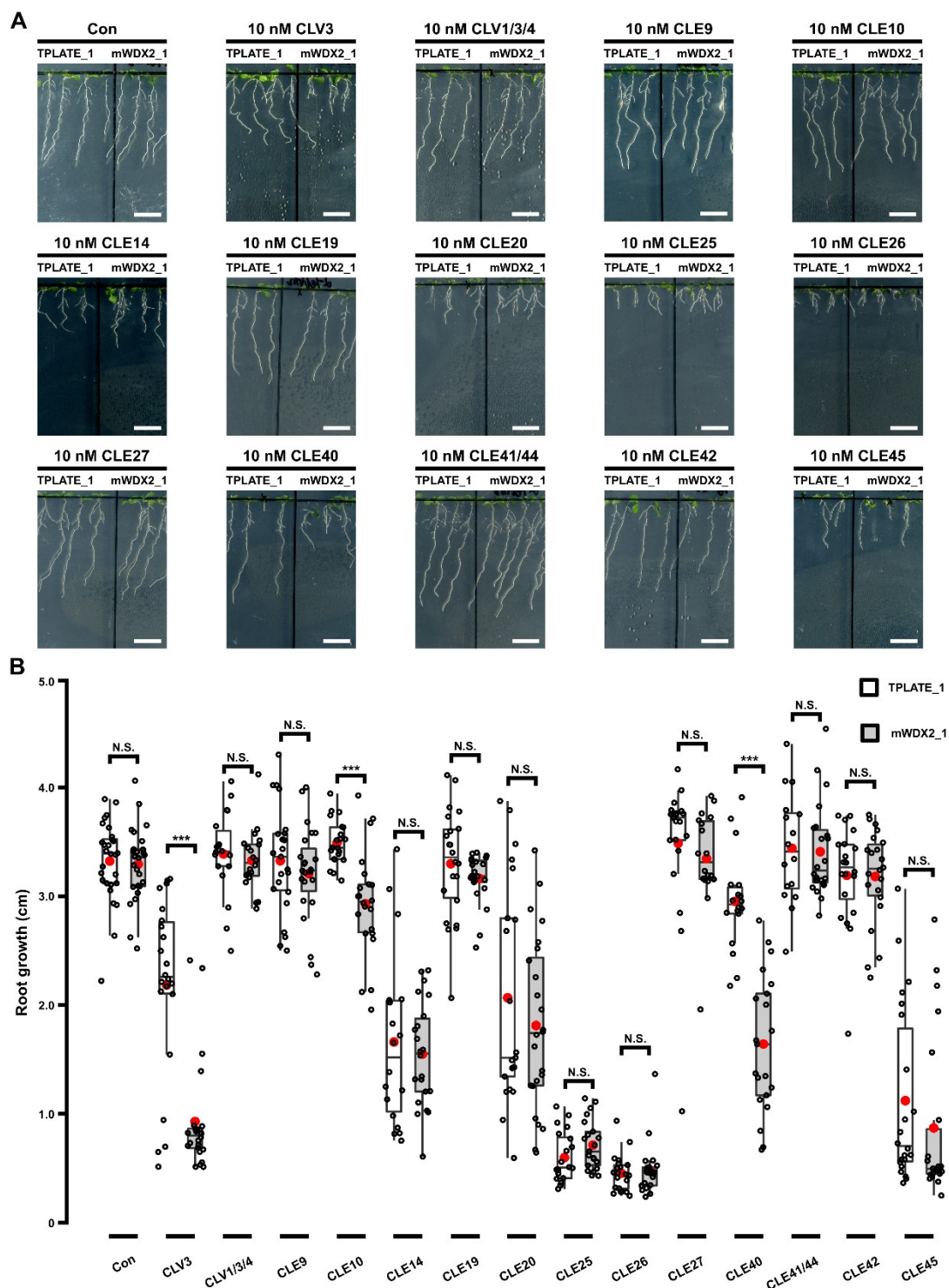


Figure S3. Destabilizing TPC results in hypersensitivity to different CLE peptides.

(A-B) Representative images and quantification of the root growth between TPLATE and mWDX2 seedlings treated with or without low doses of different CLE peptides. Seedlings were grown on $\frac{1}{2}$ MS medium supplemented with or without low doses of different CLE peptides for 8 days. Scale bar = 1cm. Primary root growth were quantified ($16 \leq N \leq 28$). ***, $P < 0.001$ for T-test. N.S., no significant difference.

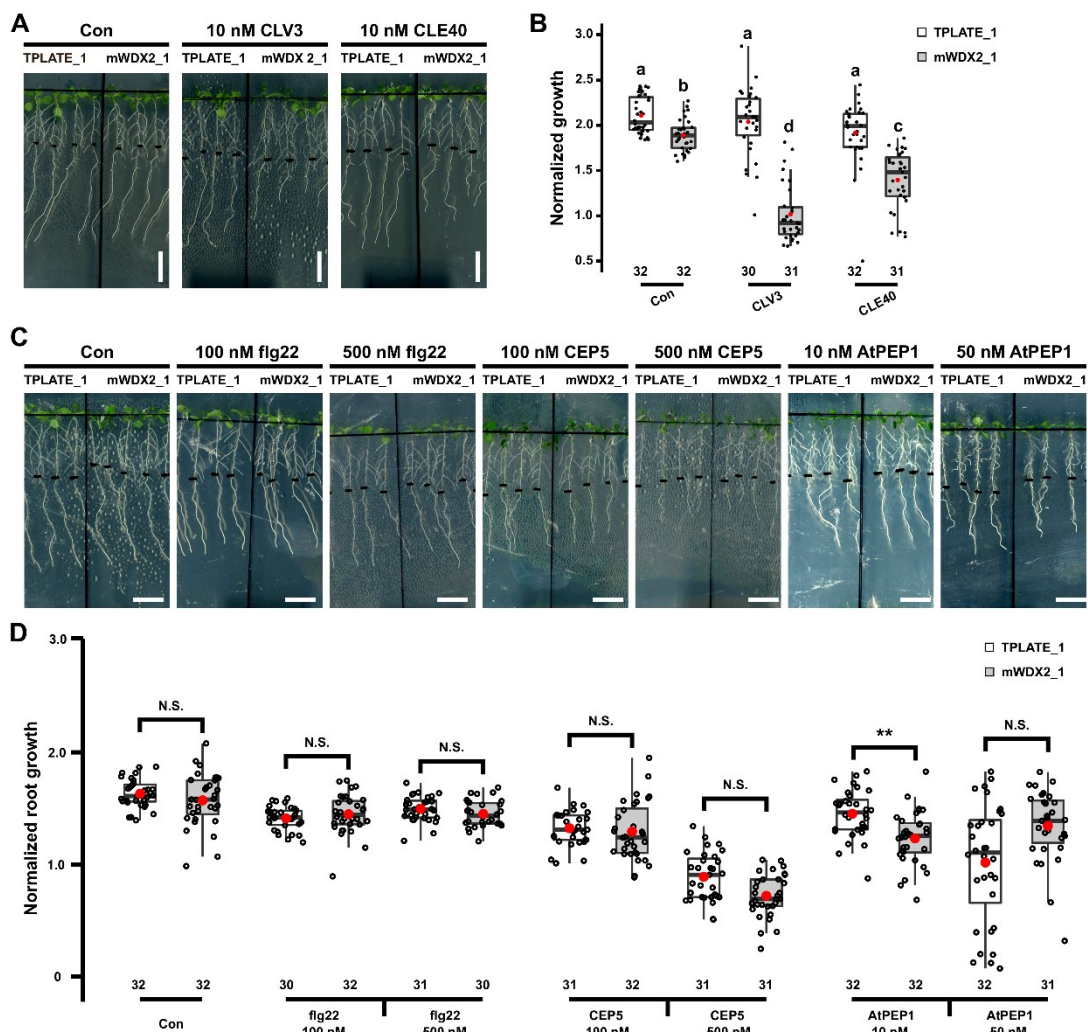


Figure S4. The hypersensitivity to CLV3 and CLE40, caused by destabilizing TPC is stronger than for other peptides.

(A-B) Representative images (A) and quantification (B) of the root growth from TPLATE and mWDX2 seedlings treated with (without) low doses of different CLV3 or CLE40 peptides. 5-day-old seedlings grown vertically on $\frac{1}{2}$ medium plate were transferred to fresh prepared $\frac{1}{2}$ MS medium supplemented with or without low doses of tested peptides and grown vertically for an additional 5 days. The root growth after transfer was normalized to the root growth before transfer. Numbers are indicated at the bottom of the graph. One-way anova, $P < 0.001$.

(C-D) Representative images (C) and quantification (D) of the root growth between TPLATE and mWDX2 seedlings treated with (without) different doses of flg22, CEP5 and AtPEP1 peptides. 5-day-old seedlings grown vertically on $\frac{1}{2}$ medium plate were transferred to freshly prepared $\frac{1}{2}$ MS medium plates supplemented with or without low doses of peptides and grown vertically for extra 5 days. The root growth after transfer was normalized to it before transfer. Numbers are indicated at the bottom of the graph. **, $P < 0.01$ for T-test. N.S., no significant difference.

Chapter 5

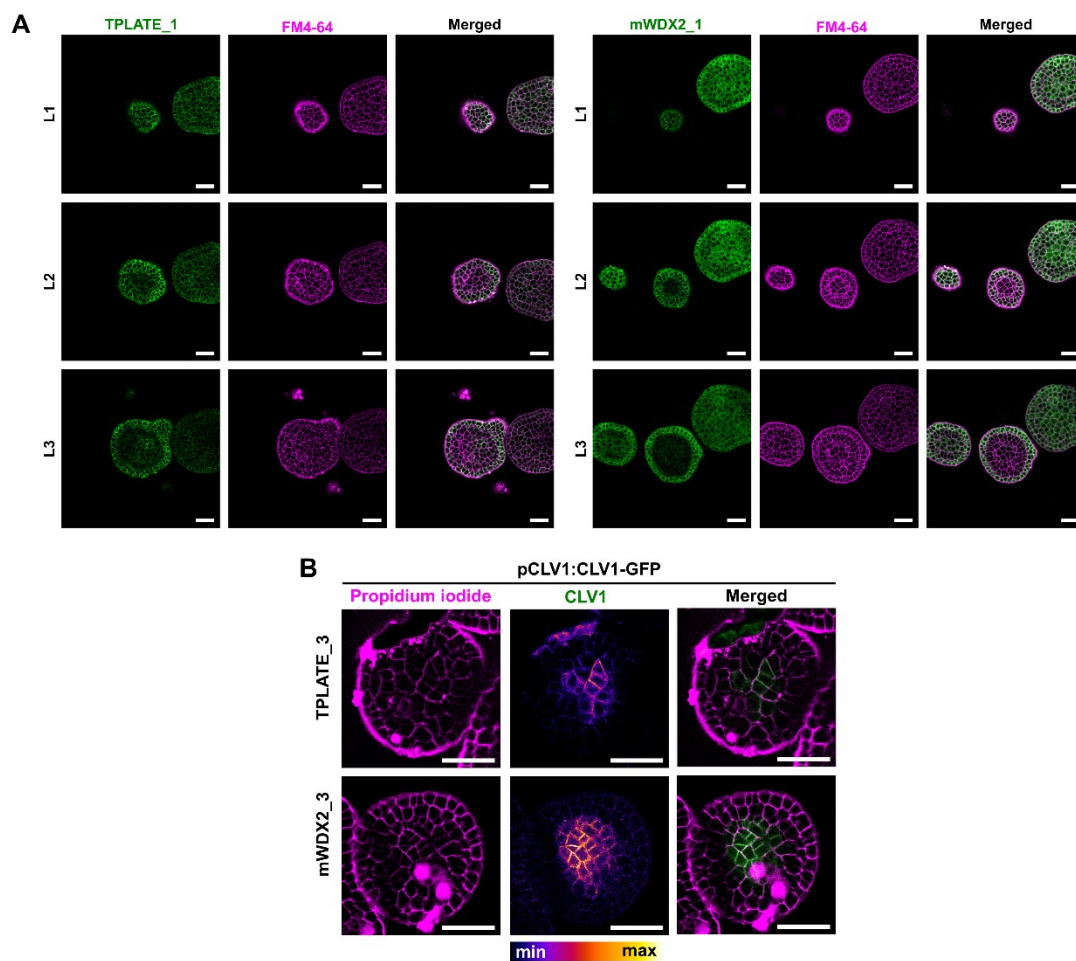


Figure S5. TPLATE is more cytoplasmic in the inflorescence meristem of mWDX2 plants compared to the TPLATE complemented lines.

(A) Consecutive confocal images (L1-L2-L3) showing the localization of TPLATE and mWDX2 in the inflorescence meristem. The PM is stained with FM4-64. Scale bar = 25 μ m.

(B) Confocal images showing enhanced PM localization of CLV1-GFP in mWDX2 flower meristems than in flower meristems of TPLATE-complemented lines. Scale bar = 25 μ m.

Chapter 5

Table 1. Information of transgenic lines used

Transgenic line	Constructs	Antibiotic selection	background
TPLATE_1	pLAT52-TPLATE-GFP	H	<i>tplate</i> (-/-)
TPLATE_2	pLAT52-TPLATE-tagRFP	H	<i>tplate</i> (-/-)
TPLATE_3	pLAT52-TPLATE-mScarlet	H	<i>tplate</i> (-/-)
mWDX1_1	pLAT52-mWDX1-GFP #1	B	<i>tplate</i> (-/-)
mWDX1_2	pLAT52-mWDX1-GFP #2	B	<i>tplate</i> (-/-)
mWDX2_1	pLAT52-mWDX2-GFP #1	B	<i>tplate</i> (-/-)
mWDX2_2	pLAT52-mWDX2-GFP #2	B	<i>tplate</i> (-/-)
mWDX2_3	pLAT52-mWDX2-mScarlet #1	H	<i>tplate</i> (-/-)

Chapter 5

Table 2. Sequence information of used CLE peptides

CLE peptide	Structure and glycosylation	
CLV3	RTVPSGPDPLHHH	RTVHypSG[Ara3]HypDPLHHH
CLE1/3/4	RLSPGGPDRHH	
CLE9	RLVPSGPNPLHN	RLVHypSGHypNPLHN+[Ara3], [Ara4] or[Ara6]
CLE10	RLVPSGPNPLHN	
CLE14	RLVPKGNPLHN	
CLE19	RVIPTGNPLHN	
CLE20	RKVKTGSNPLHN	
CLE25	RKVPNGDPIHN	
CLE26	RKVPRGPDPIHN	
CLE27	RIVPSCPDLHN	
CLE40	RQVPTGSDPLHH	
CLE41/44	HEVPSGPNPISN	
CLE42	HGVPSGPNPISN	
CLE45	RRVRRGSDPIHN	

Materials and methods

Molecular cloning

The mScarlet (Bindels et al., 2017) plasmid (Addgene) was amplified with stop codon and introduced into pDONRP2R-P3 via a Gateway BP reaction (Invitrogen) and confirmed by sequencing. To yield the mScarlet fused expression constructs, the TPLATE and mWDX2 motif substituted entry clones (Chapter 3) were combined with pHm34GW (Karimi et al., 2007), pDONRP4-P1r-Lat52 (Van Damme et al., 2006), and pDONRP2R-P3-mScarlet in triple gateway LR reactions (Invitrogen).

Arabidopsis transgenic lines and growth condition

The complemented transgenic lines expressing TPLATE-mScarlet and mWDX2-mScarlet were obtained by floral dip and identified by genotyping PCR described in Chapter 3. Transgenic lines of TPLATE and mWDX used for study in this chapter are listed in Table 1.

For all the crosses, the same reporter line or mutant plant was used as male to cross with TPLATE and mWDX2 complemented lines. To generate reporter lines into TPLATE and mWDX2 backgrounds, the reporter lines of pWUS:3xVENUS-NLS (Pfeiffer et al., 2016), pCLV3:mCherry-NLS (Pfeiffer et al., 2016), pPIN1:PIN-GFP (Benková E, 2003), pDR5:3xVENUS-N7 (Heisler et al., 2005) and pWUS-GUS (Su et al., 2009) were crossed into TPLATE_1 and mWDX2_1 complemented mutant backgrounds. The F2 plants were genotyped to obtain homozygous *tplate* mutant backgrounds. For the pWUS-GUS reporter line in TPLATE and mWDX2 complemented lines background, F3 even F4 generation plants were screened to identify homozygous plants for pWUS-GUS expression by GUS staining. To obtain dual-color marker lines of the *CLV3* and *WUS* reporter lines, the reporter line of *CLV3* and *WUS* in TPLATE or mWDX2 complemented lines were crossed.

Chapter 5

The functional pCLV1:CLV1-GFP line (Col-0 background) was kindly provided by Prof. Rüdiger Simon. The functionality of this marker was confirmed by complementation of the *clv1* mutant. Prior to crossing with TPLATE and mWDX2 transgenic lines, the pCLV1:CLV1-GFP line (Col_0 background) was backcrossed to Col-0 and a single locus expression T2 line was identified by Basta (20 mg/L) selection. The F2 Basta resistant CLV1-GFP plant was used to cross with the mScarlet fused TPLATE and mWDX2 complemented lines. In the progeny, plants homozygous for the *tplate* mutant background were identified by genotyping PCR while homozygous expression of CLV1-GFP was selected by BASTA selection.

The *clv1* null mutant *clv1-101* (Atsuko Kinoshita, 2010) was crossed into TPLATE and mWDX2 complemented lines, and the F2 plants were genotyped to achieve the *tplate clv1-101* double mutant background.

Seeds were sterilized by chlorine gas sterilization and sown on ½ MS medium plates following a 3-day vernalization at 4 degrees. For seedling experiments, seedlings were grown ½ MS media in a growth chamber under continuous light conditions at 20°C. For adult plants, one-week-old seedlings grown on ½ MS medium were transferred on soli medium and grown in a long-day (16h/8h, 20°C) growth chamber. To screen for shoot phenotypes of TPLATE as well as mWDX1 and mWDX2 plants, plants were grown in the greenhouse under long day regime with natural light.

Microtomy

The 2DAG or 5DAG seedlings were fixed with FAA for 3 days. Then seedlings were washed twice with a phosphate buffer (pH =7.2) and kept in dehydration series for 1 day and in infiltration series for extra 3 days. The roots and leaves were removed and the shoots were cut longitudinally with the microtome to generate 4 µM thick sections. Sections were stained with 0,05% Toluidine blue

Chapter 5

for 5 minutes followed by washing-off the staining solution. Then sections were mounted in DPX and kept in the fume hood for 3 days. After that, sections were ready to image.

Staining for confocal microscopy

Seedlings were treated with mPS-PI staining described before (Truernit et al., 2008). In brief, seedlings were fixed in fixative (50% methanol and 10% acetic acid) at 4°C for at least 12 h. Then seedlings were transferred to 80% ethanol and incubated at 80°C for 5 min and transferred back to fixative and incubated for another hour. Next, seedlings were rinsed with water and incubated in 1% periodic acid at room temperature for 40 min. The seedlings were rinsed again with water and incubated in Schiff reagent with propidium iodide (100 µg/mL) for 1 to 2 h or until plants were visibly stained. After PI staining, samples were cleared by chloral hydrate solution.

ClearSee treatment was done as described before (Kurihara et al., 2015; Ursache et al., 2018). Briefly, seedlings were fixed with 4% PFA following with PBS washing. Then seedlings were treated with ClearSee solution for 1 week up to 2 weeks until tissues were transparent. Then seedlings were stained with Calcofluor White (final 100 µg/ml) in ClearSee solution for 30 mins under vacuum, followed by washing in ClearSee solution for 1h.

GUS staining was performed as described before (Lammens et al., 2008). 3-day old seedlings grown on ½ MS with or without CLV3 peptide were harvested and incubated with 80% cold acetone for 30 min. After that, seedlings were washed with phosphate buffer, incubated in GUS staining solution and kept at 37 ° C in the dark for 3 hours. After GUS staining, seedlings were cleared with lactic acid and visualized with a BX51 light microscope (Olympus).

Callose staining was performed as described before (Kulich et al., 2015). Seedlings were incubated KH₂PO₄ (pH = 9.5) medium supplemented with 0.01% (w/v) aniline blue for 2 h with vacuum. After aniline blue staining, samples were

stained with PI (10 µg/mL) for 5 minutes.

Confocal imaging

Leica SP8X confocal microscope equipped with white laser was used to image. Pictures were taken with 25x (Fluotar VISIR 25x, NA = 0.95) or 40x (HC PL APO CS2, NA=1.10) water immersion objectives. The PI (excitation at 530 nm, emission at 600 - 710 nm), Calcofluor White (excitation at 405 nm, emission at 430 - 470 nm), Aniline Blue (excitation at 405 nm, emission at 490 - 4510 nm) and FM4-64 (excitation at 530 nm, emission at 650 - 750 nm), were imaged with out or with Hybrid detectors (HyDTM) a time-gated emission window between 0.3 ns - 6 ns. Signals of calcofluor white and callose channel was collected with HyDTM without gating. To visualize seedlings expressing reporter genes, fluorescence for GFP (excitation 488 nm, emission 500-540 nm), Venus (excitation 514 nm, emission 520-550 nm), mCherry (excitation 561 nm, emission 590-650 nm), were imaged respectively. Hybrid detectors (HyDTM) were used to collect the signal set with a time-gated window between 0.3 ns-6.0 ns. Individual channels of dual-color or triple-color images were imaged sequentially in line/frame model .

Transmission Electron Microscope analysis

Shoot apical meristem of four-day-old seedlings (3-day old etiolated seedlings were exposed to extra one-day light) from TPLATE and mWDX2 complemented lines were excised, immersed in 20% (w/v) BSA and frozen immediately in a high-pressure freezer (Leica Ice; Leica Microsystems, Vienna,Austria).

For immunolocalization freeze substitution was carried out in an EM AFS2 (Leica Microsystems). Over a period of four days, cells were freeze-substituted in dry acetone with 0.1% glutaraldehyde over 4 days period as follows: -90°C

Chapter 5

for 24 hours, 2°C per hour increase for 15 hours, -60°C for 16 hours, 2°C per hour increase for 15 hours, and -30°C for 8 hours. At -30°C the carriers were rinsed 3 times with acetone for 20 min each time. Samples were then slowly warmed up to 4°C. They were infiltrated stepwise over 3 days at 4°C in LR-White, hard grade (London Resin, Basingstoke, UK), and embedded in capsules. The polymerization was performed in Leica EM AFS using UV illumination over 6 days starting at 0°C and ending at 37°C. Ultrathin sections of gold interference color were made using an ultra-microtome (Leica EM UC7) and collected on formvar-coated copper slot grids. All steps of immunolabeling were performed in a humid chamber at RT. Grids were floated upside down on 25 µl of aliquots of blocking solution (5 % BSA, 1% FSG in PBS) for 20 min followed by a wash step for five times 5 min (1% BSA in PBS). Incubation in a dilution (1% BSA in PBS) of primary antibodies (anti-callose 1:1000; Biosupplies Australia) for 120 min was followed by washing five times 5 min (0.1 % BSA in PBS). The grids were then incubated with unconjugated bridging antibodies rabbit anti-mouse (Jackson ImmunoResearch) (1% BSA in PBS) for 30 min followed by incubation with PAG10nm (Cell Biology Utrecht University) and washed twice for 5 min each time with 0.1% BSA in PBS, PBS, and double-distilled water. Control experiments consisted of treating sections with PAG alone and with bridging antibodies and PAG10nm.

Sections were post-stained in a Leica EM AC20 for 30 min in uranyl acetate at 20 °C. Grids were viewed with a JEM 1400plus transmission electron microscope (JEOL, Tokyo, Japan) operating at 80 kV.

Phenotypical analysis

CLE peptides were ordered from GeneScript, the sequences of the peptides used are listed in Table 2. For shoot treatments, seedlings were grown horizontally on 1/2 MS medium supplemented with or without a certain

Chapter 5

concentration of CLV3 peptide for 3 weeks. The terminated shoot plants were counted. For root growth assays, seedlings were grown or transferred to 1/2 MS medium supplemented with or without CLE peptides or other peptides for 8 days or extra 5 days. Roots were scanned and root lengths were measured with Fiji equipped with the NeuronJ plugin.

Co-IP

Transgenic plants were ground to fine powder in liquid nitrogen and lysed with an extraction buffer (50 mM Tris (pH 7.5), 150 mM NaCl, 1 mM EDTA, 10% glycerol, 0.1% NP-40 and complete protease inhibitor cocktail (Roche)). After solubilization with the extraction buffer and incubation for 30 min at 4 °C on a rotating wheel, the samples were cleared twice at 20,000g for 10 min at 4 °C, and the supernatant was then incubated with anti-GFP magnetic beads (Miltenyi Biotec) for 2 h at 4 °C with gentle shaking. The beads were then collected and washed three times with the extraction buffer. Proteins bound on the beads were boiled with 1× SDS loading buffer for 5 min and then analysed by immunoblotting with an anti-GFP (anti-GFP HRP conjugated, 1:2,000, Miltenyi Biotec) and anti-TPLATE antibody (1:1,000, (Dejonghe et al., 2019)).

Chapter 5

References

Adamowski, M., Narasimhan, M., Kania, U., Glanc, M., De Jaeger, G., and Friml, J. (2018). A Functional Study of AUXILIN-LIKE1 and 2, Two Putative Clathrin Uncoating Factors in Arabidopsis. *Plant Cell* **30**: 700-716.

Adibi, M., Yoshida, S., Weijers, D., and Fleck, C. (2016). Centering the Organizing Center in the Arabidopsis thaliana Shoot Apical Meristem by a Combination of Cytokinin Signaling and Self-Organization. *PLoS ONE* **11**: e0147830.

Aichinger, E., Kornet, N., Friedrich, T., and Laux, T. (2012). Plant stem cell niches. *Annu Rev Plant Biol* **63**: 615-636.

Atsuko Kinoshita, S.B., Yuriko Osakabe, Shinji Mizuno, Shingo Nagawa, Yvonne Stahl, Rüdiger Simon, Kazuko Yamaguchi-Shinozaki, Hiroo Fukuda and Shinichiro Sawa. (2010). RPK2 is an essential receptor-like kinase that transmits the CLV3 signal in Arabidopsis. *Development*.

Backues, S.K., Korasick, D.A., Heese, A., and Bednarek, S.Y. (2010). The Arabidopsis dynamin-related protein2 family is essential for gametophyte development. *Plant Cell* **22**: 3218-3231.

Bashline, L., Li, S., Zhu, X., and Gu, Y. (2015). The TWD40-2 protein and the AP2 complex cooperate in the clathrin-mediated endocytosis of cellulose synthase to regulate cellulose biosynthesis. *Proc Natl Acad Sci U S A* **112**: 12870-12875.

Bate, N., Spurr, C., Foster, G.D., and Twell, D. (1996). Maturation-specific translational enhancement mediated by the 5'-UTR of a late pollen transcript. *Plant J* **10**: 613-623.

Benitez-Alfonso, Y., Faulkner, C., Pendle, A., Miyashima, S., Helariutta, Y., and Maule, A. (2013). Symplastic intercellular connectivity regulates lateral root patterning. *Dev Cell* **26**: 136-147.

Benková E, M.M., Sauer M, Teichmann T, Seifertová D, Jürgens G, Friml J. (2003). Local, Efflux-Dependent Auxin Gradients as a Common Module for Plant Organ Formation. *Cell* **115**: 591-602.

Bindels, D.S., Haarbosch, L., van Weeren, L., Postma, M., Wiese, K.E., Mastop, M., Aumonier, S., Gotthard, G., Royant, A., Hink, M.A., and Gadella, T.W., Jr. (2017). mScarlet: a bright monomeric red fluorescent protein for cellular imaging. *Nat Methods* **14**: 53-56.

Bleckmann, A., Weidtkamp-Peters, S., Seidel, C.A., and Simon, R. (2010). Stem cell signaling in Arabidopsis requires CRN to localize CLV2 to the plasma membrane. *Plant Physiol* **152**: 166-176.

Brand, U., Fletcher, J.C., Hobe, M., Meyerowitz, E.M., and Simon, R. (2000). Dependence of stem cell fate in Arabidopsis on a feedback loop regulated by CLV3 activity. *Science* **289**: 617-619.

Chapter 5

Clark, S.E., Williams, R.W., and Meyerowitz, E.M. (1997). The CLAVATA1 gene encodes a putative receptor kinase that controls shoot and floral meristem size in Arabidopsis. *Cell* **89**: 575-585.

Claus, L.A.N., Savatin, D.V., and Russinova, E. (2018). The crossroads of receptor-mediated signaling and endocytosis in plants. *J Integr Plant Biol* **60**: 827-840.

Daum, G., Medzihradzky, A., Suzuki, T., and Lohmann, J.U. (2014). A mechanistic framework for noncell autonomous stem cell induction in Arabidopsis. *Proc Natl Acad Sci U S A* **111**: 14619-14624.

Dejonghe, W., et al. (2019). Disruption of endocytosis through chemical inhibition of clathrin heavy chain function. *Nat Chem Biol* **15**: 641-649.

Deyoung, B.J., and Clark, S.E. (2008). BAM receptors regulate stem cell specification and organ development through complex interactions with CLAVATA signaling. *Genetics* **180**: 895-904.

DeYoung, B.J., Bickle, K.L., Schrage, K.J., Muskett, P., Patel, K., and Clark, S.E. (2006). The CLAVATA1-related BAM1, BAM2 and BAM3 receptor kinase-like proteins are required for meristem function in Arabidopsis. *Plant J* **45**: 1-16.

Di Rubbo, S., et al. (2013). The clathrin adaptor complex AP-2 mediates endocytosis of brassinosteroid insensitive1 in Arabidopsis. *Plant Cell* **25**: 2986-2997.

Dievart, A., Dalal, M., Tax, F.E., Lacey, A.D., Huttly, A., Li, J., and Clark, S.E. (2003). CLAVATA1 dominant-negative alleles reveal functional overlap between multiple receptor kinases that regulate meristem and organ development. *Plant Cell* **15**: 1198-1211.

Fan, L., Hao, H., Xue, Y., Zhang, L., Song, K., Ding, Z., Botella, M.A., Wang, H., and Lin, J. (2013). Dynamic analysis of Arabidopsis AP2 sigma subunit reveals a key role in clathrin-mediated endocytosis and plant development. *Development* **140**: 3826-3837.

Fletcher, J.C., Brand, U., Running, M.P., Simon, R., and Meyerowitz, E.M. (1999). Signaling of cell fate decisions by CLAVATA3 in Arabidopsis shoot meristems. *Science* **283**: 1911-1914.

Gadeyne, A., et al. (2014). The TPLATE adaptor complex drives clathrin-mediated endocytosis in plants. *Cell* **156**: 691-704.

Gaillochet, C., and Lohmann, J.U. (2015). The never-ending story: from pluripotency to plant developmental plasticity. *Development* **142**: 2237-2249.

Gaillochet, C., Daum, G., and Lohmann, J.U. (2015). O cell, where art thou? The mechanisms of shoot meristem patterning. *Curr Opin Plant Biol* **23**: 91-97.

Greb, T., and Lohmann, J.U. (2016). Plant Stem Cells. *Curr Biol* **26**: R816-821.

Guenot, B., Bayer, E., Kierzkowski, D., Smith, R.S., Mandel, T., Zadnikova, P., Benkova, E., and Kuhlemeier, C. (2012). Pin1-independent leaf initiation in Arabidopsis. *Plant Physiol* **159**: 1501-1510.

Chapter 5

Guo, Y., Han, L., Hymes, M., Denver, R., and Clark, S.E. (2010). CLAVATA2 forms a distinct CLE-binding receptor complex regulating Arabidopsis stem cell specification. *Plant J* **63**: 889-900.

Heidstra, R., and Sabatini, S. (2014). Plant and animal stem cells: similar yet different. *Nat Rev Mol Cell Biol* **15**: 301-312.

Heisler, M.G., Ohno, C., Das, P., Sieber, P., Reddy, G.V., Long, J.A., and Meyerowitz, E.M. (2005). Patterns of auxin transport and gene expression during primordium development revealed by live imaging of the Arabidopsis inflorescence meristem. *Curr Biol* **15**: 1899-1911.

Hobe, M., Muller, R., Grunewald, M., Brand, U., and Simon, R. (2003). Loss of CLE40, a protein functionally equivalent to the stem cell restricting signal CLV3, enhances root waving in Arabidopsis. *Dev Genes Evol* **213**: 371-381.

Hu, C., et al. (2018). A group of receptor kinases are essential for CLAVATA signalling to maintain stem cell homeostasis. *Nat Plants* **4**: 205-211.

Ito, Y., Nakanomyo, I., Motose, H., Iwamoto, K., Sawa, S., Dohmae, N., and Fukuda, H. (2006). Dodeca-CLE peptides as suppressors of plant stem cell differentiation. *Science* **313**: 842-845.

Janocha, D., and Lohmann, J.U. (2018). From signals to stem cells and back again. *Curr Opin Plant Biol* **45**: 136-142.

Je, B.I., et al. (2016). Signaling from maize organ primordia via FASCIATED EAR3 regulates stem cell proliferation and yield traits. *Nat Genet* **48**: 785-791.

Jeong, S., Trotochaud, A.E., and Clark, S.E. (1999). The Arabidopsis CLAVATA2 gene encodes a receptor-like protein required for the stability of the CLAVATA1 receptor-like kinase. *Plant Cell* **11**: 1925-1934.

Karimi, M., Depicker, A., and Hilson, P. (2007). Recombinational cloning with plant gateway vectors. *Plant Physiol* **145**: 1144-1154.

Kierzkowski, D., Lenhard, M., Smith, R., and Kuhlemeier, C. (2013). Interaction between meristem tissue layers controls phyllotaxis. *Dev Cell* **26**: 616-628.

Kim, S.Y., Xu, Z.Y., Song, K., Kim, D.H., Kang, H., Reichardt, I., Sohn, E.J., Friml, J., Juergens, G., and Hwang, I. (2013). Adaptor protein complex 2-mediated endocytosis is crucial for male reproductive organ development in Arabidopsis. *Plant Cell* **25**: 2970-2985.

Kitagawa, M., and Jackson, D. (2019). Control of Meristem Size. *Annu Rev Plant Biol* **70**: 269-291.

Kitakura, S., Vanneste, S., Robert, S., Lofke, C., Teichmann, T., Tanaka, H., and Friml, J. (2011). Clathrin mediates endocytosis and polar distribution of PIN auxin transporters in Arabidopsis. *Plant Cell* **23**: 1920-1931.

Krizek, B. (2009). AINTEGUMENTA and AINTEGUMENTA-LIKE6 act redundantly to regulate Arabidopsis floral growth and patterning. *Plant Physiol* **150**: 1916-1929.

Chapter 5

Kulich, I., Vojtikova, Z., Glanc, M., Ortmannova, J., Rasmann, S., and Zarsky, V. (2015). Cell wall maturation of Arabidopsis trichomes is dependent on exocyst subunit EXO70H4 and involves callose deposition. *Plant Physiol* **168**: 120-131.

Kurihara, D., Mizuta, Y., Sato, Y., and Higashiyama, T. (2015). ClearSee: a rapid optical clearing reagent for whole-plant fluorescence imaging. *Development* **142**: 4168-4179.

Lammens, T., Boudolf, V., Kheibarshekan, L., Zalmas, L.P., Gaamouche, T., Maes, S., Vanstraelen, M., Kondorosi, E., La Thangue, N.B., Govaerts, W., Inze, D., and De Veylder, L. (2008). Atypical E2F activity restrains APC/CCCS52A2 function obligatory for endocycle onset. *Proc Natl Acad Sci U S A* **105**: 14721-14726.

Lenhard, M., and Laux, T. (2003). Stem cell homeostasis in the Arabidopsis shoot meristem is regulated by intercellular movement of CLAVATA3 and its sequestration by CLAVATA1. *Development* **130**: 3163-3173.

Liu, Y., Xu, M., Liang, N., Zheng, Y., Yu, Q., and Wu, S. (2017). Symplastic communication spatially directs local auxin biosynthesis to maintain root stem cell niche in Arabidopsis. *Proc Natl Acad Sci U S A* **114**: 4005-4010.

Ma, Y., et al. (2019). WUSCHEL acts as an auxin response rheostat to maintain apical stem cells in Arabidopsis. *Nat Commun* **10**: 5093.

Mandel, T., Moreau, F., Kutsher, Y., Fletcher, J.C., Carles, C.C., and Eshed Williams, L. (2014). The ERECTA receptor kinase regulates Arabidopsis shoot apical meristem size, phyllotaxy and floral meristem identity. *Development* **141**: 830-841.

Mandel, T., Candela, H., Landau, U., Asis, L., Zelinger, E., Carles, C.C., and Williams, L.E. (2016). Differential regulation of meristem size, morphology and organization by the ERECTA, CLAVATA and class III HD-ZIP pathways. *Development* **143**: 1612-1622.

Mayer, K.F., Schoof, H., Haecker, A., Lenhard, M., Jurgens, G., and Laux, T. (1998). Role of WUSCHEL in regulating stem cell fate in the Arabidopsis shoot meristem. *Cell* **95**: 805-815.

Muller, R., Bleckmann, A., and Simon, R. (2008). The receptor kinase CORYNE of Arabidopsis transmits the stem cell-limiting signal CLAVATA3 independently of CLAVATA1. *Plant Cell* **20**: 934-946.

Muller, R., Borghi, L., Kwiatkowska, D., Laufs, P., and Simon, R. (2006). Dynamic and compensatory responses of Arabidopsis shoot and floral meristems to CLV3 signaling. *Plant Cell* **18**: 1188-1198.

Nimchuk, Z.L. (2017). CLAVATA1 controls distinct signaling outputs that buffer shoot stem cell proliferation through a two-step transcriptional compensation loop. *PLoS Genet* **13**: e1006681.

Nimchuk, Z.L., Tarr, P.T., Ohno, C., Qu, X., and Meyerowitz, E.M. (2011). Plant stem cell signaling involves ligand-dependent trafficking of the CLAVATA1 receptor kinase. *Curr Biol* **21**: 345-352.

Chapter 5

Nimchuk, Z.L., Zhou, Y., Tarr, P.T., Peterson, B.A., and Meyerowitz, E.M. (2015). Plant stem cell maintenance by transcriptional cross-regulation of related receptor kinases. *Development* **142**: 1043-1049.

Ogawa, M., Shinohara, H., Sakagami, Y., and Matsubayashi, Y. (2008). Arabidopsis CLV3 peptide directly binds CLV1 ectodomain. *Science* **319**: 294.

Paez Valencia, J., Goodman, K., and Otegui, M.S. (2016). Endocytosis and Endosomal Trafficking in Plants. *Annu Rev Plant Biol* **67**: 309-335.

Perales, M., Rodriguez, K., Snipes, S., Yadav, R.K., Diaz-Mendoza, M., and Reddy, G.V. (2016). Threshold-dependent transcriptional discrimination underlies stem cell homeostasis. *Proc Natl Acad Sci U S A* **113**: E6298-E6306.

Pfeiffer, A., et al. (2016). Integration of light and metabolic signals for stem cell activation at the shoot apical meristem. *eLife* **5**.

Poncini, L., Wyrsh, I., Denervaud Tendon, V., Vorley, T., Boller, T., Geldner, N., Metraux, J.P., and Lehmann, S. (2017). In roots of *Arabidopsis thaliana*, the damage-associated molecular pattern AtPep1 is a stronger elicitor of immune signalling than flg22 or the chitin heptamer. *PLoS ONE* **12**: e0185808.

Reddy, G.V., and Meyerowitz, E.M. (2005). Stem-cell homeostasis and growth dynamics can be uncoupled in the *Arabidopsis* shoot apex. *Science* **310**: 663-667.

Reinhardt, D., Frenz, M., Mandel, T., and Kuhlemeier, C. (2003a). Microsurgical and laser ablation analysis of interactions between the zones and layers of the tomato shoot apical meristem. *Development* **130**: 4073-4083.

Reinhardt, D., Pesce, E.R., Stieger, P., Mandel, T., Baltensperger, K., Bennett, M., Traas, J., Friml, J., and Kuhlemeier, C. (2003b). Regulation of phyllotaxis by polar auxin transport. *Nature* **426**: 255-260.

Roberts, I., et al. (2016). CEP5 and XIP1/CEPR1 regulate lateral root initiation in *Arabidopsis*. *J Exp Bot* **67**: 4889-4899.

Rodriguez-Leal, D., et al. (2019). Evolution of buffering in a genetic circuit controlling plant stem cell proliferation. *Nat Genet* **51**: 786-792.

Sanchez-Rodriguez, C., et al. (2018). The Cellulose Synthases Are Cargo of the TPLATE Adaptor Complex. *Mol Plant* **11**: 346-349.

Schoof, H., Lenhard, M., Haecker, A., Mayer, K.F.X., Jurgens, G., and Laux, T. (2000). The stem cell population of *Arabidopsis* shoot meristems is maintained by a regulatory loop between the CLAVATA and WUSCHEL genes. *Cell* **100**: 635-644.

Shinohara, H., and Matsubayashi, Y. (2015). Reevaluation of the CLV3-receptor interaction in the shoot apical meristem: dissection of the CLV3 signaling pathway from a direct ligand-binding point of view. *Plant J* **82**: 328-336.

Chapter 5

Somssich, M., Je, B.I., Simon, R., and Jackson, D. (2016). CLAVATA-WUSCHEL signaling in the shoot meristem. *Development* **143**: 3238-3248.

Somssich, M., Ma, Q., Weidtkamp-Peters, S., Stahl, Y., Felekyan, S., Bleckmann, A., Seidel, C.A., and Simon, R. (2015). Real-time dynamics of peptide ligand-dependent receptor complex formation in planta. *Sci Signal* **8**: ra76.

Soyars, C.L., James, S.R., and Nimchuk, Z.L. (2016). Ready, aim, shoot: stem cell regulation of the shoot apical meristem. *Curr Opin Plant Biol* **29**: 163-168.

Stahl, Y., Wink, R.H., Ingram, G.C., and Simon, R. (2009). A signaling module controlling the stem cell niche in Arabidopsis root meristems. *Curr Biol* **19**: 909-914.

Stahl, Y., et al. (2013). Moderation of Arabidopsis root stemness by CLAVATA1 and ARABIDOPSIS CRINKLY4 receptor kinase complexes. *Curr Biol* **23**: 362-371.

Su, Y.H., Zhao, X.Y., Liu, Y.B., Zhang, C.L., O'Neill, S.D., and Zhang, X.S. (2009). Auxin-induced WUS expression is essential for embryonic stem cell renewal during somatic embryogenesis in Arabidopsis. *Plant J* **59**: 448-460.

Truernit, E., Bauby, H., Dubreucq, B., Grandjean, O., Runions, J., Barthelemy, J., and Palauqui, J.C. (2008). High-resolution whole-mount imaging of three-dimensional tissue organization and gene expression enables the study of Phloem development and structure in Arabidopsis. *Plant Cell* **20**: 1494-1503.

Truskina, J., and Vernoux, T. (2018). The growth of a stable stationary structure: coordinating cell behavior and patterning at the shoot apical meristem. *Curr Opin Plant Biol* **41**: 83-88.

Uchida, N., and Torii, K.U. (2019). Stem cells within the shoot apical meristem: identity, arrangement and communication. *Cell Mol Life Sci* **76**: 1067-1080.

Ursache, R., Andersen, T.G., Marhavy, P., and Geldner, N. (2018). A protocol for combining fluorescent proteins with histological stains for diverse cell wall components. *Plant J* **93**: 399-412.

Van Damme, D., Coutuer, S., De Rycke, R., Bouget, F.Y., Inze, D., and Geelen, D. (2006). Somatic cytokinesis and pollen maturation in Arabidopsis depend on TPLATE, which has domains similar to coat proteins. *Plant Cell* **18**: 3502-3518.

Van Damme, D., Gadeyne, A., Vanstraelen, M., Inze, D., Van Montagu, M.C., De Jaeger, G., Russinova, E., and Geelen, D. (2011). Adaptin-like protein TPLATE and clathrin recruitment during plant somatic cytokinesis occurs via two distinct pathways. *Proc Natl Acad Sci U S A* **108**: 615-620.

Vaten, A., et al. (2011). Callose biosynthesis regulates symplastic trafficking during root development. *Dev Cell* **21**: 1144-1155.

Vernoux, T., Besnard, F., and Traas, J. (2010). Auxin at the shoot apical meristem. *Cold Spring Harb Perspect Biol* **2**: a001487.

Chapter 5

Wang, C., Yan, X., Chen, Q., Jiang, N., Fu, W., Ma, B., Liu, J., Li, C., Bednarek, S.Y., and Pan, J. (2013). Clathrin light chains regulate clathrin-mediated trafficking, auxin signaling, and development in Arabidopsis. *Plant Cell* **25**: 499-516.

Wang, J., Mylle, E., Johnson, A., Besbrugge, N., De Jaeger, G., Friml, J., Pleskot, R., and Van Damme, D. (2020). High Temporal Resolution Reveals Simultaneous Plasma Membrane Recruitment of TPLATE Complex Subunits. *Plant Physiol* **183**: 986-997.

Wang, P., et al. (2019). Plant AtEH/Pan1 proteins drive autophagosome formation at ER-PM contact sites with actin and endocytic machinery. *Nat Commun* **10**: 5132.

Williams, L., Grigg, S.P., Xie, M., Christensen, S., and Fletcher, J.C. (2005). Regulation of Arabidopsis shoot apical meristem and lateral organ formation by microRNA miR166g and its AtHD-ZIP target genes. *Development* **132**: 3657-3668.

Yadav, R.K., Tavakkoli, M., and Reddy, G.V. (2010). WUSCHEL mediates stem cell homeostasis by regulating stem cell number and patterns of cell division and differentiation of stem cell progenitors. *Development* **137**: 3581-3589.

Yadav, R.K., Perales, M., Gruel, J., Girke, T., Jonsson, H., and Reddy, G.V. (2011). WUSCHEL protein movement mediates stem cell homeostasis in the Arabidopsis shoot apex. *Genes Dev* **25**: 2025-2030.

Yamaguchi, Y.L., Ishida, T., and Sawa, S. (2016). CLE peptides and their signaling pathways in plant development. *J Exp Bot* **67**: 4813-4826.

Yamaoka, S., Shimono, Y., Shirakawa, M., Fukao, Y., Kawase, T., Hatsugai, N., Tamura, K., Shimada, T., and Hara-Nishimura, I. (2013). Identification and dynamics of Arabidopsis adaptor protein-2 complex and its involvement in floral organ development. *Plant Cell* **25**: 2958-2969.

Yoshida, S., Mandel, T., and Kuhlemeier, C. (2011). Stem cell activation by light guides plant organogenesis. *Genes Dev* **25**: 1439-1450.

Yoshinari, A., Fujimoto, M., Ueda, T., Inada, N., Naito, S., and Takano, J. (2016). DRP1-Dependent Endocytosis is Essential for Polar Localization and Boron-Induced Degradation of the Borate Transporter BOR1 in Arabidopsis thaliana. *Plant Cell Physiol* **57**: 1985-2000.

Zhou, Y., Yan, A., Han, H., Li, T., Geng, Y., Liu, X., and Meyerowitz, E.M. (2018). HAIRY MERISTEM with WUSCHEL confines CLAVATA3 expression to the outer apical meristem layers. *Science* **361**: 502-506.

Chapter Six

Conclusions and Perspectives

Chapter 6

Clathrin-mediated endocytosis (CME) is an evolutionary conserved mechanism whereby cargo proteins in the plasma membrane (PM) are recognized by adaptor protein complexes and internalized into cells via clathrin-coated vesicles (CCVs). Apart from the canonical adaptor complex Assembly Polypeptide 2 (AP-2), plant cells rely on the TPLATE complex (TPC) to execute CME (Gadeyne et al., 2014). TPC is an octameric complex that serves as an adaptor during CME in *Arabidopsis* (Gadeyne et al., 2014), and is essential for somatic and pollen development in plants (Van Damme et al., 2006; Gadeyne et al., 2014; Wang et al., 2019). Moreover, two subunits of TPC (AtEH1/Pan1 and AtEH2/Pan1), were shown to be involved in autophagy as they drive autophagosome formation at ER-PM contact sites (Wang et al., 2019). These results suggest AtEH/Pan1 proteins or the whole TPC might therefore have multiple roles in both pathways.

TPC is an evolutionary ancient adaptor complex which has been so far only been experimentally characterized in plants and in slime molds, and the complex components are not conserved in yeast and animal cells (Gadeyne et al., 2014; Hirst et al., 2014). Unlike to plants, TPC was discovered as a hexameric complex in *Dictyostelium* and is functionally dispensable (Hirst et al., 2014). The fact that plants are the only kingdom where TPC is essential for life (Gadeyne et al., 2014; Hirst et al., 2014), suggests that the initiation of CME appears to occur differently in plants than in the other model systems.

In the final Chapter, I will discuss the particular findings of my PhD study, and how the information gained opened up new hypotheses regarding TPC's function, as well as the further research plan to tackle with those.

TPC is recruited as octameric complex on the plasma membrane to fulfill its function in plant endocytosis

Although TPC was identified as an octameric complex by TAP experiments in plants (Gadeyne et al., 2014), we cannot ignore the fact that AtEH/Pan1

Chapter 6

proteins were not associated with other TPC subunits when the complex was forced into the cytoplasm by truncation of the TML subunit in plants, and also not copurified with the hexameric TPC complex in *Dictyostelium* (Gadeyne et al., 2014; Hirst et al., 2014). This suggests that the two AtEH/Pan1 subunits might be peripherally associated with a hexameric subcomplex of TPC. Visualizing the dynamic recruitment behaviors between the AtEH/Pan1 proteins and the remaining hexameric subcomplex via dual color time-lapse microscopy of CME, is the most direct way to determine whether TPC is recruited to PM as an octameric complex. However, we inferred that the temporal resolution would remain be the biggest challenge to conclude whether there is simultaneous or sequential recruitment between AtEH/Pan1 proteins and the other subunits.

Slowing down endocytosis by lowering temperature contributes to improving temporal resolution of differential recruitment

Visualizing the dynamic recruitment order between different endocytic players is a powerful way to uncover the assembly machinery of the step-wise endocytosis as well as understand the specific roles of certain endocytic proteins in plant endocytosis (Konopka and Bednarek, 2008; Fujimoto et al., 2010; Ito et al., 2012; Fan et al., 2013; Gadeyne et al., 2014; Bashline et al., 2015; Johnson and Vert, 2017; Narasimhan et al., 2020). By application of this technique, dynamin-related proteins (DRPs) were suggested as late endocytic players as they (DRP1A and DRP2B) are recruited to the PM later than clathrin (CLC) (Fujimoto et al., 2010); AP-2 proteins were revealed as earlier player as they (AP2M, AP2A1 and AP2S) appear earlier than or concomitant with CLC (Fan et al., 2013; Bashline et al., 2015; Johnson and Vert, 2017); and TPC was revealed to serve as another early endocytic player during CME, as two subunits (TPLATE and TML) are recruited to the PM earlier than or concomitant with CLC2 (Gadeyne et al., 2014; Narasimhan et al., 2020), earlier than DRP1c (Gadeyne et al., 2014), and prior to or concomitantly with the AP2 α subunit or

Chapter 6

AP2 μ (Gadeyne et al., 2014; Bashline et al., 2015). Due to the fact that endocytosis is very dynamic in plants, the temporal resolution remains the biggest challenge to monitor the dynamic recruitment of different endocytic protein players in plants.

Given that spinning disc microscopy and TIRF/VAEM microscopy are already high-speed microscopy, it appears that slowing down the whole endocytic process is a more feasible way to improve temporal resolution than looking for a faster way of imaging. With the application of the CherryTem system, we are able to cool down live samples on the microscope within minutes. The data in Chapter 2 suggest that cooling down the samples is an efficient strategy to slowdown the endocytic process as endocytosis responds immediately to lowering the temperature. The increased temporal resolution of differential endocytic players (TPLATE vs DRP1a, TPLATE vs CLC2) at low temperature compared with physiological temperature, revealed that it is a feasible and reliable tool to determine recruitment orders between different endocytic proteins.

The octameric TPC is required on the PM in plant endocytosis

The reason why AP-2 is not essential for plant endocytosis is likely caused by the formation of partially active AP-2 complexes that can still associate with the PM in individuals deficient in a given AP-2 subunit (Wang et al., 2016), which has been reported in *Caenorhabditis elegans* (Gu et al., 2013). As a consequence, plant cells can overcome the loss of single AP-2 subunits (α -, μ -, and σ -subunits) and generate a viable plant (Bashline et al., 2013; Fan et al., 2013; Kim et al., 2013; Yamaoka et al., 2013). However, knockout (TPLATE, TML, TWD40-1, TWD40-2, AtEH1 and AtEH2) or knockdown (TPLATE and TML) of single TPC subunit result in pollen lethality and seedling lethality respectively (Van Damme et al., 2006; Gadeyne et al., 2014; Wang et al., 2019), excluding the possibility that certain TPC subunits can form a partially functional

Chapter 6

subcomplex. The live cell imaging data (Chapter 2) revealed the simultaneous recruitment of TPC subunits (AtEH/Pan1 versus TPLATE, TPLATE versus TML) under both normal and lowered temperature conditions. Thus, TPC is recruited to the PM as an octameric complex. Short-term heat treatment induces the delocalization of destabilized TPLATE proteins from the PM and aggregates them in the cytoplasm, leading to the inactivation of TPC on the PM and as a consequence, a block of endocytosis (Chapter 4).

The truncated TML (TML Δ C), which forces TPC into the cytoplasm, fails to recovery AtEH/Pan1 to TPC (Gadeyne et al., 2014). Similarly, the aggregated TPLATE (mWDX) in the cytoplasm is unable to recruit AtEH2/Pan1, although it recruits DRP1a (Chapter 4). The retention of AtEH2/Pan1 on the PM when the destabilized TPLATE was aggregated in the cytoplasm, could be caused by the capacity of AtEH/Pan1 to associate with the PM independently of the other TPC subunits or, it can be attributed to the endogenous TPLATE (as F2 plants were used to image) that is still able to build-in together with AtEH/Pan for TPC assembly. The localization of AtEH2/Pan1 in the mWDX2 complemented line (*tplate* KO), in the absence of endogenous TPLATE after short term heat treatment will clarify this.

TPC versus AP-2 recruitment

It is still an open question whether TPC or AP-2 are recruited to the PM earlier. Although the majority of TPC is recruited to the PM earlier (TPLATE/TML versus AP2A1) or concomitant (TWD40-2 versus AP2M), we cannot ignore that fact rather a big population (40%) of AP-2 subunits (AP2M) exhibit earlier recruitment than TPC subunit (TWD40-2), and a mild population (less than 20%) of AP-2 subunits (AP2A1) appears earlier than TPC (TPLATE/TML) on the PM (Gadeyne et al., 2014; Bashline et al., 2015). Moreover, the situation is more complicated, as both complexes also exhibit differential departure behaviors. It is mostly observed that TPLATE/TML resides longer at the PM than AP-2,

visualized by AP2A1 (Gadeyne et al., 2014) while the majority of TWD40-2 disappear concomitant with AP2M (Bashline et al., 2015). The difference between the differential recruitment between TPC and AP-2, could be blamed on the differential recruitment between their own components. By applying dual-color live cell imaging, we were able to show the simultaneous recruitment of the octameric TPC on the PM. While recent single-color imaging work revealed the significantly different lifetimes between AP2A1 and AP2M on the PM (Johnson and Vert, 2017), suggested the possibility of differential recruitment orders among AP-2 subunits. Similar experiments could be performed to determine whether there is differential recruitment among AP2 subunits in dual-color labeled (for example AP2A1 vs AP2M) double complemented lines.

Development of tools to uncover TPC function

Many attempts have been made to manipulate plant endocytosis by interfering with the functions of the endocytic players by such as clathrin (Dhonukshe et al., 2007; Kitakura et al., 2011; Wang et al., 2013; Adamowski et al., 2018; Dejonghe et al., 2019), adaptor proteins (Bashline et al., 2013; Di Rubbo et al., 2013; Fan et al., 2013; Kim et al., 2013; Yamaoka et al., 2013; Gadeyne et al., 2014; Bashline et al., 2015; Wang et al., 2016; Sanchez-Rodriguez et al., 2018; Yoshinari et al., 2019) and dynamin-related proteins (Collings et al., 2008; Konopka and Bednarek, 2008; Backues et al., 2010; Taylor, 2011; Yoshinari et al., 2016) via genetic or chemical interference. Similarly, the lab has been aiming to uncover TPC's function in plant endocytosis via interfering with the functions of TPC subunits for a long term (Van Damme et al., 2006; Gadeyne et al., 2014; Sanchez-Rodriguez et al., 2018), and recently also by interfering with their function in autophagy (Wang et al., 2019).

The lethal phenotype of pollen and seedlings caused by loss-of-function or knockdown of TPC single subunits (except the recent identified weak allele *twd40-2-3*), however determines the infeasibility to achieve these aims via

Chapter 6

functional genetic approaches. Inducible knockdown approaches, which are able to overcome the seedling lethality caused by constitutive silencing TPC subunits, is a useful tool and has been employed to understand the roles of TPLATE in plant endocytosis as well as in seedling development (Gadeyne et al., 2014; Sanchez-Rodriguez et al., 2018). However, the low efficiency and extended time required to achieve silencing is a major issue of this approach. Short-term induction may fail to achieve adequate down-regulation of target genes, while long-term induction may result in secondary effects. Consequently, compared to viable mutants, this approach fails to provide information about TPC's function in different plant developmental stages.

The weak allele of *twd40-2-3* is a viable mutant which appears to be a useful tool to understand TPC's functions in plant endocytosis (Bashline et al., 2015). While it seems that the mild reduction of TWD40-2 in *twd40-2-3* is not strong enough, as knockout of TWD40-2 (*twd40-2-1* and *twd40-2-2*) leads to pollen lethality while this mutant only exhibited a slight reduction of root growth and elongated hypocotyl length (Gadeyne et al., 2014; Bashline et al., 2015). Although, mild reduction of TWD40-2 results in delayed dynamics of AP-2 (AP2M), and impaired endocytosis accompanied with the reduced internalization of regulation of cellulose synthase (CESA) complexes (CSCs), which resembles the inducible impaired-function of TML (Sanchez-Rodriguez et al., 2018). Combining *twd40-2-3* with mWDX-complemented *tplate* plants (Chapter 4) did not enhance the mutant phenotype in terms of root length or hypocotyl growth. Combining both weak mutants is therefore not a solution to obtaining a better tool to impair TPC-dependent endocytosis.

In addition, dominant-negative approach is another choice to manipulate TPC's function. Truncating the μ homology domain (μ HD) of TML forces it into the cytoplasm, however, still recovers certain TPC core components (Gadeyne et al., 2014). These results suggested that overexpression of the truncated TML is a potential candidate for a dominant-negative approach of TPC. However, as this will have to happen in the presence of endogenous TML, and therefore

Chapter 6

endogenous TPC, there will always be competition and it is not certain if levels of functional TPC can be depleted sufficiently with this approach and how long the induction of the truncated TML has to be maintained to achieve this.

Meanwhile, my data in Chapter 3 revealed that substituting the Sandwich or Platform subdomains located in the C-term APPENDAGE domain of TPLATE subunit, abolishes its PM recruitment and functionality which is a consequence of the complete abolishment of TPC assembly. Similar to the truncated TML, the C-term truncated TPLATE was also hypothesized to be potential candidate for dominant-negative approach of TPC in the lab. However, the development of a dominant-negative approach must meet that at least partial of the TPC subunits will be built-in together with the manipulated subunit. My results regarding the substitutions in APPENDAGE domains in the C-term of TPLATE point out that the C-term truncated TPLATE is not suitable to develop as a dominant-negative approach. On the other hand, my results however also suggest that Platform and Sandwich subdomains could be potential targets for developing effective tools to manipulate TPC functions, such as using chemical interference or CRISPR techniques.

Given that TPC functions on the PM in plant endocytosis requires the recruitment of the whole complex, disturbing the function of the fundamental TPLATE subunit in a mild way has potential to generate partially functional TPLATE allele. We employed an ingeniously targeted mutagenesis strategy to generate partial loss of function alleles of TPLATE by mutating selected motifs, which were identified based on evolutionary conservation. We identified the WDX domain as the most conserved motifs of TPLATE subunit across plants as well as in *Dictyostelium*. Our integrative TPC structure data suggested that TPLATE is centrally positioned in TPC (Yperman et al., 2020). And the WDX motif lies in a region with crucial intramolecular interactions within the TPLATE subunit and also to some extent in the region involved in interaction with other TPC subunits (particularly TML and TWD40-2) (Yperman et al., 2020). Hence, we speculate that these interactions are crucial for proper complex assembly

Chapter 6

and thus they are under strong evolutionary pressure. Substituting this motif, resulted in destabilizing TPLATE as well as the whole complex, thus dampens the efficiency of endocytosis while conserves TPLATE functionality (Chapter 3 and Chapter 4). Therefore, the destabilizing TPLATE version is a partially functional TPLATE allele which was termed mWDX.

Our MS data showed that interactions between TPLATE and the other subunits are destabilized in mWDX plants (mWDX1 and mWDX2, Chapter4). It will be interesting to test compare interaction strength between mWDX on the one hand and TPLATE on the other hand, with the other TPC subunits. Quantifiable interaction methods such as the ratiometric bimolecular fluorescence complementation (BIFC) system and the rapamycin-dependent knocksideways system developed in our lab (Grefen and Blatt, 2012; Winkler et al., 2020), will contribute to addressing this question.

mWDX is a novel conditional tool to uncover the roles of TPC on the PM

My data in Chapter 3 and Chapter 4 together reveals that mWDX is not only a partially functional TPLATE allele, but also a heat-inducible tool to inactivate TPC. I will discuss the new findings and related hypothesis regarding TPC's function with the help of this tool.

Taking it to our advantage that heat shock boosts the aggregation of destabilized proteins, we developed the destabilizing version of TPLATE, mWDX, as a heat-inducible tool to functionally inactivate TPC. Short-term heat-treatment (35 °C for 6h) delocalizes TPLATE from the PM and causes it to aggregate in the cytoplasm in mWDX2 complemented lines. This turned out to be an efficient tool to inactivate TPC on the PM and results in efficient impairment of endocytosis (Chapter 4), supporting the application of this tool to study TPC's roles on the PM.

Only few tools are available to manipulate plant endocytosis specifically on the PM. Given that clathrin localizes and functions on the PM but also at the

Chapter 6

TGN where it is likely involved in secretion (Dhonukshe et al., 2007; Robinson and Pimpl, 2014). Neither overexpression of CHC-Hub nor the application of ES9-17 enables to interfere with the functions of clathrin specifically on the PM as the non-selective competition or binding with the CHC (Kitakura et al., 2011; Dejonghe et al., 2019). Overexpression of AUXILIN (AUXILIN-like1/2) appears to block endocytosis via inhibiting the recruitment of clathrin to initiating endocytic pits by binding to and retaining all available clathrin in the cytosol. While the spots where clathrin localizes in the presence of induced auxillin could also be autophagosomes, similar to what has been shown recently that overexpression of AtEH/Pan1 could recruit clathrin to autophagosomes for degradation (Adamowski et al., 2018).

It seems that a dominant-negative of DRP1A is a potential good tool to functions on the PM, as it is exclusively recruited to the PM as endocytic foci (Konopka and Bednarek, 2008; Fujimoto et al., 2010). While overexpression of the dominant-negative dominant-negative DRP1A (DRP1A K47A) results in massive localization to discrete compartments in the cytoplasm, suggested this dominant negative tool might interfere with more than the function of DRP1A on the PM (Yoshinari et al., 2016).

The heat-inducible feature of inactivating TPC specifically on the PM provides us with the unique opportunity to understand the step-wise process of endocytosis such as viewing CCPs budding from the plasma membrane. TPC is speculated to be an initiation player during CME in plants, it is therefore necessary to understand how CCPs budding will be on the plasma membrane when TPC function is perturbed. Investigating the CCVs curvature with the 'unroofed' *Arabidopsis* protoplasts (Narasimhan et al., 2020), obtained from mWDX complemented lines after short-term heat treatment will contribute to understanding TPC's roles in CCVs development.

mWDX links TPLATE-dependent endocytosis to the regulation of ROS homeostasis

Heat stress always leads to excessive reactive oxygen species (ROS) accumulation which is harmful to plants and results in cell death (Sedaghatmehr et al., 2019; Yu et al., 2019; Tang et al., 2020). The whitening cotyledons phenotype could be caused by ROS accumulation in mWDX2 mutants under heat stress (Chapter 4). Recent work showed that ROS accumulation under heat stress is light-dependent, as dark treatment abolished ROS accumulation and thus inhibited the lesion-mimicking phenotype (Tang et al., 2020). Our preliminary data show that the whitening cotyledon phenotype, which correlates with the seedling lethality in mWDX2 complemented lines under long-term heat stress is inhibited by constant dark treatment. (Fig S1). These results are similar to recent work in rice (Tang et al., 2020), indicating that the observed seedling lethality is likely caused by the dysregulation of ROS under impaired/loss function of TPC. However, further experiments such as ROS staining (DAB staining and NBT staining) are required to confirm the accumulation of ROS in mWDX2 complemented lines under heat stress. In addition, the internalization of the NADPH oxidase RboHD, which is involved in the production of apoplastic ROS (Mittler, 2017; Qi et al., 2017), undergoes clathrin-independent microdomain-associated internalization as well as CME (Hao et al., 2014). Thus, RboHD is a potential cargo which requires TPC for its internalization. To further investigate this, interaction between TPC and RboHD via BiFC and Co-IP could be performed, similarly as our analyses which linked TPLATE to CLV1 (chapter 5). Also, the accumulation of RboHD on the plasma membrane by immunolocalization could be examined and the dynamics of RboHD in WDX complemented lines under/after short-term heat stress could be analyzed.

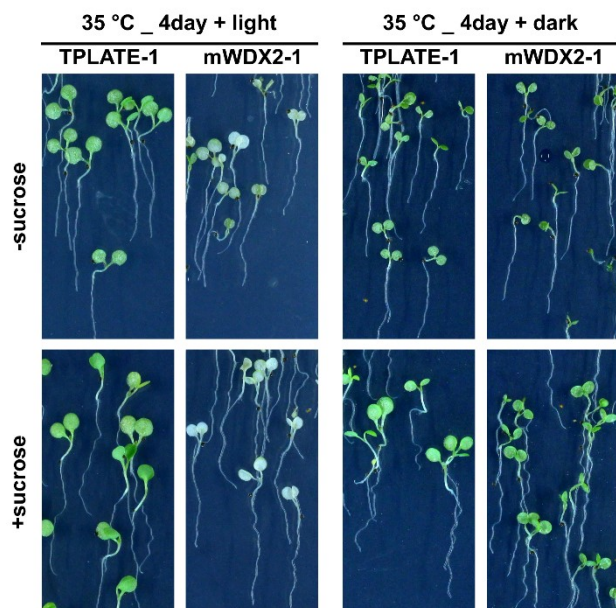


Figure S1. Darkness inhibits whitening of the mWDX2 cotyledons under heat stress.

Phenotypical comparison between TPLATE and mWDX2 complemented lines in response to heat stress under light or dark conditions. Seedlings were grown vertically at 20 °C for 5 days and then moved to 35 °C for extra 4 days under continuous light or darkness supplemented with or without sucrose.

mWDX reveals that TPC function is not required for autophagosome formation

The requirement of AtEH/Pan1 for autophagy, and the observation that other TPC subunits are also involved, brings the question whether the whole TPC is required for autophagy (Wang et al., 2019). Mild downregulation of AtEH1/Pan1 results in a strong susceptibility to nutrient depleted conditions, especially to fixed carbon starvation. If the whole TPC is required for autophagy, mWDX is expected to exhibit susceptibility to fixed carbon starvation as the whole TPC is already destabilized under physiological temperature. Our carbon starvation experiments in Chapter 4 reveal that the whole TPC is not required for autophagy under nutrient depleted conditions at permissive temperatures. However, the insusceptibility of mWDX plants to fixed carbon starvation could also be blamed to the possibility that there is still enough TPC present to

Chapter 6

initiate/execute autophagy. Short-term heat treatment which inactivates TPC via aggregating destabilized TPC in the cytoplasm in our mWDX2 complemented lines, however failed to dampen autophagosome formation. This further supports that the whole TPC is not required for autophagy.

The fact that AtEH2/Pan1 is not recruited to TPLATE aggregated structure, points to the possibility that AtEH/Pan1 proteins are required for autophagy independent of other TPC subunits. However, we currently are limited to heat stress as we require this treatment to inactivate TPC. Reduced *AtEH/Pan1* expression has so far only been linked to nutrient stress, not to heat stress. Further experiments are required to prove AtEH/Pan1 proteins are required for autophagosomes formation under heat stress. The quantification of autophagosome formation upon down-regulation of AtEH/Pan1 under heat stress is the logical next step.

mWDX associates TPLATE-dependent endocytosis with shoot apical meristem maintenance

Mild destabilization of TPC in mWDX complemented lines results in a predominant double-shoot phenotype under physiological conditions (Chapter 5), which is caused by the splitting of the meristem, randomized cell identity and disordered patterning in the vegetative SAM. This novel phenotype was not observed in the weak *twd40-2-3* allele (Bashline et al., 2015) and or other impaired-function endocytic players such as clathrin (Kitakura et al., 2011; Wang et al., 2013; Adamowski et al., 2018), AP-2 (Fan et al., 2013; Kim et al., 2013; Yamaoka et al., 2013) and dynamins (Collings et al., 2008; Backues et al., 2010; Mravec et al., 2011). The reason why this phenotype has not been reported in endocytic player mutants could be caused by either inadequate or overwhelming modulation of plant endocytosis. Due to destabilizing TPC, we hypothesize that the pLAT52 promoter possesses weak activity in the vegetative meristem, and therefore fails to provide sufficient TPC for plant

Chapter 6

endocytosis to maintain the SAM homeostasis in mWDX complemented lines. Further experiments to explain the meristem developmental dynamics by the temporal-spatial behaviour of the pLAT52 promoter have been discussed in Chapter 5.

Due to the deficient endocytosis in our mWDX complemented line, we could trace this phenotype back to impaired internalization of CLV1-type receptors from the PM in the vegetative and flower meristems as well as ectopic deposition of callose and thick cell walls in the vegetative meristems. The ectopic callose deposition and thick wall observed in the mWDX2 meristems, on the one hand might block the cell-to-cell communication (such as WUS movement and CLV3 migration) between different functional zones, on the other hand, it may also contribute to the dead/differentiated cells at the summit and central zone of the meristem. Further experiments to convert the mWDX2 phenotype such as removing the ectopic callose deposition via overexpression of the callase PDBG1 have been discussed in Chapter 5.

The homeostasis of reactive oxygen species (ROS) is essential for SAM maintenance as different forms of ROS have antagonistic roles in plant stem cell regulation (Huang et al., 2019). In the Arabidopsis SAM, enrichment of O_2^- in stem cells activates the WUSCHEL gene to maintain stem cell activities, whereas H_2O_2 accumulation in the peripheral zone (PZ) promotes cell differentiation. Moreover, H_2O_2 negatively regulates O_2^- biosynthesis in stem cells, and increasing H_2O_2 levels or scavenging O_2^- leads to the termination of stem cells (Zeng et al., 2017). TPLATE-dependent endocytosis has been hypothesized to regulate the ROS homeostasis. Consequently, dysregulation of ROS caused by deficient TPLATE-dependent endocytosis may also contribute to the dead/differentiated cells at the summit and central zone in WDX2 vegetative meristem. Similarly, further experiments such as ROS staining (DAB staining and NBT staining) are required to examine the distribution of ROS in mWDX2 vegetative meristems.

Chapter 6

We speculated the ectopic callose deposition likely blocks the cell-to-cell communication in mWDX2 vegetative meristems. The CLV3 peptide has never been localized *in vivo*, so we failed to show how it could diffuse in mWDX2 vegetative meristem (Kitagawa and Jackson, 2019). Recent work showed an inactive version of WUS (WUS-delta Box) driven by the ML1 promoter was able to move to the L2 and L3 layer cells, which represents an ideal candidate to evaluate the cell-to-cell communication in mWDX2 meristems. Comparing the movement of labelled ML1-driven WUS-delta Box in TPLATE and mWDX2 vegetative meristems will contribute to understand the effect of mWDX on cell-to-cell communications.

In addition to the strategy to visualize the movement of proteins between cell layers in the SAM, genetic approaches combining mWDX2 complemented lines to the EMS missense mutation *wus-7* (Graf et al., 2010; Lin et al., 2016), the dominant-negative *clv1-8* (Dievart et al., 2003) and the *clv3-9* null mutant (Nimchuk et al., 2015) will also help to answer what happens in mWDX2 vegetative meristems. For example, examining whether there will be enhanced phenotype in the combination of mWDX2 (*tplate* homo) with *wus-7* (heterozygous or homozygous) will help to understand the effect of blocking the movement of WUS on SAM formation from a genetic point of view. Examining the phenotype of the combination of mWDX2 with the dominant-negative *clv1-8* will contribute to understanding whether TPLATE-dependent endocytosis is also involved in the internalization of other types of receptors. Moreover, examining the phenotype of the combination of mWDX2 with the *clv3-9* will contribute to evaluating the effect of thick cell wall and ectopic callose deposition on the diffusion of CLV3 as well as other peptides function in SAM maintenance.

Is TPLATE-dependent endocytosis required root apical meristem maintenance?

The root apical meristem (RAM) is essential for plants to generate their underground tissues. Similar to SAM, cell-to-cell communication between the quiescent center (QC) and the surrounding cells is also essential for RAM to maintain the quiescence in the QC and stemness in the stem cell niche (SCN) (Drisch and Stahl, 2015; Uchida and Torii, 2019). It has been shown that blocking the symplastic communication (mediated by plasmodesmata) between QC and the surrounding cells by ectopic overexpression of an inducible gain-of-function mutations in CALLOSE SYNTHASE3 (CALS3) (in QC), results in disruption of SCN maintenance including QC division, columella stem cells (CSCs) division and disorganized columella (Liu et al., 2017). Similar to SAM, we also observed disruption of SCN maintenance such as CSCs division and disorganized patterning in the RAMs of WDX2 roots which might be the consequence of the ectopic callose deposition around QC in mWDX2 roots (Fig S2). These results initially link TPLATE-dependent endocytosis to RAM maintenance as well. However, the mechanism requires to be further studied.

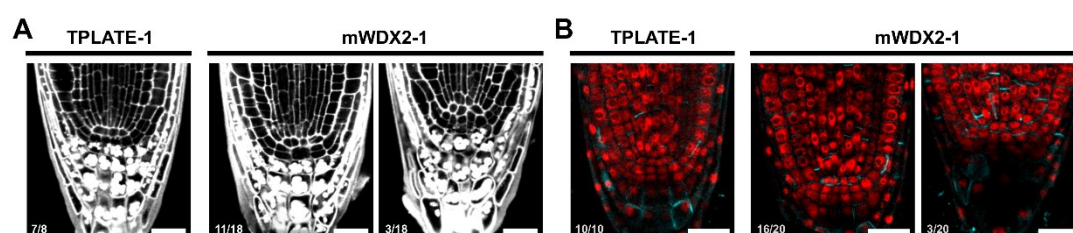


Figure S2. Destabilizing TPC results in disorganized root apical meristem patterning, which correlates with ectopic callose deposition around QC.

(A-B) Representative images of root apical meristems in TPLATE and mWDX2 complemented lines. The 4- or 5-day old seedlings were treated with mPS-PI staining (A) or aniline blue staining and co-stained with PI (B). Scale bar = 25 μ m. The numbers in panel (A) indicate the amount of seedlings showing normal (TPLATE) or disorganized root apical meristem patterning (mWDX2) out of the total number of seedlings imaged. The numbers in panel (B) indicate the amount of seedlings showing normal callose deposition (TPLATE) or ectopic callose deposition

around QC (mWDX2) out of the total number of seedlings imaged.

Is manipulation of TPC's function potentially applicable to agriculture?

Manipulation of meristem size pathways have been reported to increase yield in tomato and maize, including increase the size of fruits and the number of seeds (Je et al., 2016; Rodriguez-Leal et al., 2017). Given the enlarged meristem as well as double shoots which may form more branches to generate seeds, we also compared the seeds size as well as yields between TPLATE and mWDX2 under physiological conditions. Generally, mWDX2 exhibited enlarged seed sizes as well as possessed increased seed yields (Fig S3). Our initial data (not shown) already confirmed the functionality of removing the mWDX domain in TPLATE as well as the double-shoot phenotypes. These data together reveal the potential application of improving yields in crops by applying CRISPR/Cas9 mutagenesis to manipulate TPC's functions. However, attempts will have to be made to avoid causing too high instability of TPC, which could be boosted by elevated temperatures as this will be detrimental for plant growth.

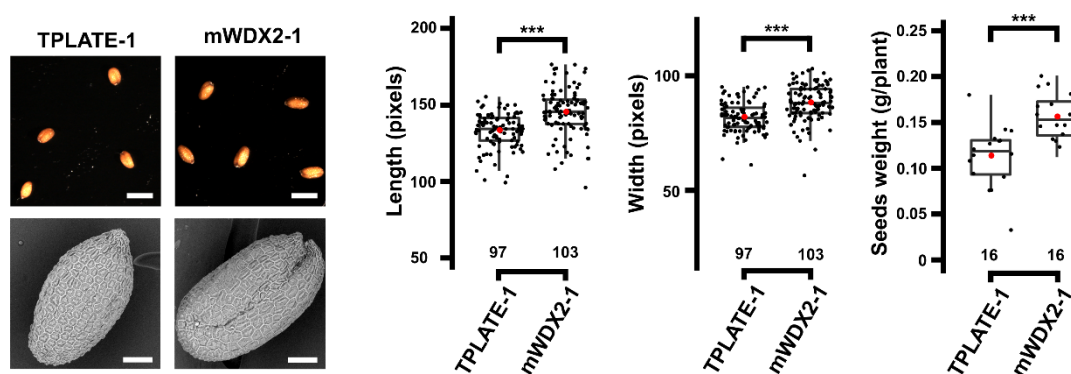


Figure S3. Destabilizing TPC results in enlarged seeds and improved yields

Representative images and quantification of seeds from TPLATE and mWDX2 complemented lines. Seeds were imaged with Leica bino (upper panel) and Table electronic microscopy (Hitachi TEM, lower panel). Scale bars equal to 650 μm (200 pixels, upper) or 100 μm (lower). Number are indicated at the bottom. ***, P<0.001 for Ttest.

Chapter 6

During my PhD research, many experiments have been initiated to uncover TPC's function in autophagy, endocytosis as well as plant development. We achieved to possess functionally complemented lines for several TPC subunits (TPLATE, TML, AtEH1/Pan1 and AtEH1/Pan1, TWD40-1 and TWD40-2). We now have a much more detailed insight on how this complex operates and we now possess tools to conditionally inactivate the complex, albeit with the restriction of high temperature. We will mainly focus on answering the following questions in the recent future: How is the recruitment of AtEH/Pan1 at the PM affected in the absence of TPC under heat stress? Are AtEH/Pan1 proteins required for autophagosome formation under heat stress? How does TPLATE-dependent endocytosis regulate ROS homeostasis? How is the movement of WUS affected in the SAM of mWDX plants and what causes the centrally positioned cell death/differentiation in mWDX2 vegetative SAMs?

References

- Adamowski, M., Narasimhan, M., Kania, U., Glanc, M., De Jaeger, G., and Friml, J.** (2018). A Functional Study of AUXILIN-LIKE1 and 2, Two Putative Clathrin Uncoating Factors in Arabidopsis. *Plant Cell* **30**: 700-716.
- Backues, S.K., Korasick, D.A., Heese, A., and Bednarek, S.Y.** (2010). The Arabidopsis dynamin-related protein2 family is essential for gametophyte development. *Plant Cell* **22**: 3218-3231.
- Bashline, L., Li, S., Zhu, X., and Gu, Y.** (2015). The TWD40-2 protein and the AP2 complex cooperate in the clathrin-mediated endocytosis of cellulose synthase to regulate cellulose biosynthesis. *Proc Natl Acad Sci U S A* **112**: 12870-12875.
- Bashline, L., Li, S., Anderson, C.T., Lei, L., and Gu, Y.** (2013). The endocytosis of cellulose synthase in Arabidopsis is dependent on mu2, a clathrin-mediated endocytosis adaptin. *Plant Physiol* **163**: 150-160.
- Collings, D.A., Gebbie, L.K., Howles, P.A., Hurley, U.A., Birch, R.J., Cork, A.H., Hocart, C.H., Arioli, T., and Williamson, R.E.** (2008). Arabidopsis dynamin-like protein DRP1A: a null mutant with widespread defects in endocytosis, cellulose synthesis, cytokinesis, and cell expansion. *J Exp Bot* **59**: 361-376.
- Dejonghe, W., et al.** (2019). Disruption of endocytosis through chemical inhibition of clathrin heavy chain function. *Nat Chem Biol* **15**: 641-649.
- Dhonukshe, P., Aniento, F., Hwang, I., Robinson, D.G., Mravec, J., Stierhof, Y.D., and Friml, J.** (2007). Clathrin-mediated constitutive endocytosis of PIN auxin efflux carriers in Arabidopsis. *Curr Biol* **17**: 520-527.
- Di Rubbo, S., et al.** (2013). The clathrin adaptor complex AP-2 mediates endocytosis of brassinosteroid insensitive1 in Arabidopsis. *Plant Cell* **25**: 2986-2997.
- Dievart, A., Dalal, M., Tax, F.E., Lacey, A.D., Huttly, A., Li, J., and Clark, S.E.** (2003). CLAVATA1 dominant-negative alleles reveal functional overlap between multiple receptor kinases that regulate meristem and organ development. *Plant Cell* **15**: 1198-1211.
- Drisch, R.C., and Stahl, Y.** (2015). Function and regulation of transcription factors involved in root apical meristem and stem cell maintenance. *Front Plant Sci* **6**: 505.
- Fan, L., Hao, H., Xue, Y., Zhang, L., Song, K., Ding, Z., Botella, M.A., Wang, H., and Lin, J.** (2013). Dynamic analysis of Arabidopsis AP2 sigma subunit reveals a key role in clathrin-mediated endocytosis and plant development. *Development* **140**: 3826-3837.
- Fujimoto, M., Arimura, S., Ueda, T., Takanashi, H., Hayashi, Y., Nakano, A., and Tsutsumi, N.** (2010). Arabidopsis dynamin-related proteins DRP2B and DRP1A participate together in clathrin-coated vesicle formation during endocytosis. *Proc Natl Acad Sci U S A* **107**: 6094-6099.
- Gadeyne, A., et al.** (2014). The TPLATE adaptor complex drives clathrin-mediated endocytosis in plants. *Cell* **156**: 691-704.

Chapter 6

Graf, P., Dolzblasz, A., Wurschum, T., Lenhard, M., Pfreundt, U., and Laux, T. (2010). MGOUN1 encodes an Arabidopsis type IB DNA topoisomerase required in stem cell regulation and to maintain developmentally regulated gene silencing. *Plant Cell* **22**: 716-728.

Grefen, C., and Blatt, M.R. (2012). A 2in1 cloning system enables ratiometric bimolecular fluorescence complementation (rBiFC). *Biotechniques* **53**: 311-314.

Gu, M., Liu, Q., Watanabe, S., Sun, L., Hollopeter, G., Grant, B.D., and Jorgensen, E.M. (2013). AP2 hemicomplexes contribute independently to synaptic vesicle endocytosis. *eLife* **2**: e00190.

Hao, H., Fan, L., Chen, T., Li, R., Li, X., He, Q., Botella, M.A., and Lin, J. (2014). Clathrin and Membrane Microdomains Cooperatively Regulate RbohD Dynamics and Activity in Arabidopsis. *Plant Cell* **26**: 1729-1745.

Hirst, J., Schlacht, A., Norcott, J.P., Traynor, D., Bloomfield, G., Antrobus, R., Kay, R.R., Dacks, J.B., and Robinson, M.S. (2014). Characterization of TSET, an ancient and widespread membrane trafficking complex. *eLife* **3**: e02866.

Huang, H., Ullah, F., Zhou, D.X., Yi, M., and Zhao, Y. (2019). Mechanisms of ROS Regulation of Plant Development and Stress Responses. *Front Plant Sci* **10**: 800.

Ito, E., Fujimoto, M., Ebine, K., Uemura, T., Ueda, T., and Nakano, A. (2012). Dynamic behavior of clathrin in Arabidopsis thaliana unveiled by live imaging. *Plant J* **69**: 204-216.

Je, B.I., et al. (2016). Signaling from maize organ primordia via FASCIATED EAR3 regulates stem cell proliferation and yield traits. *Nat Genet* **48**: 785-791.

Johnson, A., and Vert, G. (2017). Single Event Resolution of Plant Plasma Membrane Protein Endocytosis by TIRF Microscopy. *Front Plant Sci* **8**: 612.

Kim, S.Y., Xu, Z.Y., Song, K., Kim, D.H., Kang, H., Reichardt, I., Sohn, E.J., Friml, J., Juergens, G., and Hwang, I. (2013). Adaptor protein complex 2-mediated endocytosis is crucial for male reproductive organ development in Arabidopsis. *Plant Cell* **25**: 2970-2985.

Kitagawa, M., and Jackson, D. (2019). Control of Meristem Size. *Annu Rev Plant Biol* **70**: 269-291.

Kitakura, S., Vanneste, S., Robert, S., Lofke, C., Teichmann, T., Tanaka, H., and Friml, J. (2011). Clathrin mediates endocytosis and polar distribution of PIN auxin transporters in Arabidopsis. *Plant Cell* **23**: 1920-1931.

Konopka, C.A., and Bednarek, S.Y. (2008). Comparison of the dynamics and functional redundancy of the Arabidopsis dynamin-related isoforms DRP1A and DRP1C during plant development. *Plant Physiol* **147**: 1590-1602.

Lin, T.F., Saiga, S., Abe, M., and Laux, T. (2016). OBE3 and WUS Interaction in Shoot Meristem Stem Cell Regulation. *PLoS ONE* **11**: e0155657.

Chapter 6

Liu, Y., Xu, M., Liang, N., Zheng, Y., Yu, Q., and Wu, S. (2017). Symplastic communication spatially directs local auxin biosynthesis to maintain root stem cell niche in Arabidopsis. *Proc Natl Acad Sci U S A* **114**: 4005-4010.

Mittler, R. (2017). ROS Are Good. *Trends Plant Sci* **22**: 11-19.

Mravec, J., et al. (2011). Cell plate restricted association of DRP1A and PIN proteins is required for cell polarity establishment in Arabidopsis. *Curr Biol* **21**: 1055-1060.

Narasimhan, M., Johnson, A., Prizak, R., Kaufmann, W.A., Tan, S., Casillas-Perez, B., and Friml, J. (2020). Evolutionarily unique mechanistic framework of clathrin-mediated endocytosis in plants. *eLife* **9**.

Nimchuk, Z.L., Zhou, Y., Tarr, P.T., Peterson, B.A., and Meyerowitz, E.M. (2015). Plant stem cell maintenance by transcriptional cross-regulation of related receptor kinases. *Development* **142**: 1043-1049.

Qi, J., Wang, J., Gong, Z., and Zhou, J.M. (2017). Apoplastic ROS signaling in plant immunity. *Curr Opin Plant Biol* **38**: 92-100.

Robinson, D.G., and Pimpl, P. (2014). Clathrin and post-Golgi trafficking: a very complicated issue. *Trends Plant Sci* **19**: 134-139.

Rodriguez-Leal, D., Lemmon, Z.H., Man, J., Bartlett, M.E., and Lippman, Z.B. (2017). Engineering Quantitative Trait Variation for Crop Improvement by Genome Editing. *Cell* **171**: 470-480 e478.

Sanchez-Rodriguez, C., et al. (2018). The Cellulose Synthases Are Cargo of the TPLATE Adaptor Complex. *Mol Plant* **11**: 346-349.

Sedaghatmehr, M., Thirumalaikumar, V.P., Kamranfar, I., Marmagne, A., Masclaux-Daubresse, C., and Balazadeh, S. (2019). A regulatory role of autophagy for resetting the memory of heat stress in plants. *Plant Cell Environ* **42**: 1054-1064.

Tang, Y., Gao, C.C., Gao, Y., Yang, Y., Shi, B., Yu, J.L., Lyu, C., Sun, B.F., Wang, H.L., Xu, Y., Yang, Y.G., and Chong, K. (2020). OsNSUN2-Mediated 5-Methylcytosine mRNA Modification Enhances Rice Adaptation to High Temperature. *Dev Cell* **53**: 272-286 e277.

Taylor, N.G. (2011). A role for Arabidopsis dynamin related proteins DRP2A/B in endocytosis; DRP2 function is essential for plant growth. *Plant Mol Biol* **76**: 117-129.

Uchida, N., and Torii, K.U. (2019). Stem cells within the shoot apical meristem: identity, arrangement and communication. *Cell Mol Life Sci* **76**: 1067-1080.

Van Damme, D., Coutuer, S., De Rycke, R., Bouget, F.Y., Inze, D., and Geelen, D. (2006). Somatic cytokinesis and pollen maturation in Arabidopsis depend on TPLATE, which has domains similar to coat proteins. *Plant Cell* **18**: 3502-3518.

Wang, C., Yan, X., Chen, Q., Jiang, N., Fu, W., Ma, B., Liu, J., Li, C., Bednarek, S.Y., and Pan, J. (2013). Clathrin light chains regulate clathrin-mediated trafficking, auxin signaling, and development in Arabidopsis. *Plant Cell* **25**: 499-516.

Chapter 6

Wang, C., et al. (2016). Differential Regulation of Clathrin and Its Adaptor Proteins during Membrane Recruitment for Endocytosis. *Plant Physiol* **171**: 215-229.

Wang, P., et al. (2019). Plant AtEH/Pan1 proteins drive autophagosome formation at ER-PM contact sites with actin and endocytic machinery. *Nat Commun* **10**: 5132.

Winkler, J., Mylle, E., De Meyer, A., Pavie, B., Merchie, J., Gronès, P., and Van Damme, D. (2020). Rapamycin-dependent delocalization as a novel tool to reveal protein-protein interactions in plants.

Yamaoka, S., Shimono, Y., Shirakawa, M., Fukao, Y., Kawase, T., Hatsugai, N., Tamura, K., Shimada, T., and Hara-Nishimura, I. (2013). Identification and dynamics of Arabidopsis adaptor protein-2 complex and its involvement in floral organ development. *Plant Cell* **25**: 2958-2969.

Yoshinari, A., Fujimoto, M., Ueda, T., Inada, N., Naito, S., and Takano, J. (2016). DRP1-Dependent Endocytosis is Essential for Polar Localization and Boron-Induced Degradation of the Borate Transporter BOR1 in Arabidopsis thaliana. *Plant Cell Physiol* **57**: 1985-2000.

Yoshinari, A., Hosokawa, T., Amano, T., Beier, M.P., Kunieda, T., Shimada, T., Hara-Nishimura, I., Naito, S., and Takano, J. (2019). Polar Localization of the Borate Exporter BOR1 Requires AP2-Dependent Endocytosis. *Plant Physiol* **179**: 1569-1580.

Yperman, K., et al. (2020). The TPLATE subunit is essential for structural assembly of the endocytic TSET complex.

Yu, W., Wang, L., Zhao, R., Sheng, J., Zhang, S., Li, R., and Shen, L. (2019). Knockout of SIMAPK3 enhances tolerance to heat stress involving ROS homeostasis in tomato plants. *BMC Plant Biol* **19**: 354.

Zeng, J., Dong, Z., Wu, H., Tian, Z., and Zhao, Z. (2017). Redox regulation of plant stem cell fate. *EMBO J* **36**: 2844-2855.

Acknowledgments

In the last part of my thesis, I would like to take this opportunity to acknowledge many people who have guided me, helped me, and encouraged me during my PhD study.

First and foremost, I would like to apply my deepest appreciation to my promoter Daniel, who provided me the great opportunity to pursue my PhD in such an excellent group five years ago. Thanks for guiding me to the kingdom of plant endocytosis as well as teaching live-cell imaging techniques. As I started my PhD study with a scarce molecular biology background, which is not easy for me as well as for you. I can still remember we communicated on the pages, and you explained to me patiently and wrote down the short-term plan cautiously at the start. I can still remember you guided me on how to perform genotyping PCR, how to plant Arabidopsis and do the floral dips, and how to image the epidermis cells in the roots, et al. I appreciate your patient guidance, your timely communications when I have nice results or questions, your kind explanations to my questions, your encouragements when I made progress, your inspiring suggestions and the freedom you gave me to perform experiments, as well as your timely and cautious revisions on the manuscripts and my thesis. Without your full support, I cannot achieve my PhD. Thank you, Daniel! You are a great mentor for my study and my life.

Then I want to give my special thanks to my co-promoter, Jenny. I appreciate your support for my BOF funding application, as well as valuable comments and all kinds of help for my projects.

I would also like to thank all the members of my PhD Examination Board for spending precious time on evaluating my thesis and providing valuable comments and kind advice to improve my thesis greatly.

I want to acknowledge the China Scholarship Council (CSC) and the Special Research Funds of Ghent University (BOF) for the financial support.

Many thanks to my dear colleagues, Roman, Klaas, Qihang, Evelien, Peter, Michaël, Joanna, Deepanksha, Michael, Andreas, and Jonathan for their kind help in these years. Especially, I appreciate Roman, Klaas, and Peter for the constructive discussions and critical comments for manuscript preparation as well as the efforts in chemical biology experiments and data analysis. I learned a lot from you. I appreciate the guidance from Evelien at the start of my study as well as the efforts for the annoying image data analysis. I also appreciate Qihang and Michaël, for helping me with big-scale experiments and taking care of my plants. I cherish all the good times and vivid memories spent together with our Alice group from the sparkling brainstorming to the colorful group activities. They are precious memories of my PhD life.

I want to thank all the collaborators who contribute to this work. Without your efforts, I am not able to obtain so many fantastic results. I also want to give a big thanks to all the colleagues in PSB support teams for providing such a pleasant atmosphere to work.

I also want to thank our Chinese community for their help, encouragement and support. Zongcheng and Baojun, you are so knowledgeable and can always explain my question clearly. I treasure the time we spent together for the drinking and foods, tea and chatting, traveling, and playing games with you: Qing, Xiuyang, Shanshuo, Ting, Xinyu, Ke, Cheng, Yaowei, Boyu, Xiangyu, Ji, Xiaopeng, Panfeng, Yuanke, Qing, and all the Chinese group.

Additionally, I also want to thank my best friends out of PSB: Hanxiang, Genlin, Yingjie, Qing, and Yufeng, for their encouragements and suggestions when I feel confused. I appreciate and miss the time we spent together in room 634, SCAU.

Finally, I would like to dedicate my most gratitude to my parents and girlfriend for their accompany, support, and encouragement. I appreciate my girlfriend Qi, preparing delicious food and taking care of my daily life although she has to tackle her PhD. I appreciate the endless love and support from my parents that support me to move forward.

Curriculum Vitae

Personal information

Name: Jie Wang
Gender: Male
Date of birth: 21-07-1990
Place of birth: Sanmenxia, Henan, China

Education

2015.09 - present

PhD

Ghent University / VIB – Gent, Belgium
Thesis: Dynamic recruitment and the physiological roles of the TPLATE complex in plant endocytosis
Promotor: Prof. Dr. Daniel Van Damme
Co-promotor: Prof. Dr. Eugenia Russinova
Funded by:
Special Research Fund from Ghent University, 2015 - 2019
China Scholarship Council (CSC) scholarship, 2015 - 2019

2012.09 - 2015.06

Master of Agriculture

South China Agricultural University - Guang Zhou, China
Thesis: Uptake mechanism and translocation of fluorescent glucose-fipronil conjugates in *Ricinus communis*
Promotor: Prof. Dr. Hanhong Xu
National Scholarship for Postgraduates, Ministry of Education of China
Award for Outstanding Graduates, SCAU

2008.09 - 2012.06

Bachelor of Engineering

Henan Agricultural University - Zheng Zhou, China.

Conferences

- 2019.10 **International Symposium on Frontiers in Plant Cell Biology and Modern Forestry Researches**
Hang Zhou, China
Poster : The octameric TPLATE complex is recruited to the plasma membrane as a whole
- 2018.9 **21th European Network for Plant Endomembrane Research Meeting**
Vienna, Austria
Poster : TPLATE complex-dependent endocytosis is involved in shoot apical meristem patterning
- 2017.9 **20th European Network for Plant Endomembrane Research Meeting**
Prague, Czech Republic
Oral Presentation : Lowering temperature: monitoring the relative PM recruitment of endocytic proteins with enhanced temporal resolution?
- 2016.9 **19th European Network for Plant Endomembrane Research Meeting**
Bordeaux, France
Poster : Relative PM recruitment of TPLATE complex subunits and dissecting the function of TPLATE during Clathrin-mediated endocytosis in *Arabidopsis*

Publications

equal contribution (co-first author)

1. **Wang, J.**, Mylle, E., Johnson, A., Besbrugge, N., De Jaeger, G., Friml, J., Pleskot, R., and Van Damme, D. (2020). High temporal resolution reveals simultaneous plasma membrane recruitment of TPLATE complex subunits. *Plant physiology*.
2. Wang, P., Pleskot, R., Zang, J., Winkler, J., **Wang, J.**, Yperman, K., Zhang, T., Wang, K., Gong, J., Guan, Y., et al. (2019). Plant AtEH/Pan1 proteins drive autophagosome formation at ER-PM contact sites with actin and endocytic machinery. *Nature communications* 10, 5132.
3. Arora, D., Abel, N.B., Liu, C., Van Damme, P., Yperman, K., Eeckhout, D., Vu, L.D., **Wang, J.**, Tornkvist, A., Impens, F., et al. (2020). Establishment of Proximity-dependent Biotinylation Approaches in Different Plant Model Systems. *Plant Cell*.
4. Klaas Yperman[#], **Jie Wang**[#], Dominique Eeckhout, Joanna Winkler, Lam Dai Vu, Michael Vandorpe, Peter Grones, Evelien Mylle, Michael Kraus, Romain Merceron, Jonah Nolf, Eliana

Mor, Pieter De Bruyn, Remy Loris, Martin Potocký, Savvas N. Savvides, Bert De Rybel, Geert De Jaeger, Daniel Van Damme, and Roman Pleskot (2020). Structural basis for the evolution of the endocytic TSET complex in plants. (Manuscript is currently under review)

5. **Jie Wang**, Klaas Yperman, Peter Grones, Qihang Jiang, Evelien Mylle, Eliana Mor, Jonah Nolf, Dominique Eeckhout, Geert De Jaeger, Bert De Rybel, Roman Pleskot, and Daniel Van Damme (2020). Conditional destabilization of the TPLATE complex impairs endocytic internalization. (Manuscript is currently being submitted for publication).

Publications related to Master Research projects

6. **Wang, J. #**; Lei, Z. #; Mao, G.; Wen, Y.; Xu, H., A novel fluorescent conjugate applicable to visualize the translocation of glucose-fipronil. *Journal of Agricultural and Food Chemistry*. 2014, 62 (35), 8791-8798.

7. Qin, P. #; **Wang, J. #**; Wang, H.; Wen, Y.; Lu, M.; Li, Y.; Xu, Y.; Xu, H., Synthesis of Rotenone-O-monosaccharide derivatives and their phloem mobility. *Journal of Agricultural and Food Chemistry*. 2014, 62 (20), 4521-4527.

8. Lei, Z. #; **Wang, J. #**; Mao, G.; Wen, Y.; Tian, Y.; Wu, H.; Li, Y.; Xu, H., Glucose Positions Affect the Phloem Mobility of Glucose–Fipronil Conjugates. *Journal of Agricultural and Food Chemistry*. 2014, 62 (26), 6065-6071.

9. Lei, Z. #; **Wang, J. #**; Mao, G.; Wen, Y.; Xu, H., Phloem mobility and translocation of fluorescent conjugate containing glucose and NBD in castor bean (*Ricinus communis*). *Journal of Photochemistry and Photobiology B-Biology*. 2014, 132, 10-16.

10. Jia, J.; Zhu, L.; Jin, X.; **Wang, J.**; Zhang, W.; Wu, H.; Xu, H., 2,4-Dichlorophenoxyacetic acid functionalized gold nanoparticles: synthesis, characterization and biological effects. *Journal of Materials Chemistry B*. 2014, 2 (21), 3299-3305.

11. Lei, ZW. #; **Wang, J. #** Synthesis and application of clickable and biocompatible fluorescent glycosyl labels. *Dyes and Pigments*. 2015. 113: p. 627-633.

12. Mao, GL.; **Wang, J.**; Lei, ZW.; Xu, FF.; Zhang, ZX.; Xu, HH., Root uptake and long-distance root-shoot translocation of a glucose-fipronil conjugate in soybeans (*Glycine max*). 13th IUPAC international congress of pesticide chemistry. San Francisco, California, USA, 2014, P 42.

Courses and Training

Practical English 3-5, UCT, Ghent University	2015 .10 - 2016. 12
Scientific Writing & Oral Presentations, VIB	2017. 06
Summer School in Advanced Light Microscopy, VIB	2017. 06

